UNIVERSITY OF CALIFORNIA SAN DIEGO

Neural computations for behaviorally relevant information storage and retrieval from seconds to hours

A dissertation submitted in partial satisfaction of the requirements
for the degree Doctor of Philosophy

in

Biology

by

Siavash Ahmadi

Committee in charge:

Professor Jill K. Leutgeb, Chair
Professor Robert E. Clark
Professor Stefan Leutgeb
Professor Terrence J. Sejnowski
Professor John T. Wixted

2020

The Dissertation of Siavash Ahmadi is approved, and it is acceptable in quality and form for publication on microfilm and electronically:

Chair

University of California San Diego

2020

DEDICATION

To my family

TABLE OF CONTENTS

LIST OF FIGURES

ACKNOWLEDGEMENTS

It is often said that finishing a PhD is a hard and arduous undertaking but writing the acknowledgement section of the dissertation is feeling just as hard. It is obvious to me that many people have been instrumental in my path to where I currently am, but finding the right words to properly express my gratitude to them is the challenge here. The person most responsible for your growth as a budding scientist is your advisor and I am first and foremost grateful to her for helping me get through this. Jill certainly took a massive gamble on me when she admitted me directly into her lab seven years ago. At the time, I knew little about neuroscience, and certainly nothing about doing experiments or working with animals. Jill gave me much freedom to explore and fail (as I did many times, big and small). She guided me to learn how to find the right questions, identify the steps to address them, compose my thoughts and ideas and express them cogently, and present my findings persuasively. I am grateful to her for supporting me all along.

I would like to thank my committee members, Stefan Leutgeb, Terry Sejnowski, John Wixted, and Bob Clark for their critical appraisal of my progress every year and their ideas to help move the projects forward. Several of the findings I present in the dissertation stem from their feedback. Because we shared lab space, I interacted with Stefan significantly. Stefan has taught me much about how to think critically of all scientific results, be it my own or others'. He has generously spent innumerable hours sitting down with me to work on data analysis or edit drafts, and so kindly supported me through some difficult times. I have also been tremendously lucky that Terry contributed to my growth in so many ways, but I am particularly grateful to him for almost singlehandedly convincing me – one day during tea time at his lab – to want to continue down an academic path. I do not know if he remembers this episode, but I always will.

Of particular importance to my PhD coming to a conclusion were Veronica Piatti, Takuya Sasaki and Marta Sabariego who collected the data that I reanalyzed in Chapter 2 of the dissertation. Frequent interactions with them were critical to understand the data sets and successfully continue the analyses. In addition to that, Veronica taught me many things about rats, doing experiments and the procedures I had to do afterwards. I would also like to express special thanks to Christian Leibold of LMU Munich for his general support and direct involvement with the development and analysis of the computational model presented in Chapter 2. Many of the other things I learned were also a result of my interactions with my lab mates. I am particularly thankful to Laura Ewell who taught me a lot about how to be a PhD student. Laura, her husband Jon, and I shared nice discussions about the English language together. I learned how to build hyperdrives from Mandy Wong to whom I am thankful for it. I thank Silvia Viana da Silva for all the banter we shared about football and for listening to my stories. I'm sorry if I bore you to death, Silvia! I also spent a significant amount of time with Clare Quirk talking about being PhD students. Those conversations were vital to my survival in grad school. Ipshita Zutshi unwittingly taught me how to be more humble and communicate better. She too aided me in honing my grad school survival skills, provided insightful and intelligent feedback on my research projects, and aided me with troubleshooting things, not to mention her generous help during first year classes and qualifying exam. Anna-Lena Schlenner assisted me with collecting some experimental data for a few months which was important to keeping some minimal semblance of sanity while I was awaiting my US visa to return to the lab. Ario Ramezani and Christopher Luong also provided significant assistance in the experimental parts of my projects, including animal training, data collection, and post-mortem tissue processing. Down in the vivarium were perhaps the real heroes of the lab: the rats. I will always remember

you guys. Vivarium staff Neil Batista, who was very friendly, greatly helped me in taking care of the rats.

Many of my previous professors have been crucial in my path until today. I am thankful to Prof. Yahya Tabesh who was my undergraduate advisor and professor in a couple of algorithms courses. Prof. Rasool Ramezanian reinvigorated my passion for research and taught me exciting topics such as game theory, new to me at the time. The reason I am writing my PhD dissertation in systems neuroscience and not some other endeavor is without a doubt attributable to Prof. Rens Bod. Prof. Bod is a linguist, but when I was in Amsterdam he advised me to start working with Francesco Battaglia. Francesco, to whom I am much obliged, took me on as a master's intern student and taught me a lot along the way which prepared me to start my PhD. And the rest is history.

When I joined the PhD program, I was living in perpetual fear. The last biology course I had taken was about 9 years prior and, embarrassingly, I did not know some basic concepts in biology. Of course, we were required at the time to complete a three course sequence, molecular biology, cellular biology, and genetics. There is absolutely no doubt in my mind that I would have failed at least one of these graduate level courses in a subject matter so foreign to me at the time if it wasn't for the generosity of my classmates who helped me learn the material and do the assignments to stay afloat. Angela, Varoth, Yeara, Mizu, Meiyan, Hyeson, Mai, Bu, Alison, Ipshita: thank you all. I am also thankful to the fellow students in the Neurocircuits graduate seminars for their continual critical feedback on my work.

Many friends have helped throughout the years to reach this point, before and after I started my PhD. One of the most amazing friends I have known is Ben Brandenburg who was my classmates while I was a master's student in Amsterdam. Ben was incredibly generous in

every way. He opened his home to me for three months between when I finished my internship in the Leutgeb lab and when started here as a PhD student. Had it not been for him, I would have had an unfathomably stressful time and been stranded god knows where in the Netherlands that summer. Ben has always had my back and I always look forward to talking to him on the phone and share PhD chronicles or hear about the French countryside, in which I find great joy. I am extremely grateful to Ron and Nicola who graciously welcomed me in their home at the beginning of my PhD which was especially helpful at that stage. They also helped me adjust to the San Diego way of life throughout the years, be it by having me over for Thanksgiving or a nice dinner out. I always appreciated it all. I cannot leave San Diego without mentioning Enoch who has been a terrific friend, the first I found in this city a month after arriving here for the first time as a master's student. He has taught me how to be a better person. Enoch has been incredibly supportive through it all and key to why I had a successful postdoc interview—I am forever indebted to him. Bahram who I got to know almost by accident is probably the person I spent the most amount of time talking with about personal matters over the last several years. Bahram was my therapist and I was his. Being a brilliant scientist himself, Bahram showed great interest in what I was doing in the lab so naturally we spent countless hours discussing science, coming up with new experimental designs, and identifying key questions in the neuroscience of learning and memory. Life would definitely not have been the same without knowing Bahram. Augustine was the reason I found a way to play soccer every week, which cleansed my brain. Andre made it fun playing on the field, and planned great hikes and camping trips which I enjoyed a lot.

Family is what I cherish the most. It is an unfortunate turn of events that I have been unable to visit my parents and brother for four and a half years, and my sister for about two. I

love you all beyond words can express. I am forever and ever indebted to my uncle, Aydin, who is probably the most critical link in the chain that has led me down my current path. I love you very much and I hope to repay your kindness by doing what you would expect me to: work hard, love what I do, and give back. I owe what I have to all of you and miss you achingly.

Chapter 1, in full, is material that is unpublished and coauthored by Ahmadi, S, Leutgeb, S, and Leutgeb, JK. The dissertation author was the primary investigator and author of this material.

Chapter 2, in full, is currently being prepared for submission for publication of the material by Ahmadi, S, Sasaki, T, Sabariego, M, Leibold, C, Leutgeb, S, and Leutgeb, JK. The dissertation author was the primary investigator and author of this material.

VITA

2011 Bachelor of Science, Sharif University of Technology, Tehran, Iran
2013 Master of Science, University of Amsterdam, Amsterdam, The Netherlands
2020 Doctor of Philosophy, University of California San Diego, USA

PUBLICATIONS

Sasaki, T., Piatti, V. C., Hwaun, E., Ahmadi, S., Lisman, J. E., Leutgeb, S., & Leutgeb, J. K. (2018). Dentate network activity is necessary for spatial working memory by supporting CA3 sharp-wave ripple generation and prospective firing of CA3 neurons. *Nat Neurosci* **21**, 258–269. dx.doi.org/10.1038/s41593-017-0061-5.

Sabariego, M., Schönwald, A., Boublil, B. L., Zimmerman, D. T., Ahmadi, S., Gonzalez, N., Leibold, C., Clark, R. E., Leutgeb, J. K., & Leutgeb, S. (2019). Time cells in the hippocampus are neither dependent on medial entorhinal cortex inputs nor necessary for spatial working memory. *Neuron* **102**(6), 1235–1248. dx.doi.org/10.1016/j.neuron.2019.04.005.

Ahmadi, S., Sasaki, T., Sabariego, M., Leibold, C., Leutgeb, S., & Leutgeb, J. K. Distinct roles of dentate gyrus and medial entorhinal cortex inputs for phase precession and temporal correlations in hippocampal CA3 place cells. *In preparation*.

Ahmadi, S., Leutgeb, S., & Leutgeb, J. K. Reorganization of hippocampal population patterns during memory retention over hours. *In preparation*.

FIELDS OF STUDY

Major Field: Biological Science (Neuroscience)

Studies in Biology, PhD
Professor Jill K. Leutgeb

Studies in Brain and Cognitive Sciences, MSc
Professor Francesco P. Battaglia

Studies in Computer Science, BSc
Professor Rasool Ramezanian

ABSTRACT OF THE DISSERTATION

Neural computations for behaviorally relevant information storage and retrieval from seconds to hours

by

Siavash Ahmadi

Doctor of Philosophy in Biology

University of California San Diego, 2020

Professor Jill K. Leutgeb, Chair

Episodic memories unfold in space and time, typically in a sequential manner. The hippocampus, being an effective sequence generator, critically supports the acquisition and recall of episodic memories. Further, it is thought to accomplish this by implementing a “cognitive map”—and internal representation of relations among external events. However, several aspects of how the encoding, maintenance, and retrieval of sequences are mediated at the hippocampal neuronal level are not well-understood. Moreover, it is unclear how the hippocampus continues to process established cognitive maps to use them for guiding behavior at a later time. My thesis consists of two studies combining experimental and computational approaches in which I

demonstrate how the hippocampus implements sequential computations to support episodic memory. To understand how the hippocampus might act as a cognitive map, first I examine how animals display stable memory-guided behaviors despite substantial reorganization of representations in the hippocampus code for space (i.e., change in the correspondence of neural activity to constant external/internal variables). In this study, I uncover several aspects of neural dynamics in terms of spatial and temporal co-firing of neural ensembles which support memory. I also investigate how subpopulations representing specific memories are reactivated after learning to support future memory retrieval. In the second study, I investigate the phenomenon of phase precession which is thought to constitute the “low-level” basis for forming and orchestrating multi-neuronal sequential activity that is repeatedly manifested in behavior. By independently controlling converging inputs (DG and MEC) onto the same neural network (hippocampal CA3), I elucidate the distinct roles of these inputs in organizing the temporal codes of CA3. I propose a simple computational model that explains the observations and makes quantitative predictions for future testing. I conclude by discussing how the phenomena discovered in the two studies are related, and propose a framework for testing my predictions in future experiments. Together, these investigations advance our understanding of hippocampal dynamics that support encoding, maintenance, and retrieval processes by dissecting multiple circuits and distinct neuronal populations within them.

INTRODUCTION

Episodic memory and the brain structures supporting it

Language, symbolic reasoning, a sophisticated theory of mind, and the ability to produce and appreciate art might set us apart from other animals, but what distinguishes us from *each other* no doubt stems from our personal *autobiographical*, or *episodic*, memory. Memories of our childhood, our parents, friends, life events, and personal secrets are what make us who we are as individuals. Without them, we might still possess the uniquely human cognitive abilities, but we would no longer be who we used to be. In this dissertation, I investigate the neural mechanisms underlying some forms of episodic memories that are thought to establish them over a few seconds and maintain them for many hours and days.

In psychology and neuroscience, episodic or autobiographical memory is defined as the memory of events that take place within a spatial and temporal context. An instance of an episodic memory may be remembered as "I bought bread from the bakery yesterday morning." In humans, episodic memory is accompanied by autonoetic consciousness (Tulving, 1983) whereby a personally experienced event is remembered as such. Autonoetic consciousness is one's ability to imagine oneself back within the remembered memory as if it were happening at the moment of imagination. Furthermore, episodic memory is distinguished from semantic memory which is the memory of facts expressible in propositional form and crucially lacks an autonoetic nature (e.g., "Paris is the capital of France").

Our ability to probe specific brain regions responsible for storing episodic memories arguably began with the classic work of Scoville and Milner (Scoville & Milner, 1957) where they reported the case of patient H.M. who, for medical reasons regarding his intractable

epilepsy, had gone through brain surgery where portions of his medial temporal lobe were resected. H.M.'s surgery caused him to lose his ability to form new memories. Intriguingly, H.M.'s other cognitive abilities such as his intelligence, reasoning and language abilities remained intact after the surgery. Even more fascinating was the fact that, H.M.'s memory loss was specific to the episodic and semantic varieties: procedural ("muscle") memory, perceptual learning, and skill learning had all remained intact. Furthermore, H.M. retained his short-term, "working" memory such that he could hold short conversations or retain information for minutes by constantly rehearsing it. In addition to helping establish the memory taxonomy of declarative versus non-declarative (Squire, 1992), these observations established, for the first time, that the former is attributable to a circumscribed part of the brain, namely the hippocampus and its associated areas such as the entorhinal cortex (Scoville & Milner, 1957). Subsequent studies of H.M. (Corkin, 1984, 2002) as well as other memory loss patients (e.g., Rosenbaum *et al.* (2005)) demonstrated that the neural substrates for episodic memories could be further distinguished from those supporting merely semantic memories (Gordon Hayman, Macdonald, & Tulving, 1993; O'Kane, Kensinger, & Corkin, 2004; Rosenbaum *et al.*, 2005; Tulving, Hayman, & Macdonald, 1991). Postmortem histology and brain reconstruction (Annese *et al.*, 2014) confirmed that H.M.'s brain lesions were extensive and included a deafferented hippocampus and additional structures in the medial temporal lobe including the entorhinal cortex (Annese *et al.*, 2014; Corkin, Amaral, González, Johnson, & Hyman, 1997).

Circuitry of the hippocampus and entorhinal cortex

The hippocampal formation and the entorhinal cortex are part of the greater parahippocampal region (Witter, Groenewegen, Lopes da Silva, & Lohman, 1989). The parahippocampal region is the locus of convergence of multiple sensory information sources that

are eventually routed through the hippocampus through the superficial layers (layers II and III) of entorhinal cortex (EC). Early anatomical studies identified at least two major subdivisions in the medial and lateral aspects of the entorhinal cortex with distinct cytoarchitectonic and connectivity profiles. The superficial EC consists of two principle neuron types, the stellate and pyramidal cells, which form extensive intrinsic recurrent networks. Entorhinal cortex layer II (ECII) and layer III (ECIII) pyramidal cells' projections are largely confined to the EC, while the ECII stellate cell population forms the primary source of direct input to the dentate gyrus (DG) and CA3 subregions of the hippocampus (HPC). ECIII stellate cells target the interneurons of the CA1 subregion in HPC. Both ECII and ECIII stellate cells send axons to area CA2 in HPC. These direct, monosynaptic connections from superficial EC to HPC are termed the perforant pathway (PP). Within HPC, DG comprises the granule cell and mossy cell populations. The granule cells of DG are the most numerous cell type in HPC (> 1,000,000) and send their axons (termed "mossy fibers") to the pyramidal cells of CA3. The mossy cells of DG, in turn, receive CA3 projections and project back to the DG granule cells. The roughly 250,000 pyramidal cells of the CA3 region project to area CA1 as well as form relatively extensive recurrent connections onto other pyramidal cells in CA3. In addition to receiving indirect ECIII and direct CA3 input, CA1 neurons also receive inputs from area CA2. CA1, containing roughly ~350,000 tightly packed pyramidal cell bodies in its stratum pyramidale, acts as the main output path of the hippocampus, projecting to the subicular structures as well the deep layers (V and VI) of EC. It is now worth reviewing, in some detail, the computational considerations that arise from the anatomical properties just described.

The potential function of the different subregions of the hippocampus might be analyzed based on the cytoarchitecture, connectivity, and electrophysiological properties of each region.

Figure 0.1: Simplified schematic of the anatomical connections of the EC-HPC circuit. Information generally flows from the superficial layers (II/III) of the entorhinal cortex (EC) through the hippocampus (HPC) to the deep layers (V/VI) of EC, with the arrows indicating monosynaptic connections. The curved arrow on the right indicates the direction of this information flow. The perforant pathway, indicated in orange, originates in ECII and makes monosynaptic contacts onto DG, CA3, and CA2. The temporoammonic pathway, indicated in purple, originates from ECIII and makes monosynaptic contacts onto CA1 and CA2. Within HPC, DG granule cells send their mossy fibers to CA3 and CA2. CA3, in turn, projects to CA2 and CA1, with CA2 providing an additional input to CA1. CA1 acts as the output circuit of the hippocampus and sends its axons to ECV/VI.

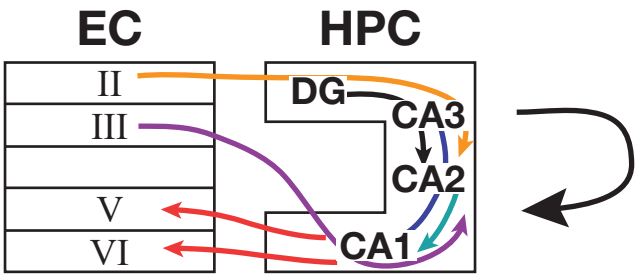
EC
HPC
II
III
V
VI
DG
CA3
CA2
CA1

DG has been proposed to generate an efficient, orthogonalized code (Rolls, 1989, 1996). Here, "efficiency" refers to the idea that only those patterns that do occur in the input (but not those that are rare or never occur) are learned by the DG system. This, in effect, compresses the input for encoding. Moreover, "orthogonal" refers to the statistical independence of the set of encoded patterns. Orthogonalization can be achieved by a combination of two features: first, the number of DG granule neurons is far greater than the number of stellate neurons in the layer II of the entorhinal cortex where almost all entorhinal and the bulk of parahippocampal inputs to DG originate ((Gatome, Slomianka, Lipp, & Amrein, 2010; Kitamura *et al.*, 2014; Varga, Lee, & Soltesz, 2010; Witter *et al.*, 1989); > 1,000,000 vs. < 40,000 in the rat). Because the synapses of each DG neuron may be thought of as having randomly distributed weights with respect to a new memory item to be stored, this expansion in the dimensionality of input ensures that the probability of the same neuron being activated in response to similar inputs is very low. Second, competitive learning may lead to a winner-take-all scheme in which the subpopulation with the highest drive due to a given input will suppress the activity of neighboring neurons via lateral inhibition, thereby increasing the signal-to-noise ratio (Dasgupta, Stevens, & Navlakha, 2017; Rolls, 1996). The very low probability ($< 10^{-4}$) of a CA3 cell being contacted by a DG mossy fiber (Amaral, Ishizuka, & Claiborne, 1990) also make it more likely that distinct CA3 representations are activated by various DG inputs, a function termed pattern separation (Hainmueller & Bartos, 2020; Rolls, 1996). These theoretical insights regarding pattern separation are experimentally supported by the observation that small changes in the environmental features lead to both a substantial decorrelation in the dentate gyrus population code and the recruitment of distinct statistically independent CA3 populations (Leutgeb, Leutgeb, Moser, & Moser, 2007). Calcium imaging (GoodSmith *et al.*, 2017), juxtacellular

(GoodSmith *et al.*, 2017), and optogenetically tagged electrophysiological (Senzai & Buzsáki, 2017) recording from mossy and granule cells of the dentate gyrus suggested that the findings of Leutgeb *et al.* (2007) on pattern separation by DG may primarily but not exclusively (GoodSmith, Lee, Neunuebel, Song, & Knierim, 2019) reflect the contributions of the mossy cells or adult-born granule neurons (Danielson *et al.*, 2016).

The CA3 region forms a recurrently connected network which can accomplish autoassociation. Analyses of this architecture (Marr, 1971; Rolls, 1996; Treves & Rolls, 1994) have suggested that after storing orthogonalized DG input patterns, CA3 can facilitate reliable retrieval of stored patterns given only a partial corresponding input. In this manner, the DG input can serve as an index code, while the CA3 performs pattern completion (Knierim & Neunuebel, 2016; Rebola, Carta, & Mulle, 2017; Rolls, 2013). CA3 sends backprojections to DG (Scharfman, 2007) which may aid the retrieval process (Hainmueller & Bartos, 2020; Lisman, 1999). CA3 neurons maintain a stable response to minor changes in the environment (Colgin *et al.*, 2010; Leutgeb *et al.*, 2005a; Leutgeb & Leutgeb, 2007; Leutgeb, Leutgeb, Treves, Moser, & Moser, 2004; Vazdarjanova & Guzowski, 2004), suggesting autoassociative dynamics govern the CA3 circuit as an error correction/pattern completion mechanism as suggested by theoretical inquiries (Treves & Rolls, 1992; Tsodyks, 1999). Since CA3 neurons receive both DG and EC inputs, there may be a division of labor in terms of encoding and retrieval between the two inputs. In this view, the relatively weak, associatively modifiable synapses of the PP (EC input) provide the processed input modalities from the various sensory areas, whereas the strong non-associative DG inputs act as an unsupervised teacher that are useful at the encoding stage, but should remain inactive during retrieval (Treves & Rolls, 1992). Indeed, experimental data have shown that DG inputs are strong enough to act as a “detonator” for CA3 spiking (Henze, Wittner,

& Buzsáki, 2002; McNaughton & Morris, 1987). Larson and Lynch (1986) showed that a "priming" stimulus followed 200 milliseconds later by a second stimulation can induce strong potentiation in the hippocampus, supporting the dual-input encoding scheme (Bittner *et al.*, 2015). By exposing rats to a novel (i.e., previously not experienced) modified Hebb-Williams maze (in which rats are required to navigate with as short a path as possible between a start and end location) , Lee and Kesner (2004) provided evidence for a dissociation between the roles of the DG and EC inputs in encoding and retrieval processes, respectively. The rats performed 10 trials a day over the course of three learning days. It was argued that intact encoding and retrieval would be predictive, respectively, of within-day and between-day reduction in navigation errors. By this logic, Lee and Kesner (2004) showed an encoding deficit in rats with DG-to-CA3 input lesions, and a retrieval deficit in rats with EC lesions. Further, comparison of contra- with ipsilateral DG-CA3 lesions supported the notion than DG and CA3 work together to support encoding, but not retrieval (Jerman, Kesner, & Hunsaker, 2006). Finally, CA3 has been shown to be important for fast one-trial learning of spatial memories (Kesner, Hunsaker, & Warthen, 2008; Nakashiba, Young, McHugh, Buhl, & Tonegawa, 2008; Nakazawa *et al.*, 2003) as well as recalling a memory when presented only with partial cues (Nakazawa *et al.*, 2002).

CA2, situated anatomically between CA3 and CA1 regions, is the studied region of the hippocampus studied least (Dudek, Alexander, & Farris, 2016). In part, the lack of extensive research into CA2 is due to the small size of this region and the fact that it has been difficult to define its boundaries conclusively. However, recent advances have made possible to identify and record from CA2. In terms of EC-HPC connectivity, CA2 receives inputs from both layers II and III of EC as well as from CA3 (Chevaleyre and Siegelbaum (2010); Rowland *et al.* (2013); but see Kohara *et al.* (2014)). However, while ECIII inputs to CA2 are strongly excitatory, CA3

Schaffer collaterals provide a large inhibitory drive in CA2 (Chevaleyre & Siegelbaum, 2010). CA2, in turn, sends strong excitatory projections to the deep sublayer CA1 (Chevaleyre & Siegelbaum, 2010; Kohara *et al.*, 2014), as well as to ECII (Rowland *et al.* (2013); but see Cui, Gerfen, and Young (2013)). CA2 has been shown to be important for social memory (Hitti & Siegelbaum, 2014) and proposed to provide a degraded copy of a memory to CA1 where a stable version of the same memory can be combined with the CA2 input to "timestamp" stored patterns in support of episodic memory (Mankin, Diehl, Sparks, Leutgeb, & Leutgeb, 2015). Intriguingly, in stark contrast to the CA3 where representations remain stable over long time periods, the representations of CA2 temporally evolve despite the fact that it forms recurrent connections (Okamoto & Ikegaya, 2019), although this representational instability could be due to a combination of a somewhat lower recurrence rate (1.4% versus 1-4%; (Amaral *et al.*, 1990; Bennett, Gibson, & Robinson, 1994; Guzman, Schlögl, Frotscher, & Jonas, 2016; Okamoto & Ikegaya, 2019; Rolls, 2013; Witter, 2007)), inhibitory modulation (Sun *et al.*, 2017), and/or distinct plasticity rules (Carstens & Dudek, 2019). Through its backprojections to CA3, CA2 can also regulate the overall network excitability in the hippocampus (Boehringer *et al.*, 2017).

Finally, CA1 receives excitatory inputs from ECIII with feedforward inhibition from ECII through its distal interneurons (Kitamura *et al.*, 2014; Milstein *et al.*, 2015). In addition to the EC input, CA1 receives inputs from CA3 and CA2. The major outputs of CA1 end in the deep (layers V/VI) of EC as well as the subiculum. The CA1 circuit of the hippocampus has been proposed to serve multiple functions. Levy (1989) proposed that CA1 is a predictive network that compares a "preprocessed" version of incoming information from CA3 to the direct input of EC in order to produce a predictive representation. Rolls (2010) proposes that CA1 recodes discrete memory items, the constituents of episodic memory, to generate an appropriate recall

cue to be sent to neocortex. In this way, memory consolidation, the transfer of recently acquired memories to neocortex, could occur or older memories previously stored in neocortex could be reinstated (Bosch, Jehee, Fernández, & Doeller, 2014; Goode, Tanaka, Sahay, & McHugh, 2020; Hindy, Avery, & Turk-Browne, 2019; Nyberg, McLntosh, Houle, Nilsson, & Tulving, 1996; Pacheco Estefan *et al.*, 2019; Tanaka *et al.*, 2014). Due to its relatively dense packing of pyramidal cells and anatomical position, CA1 is the most readily accessible region of the hippocampus both for electrophysiological recordings and, more recently, optical monitoring of neural activity. Consequently, CA1 is perhaps the most well-studied hippocampal network.

A synaptic theory of memory

The first refined theory on how stimuli can effect lasting cellular changes that allow the brain to store and later recall memories was articulated by Donald Hebb. Hebb proposed that the "repeated or persistent" excitation of a post-synaptic cell B by a pre-synaptic cell A results in physiological processes in at least one of the two cells that increase the efficacy of A → B communication (Hebb, 1949). This process explains "associative" or "Hebbian" learning whereby two simultaneously occurring stimuli become associated in appropriate cellular substrates in the brain such that the activation of one facilitates the activation of the other. The first experimental evidence for a cellular mechanism that could underlie this form of learning in the mammalian brain was discovered in 1973. Bliss and Lømo (1973) reported that perforant path (EC to DG input) synaptic efficiency abruptly increased following brief yet strong trains of stimuli activating the perforant path axons which was sustained for many hours. The discovery of such "long-term potentiation" (LTP) triggered a whole new field in memory research that has led to a plethora of studies identifying its detailed cellular and molecular mechanisms (Nicoll, 2017). Although both pre- and post-synaptic molecular mechanisms may be involved in the

induction and expression of LTP (Bliss & Collingridge, 1993; Nicoll & Schmitz, 2005), a preponderance of evidence favors a stronger post-synaptic role (Granger & Nicoll, 2014). A key characteristic of postsynaptic LTP is the instrumental involvement of N-methyl-D-aspartate (NMDA) receptors (Collingridge, Kehl, & McLennan, 1983).

Of direct relevance to the mechanisms of hippocampal learning and memory is psychopharmacological evidence that LTP is important in the process. Morris, Anderson, Lynch, and Baudry (1986) showed that NMDA receptor blockade with agent AP-V impairs behavioral memory performance, likely through disruption of LTP (Morris *et al.*, 1986). Later studies corroborated this view by showing that hippocampal LTP was necessary (Castro, Silbert, McNaughton, & Barnes, 1989; Moser, Krobert, Moser, & Morris, 1998) and sufficient (Tang *et al.*, 1999) for spatial navigation, and that, conversely, spatial navigation effected LTP in the hippocampus (Martin, Grimwood, & Morris, 2000; McNaughton, Barnes, Rao, Baldwin, & Rasmussen, 1986). Together, these studies identified the synapse as a very appealing locus for the encoding, retention, and recall of memories. In the field of hippocampus-dependent spatial navigation and memory, this guided future research into how hippocampal activity patterns can orchestrate synaptic changes in support of memory (Magee & Grienberger, 2020).

Place selectivity, cognitive map, and the neural basis of memory

As reviewed earlier, the episodic memory deficits observed in patient H.M. were attributable to the loss of medial temporal lobe structures, including the hippocampus. Motivated by this, and to understand how neurons in the hippocampus responded to various stimuli, in particular memory-related variables, John O’Keefe placed microelectrodes into the CA1 region of the hippocampus of rats and recorded unit spiking activity (O'Keefe & Dostrovsky, 1971).

Observing that many hippocampal units responded only when the animals were placed in specific locations within the environment, it was concluded that the hippocampus provides the rest of the brain with a spatial map useful for navigation behaviors. This was particularly interesting because of the experiments of Edward C. Tolman (Tolman, 1948) wherein he had concluded that rats learning mazes establish a map of their environment in their brain to help them find routes and environmental relationships. Hence, the spatially selective spiking of hippocampal cells gave them the moniker “place cells.” To explain this observation as well as the memory deficits of H.M., O’Keefe and Dostrovsky proposed that the hippocampus serves as a cognitive map in the brain (O'Keefe & Nadel, 1978).

Working with John O’Keefe, Richard Morris published a landmark study in which he and colleagues showed that, in rats, the hippocampus was specifically required to solve what’s now known as the Morris water maze. The Morris water maze consists of a large, circular water tank filled with opaque water (made opaque with milk or chalk) with a small platform submerged just below water level, located somewhere in the tank. Rats are placed in the water at random locations in each trial. Because rats do not like being in water, they start swimming around until they find the hidden platform and climb on it to escape. Within a few trials (< 10), rats learn the location of the hidden platform so that, unlike in the first couple of trials where they swam randomly in search of the platform, they can subsequently swim directly to the platform from any starting position. Morris, Garrud, Rawlins, and O'Keefe (1982) showed that rats with hippocampal lesions, but not cortical lesions, lost the ability to learn the location of the hidden platform by observing that these rats continued to take circuitous paths to the platform, indicating a lack of place learning and/or navigation ability.

Representation of the content of experience in the hippocampus

To represent episodic events, the brain need store not only a *where* component, but also a *what* component. Soon after the first report of spatially restricted hippocampal activity (O'Keefe & Dostrovsky, 1971), John O'Keefe was in fact the first to suggest that the hippocampus could combine location information from a landmark-independent navigation system with information regarding the content of an experience or environmental features (O'Keefe, 1976). However, this idea was a theoretical postulate and was not demonstrated experimentally. To examine how various features of a given experience are represented by the hippocampus, classically hippocampal neurons are monitored while animals explore an environment looking for experimenter-provided food. For example, (Muller & Kubie, 1987) were the first to describe the response of place cells to changes in sensory stimuli, such as the coherent rotation of place field locations with a rotation of the cue card in a cylindrical enclosure. Bostock, Muller, and Kubie (1991) reported that replacing a familiar white cue card on the wall of a cylindrical enclosure with a black cue card leads to the gradual divergence of the distribution and response intensity of place fields in the hippocampus. Hippocampal cells can also encode navigation-related variables such as direction of movement and velocity (McNaughton, Barnes, & O'Keefe, 1983). In a T-maze where rats were required to alternate between running down the left or right side of the maze to receive a food reward, spatially selective CA1 cells responded differentially on left- or right-bound trajectories in the same position (Wood, Dudchenko, Robitsek, & Eichenbaum, 2000). The first clear and conclusive evidence that the *what* and *where* of an experience can be simultaneously encoded by the hippocampus, however, came from CA3 data in rats exploring two similar but distinct environments, thereby excluding variables such as behavioral context (Wood *et al.*, 2000) or directional orientation (McNaughton *et al.*, 1983). In response to subtle

environmental changes (such as the color or shape of it), hippocampal place cells modulate the rate at which they emit spikes, thereby encoding episodic content without compromising location information represented by the place field position (Leutgeb *et al.*, 2005b). In contrast, place field positions completely reorganize in response to dramatic changes in the environment, such as moving from one experiment room to another. It is also noteworthy that because the task-specific non-spatial response of the hippocampus can override its spatial representations (Wood, Dudchenko, & Eichenbaum, 1999), the hippocampus can be thought of as a general device storing relationships between external entities (Eichenbaum & Cohen, 2014; Lisman *et al.*, 2017; Whittington *et al.*, 2020). Hippocampal cells are also known to display sustained activity in well-defined "time fields" during working memory task delays (MacDonald, Lepage, Eden, & Eichenbaum, 2011; Pastalkova, Itskov, Amarasingham, & Buzsáki, 2008), though this mode of firing does not seem to be directly involved in supporting working memory functions (Sabariego *et al.*, 2019).

Upstream of the hippocampus, both spatial and non-spatial coding is observed. The medial portion of EC contains many different types of spatially modulated cells (Sasaki, Leutgeb, & Leutgeb, 2015; Sugar & Moser, 2019). These include the famous grid cells that fire in regular hexagonal patterns that tessellate the entire environment during exploration (Hafting, Fyhn, Molden, Moser, & Moser, 2005); head direction-tuned cells with or without conjunctive tuning of other variables (Sargolini *et al.*, 2006), border cells, which are active along environmental edges (Solstad, Boccara, Kropff, Moser, & Moser, 2008); speed cells, whose firing rate is tightly related to movement speed (Kropff, Carmichael, Moser, & Moser, 2015); as well as spatially modulated cells with irregular firing patterns (Diehl, Hon, Leutgeb, & Leutgeb, 2017). MEC firing patterns, specifically those of grid cells, can rearrange their firing rate

reminiscent of hippocampal rate remapping thought to encode the content of episodic events (Diehl *et al.*, 2017; Diehl, Hon, Leutgeb, & Leutgeb, 2019). The firing patterns in the lateral portion of EC are dominated by the non-spatial variables of experience. LEC cells are strongly responsive to objects and object place relationships (Deshmukh & Knierim, 2011; Hargreaves, Rao, Lee, & Knierim, 2005).

Drifting place code for time

The early developments enumerated above gave birth to the subsequent explosion in neurophysiological research into the neural underpinnings of memory processing, lost in patients like H.M. following hippocampal damage. Consequently, many attempts were made to identify the specific role of the hippocampus in flexible navigation and/or to identify the key players required to support the building and deployment of a cognitive map. McNaughton *et al.* (1983) were the first to identify a velocity signal in the hippocampus. Later, it was shown that self-motion is required for place cell discharge Foster, Castro, and McNaughton (1989). In an important early study, (Thompson & Best, 1990) recorded the activity of hippocampal units over timescales much longer than previously examined. If the hippocampus were indeed important to store memory related representations, it was argued, its activity should remain stable in the absence of environmental change. Thompson and Best (1990) found that putative single hippocampal cells to a large extent retained their place selectivity for up to several months. An important caveat of this study, however, was that sampling of the hippocampal population was sparse both anatomically and temporally: even though some individual cells might retain stable place selectivity over a long time, at the population level, this might not be the case. Moreover, because the months-long recordings were sampled periodically (as opposed to continuously), it was not clear how dynamic the place selectivity profiles could be.

Recent advances in recording technologies have made it possible to continually monitor the activity of large ensembles of neurons from various hippocampal regions. Using tetrodes, Mankin *et al.* (2012) were the first to perform large-scale electrophysiological ensemble recordings of the same set of neurons in areas CA1 and CA3 of rat hippocampus over a period of up to 60 hours. This pivotal study demonstrated that the population level representations in CA3 are largely stable across extended time periods, but CA1 representations drift in the absence of any overt changes in the environment, the experience, or behavior of the animals. By comparing hippocampal representations across 24-h long intervals, the authors further showed that the place selective activity patterns are not under the influence of circadian rhythms. Ziv *et al.* (2013) used calcium imaging to monitor activity in very large sets (up to 1040) of CA1 neurons over weeks. They reported that ~15-25% of cells were common between, and had stable place representations across, any two sessions. These studies extended the findings of an earlier study by Manns, Howard, and Eichenbaum (2007) where the authors investigated the question of how changes in hippocampal representations may help rats perform a memory task that depended on their estimate of temporal context. It was reported that a greater change in representations for temporally distant contexts and a lesser change in temporally proximal ones correlated with better behavioral performance (Manns *et al.*, 2007).

The findings of Mankin *et al.* (2012) suggested that an important ingredient of episodic memories, namely the *when*, may in fact be encoded by the hippocampus. In principle, a time-varying and a time-constant representation of the same event can be compared to estimate elapsed time since the occurrence of the event, as suggested by previous computational studies (Estes, 1955; Howard & Kahana, 2002; Mensink & Raaijmakers, 1989). To further investigate this hypothesis, Mankin *et al.* (2015) recorded from large ensembles of all three hippocampal

regions CA1, CA2, and CA3, over extended time periods and in two spatial contexts while rats randomly foraged for food. Representations in CA2 evolved almost exclusively in response to elapsed time, but not to a change in context (Mankin *et al.*, 2015). In contrast, and as expected (Mankin *et al.*, 2012), CA1 representations changed to a moderate degree in response to both elapsed time and different contexts. CA3 representations remained largely stable across time, but responded strongly to contextual differences. In view of prior computational work on the representation of time of episodic memories, these results were reminiscent of the circuitry of the hippocampus with CA3 and CA2 fields projecting to CA1 where a stable representation of the same context (CA3 input) can be compared to and combined with a time-varying representation of the environment (CA2 input) to "timestamp" episodic memories and thus estimate elapsed time. Similar ideas were explored by Rubin, Geva, Sheintuch, and Ziv (2015) using calcium imaging in CA1. While the Mankin et al. study had the obvious advantage that all hippocampal subregions, including the areas inaccessible to imaging techniques, were sampled, Rubin et al. characterized the dynamics of the CA1 code over even longer time periods. It was shown that the CA1 code possesses a global aspect that changes gradually across days irrespective of the particular behavioral context, and that it may be used to computationally estimate the time at which a representation was recorded (Rubin *et al.*, 2015).

The above studies together suggest that representational drift might be a *bona fide* signal in the hippocampal code. In fact, representational drift has been reported in other brain areas (Driscoll, Pettit, Minderer, Chettih, & Harvey, 2017; Gallego *et al.*, 2018; Rokni, Richardson, Bizzi, & Seung, 2007) and suggested to serve specific computational functions (Rule, O'Leary, & Harvey, 2019). This view raises the question of what aspects of the code remain invariant with respect to a given behaviorally relevant variable, such as the geometry of the environment or

reward-place contingencies (Clopath, Bonhoeffer, Hübener, & Rose, 2017). This view will be referred to as the "reorganization theory" in this thesis. On the other hand, studies to uncover the physical locus of stored memories in the brain (Tonegawa, Liu, Ramirez, & Redondo, 2015) suggest that, at least in the memory system, the reactivation of the same ensemble of cells active at the time of memory acquisition is tantamount to the recall of the stored set of stimuli (Josselyn & Tonegawa, 2020). This view will be referred to as the "engram theory" in this thesis. Thus, it is unclear how the two hypotheses – the engram theory, where reactivation of an ensemble of neurons with a stable identity leads to memory retrieval, and the reorganization theory whereby representational drift is a feature of the distributed code, perhaps useful to encode time – can be reconciled.

Of note, in the studies where representational drift was reported in the hippocampus (Mankin *et al.*, 2015; Mankin *et al.*, 2012; Rubin *et al.*, 2015; Ziv *et al.*, 2013), the subjects were not actively engaged in a memory task. Since memory demand and/or attentional process can enhance coding fidelity in the hippocampus (Muzzio *et al.*, 2009), the representational drift in the hippocampus over extended time periods may be explained by task conditions. Furthermore, the engram theory arises mainly from studies of a particular memory process known as contextual fear conditioning (CFC), typically with genetic cell tagging and optogenetic reactivation methods as tools to study encoding and retrieval. If the mode of memory circuit engagement in CFC differs systematically from that in spatial memory and navigation tasks, the theories may not be at odds after all. Moreover, if the characteristics of the tools used to probe the brain elicit non-physiological operation modes, it would not be surprising to observe that the reactivation of the same cells in the hippocampus would lead to the behaviorally measured retrieval of contextual fear memories. For instance, in a mouse model of Alzheimer's disease

unable to retrieve specific memories with natural recall cues, the optogenetic reactivation of a memory engram leads to the behavioral expression of the memory (Roy *et al.*, 2016). Thus, the overexpression of activity in memory-related brain circuits by optogenetics might override the reorganization expected from a naturally drifting code as posited by the reorganization theory. Together, these arguments necessitate further investigation to tease apart the memory-related factors enumerated above and to clarify the distinctions between the reorganization and engram theories.

What determines the allocation of memory traces to specific neurons?

For over a century, *where* in the brain memories are stored has remained an enigma (Josselyn, Köhler, & Frankland, 2017; Schacter, Eich, & Tulving, 1978). Lashley famously carried out experiments with rats to identify a specific locus for memory to no avail. He trained rats to learn mazes and tested them after lesioning various areas of the cortex and found that memory deficits correlated with the total amount of lost cortical tissue rather than lesions to specific cortical areas (Lashley, 1950). Studies of patient H.M. (Scoville & Milner, 1957) brought us closer the anatomical structure housing episodic memories, but a cellular and molecular understanding seemed out of reach without the appropriate tools. Recently, with the advent of advanced genetic engineering methods our understanding of this matter has greatly advanced (Josselyn & Tonegawa, 2020). Like other cells in the body, neurons are complex factories. Neural activity, primarily characterized by the generation of action potential spikes, can trigger cascades of subcellular events that regular homeostasis and the future responses of the cell to incoming stimuli. One of the most interesting such subcellular events is the expression of immediate early genes (IEGs). IEGs were discovered in the context of cell signaling of mitogenic stimuli in cancer research (Kelly, Cochran, Stiles, & Leder, 1983), and were found to

be expressed in response to diverse forms of stimuli including neurotrophic factors (Kelly *et al.*, 1983), and cholinergic agonists by depolarization via voltage-dependent calcium channels of adrenal gland-derived cells (Greenberg, Ziff, & Greene, 1986; Morgan & Curran, 1986). IEG expression in the brain was first discovered when the convulsant Metrazole was administered to neurons to study Metrazole-induced epileptic seizures (Morgan, Cohen, Hempstead, & Curran, 1987). Taking advantage of the relationship between neural activation and IEG expression (Morgan & Curran, 1989), Guzowski, McNaughton, Barnes, and Worley (1999) used microscopy together with ensemble neurophysiological recordings to show that CA1 cells expressing the immediate-early gene Arc can be identified as having been active when rats visited different environments. Building on these tools, Reijmers, Perkins, Matsuo, and Mayford (2007) genetically tagged c-fos-active neurons of basolateral amygdala to show that during recall the same neurons active at encoding were reactivated, resulting in the behavioral expression of fear memories. Interestingly, the artificial reactivation of tagged neurons with optogenetics is sufficient to elicit a behavioral fear response (Liu *et al.*, 2012). For the first time, a cellular substrate was hence identified as the physical locus of a memory.

What determines which neurons are recruited to encode a memory under natural conditions? Direct synaptic input cannot explain this because even though a large fraction of neurons in a brain region might be involved in receiving and locally processing the same input, only a small proportion of the neurons in that area will acquire the memory (Repa *et al.*, 2001). On the other hand, the neuronal expression level of cAMP response element-binding protein (CREB) correlates with the probability of the involvement of a neuron in representing a memory (Han *et al.*, 2007), while its artificial overexpression and inhibition can bias or preclude the neurons to be recruited to the engram (Yiu *et al.*, 2014; Zhou *et al.*, 2009). CREB overexpression

also increases the propensity of a neuron for synaptic plasticity and helps the consolidation process (Zhou *et al.*, 2009). However, as CREB is involved in a multitude of cellular processes, these results per se do not imply a causal role for it in memory allocation. Because CREB regulates excitability (Zhou *et al.*, 2009), an influential theory (Rogerson *et al.*, 2014; Silva, Zhou, Rogerson, Shobe, & Balaji, 2009) proposed neuronal excitability as an attractive variable determining memory allocation because it elegantly explains memory allocation. The idea that intrinsic excitability regulates neuronal selectivity is also corroborated by intracellular recordings and manipulations in the hippocampus. Place cells in a novel environment have higher excitability than silent cells (Epsztein, Brecht, & Lee, 2011); conversely, when silent CA1 cells are made more excitable by current injection, they form new place fields (Lee, Lin, & Lee, 2012). Examination of the expression of place fields across multiple environment and experimental conditions demonstrated that CA1 cells have an intrinsic "propensity" that dictates spatial selectivity (Lee, Briguglio, Cohen, Romani, & Lee, 2020). Importantly, propensity was shown to be determined by cell excitability through intracellular recordings (Lee *et al.*, 2020). Within the neuronal population, intrinsic excitability naturally fluctuates such that different subsets of neurons become more or less likely to participate in memory representations (Cai *et al.*, 2016). Such fluctuations in excitability segregate ensembles for different memories in time which can be used to encode their temporal continuity (Cai *et al.*, 2016). Lastly, after acquisition, excitability significantly influences neuronal reactivation during subsequent sleep (Mizunuma *et al.*, 2014), presumably for further potentiation and consolidation (van de Ven, Trouche, McNamara, Allen, & Dupret, 2016).

Aside from excitability, reward signals can modulate the expression of place selectivity in the hippocampus. Reward information is directly represented in the hippocampus (Gauthier &

Tank, 2018), but non-reward cells also tend to cluster their place fields near reward (Dupret, O'Neill, Pleydell-Bouverie, & Csicsvari, 2010) or behaviorally relevant locations (Hok *et al.*, 2007; Hollup, Molden, Donnett, Moser, & Moser, 2001). Direct photostimulation of dopaminergic inputs from ventral tegmental area (Mamad *et al.*, 2017; McNamara, Tejero-Cantero, Trouche, Campo-Urriza, & Dupret, 2014) and locus coeruleus (Takeuchi *et al.*, 2016), both dopaminergic hubs (Kempadoo, Mosharov, Choi, Sulzer, & Kandel, 2016), to hippocampal neurons at specific locations on a maze enhances and stabilizes the place memory and representations of that location (Mamad *et al.*, 2017; McNamara *et al.*, 2014). The contribution of locus coeruleus (Takeuchi *et al.*, 2016) could, however, be mediate through pronounced arousal during memory performance (Breton-Provencher & Sur, 2019). In addition, attention (Kentros, Agnihotri, Streater, Hawkins, & Kandel, 2004; Muzzio *et al.*, 2009) and novelty detection (Fyhn, Molden, Hollup, Moser, & Moser, 2002) mechanisms can also enhance place field expression and stability in the rodent hippocampus.

Oscillations, brain states, and the two-stage model of memory

The various cellular processes in the brain – including the ionic fluxes, synaptic currents, action potentials, and calcium spikes – produce voltage differentials with respect to a reference point (Buzsáki, Anastassiou, & Koch, 2012). The electric fields resulting from such voltage differentials can be measured with electrodes placed in the extracellular space. Depending on the spatial organization of the sources and the degree of their temporal synchronization, voltage differentials can manifest as oscillations in the local field potentials (LFPs). Such regular rhythmic activity constitutes an important mode of information processing in addition to neuronal spiking (Arnal & Giraud, 2012; Buzsáki, 2006; Sejnowski & Paulsen, 2006). Brain oscillations have been implicated in such functions as sparsening of the neural code (Perez-Orive

et al., 2002), facilitating interareal communication (Colgin *et al.*, 2009; Womelsdorf *et al.*, 2007), attentional processes (Taylor, Mandon, Freiwald, & Kreiter, 2005; Womelsdorf *et al.*, 2007), sensory perception (Gray & Singer, 1989), cognitive control (Helfrich & Knight, 2016), and even consciousness (Vesuna *et al.*, 2020). In the hippocampus, different oscillation frequencies are associated with different behavioral and cognitive functions (Buzsáki, 2006; Buzsáki, Lai-Wo S, & Vanderwolf, 1983; Colgin, 2016; Leung, Da Silva, & Wadman, 1982; Vanderwolf, 1969).

The most prominent oscillatory band in the hippocampus LFP is the 6-10 Hz rhythm, termed "theta," named so after "thalamus" (Niedermeyer, 1999; Walter & Dovey, 1944) because early studies of thalamic lesions shifted the oscillation frequency of the alpha band (8-12 Hz in primates) lower to a new band (Kennard, 1943). Theta oscillations are observed throughout the hippocampus during rapid eye movement (REM) sleep and wakefulness, specifically during locomotion, and attentive and voluntary behaviors (Vanderwolf, 1969; Whishaw & Vanderwolf, 1973). Theta is thought to originate through a combination of cellular and circuit interactions between subcortical, entorhinal and local inhibitory networks in the hippocampus (Buzsáki *et al.*, 1983; Buzsáki & Moser, 2013; Colgin, 2013; Colgin, 2016). In the upstream EC, theta is selectively expressed in the medial portion of the entorhinal cortex (Deshmukh, Yoganarasimha, Voicu, & Knierim, 2010). Higher frequency gamma oscillations (30-120 Hz) occur during both wakefulness and sleep in local neuronal processing (Colgin, 2016; Colgin *et al.*, 2009), and have been proposed to support encoding of current sensory information in memory tasks (Colgin, 2016), information routing (Colgin *et al.*, 2009), memory retrieval (Shirvalkar, Rapp, & Shapiro, 2010), and working memory (Sasaki *et al.*, 2018; Yamamoto, Suh, Takeuchi, & Tonegawa, 2014). The third prominent set of LFP oscillations is observed in the fast 150-250 Hz band,

which is termed the ripple band oscillations or ripples for short. Ripples are a prominent oscillation in the CA1 pyramidal cell layer (Buzsáki, 2015) and CA3 (Sasaki *et al.*, 2018), and temporally coincide with sharp-wave events initiated in CA3 (Buzsáki, 1986). The co-occurrence of sharp wave and ripple oscillations has given rise to the term sharp wave-ripple (SWR; Ylinen *et al.* (1995)). SWRs occur primarily in quiescent wakefulness and non-REM sleep (Buzsáki, 2015) and can be triggered by distinct mechanisms in CA2 (Okamoto & Ikegaya, 2019; Oliva, Fernández-Ruiz, Buzsáki, & Berényi, 2016) or CA3 (Buzsáki, 1986, 2015; Ylinen *et al.*, 1995). Hippocampal SWRs can affect cortical targets (Chrobak & Buzsáki, 1994).

Animal behavior can be viewed as a two-stage process: preparatory (i.e., exploratory or goal-directed) and consummatory (i.e., immobility, sleep). Coincidentally, the theta and ripple band oscillations occur predominantly during preparatory and consummatory behaviors, respectively (Buzsáki, 2015). Accordingly, two prominent "brain states" can be characterized by the mode of oscillatory voltage fluctuations in the rodent. By "default," namely when the extrahippocampal inputs are severed, the hippocampus constantly generates sharp wave events (Buzsáki *et al.*, 1983). When the extrahippocampal inputs dominate, however, such as during locomotion, the hippocampus switches to a different oscillatory regime where theta is most prominent (Buzsáki *et al.*, 1983). With the memory deficit profile of H.M. in mind (Scoville & Milner, 1957), Buzsáki (1989) synthesized his physiological findings in the study of hippocampal oscillations to propose a "two-stage" model of memory encoding and consolidation. If the hippocampus is required for the rapid acquisition of memories, the naturally occurring physiological signatures would be good candidates with which to support this function. Accordingly, during learning in the preparatory theta brain state neocortical input imprints a temporary trace of experience in the hippocampal network. This constitutes the first stage of

memory consolidation. In the second stage, which unfolds during the consummatory brain state, the newly formed hippocampal memory trace is transferred to neocortex through the re-expression of activity and potentiation of appropriate synapses during the abundant SWRs (Vyazovskiy, Cirelli, Pfister-Genskow, Faraguna, & Tononi, 2008). A feature of this system would be that it supports one-shot learning (a fundamental feature of episodic memory) because it can quickly acquire information and repeatedly try to incorporate it into the knowledge reservoir through ample "offline" repetitions.

From a purely computational perspective, Marr (1971) was the first to propose that memory consolidation can happen if the hippocampus acquires everyday memories and plays them back to the neocortex so that it can store them long-term as well as extract categories and abstractions from this data. Pavlides and Winson (1989) were the first to examine neuronal spiking activity in post-experience sleep, and found that hippocampal neurons' spiking became more prominent if the same neurons became activated during exploration immediately preceding the sleep. Wilson and McNaughton (1994) explored a similar idea by simultaneously recording large numbers of CA1 neurons and showed that CA1 neuronal correlations were strongly reactivated in post-experience sleep, suggesting that the spike content of SWR was determined by learning and was not random. A landmark computational study by McClelland, McNaughton, and O'Reilly (1995) further corroborated computational basis of the idea that the hippocampus is a fast-learner and the neocortex a slow one. This study was motivated by the observations that hippocampal damage produces temporally graded retrograde amnesia (i.e., amnesia that is most severe for the most recent memories and less severe for more remote ones; Kim and Fanselow (1992); Scoville and Milner (1957); Squire (1992); Zola-Morgan and Squire (1990)) and provided an account of why this must be the case: that shared structure of events and experiences

can be learned in a gradual and interleaved manner by neocortex while minimizing catastrophic interference among learned materials. In this scheme, the hippocampus acts as a temporary storage of newly acquired information so that this information does not interfere with established neocortical knowledge or memories. Furthermore, this "consolidation" process is temporally extended to allow the system to extract shared structure by interleaving new learning with exposure to exemplars of existing knowledge (Káli & Dayan, 2004; McClelland *et al.*, 1995). The synchrony between various neurophysiological signatures of memory processing across the hippocampus and neocortex lends further support to these ideas. SWRs and neocortical spindles (transient 7-14 Hz oscillations linked to memory functions; Peyrache and Seibt (2020)) act in a coordinated way (Peyrache, Battaglia, & Destexhe, 2011; Siapas & Wilson, 1998), while SWRs coincide with cortical down-state to up-state transitions (Battaglia, Sutherland, & McNaughton, 2004). Together, these theoretical, computational, and experimental data and ideas lay the groundwork for the future exploration of memory encoding and consolidation processes.

In the last two decades, studies of hippocampal reactivation during SWRs have focused on three avenues. First, improvement in recording technology has allowed an increase in the number of simultaneously recorded neurons and thus detailed characterization of the reactivation events themselves, plus the conditions under which they occur. Second, the mechanisms of neuronal reactivation and its physiological effects on the network have been investigated. Third, the relation between offline reactivation and various behavioral variables and mnemonic processes have been further elucidated. These results are reviewed next.

Replay: properties, mechanisms, and role in memory

The computational and theoretical studies reviewed above suggest that everyday experiences may be recapitulated by neural activity during sleep. Intuitively, we also know that dreaming in sleep sometimes matches previous experiences. Motivated by this, Pavlides and Winson (1989) showed, for the first time, that single hippocampal neurons that were active during a given experience were more likely to be active in the subsequent REM sleep compared to those neurons that did not spike in behavior. Later, comparison of sequential neuronal spiking during pre- and post-experience sleep revealed that the patterns of post-experience spiking reflect the order in which the neurons fired during exploration (Skaggs & McNaughton, 1996). This experience-dependent ordering and re-expression of neuronal pairs became known as "replay," but it was not until later that with improved recording and statistical methods large-scale sequences of neuronal reactivation were confirmed in REM (Louie & Wilson, 2001) and non-REM, slow-wave sleep (SWS) (Lee & Wilson, 2002; Nádasdy, Hirase, Czurkó, Csicsvari, & Buzsáki, 1999).

Studying hippocampal activity patterns during sleep before and after experience allows one to segregate the role of memory-related and sensory-related changes in the brain. A common feature of replay events is that they coincide with hippocampal sharp-wave ripples (Kudrimoti, Barnes, & McNaughton, 1999; Lee & Wilson, 2002; Nádasdy *et al.*, 1999). SWRs and the associated burst of spiking in hippocampal neurons influence cortical activity and induce synaptic changes (Buzsáki, 1986; Chrobak & Buzsáki, 1994; Sadowski, Jones, & Mellor, 2016; Ylinen *et al.*, 1995), which is consistent with a role for replay in transferring acquired memories to neocortex (Buzsáki, 1989). This idea is further supported by the fact that hippocampal reactivation was strongest following a novel experience (Cheng & Frank, 2008; Kudrimoti *et al.*, 1999). However, because sharp-wave ripples also occur during quite wakefulness, a natural

question is whether replay occurs in conjunction with ongoing behavior. Recordings from large ensembles of CA1 neurons showed that replay does in fact occur when rats were consuming a reward at either end of a linear track where they ran back and forth (Foster & Wilson, 2006). Intriguingly, the sequence of place field reactivation that the rats experienced while running from one end to the other end of the track replayed in reverse order: the most recently traversed place fields fired first in the sequence, while the place fields traversed first on a track journey fired last in the sequence. Theories of reinforcement learning suggested a role for such reverse replay in evaluating the value of recent experience (Foster & Wilson, 2006). As such, reverse replay would provide a mechanism for the hippocampus to relate the reward information available at the end of a trajectory to the sequence of spatial locations that led the rat to its current position. In fact, when outcomes are rewarded, replay becomes more prevalent and robust (Singer & Frank, 2009), supported by the dopaminergic system (McNamara *et al.*, 2014).

The idea that awake replay may have a role in the online evaluation of sequences was further supported by the observation that sequences play out in forward order in anticipation of upcoming trajectories (Diba & Buzsáki, 2007). When rats are performing a two-alternative spatial working memory task, hippocampal sequences were shown to alternate between depicting one or the other of the possible choices (Johnson & Redish, 2007) in a manner dependent on prior experience (Jackson, Johnson, & Redish, 2006; O'Neill, Senior, Allen, Huxter, & Csicsvari, 2008; Singer, Karlsson, Nathe, Carr, & Frank, 2010). The prevalence and quality of replay in a spatial working memory task was shown to be related to correct choices (Singer, Carr, Karlsson, & Frank, 2013). Replay was also shown to extend to spatial locations far from the animal's current location within the same environment (Davidson, Kloosterman, & Wilson, 2009), or a different environment (Gupta, van der Meer, Touretzky, & Redish, 2010; Karlsson & Frank,

2009). The role of awake replay in online choice evaluation is also supported by the stronger hippocampal-prefrontal interactions during wakefulness compared to sleep (Shin, Tang, & Jadhav, 2019; Tang & Jadhav, 2019).

To establish a causal link between replay and memory, multiple strategies have been employed. Because replay is associated with the incidence of SWRs, closed-loop detection and disrupting SWRs during sleep and wakeful behavior has been used as a relatively straightforward way to inhibit replay and study its effects on learning and memory. SWRs disruption by electrical stimulation during sleep and (Girardeau, Benchenane, Wiener, Buzsáki, & Zugaro, 2009) awake behavior (Jadhav, Kemere, German, & Frank, 2012) impairs subsequent or ongoing spatial memory performance. Disruption of SWR-associated spiking impaired the development and stabilization of representations for new goal locations (Roux, Hu, Eichler, Stark, & Buzsáki, 2017) or a novel environment (van de Ven *et al.*, 2016). Conversely, selective artificial stimulation of the medial forebrain bundle, a carrier of reward information, during the reactivation of specific place cells in SWR biases exploration behavior toward the place fields of the artificially conditioned cells (de Lavilléon, Lacroix, Rondi-Reig, & Benchenane, 2015). Furthermore, direct recordings of hippocampal and neocortical activity shows functionally relevant communication between the two systems during sharp-wave ripples (Khodagholy, Gelinas, & Buzsáki, 2017; Maingret, Girardeau, Todorova, Goutierre, & Zugaro, 2016). Gridchyn, Schoenenberger, O'Neill, and Csicsvari (2020) trained rats to locate goal locations in two separate environments and disrupted reactivated neuronal spiking in subsequent sleep for one of the two environments. This clever experimental design allowed the authors to harness the environment-specific firing selectivity of hippocampal cells to simplify the online replay decoding processes. Memory performance was impaired only in the environment whose

associated replay events were selectively interfered with (Gridchyn *et al.*, 2020). More sophisticated online decoding methods have also been used to show a role for awake replay in memory task performance (Ciliberti, Michon, & Kloosterman, 2018). Computational modeling (Káli & Dayan, 2004) and experimental data (Rasch & Born, 2007) both support the idea that replay helps the brain maintain memories in the face of representational changes (Mankin *et al.*, 2015; Mankin *et al.*, 2012; Rule *et al.*, 2019).

As pointed out in some of the literature reviewed above, conventional experimental protocols have shown, by comparing pre- and post-experience sequential reactivation, that experience can produce changes in the patterns of population burst during SWRs. There are two modes of learning-related changes can be distinguished in such protocols. In studies where a novel environment is experience by animals, the experience of novelty itself has been shown to promote reactivation patterns in subsequent rest (Cheng & Frank, 2008). This can reflect the encoding of information about the color, geometry, scale or other factor determined by the environment. On the other hand, because animals are typically kept in home cages where neuronal activity is minimal (Chawla *et al.*, 2005), reactivation after the only notable experience of the animals on a given day might be the driver of the heightened excitability in the hippocampus. Thus, there are at least two factors that are intermingled in the conventional setting. Complementary to this, if environment-, novelty- and experience-specific factors are held constant, flexible learning of new goal locations on each day may drive reactivation in a different manner than tested using conventional paradigms. Another aspect of post-experience dynamics that remains unknown is for how long and with what fidelity reactivation dynamics continue to unfold after initial learning. Previous studies have monitored this activity for only short (~30 min) periods. If the animals are required to remember information for many hours to

guide their future behavior, one might expect to see dynamic changes in neural activity for the duration of sleep periods in between learning and testing. Further, the animals in these studies rested in the same location as the learning and testing took place, perhaps biasing the content of replay. Finally, it is unclear whether different neuronal subpopulations participate in reactivation to the same extent and whether these dynamics change if learned information must be retained for future memory testing.

Role of theta in plasticity and orchestrating sequential activity for the rapid encoding of episodic memory for later replay

So far, we have discussed the role of offline reactivation in promoting the long-term storage of recently acquired memories. Here we review the evidence for how plasticity is regulated during acquisition, specifically by theta oscillations marking preparatory brain states. Among many functions attributed to theta oscillations (Colgin, 2013), two features are of particular interest. First, theta has been shown to play a role in the regulation of neural plasticity. Following initial suggestions that stimulation patterns at theta-like intervals can enhance plasticity (Larson, Wong, & Lynch, 1986), Huerta and Lisman (1993) elicited theta oscillations in LFPs by activating septal cholinergic cells and showed that theta regulated neural plasticity in a phase-dependent manner. Huerta and Lisman (1995) showed that the synaptic strength of CA1 cells can be efficiently enhanced or reduced by single bursts resembling those occurring *in vivo* if delivered at specific phases of theta oscillations. Thus, in principle, the hippocampus networks can exploit these properties to optimize memory functions.

The second intriguing feature of theta is its relationship to the spiking of individual hippocampal neurons. As a rat moves about the environment, place cells become active in their

spatial receptive fields and quiet down after the animal leaves the place field of each cell. At the same time, theta oscillations occur robustly while the animal is running. In general, by virtue of their generation mechanism (Colgin, 2013) the peak and trough phases of theta oscillations reflect the trough and peak of the collective firing rate of the population, respectively. This means that any given place cell is more likely to emit spikes while theta is at its trough. Within its place field a cell will fire over multiple theta cycles for as long as the animal is physically in the field. However, as an animal runs through the field from one side to the other, its spiking follows a precise relationship to the theta cycle: spikes emitted early in the field (near the entry point) will be more likely to occur at the end of the theta cycle, whereas spikes emitted late in the field (near the exit point) will be more likely to occur at the early phase of the theta cycle. In between the entry and exit from the place field, the spikes follow a roughly linear relationship with theta phase. In brief, the theta phase of spikes appear to advance to earlier and earlier part of the cycle as the animal progresses further and further into the field until exit. This phenomenon is referred to as "theta phase precession," first reported by O'Keefe and Recce (1993). Phase precession is observed throughout the hippocampus (Skaggs, McNaughton, Wilson, & Barnes, 1996), and is known to provide additional spatial information alongside firing rate (Harris *et al.*, 2002; Huxter, Burgess, & O'Keefe, 2003; Skaggs *et al.*, 1996).

Assuming each hippocampal cell is exhibiting phase precession while the animal is running, the spikes from a few cells with a series of partially overlapping place fields will be organized in the theta cycle to reflect the order in which they are traversed. Theta-nested sequences thus organized are called hippocampal "theta sequences" (Dragoi & Buzsáki, 2006; Foster & Wilson, 2007). It should be noted that while the phase precession and theta sequence phenomena seem to be tightly intertwined, they need not be mutually interdependent. For

example, random variations in the preferred phase of individual cell spiking over successive theta cycles can in principle scramble the order of spikes while preserving the precession effect (Feng, Silva, & Foster, 2015; Foster & Wilson, 2007; Middleton & McHugh, 2016). On the contrary, cells can maintain a tight spike ordering without reducing their average theta phase over the course of a place field traversal. At any rate, phase precession can in theory act as the organizing mechanism for the formation of theta sequences. The potential physiological significance of theta sequence formation is underscored by the fact that the behaviorally relevant time course of place cell spiking during exploration (a few seconds) can be effectively compressed to less than about 125 ms and repeated several times during a multi-field trajectory. This can facilitate neural plasticity via spike timing-dependent plasticity (STDP; Bi and Poo (1998); Feldman (2012); Markram, Lübke, Frotscher, and Sakmann (1997); Mishra, Kim, Guzman, and Jonas (2016)) to rapidly encode episodic events experienced only once (Dragoi, Harris, & Buzsáki, 2003; Skaggs *et al.*, 1996). In addition, theta phase precession and theta sequences can provide a mechanism for quick evaluation of possible decisions via hippocampal-cortical communication (Jones & Wilson, 2005; Schmidt, Duin, & Redish, 2019; Wikenheiser & Redish, 2015).

Theoretical interpretations of phase precession generally postulate a role for prediction or cued recall of upcoming sequences (Jaramillo & Kempter, 2017; Jensen & Lisman, 1996; Lisman & Redish, 2009; Lisman, Talamini, & Raffone, 2005; Maurer & McNaughton, 2007; Sanders, Rennó-Costa, Idiart, & Lisman, 2015). Hippocampal networks evolve through a combination of internal dynamics and external influences (Buzsáki & Tingley, 2018; Czurkó, Hirase, Csicsvari, & Buzsáki, 1999; Pastalkova *et al.*, 2008; Wang, Romani, Lustig, Leonardo, & Pastalkova, 2015). Accordingly, the theta cycle can be said to orchestrate neural computations

(Buzsáki, 2006) in terms of internally- and externally dominated dynamics (Lisman & Redish, 2009; Lisman *et al.*, 2005; Maurer & McNaughton, 2007; Sanders *et al.*, 2015). Although phase precession is not observed when rats run in a running wheel without a memory task (Hirase, Czurkó, Csicsvari, & Buzsáki, 1999), if the running wheel is used as a delay period in the context of a spatial working memory task, hippocampal cells show phase precession that gives rise to theta sequences depicting the future decision of the rat (Pastalkova *et al.*, 2008). Moreover, when rats are trained to jump in anticipation of a foot shock, hippocampal cells show location-independent phase precession whose temporal profile is consistent with the interpretation that the phase advancement of spikes is a predictive signal (Lenck-Santini, Fenton, & Muller, 2008). Thus, during phase precession spike phase appears to follow two stages across its place field: a "predictive" phase precession, along with a phase cluster representing the "true" place field (Sanders *et al.*, 2015; Yamaguchi, Aota, McNaughton, & Lipa, 2002).

On the population level, statistical mapping of the identity of multiple cells of a theta sequence to external position (i.e., neural decoding) uncovers paths at the current location, behind, or ahead of the animal at early, mid, and late theta phases (Gupta, van der Meer, Touretzky, & Redish, 2012; Johnson & Redish, 2007; Wang, Foster, & Pfeiffer, 2020). The neural coding properties, information processing delays, and theoretical considerations regarding the architecture of DG and CA3 suggest that their mutual interaction may be important for encoding, and by extension, for phase precession (Jerman *et al.*, 2006; Lisman *et al.*, 2005). Accordingly, DG circuit can relay an incoming item to CA3 to cue the recall of the rest of the sequence. However, an error correction mechanism would be necessary to ensure the errors at each step in recalling the sequence do not accumulate to a catastrophic degree. This error correction mechanism is proposed to be accomplished by the reciprocal DG-CA3 connections

(Lisman, 1999; Lisman *et al.*, 2005). The DG-CA3 interactions then provide the look-ahead signal late in the cycle, while the representation of current location can be triggered by EC input (Sanders *et al.*, 2015). This model provides an explanation for the modulation of plasticity by theta oscillations (Huerta & Lisman, 1993) by positing segregated encoding and retrieval on a fast timescale. During learning, the spikes from cells with overlapping place representations can be encoded in a well-organized sequence late in the theta cycle, and later reactivation in offline brain states to further potentiate the appropriate connections (Redish & Touretzky, 1998). At the same time, previously stored associations can be recalled early in the cycle to guide navigation (Redish & Touretzky, 1998; Sanders *et al.*, 2015).

These theoretical considerations implicate the segregation of different inputs in the theta cycle as a beneficial coding scheme. Indeed, hippocampal circuits can also organize their timing to maximize activity, and perhaps optimize plastic circuit changes, in circumscribed portions of the theta cycle (Mizuseki, Sirota, Pastalkova, & Buzsáki, 2009; Robbe *et al.*, 2006). Extrahippocampal inputs perhaps play a major role in supporting this theta cycle-specific organization because brief electrical stimulation does not disrupt the spike theta phase predicted by the normal progression of phase precession (Zugaro, Monconduit, & Buzsáki, 2005). In the absence of MEC, hippocampal phase precession is greatly, but not entirely, abolished (Schlesiger *et al.*, 2015). The remaining precession can in principle be supported in part by LEC inputs. In support of this hypothesis, during an object recognition task (Robinson *et al.*, 2017), phase precession is not impaired by MEC inaction in object responsive CA1 cells, which may receive maximal input from LEC (Deshmukh & Knierim, 2011; Hargreaves *et al.*, 2005). What's more, consideration of other oscillatory components in the neural activity further supports this notion. Gamma oscillations are typically considered to consist of two distinct sub-bands (Colgin, 2016):

slow (25-55 Hz) and fast (60-100 Hz). In the hippocampus, fast gamma oscillations reflect an increase in input originating from EC (Colgin *et al.*, 2009; Mizuseki *et al.*, 2009; Pernía-Andrade & Jonas, 2014; Schomburg *et al.*, 2014). In contrast, slow gamma corresponds to local input in the hippocampus (Bragin *et al.*, 1995; Colgin *et al.*, 2009; Csicsvari, Jamieson, Wise, & Buzsáki, 2003; Kemere, Carr, Karlsson, & Frank, 2013). For example, in the CA3 circuit, slow gamma is likely inherited from DG (Hsiao, Zheng, & Colgin, 2016). When slow gamma is present, place cell spiking mainly occurs in the first half of the place field (Bieri, Bobbitt, & Colgin, 2014). Furthermore, spike phase relationships as well as current source density analyses suggest that EC input dominates during the second half of place field passage (Bieri *et al.*, 2014; Mizuseki *et al.*, 2009; Schomburg *et al.*, 2014). This view is consistent with the results of cell type specific manipulations which led to selective disruption of spiking in the first and second halves of place fields (Royer *et al.* (2012); but see Fernández-Ruiz *et al.* (2017) who suggest the opposite).

The idea that phase precession and theta sequence mechanisms can prime the appropriate synapses for further potentiation has received empirical support. Experiments investigating the relationship between theta state firing and subsequent replay reveal that co-firing strength in behavior is predictive of subsequent replay quality (O'Neill *et al.*, 2008). After performing a memory task, but not after random foraging, interference with the incidence of SWRs, and presumably replay, led to an NMDA-receptor dependent compensatory increase in the incidence rate of SWRs (Girardeau, Cei, & Zugaro, 2014), suggesting temporary changes during learning primed the hippocampal network for further potentiation during SWR-associated firing. Phase precession can be reduced without affecting place selective firing if rats are passively transported across the place fields of multiple cells (Cei, Girardeau, Drieu, Kanbi, & Zugaro, 2014). Exploiting this, Drieu, Todorova, and Zugaro (2018) showed that post-experience replay was

impaired without phase precession and theta sequences, suggesting a link between theta-modulated firing in preparatory brain states and SWR-associated synaptic modifications in ensuing consummatory brain states. Studies of hippocampal spiking during post-natal development demonstrate that experience dependent replay of sequence established during navigation emerge in concert with theta sequences (Farooq, Sibille, Liu, & Dragoi, 2019; Muessig, Lasek, Varsavsky, Cacucci, & Wills, 2019), but after phase precession has developed (Langston *et al.*, 2010). Extrahippocampal input from the MEC is also required to flexibly form replay sequences (Chenani *et al.*, 2019). These studies demonstrate the coordinated interplay between theta- and SWR-associated sequential activity in service of learning and memory.

Despite this wealth of knowledge, the mechanisms of phase precession are not well-understood. Although these data together with computational modeling (Chance, 2012; Thurley, Leibold, Gundlfinger, Schmitz, & Kempter, 2008) suggest that it is possible that phase precession requires the interaction of two theta-modulated excitatory inputs, this hypothesis has not been directly investigated when hippocampal circuits are engaged in supporting ongoing memory-guided behavior. Other computational models of phase precession have mostly focused on network interactions (Losonczy, Zemelman, Vaziri, & Magee, 2010; Romani & Tsodyks, 2015; Tsodyks, Skaggs, Sejnowski, & McNaughton, 1996; Wallenstein & Hasselmo, 1997) or cellular mechanisms (Harvey, Collman, Dombeck, & Tank, 2009; Magee, 2001). Inhibitory interneurons can contribute to brain computations in complex ways, including division, subtraction, task variable representations, pattern separation, and gain control (Fu *et al.*, 2014; Kvitsiani *et al.*, 2013; Lapray *et al.*, 2012; Markram *et al.*, 2004; Roux & Buzsáki, 2015; Wilson, Runyan, Wang, & Sur, 2012; Wilson & Laurent, 2005). But, inhibitory circuits are generally considered to provide “disinhibition time windows” during which excitatory input can drive

spiking. Combined with the phase interaction of excitation and inhibition this can give rise to the precession effect (Kamondi, Acsády, Wang, & Buzsáki, 1998; Lengyel, Szatmáry, & Érdi, 2003; Mehta, Lee, & Wilson, 2002). What, if any, aspects of phase precession is controlled by specific input components in the EC-HPC circuit has not been investigated thoroughly. Additionally, whether phase precession arising de novo in each stage of the processing pipeline – within the DG, CA3, or CA1 – is not known. If phase precession is generated *de novo*, it would be important to know whether it arises in the intrinsic circuitry of each region or multiple inputs are combined to produce it. It is also possible that the EC-specific phase precession (Hafting, Fyhn, Bonnevie, Moser, & Moser, 2008; Reifenstein *et al.*, 2016) can be inherited directly by downstream hippocampal areas (D'Albis, Jaramillo, Sprekeler, & Kempter, 2015; Jaramillo, Schmidt, & Kempter, 2014).

What do the neurons of the hippocampus *really* represent?

Despite the enormous complexity of artificial deep neural networks (DNNs), there exists a straightforward and simple explanation for the representations that develop with training these networks: each neuron is a nonlinear feature detector. In other words, DNNs, at least of the classifier variety, untangle the highly non-linear features of their input so that an input can be sorted into an appropriate category (Bengio, Courville, & Vincent, 2013; LeCun, Bengio, & Hinton, 2015). While we have an intuitive interpretation of hippocampal single neuron responses, quantitatively speaking it is still not clear what *exactly* these cells represent. This means that we do not have a theory that can predict to what extent each neuron will alter its activity patterns in response to a particular input, and how its activity patterns inform the downstream networks to do further computations.

One view of the nature of hippocampal representations is that the set of place selective firing profiles, or a place map, is the expression of the attractor states of a navigation system (McNaughton, Battaglia, Jensen, Moser, & Moser, 2006; Redish & Touretzky, 1998). These ideas were first developed based on the experimental data obtained from the hippocampus (Samsonovich & McNaughton, 1997), but after the discovery of grid cells and other specialized cell types in the MEC (Buzsáki & Moser, 2013) it became clear that the MEC circuit is better suited to represent location based on self-motion cues (McNaughton *et al.*, 2006). Further complicating the early interpretations was the fact that the hippocampus can represent the ongoing context through its firing rate profiles (Bostock *et al.*, 1991; Leutgeb, Leutgeb, Moser, & Moser, 2005c; Muller & Kubie, 1987; Wood *et al.*, 1999; Wood *et al.*, 2000). A reinforcement learning-based model that combines self-motion and temporal difference learning to provide consistent spatial coordinates has also been proposed (Foster, Morris, & Dayan, 2000), though this model seems inconsistent with the accumulation of place fields at behaviorally relevant locations (Fyhn *et al.*, 2002; Hok *et al.*, 2007).

Prior experience of the animal during learning has a significant effect on how intuitively defined contexts are represented in the hippocampus. For example, CA3 circuits display intermediate representations in morphed environments between two square and circle end points if the rats are trained in the same place in the end point arenas (Leutgeb *et al.*, 2005a), but not if they are trained in separate places (Colgin *et al.*, 2010; Wills, Lever, Cacucci, Burgess, & O'Keefe, 2005). So whether the population is said to represent a given context depends on more factors than the present set of stimuli. Thus, interpretations may be complicated if we do not have a good definition of what constitutes a context. Perhaps the first formal definition of a "context" was given by Fuhs and Touretzky (2007). Accordingly, what defines a context is "not

a particular class of stimuli […] or behaviors […], but a set of time windows within which the statistical structure of sensory experiences and behaviors is stable" (Fuhs & Touretzky, 2007). Thus, the hippocampal response is its best estimate of the parameters of a statistical inference model about the current context that can inform behavior. When the context is inferred to have sufficiently changed to warrant learning a complex new model, the hippocampus will undergo remapping (Sanders, Wilson, & Gershman, 2020).

Recent theories of hippocampal representations take inspiration from reinforcement learning to cast the hippocampus as a general purpose computing machine suited for computations that rely on learned relations (Stachenfeld, Botvinick, & Gershman, 2017). The reinforcement learning framework is concerned with an agent interacting with its environment. Interaction here is two-way. The agent influences the environment through its actions while the environment influences the agent by rewarding it (rewards can be 0 or negative, i.e., neutral or punishing outcomes). The agent is thus faced with a computational task: to learn the action-reward contingencies in the context of its environment. To optimize its resources for this computational task, the agent must *represent* the relevant information in an effective manner. The successor representation is one such representation scheme (Gershman, 2018), and is proposed to be exactly what the hippocampus learns and represents (Stachenfeld *et al.*, 2017). Therefore, the place selective responses of the hippocampus are its best prediction of the discounted future occupancy of the rat at each location. This information is relayed to other brain areas to be combined with estimates about reward outcomes to guide behavior (Stachenfeld *et al.*, 2017). Hence, this model implies that when rats learn reward-place contingencies in a memory task, their exploration behavior should be correlated with place field activity in the environment. In agreement with this prediction, a recent study reported that the targeted

stimulation of place fields expressed at behaviorally relevant locations biases the animals to visit those locations (Robinson *et al.*, 2020). A generalized unsupervised method, called the Tolman-Eichenbaum Machine, proposes a framework for factorizing representations that correspond to different aspects of knowledge and flexibly combining them to represent novel experiences (Whittington *et al.*, 2020). In this way, solving one task (i.e., learning structural knowledge) can be used in spatial and non-spatial domains to explain a wide variety of empirically observed phenomena of hippocampal coding (Whittington *et al.*, 2020).

The importance of memory task engagement in the study of hippocampal computations

As discussed earlier episodic memories can be characterized as combining an event content (the what; "I bought bread") that took place in a spatial context (the where; "from the bakery") and temporal context (the when; "yesterday morning"), coupled with autonoetic consciousness. Hence, in the strictest sense, understanding the neural mechanisms of episodic memory is possible only in humans. However, by analogy the ability to use stored information in terms of the conjunction of the what, the where, and the when of experiences is analogously referred to as episodic-like memory (Eichenbaum, Fortin, Ergorul, Wright, & Agster, 2005). Episodic-like memory has been rather extensively documented in multiple species, including rats (Babb & Crystal, 2005, 2006; Clayton & Dickinson, 1998; Kart-Teke, De Souza Silva, Huston, & Dere, 2006; Naqshbandi, Feeney, McKenzie, & Roberts, 2007; Roberts *et al.*, 2008; Schwartz, Hoffman, & Evans, 2005). Consequently, rats have been recently used as model organisms for the study of episodic memory. However, crucially, the vast majority of modern neuroscientific research into hippocampal information processing has largely investigated it *outside* the scope of a memory task, thus undermining the interpretation of their relevance for mnemonic function.

Preview of the dissertation

To test whether hippocampal activity patterns hypothesized to be involved in estimating elapsed time (Mankin *et al.*, 2015) indeed allow for episodic-like memory, rats can be trained to distinguish between a short (e.g., 30 minutes long) and long (e.g., 6 hours long) delay period by learning to associate each delay with a distinct spatial location. Hippocampal population activity patterns can then be analyzed in relation to behavioral responses and performance for a test of the hypothesis. However, before this can be ascertained, one must first establish whether hippocampal populations exhibits a greater, diminished, or similar rate of reorganization while rats are required to encode and retain spatial information to guide their goal-directed behavior many hours later, compared to when they are not required to do so. Learning the structure of an 8-arm radial maze and place-reward contingencies on it (Olton & Samuelson, 1976) is known to depend on hippocampal circuits (Olton, Walker, & Gage, 1978), including DG (McNaughton, Barnes, Meltzer, & Sutherland, 1989; Sasaki *et al.*, 2018).

To determine the rate of hippocampal population response reorganization during the performance of a spatial memory task over many hours, we developed a delayed-matching-to-place task and trained rats on it while monitoring hippocampal CA1 neural activity. Compared to a control condition in which rats engaged in a "memory-less" task behaviorally matched the experimental condition, the memory task condition caused a significantly greater code reorganization over six hours. This was manifest both at the level of single cells and pairwise correlations between them, resulting in the degradation of the spatial information conveyed by the hippocampus after many hours. In spite of this degradation, a distinct subset of neurons began to overrepresent the goal location immediately after the rats' first time exploring the goal location each day. This goal selective population exhibited properties consistent with higher

intrinsic excitability. Our experimental design also allowed us to examine the evolution and peculiarities of post-learning neural activity patterns for many hours. We discovered that cells were biased by memory task performance to fire in long-duration SWRs. Goal cells, in particular, were also more likely to fire in SWRs. Finally, the reorganization of place representations in the memory task led to the clustering of neural activity on arms most visited by the rats in the memory task, suggestive of a mechanistic role in guiding animal behavior. These results, presented in full in chapter 1, elucidate how memory-related representations are processed offline and retained for future retrieval.

In chapter 2, we investigate the complementary physiological processes, namely encoding during online states. As suggested by earlier arguments, DG and CA3 work together to support encoding the initial traces of memory to be further processed in offline states. Phase precession in this network is likely to play a critical role. However, the generation mechanisms of phase precession with respect to various circuit inputs are not well-understood. Studying CA3 phase precession allowed us to independently control one of its two major theta-modulated excitatory inputs, namely DG and MEC. We examined CA3 spiking with or without DG and/or MEC inputs while rats performed a hippocampal dependent working memory task. We found that both inputs are necessary for intact CA3 phase precession. However, we discovered a double dissociation as well. Whereas the DG-CA3 circuit was capable of supporting precise spiking late in the theta phase (prospective/predictive coding) without MEC input, the DG input was indispensable for this function when MEC was intact. Furthermore, spiking order of pairs of CA3 cells in the theta cycle, normally matching the behavioral sequence of place field traversals, was found to no longer match the behavioral sequence without intact DG inputs, even in those CA3 cells that had some remaining phase precession. In contrast, MEC lesions did not affect this

phenomenon, even in cells with significantly impaired phase precession. We developed a computational model that explained the empirical findings and made testable predictions regarding the role of each input, including the inhibitory interneuron network, in orchestrating precise spike timing during theta, important for memory encoding processes.

Chapter 3 concludes the dissertation by synthesizing the findings of chapters 1 and 2. In addition, the implications of the findings and the most promising future research directions are discussed. Specific predictions and experimental designs to test them are also developed.

CHAPTER 1: Reorganization of hippocampal population patterns during memory retention over hours

Abstract

Hippocampal place cells are thought to support memory-guided navigation by encoding map-like representations of an animal's environment—activity patterns tied to internal and/or external variables, such as animal position (Grieves & Jeffery, 2017). In the absence of a behavioral task, these representations undergo continual spontaneous reorganization, typically detectable only after an extended amount of time (on the scale of hours) has elapsed (Mankin *et al.*, 2012). Consequently, because hippocampal patterns can be faithfully re-expressed across minutes-long intervals, the reinstatement of the previously encoded patterns upon re-exposure to the same environment is taken to be the basis of memory retrieval and, by extension, goal-directed navigation (Dupret *et al.*, 2010; Gridchyn *et al.*, 2020; Josselyn & Tonegawa, 2020; Roux *et al.*, 2017; Singer *et al.*, 2013). However, it is unclear how on substantially longer timescales the reorganized representations of a static environment can still be valid and informative for navigation. We trained two groups of rats to perform a spatial memory task and a non-memory task on an 8-arm radial maze. In the memory version, rats learned a new goal-arm location each morning and were tested 6 hours later for memory retention. In the non-memory version, rats performed a behaviorally matched task without a consistently rewarded location. Compared to the non-memory task, a number of findings were revealed in the memory task: (1) Single-cell place representations were less stable, leading to degradation of position decoding accuracy over time. (2) During memory retention between the learning and test phases, strong spatial co-firing between cell pairs diminished, while strong pairwise spike train correlations

were preserved to a larger extent than weak ones. (3) Despite instability in the spatial code, a distinct population coded for new goal location information, and pairwise spatial correlations of goal cells tended to be better preserved than those of non-goal cells. (4) During sleep in the six-hour retention period between learning and testing, spiking was preferentially recruited in long-duration sharp wave ripples (SWRs). (5) Pairwise coactivation from the learning phase was more strongly re-expressed in SWRs during the retention period and during sleep after testing. Taken together, our results establish that neuronal activity patterns show substantial instability during memory retention over hours without interfering with task performance. Thus, in principle, the functional neural subpopulations emerging in concert with memory task performance could support memory-guided behavior. These findings segregate memory-related network dynamics from coding for more consistently remembered environmental features, such as space and context.

Introduction

The rodent hippocampus is thought to support spatial memory by providing a map of the environment encoded in the spiking of its cells at precise spatial locations (Buzsáki & Moser, 2013). Single cell and population level analyses of this code have demonstrated that hippocampal cells retain stable place fields from seconds to minutes (Diehl *et al.*, 2019; Leutgeb *et al.*, 2004; Sasaki *et al.*, 2015). In general, in a novel environment, CA1 place fields start out broad and imprecise, conveying low spatial information but as the animal learns the conjunction of all features that define the environment the place fields become more precise and stable (Karlsson & Frank, 2008). As time passes, these representations drift, with the drift being readily detectable on the timescale of hours or longer (Mankin *et al.*, 2012; Ziv *et al.*, 2013). By utilizing this drifting code, the output area of the hippocampus, CA1, can in principle compute the time since a memory was acquired by comparing a temporal context encoded by a constantly drifting population code originating from CA2, and a high-fidelity copy of the memory stored in CA3 (Mankin *et al.*, 2015). However, if extrahippocampal networks should rely on receiving accurate spatial information from CA1, a temporally drifting CA1 code will be problematic unless there is concurrent and fast recalibration of downstream areas (Rule *et al.*, 2019). Since learning in the hippocampus occurs faster than in neocortex (McClelland *et al.*, 1995), other strategies must exist to ensure reliable computations. One hypothesis is that once animals engage in active encoding and retaining task-related information, the hippocampal code stabilizes, obviating neocortical recalibration. Alternatively, the hippocampal code for space may reorganize in a heterogeneous way in a memory task, accelerated in some cells but more stable in others.

During an experience, the hippocampal networks undergo changes that are evident when neuronal co-firing is compared after exploration of a novel environment relative to that prior to

exploration. In particular, neuronal co-firing is significantly enhanced post-experience compared to the pre-experience baseline (Skaggs & McNaughton, 1996; Wilson & McNaughton, 1993). This also indicates that learned associations continue to be processed in post-experience offline states. This active offline processing predominantly takes place during sharp-wave ripple (SWR)-associated firing (Nádasdy *et al.*, 1999), and important for memory and affects subsequent spatial selectivity profiles of hippocampal cells (Norimoto *et al.*, 2018; Roux *et al.*, 2017). Yet, the hours-long time course of this process after an experience is not known. If SWR-related activity continues for many hours post-experience, this would put its proposed role in place map stabilization (Roux *et al.*, 2017) at odds with population reorganization over a relatively long time periods (hours to days). Alternatively, SWR participation of hippocampal neurons could be selective, with a dichotomy in the identity of the cells that fire in SWRs determined by their spatial selectivity during exploration. Furthermore, it is unclear how SWR-associated spiking patterns change when information is learned and activity retained over many hours to guide behavior. When the environment is novel (as in most previous studies of SWR-related firing), SWRs occur at a pronounced rate (Cheng & Frank, 2008; Singer & Frank, 2009), potentially facilitating the rapid formation and stabilization of spatial maps. When rats perform a task in a highly familiar environment, however, the reduced incidence rate of SWRs could lead to increased place map reorganization, potentially undermining spatial memory performance. Alternatively, task performance per se might promote stable place selectivity (Kentros *et al.*, 2004). These factors can be dissociated if memory-dependent behavior is paired with a non-memory control.

To answer the above questions, we trained rats to perform one of two tasks on an 8-arm radial maze. The first group performed a memory task where, each day, they learned the location

of a reward at the end of one arm and were tested six hours later. The second group performed a non-memory version of this task in which the rewarded location was inconsistent and random to prevent the establishment of a reward-place association. This control group shared all behavioral variables without learning a new goal arm allowing us to determine whether network dynamics can be ascribed to experience or learning, and place map stability on memory load. We thus monitored the same population of CA1 neurons in learning, retention, and testing periods to directly assess the stability of hippocampal representations during behavior as well as the dynamics of the network during rest in the six hour retention period. We found that, compared to the non-memory task, memory task performance caused single-cell place representations to be less stable, leading to degradation of position decoding accuracy over time. In addition, we observed pronounced reorganization in correlations between pairs of spatial maps and pairs of spike trains. Despite this reorganization, a distinct population of neurons preferentially represented the goal location, and tended to have better preserved spatial coding between learning and retrieval. Furthermore, during rest in the six-hour retention period, spiking was preferentially recruited in long-duration sharp wave ripples. Finally, pairwise coactivation from the learning phase was more strongly re-expressed in SWRs during the retention period and during sleep after testing.

Results

The memory based behavioral paradigm

We developed a delayed match-to-place spatial memory task in which rats (N = 9) learned the location of a food reward available at the end of a goal arm on an 8-arm radial maze (Figure 1.1A). The goal arm was pseudorandomly chosen for each session to induce daily

memory updates. We trained the rats to freely explore the maze in blocks of 5-6 trials (labeled S0-S5; whole block labeled “SAMPLE”) and learn and remember the goal arm in each experimental session which was baited consistently in every trial. The rats had access only to the goal arm in S0, but to all arms subsequently. To isolate the effect of learning a new goal location every day, a control group of rats (N = 4) performed a non-memory variation of this task in which the baited arm was pseudorandomly chosen for each trial rather than for a whole session to ensure that no location would be reliably informative to be remembered for future reward seeking behavior.

Rats were tested for their memory of the goal arm six hours after the end of the SAMPLE phase. For brevity we will refer to the arm visited in S0 by the rats in the non-memory group also as the goal arm (see Methods). We quantified the behavioral performance by two measures: the time from the start of the TEST trial to the rats’ first visit to the reward zone of the goal arm, or their rank of first entry to that arm. Rats trained to perform the memory task visited the goal arm sooner than those performing the non-memory task (Figure 1.1B; rank sum = 909, z-stat = -3.043, $p = 0.0023$, Wilcoxon’s rank sum; $t_{54} = -3.20$, $p = 0.0023$, two-sample t-test). Testing the rats for their memory of the goal arm after only 30 minutes indicated that rats in both tasks acquired the memory of the first visited arm despite it not being consistently baited in the non-memory task (Figure 1S.1A). Comparing this to the results of testing the rats after six hours (Figure 1.1B) suggests that although the goal arm is remembered by all rats for the initial 30 minutes post-learning, only in the memory task do rats remember the goal arm for up to a minimum of six hours (until tested). We estimated the distribution of arm entry rank data via simulations based on observed turn data (Figure 1S.1B; see Methods for simulation details) and observed that, by the rank-of-entry measure, performance was better than what would be

Figure 1.1: Accurate spatial localization does not explain spatial navigation and performance in a memory task. (A) Behavioral tasks. **(B)** Behavioral performance. **(C)** Spatial coding in the hippocampus. “S” and “T” labels indicate the place maps of the same cell in the SAMPLE and TEST phases, respectively. The bottom half of examples had a cluster quality score of 4, except the example from rat 897 which had a score of 5. **(D)** The spatial correlation of hippocampal place maps across the two phases of the behavioral tasks. **(E)** The hippocampal code is more unstable when the animals perform a memory task. **(F)** Pure location is inconsistent with the oft-proposed function of the hippocampus, namely accurate localization. **(G)** The median absolute error of the Bayesian decoder increases only in the memory task, presumably due to greater instability of the maps shown in (D-E). **(H)** The spatial instability of the maps or the drop in decoder accuracy are not due to degenerate place coding in the hippocampus, such as lower spatial selectivity or loss of place fields. (Top) Fraction of all cells with a place field in SAMPLE but not TEST (“S only”), TEST but not SAMPLE (“T only”), SAMPLE and TEST (“S+T”) and cells that did not form a place field in either SAMPLE or TEST (“Neither”). (Bottom) The hippocampus displayed greater spatial selectivity across the two phases of the memory, but not the non-memory, task, as evidence by the higher proportion of cells expressing a place field in the memory task.

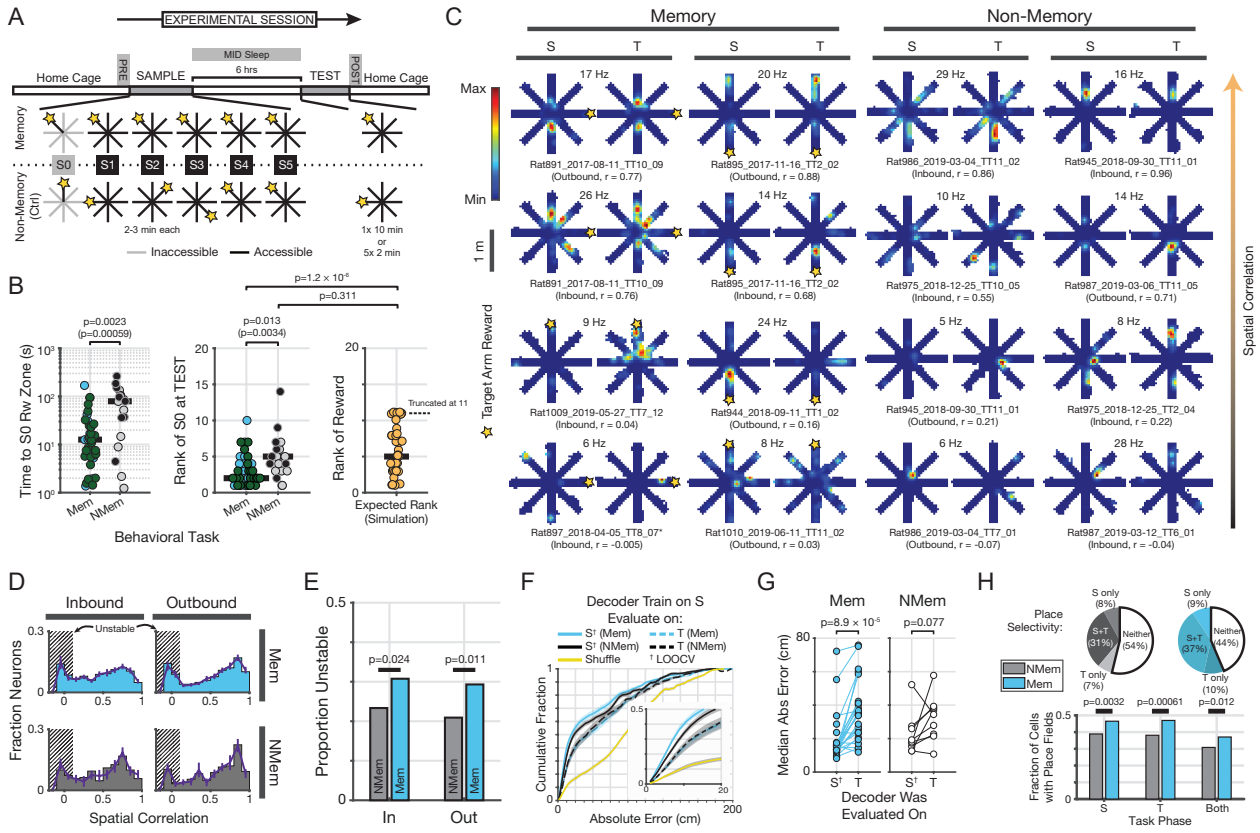
A
EXPERIMENTAL SESSION
MID Sleep
6 hrs
Home Cage
PRE
SAMPLE
TEST
POST
Home Cage
Memory
S0
S1
S2
S3
S4
S5
Non-Memory (Ctrl)
2-3 min each
1x 10 min or 5x 2 min
Inaccessible
Accessible
B
p=1.2 × 10⁻⁶
p=0.311
p=0.0023 (p=0.00059)
p=0.013 (p=0.0034)
Time to S0 Rw Zone (s)
Rank of S0 at TEST
Rank of Reward
Truncated at 11
Mem
NMem
Expected Rank (Simulation)
Behavioral Task
C
Memory
Non-Memory
S
T
Max
Min
1 m
Target Arm Reward
Spatial Correlation
17 Hz
Rat891_2017-08-11_TT10_09 (Outbound, r = 0.77)
20 Hz
Rat895_2017-11-16_TT2_02 (Outbound, r = 0.88)
29 Hz
Rat986_2019-03-04_TT11_02 (Inbound, r = 0.86)
16 Hz
Rat945_2018-09-30_TT11_01 (Inbound, r = 0.96)
26 Hz
Rat891_2017-08-11_TT10_09 (Inbound, r = 0.76)
14 Hz
Rat895_2017-11-16_TT2_02 (Inbound, r = 0.68)
10 Hz
Rat975_2018-12-25_TT10_05 (Inbound, r = 0.55)
14 Hz
Rat987_2019-03-06_TT11_05 (Outbound, r = 0.71)
9 Hz
Rat1009_2019-05-27_TT7_12 (Inbound, r = 0.04)
24 Hz
Rat944_2018-09-11_TT1_02 (Outbound, r = 0.16)
5 Hz
Rat945_2018-09-30_TT11_01 (Outbound, r = 0.21)
8 Hz
Rat975_2018-12-25_TT2_04 (Inbound, r = 0.22)
6 Hz
Rat897_2018-04-05_TT8_07* (Inbound, r = -0.005)
8 Hz
Rat1010_2019-06-11_TT11_02 (Outbound, r = 0.03)
6 Hz
Rat986_2019-03-04_TT7_01 (Outbound, r = -0.07)
28 Hz
Rat987_2019-03-12_TT6_01 (Inbound, r = -0.04)
D
Inbound
Outbound
Unstable
Fraction Neurons
Mem
NMem
Spatial Correlation
E
Proportion Unstable
p=0.024
p=0.011
In
Out
F
Decoder Train on S
Evaluate on:
S† (Mem)
S† (NMem)
Shuffle
T (Mem)
T (NMem)
† LOOCV
Cumulative Fraction
Absolute Error (cm)
G
Mem
NMem
p=8.9 × 10⁻⁵
p=0.077
Median Abs Error (cm)
S†
T
Decoder Was Evaluated On
H
Place Selectivity:
NMem
Mem
S only (8%)
S+T (31%)
Neither (54%)
T only (7%)
S only (9%)
S+T (37%)
Neither (44%)
T only (10%)
p=0.0032
p=0.00061
p=0.012
Fraction of Cells with Place Fields
S
T
Both
Task Phase

expected by chance only in the memory task (Figure 1.1C; Mem vs. Sim rank sum = 1071794.5, z-stat = -4.70, $p = 1.3 \times 10^{-6}$; NMem vs. Sim rank sum = 888826.5, z-stat = -0.492, p = 0.311). Importantly, this confirmed that the difference in performance between the two versions of the task was indeed due to a memory effect as opposed to arising from diverging behavioral strategies or other latent variables. Thus, training history and the repeated receipt of reward at a constant location in each session were crucial for the long-term (i.e., hours-long) retention of the spatial information required to solve the memory task. Furthermore, our task design and training protocol were effective and rats did learn the tasks as intended.

Memory task engagement destabilizes hippocampal spatial representations

The prevailing view of hippocampal function is that it computes a stable code for acquired memories (Eichenbaum, 2017), which in rodents is predominantly and overtly in the spatial domain (O'Keefe & Nadel, 1978). This code is then routed to downstream areas to guide behavior on the basis of spatial memories (Morris *et al.*, 1982; Redish & Touretzky, 1998; Sanders *et al.*, 2015). A large body of literature has corroborated this view by primarily showing that the hippocampal code indeed contains very substantial spatial information (Brown, Frank, Tang, Quirk, & Wilson, 1998; Davidson *et al.*, 2009; Frank, Brown, & Wilson, 2000; Gonzalez, Zhang, Harutyunyan, & Lois, 2019; Pfeiffer & Foster, 2013; Wikenheiser & Redish, 2015; Wilson & McNaughton, 1993; Zhang, Ginzburg, McNaughton, & Sejnowski, 1998; Ziv *et al.*, 2013). It is known that in an open field paradigm hippocampal neural representations become decorrelated as a function of elapsed time (Mankin *et al.*, 2012). If the previously observed representation changes (Mankin *et al.*, 2012) were due to the lack of a behaviorally relevant objective, we would expect to see more stable maps in our memory task. Moreover, previous

experiments were done over relatively short time periods and/or in the absence of a memory task, leaving unanswered to what extent hours-long code reorganization would affect spatial memory performance.

Our paradigm requires that spatial information be learned and retained over extended time scales on the 8-arm radial maze. Furthermore, we follow the same population of neurons after learning a new goal through six hours of memory retention until testing and memory retrieval. In addition, our control group allows us to dissociate the task-specific learning from expected learning of environmental features or passage of time. Thus, to ask how hippocampal representations in our novel paradigm compare to those in classic open-field or linear track paradigms without an explicit memory task and studied over much shorter intervals, we proceeded to quantify the spatial stability of single cell place maps across the SAMPLE and TEST behavioral epochs. After confirming the success of the training protocol and the robustness of behavioral performance, a subset of 24 (memory) and 9 (non-memory) individual sessions (where testing took place 6 hours after SAMPLE) were selected for analysis of neural dynamics (fig 1.1B; neurons N = 1795 from 34 sessions). Surprisingly, we observed that, compared to the non-memory task, memory task performance led to a greater amount of change in the within-cell spatial map correlations over extended time intervals (Figure 1.1C-D). Quantitatively, the proportion of cells that were uncorrelated or only weakly correlated was higher in the memory task compared to the non-memory task (Figure 1.1E; 29.3% vs. 20.9%, $p = 0.0114$, $\chi^2 = 6.40$, chi-squared test). This was not due to poor cluster quality as the patterns were replicable when the analysis was restricted to the clusters with the highest quality scores (27.7% vs. 18.9%, $p = 0.0476$, $\chi^2 = 3.92$, chi-squared test). Thus, when rats are required to retain spatial

information for extended periods of time, the representations of single hippocampal cells undergo a greater amount of reorganization than when they passively explore the environment.

Position estimation suffers from reduced spatial stability of place representations

To ask how despite greater instability in the hippocampal neural code the rats could successfully perform the memory task, we compared the generalization ability of a Bayesian decoder across the SAMPLE and TEST epochs. Specifically, we reasoned that if the hippocampus helps the rats solve the memory task by providing an accurate map-like representation of the environment, the increased instability of the neural code due to the memory task should have no material impact on the ability of a downstream decoder to locate the rats from neural activity. For instance, such a population decoder might be able to extract stable spatial information even though individual cell representations change over time. Using five-fold cross validation, we were able to decode the instantaneous position of the rat better than chance in both tasks and for both behavioral epochs (Figure 1.1F; see Methods). However, the decoder generalized better to the TEST epoch in the non-memory task compared to the memory task (Figure 1.1F, inset; compare the difference between the memory curves (blue) with the difference between the non-memory curves (gray)). Quantitatively, the median absolute error increased significantly between the SAMPLE and TEST epochs only in the memory task (Figure 1.1G). This drop in the decoder performance was not due to disparate place selectivity profiles of hippocampal cells in the two tasks (Figure 1.1H). These data are inconsistent with the hypothesis that the function of the hippocampus in solving our spatial memory task is to broadcast an accurate position estimate within the map of an environment.

Memory task modulates pairwise place representation and spiking dynamics

We next hypothesized that higher-order neural dynamics might mediate the successful performance of the rats in the memory task. To test this, we first examined to what extent pairwise correlations between spatial representations were maintained across the two tasks. Whereas a positive correlation between two cells' place maps is indicative of sufficiently overlapping place fields, a zero or negative correlation would be inconclusive about the exact relationship between the spatial receptive fields of the cells (Figure 1.2A). Therefore, to assess how place selectivity is co-modulated between cell pairs, we focused on positively correlated cell pairs and asked to what extent such positive correlations are maintained across the SAMPLE and TEST epochs in each task. 44.0% and 34.9% of all cell pairs in the memory task had a positive map correlation in the SAMPLE and TEST epochs (Figure 1.2B). However, while in the non-memory task the percentage of cell pairs with a positive map correlation at SAMPLE (45.7%) was similar to that in the memory task, only 28.9% had a positive correlation in TEST epochs (Figure 1.2B). Of the positively correlated cell pairs in the SAMPLE epoch 51.0% in the memory task and 44.5% in the non-memory task were still positively correlated at TEST (Figure 1.2C; $p = 6.8 \times 10^{-17}$, $\chi^2 = 69.73$, chi-squared test), indicating that changes in the spatial selectivity of these pairs was more coherent in the memory task. The amount of change in the pairwise map correlations was a function of the initial correlation strength of the pairs (Figure 1.2D). In particular, whereas the weakly- and moderately-correlated pairs (pairs with $r < 0.1$ and $0.1 < r < 0.4$, respectively) reorganized similarly across the two tasks (Figure 2D, left and middle panels, Cohen's effect size $d < 0.061$), the strongly correlated cell pairs retained their strong correlation to a greater extent in the non-memory task (Figure 2D, right panel, Cohen's effect

size d = -0.535). Thus, while pairs of place cells are more likely to retain their similar spatial selectivity profile across task phases in the memory task compared to the non-memory task, changes in spatial co-selectivity originate primarily in the cells with the most highly similar firing patterns.

The place representation correlations are coarse measures of coherent population changes and only account for firing rates. To gain insights into how the precise relative spike timing of the cells is preserved throughout the experimental sessions, we examined the spike trains by calculating the correlation coefficient between pairs of spike count vectors (Figure 2E; see Methods). At SAMPLE, about 95% of the spike train correlation values lay between -0.06 and 0.128 in both tasks, with almost all (99.8%) significant (at $\alpha = 10^{-4}$) values being positive (Figure 1.2F). While a similar proportion of all spike train pairs were significantly correlated in both tasks (Figure 1.2F), a higher percentage of trains positively correlated at SAMPLE were correlated at TEST in the non-memory task (Figure 1.2G, memory vs. non-memory: 23.0% vs. 32.0%, $t_{31} = -2.17$, $p = 0.038$, two sample t-test). Inspection of the correlation matrices across SAMPLE and TEST suggested that low and high correlation values are affected differently (Figure 1.2H). Indeed, quantile-quantile plots (QQ-plots) comparing the shape of distributions across the two epochs supported this observation (Figure 1.2I).

To compare how small and large correlations changed from SAMPLE to TEST across the two tasks, we quantified two features of the QQ-plots for each session. The “flattening” of the portion of the QQ-plots between 0 and 0.01 was taken to be a proxy for how small correlations changed, whereas the deviation of points greater than 0.05 was taken to be a proxy for how large correlations changed (Figure 1.2I; see Methods). At the population level, strongly correlated values became more extreme, while weakly correlated values were further diminished in the

Figure 1.2: Pairwise spatial firing and temporal firing correlations are preferentially reduced in the memory task. (A) Example place maps pairs with relatively stable and unstable co-firing. **(B)** The distribution of all place map correlation values in the memory task (left) and in the non-memory task (right) for the SAMPLE (solid line) and TEST (shaded histograms) epochs. The marked rectangular area is blown up in the inset for clarity. Notice that in the memory task the overall distribution is similar between SAMPLE and TEST, while in the non-memory task the TEST distribution is reduced. This is because the values are normalized to represent a fraction of all possible map pairs so if a place cell stops firing at TEST, it contributes to the denominator without contributing to the numerator in the normalization step. **(C)** Compared with the non-memory task, a higher proportion of place cells in the memory task retained their co-firing from SAMPLE to TEST. **(D)** Distribution of spatial firing map correlation changes between SAMPLE and TEST epochs for pairs with low ($r < 0.1$), moderate ($0.1 < r < 0.4$), or high ($r > 0.4$) correlation at SAMPLE. Cell pairs with the most similar spatial co-firing patterns (High) saw a greater amount of reduction in their co-firing at TEST in the memory versus the non-memory task. **(E)** Schematic of the computational steps for estimating spike train correlations. **(F)** Distribution of spike train correlations in the memory (top) and non-memory (bottom) tasks for the SAMPLE (solid line) and TEST (shaded) epochs. **(G)** In the memory task, a lower proportion of cells retained their spike train correlation between SAMPLE and TEST epochs. **(H)** Example spike train correlation matrices from the memory task. **(I)** QQ-plot of example correlation matrices from (H). How the changes in strong and weak values are quantified is graphically displayed. **(J)** Quantification of changes in strong and weak spike train correlations from all sessions of each task. **(K)** In both tasks, cell pairs with strongly correlated spike trains were more likely to retain their correlation between SAMPLE and TEST. Retention is quantified as the fraction of pairs at SAMPLE that were significantly correlated at TEST. Weak correlations: $r < 0.05$, Strong correlations $r > 0.05$.

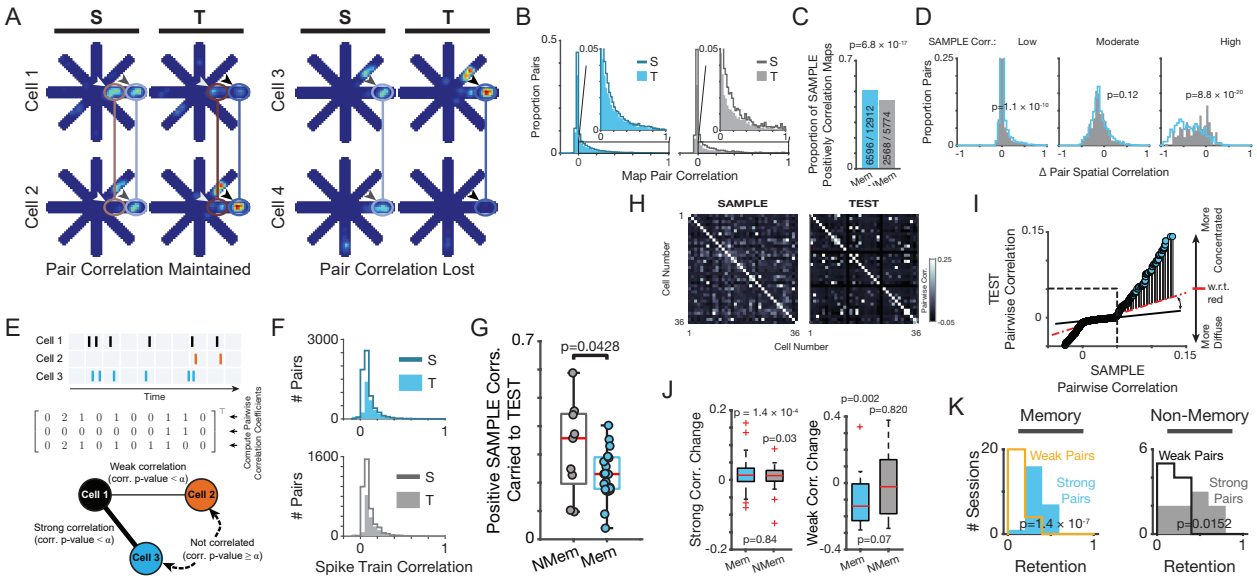
A
S
T
Cell 1
Cell 2
Cell 3
Cell 4
Pair Correlation Maintained
Pair Correlation Lost
B
Proportion Pairs
Map Pair Correlation
C
Proportion of SAMPLE Positively Correlation Maps
p=6.8 × 10^-17
6696 / 12912
2568 / 5774
Mem
NMem
D
SAMPLE Corr.:
Low
Moderate
High
Proportion Pairs
p=1.1 × 10^-19
p=0.12
p=8.8 × 10^-20
Δ Pair Spatial Correlation
E
Cell 1
Cell 2
Cell 3
Time
Correlate Pairwise Correlation Coefficients
Weak correlation
(corr. p-value < α)
Strong correlation
(corr. p-value < α)
Not correlated
(corr. p-value ≥ α)
F
Pairs
Spike Train Correlation
G
Positive SAMPLE Corrs. Carried to TEST
p=0.0428
NMem
Mem
H
SAMPLE
TEST
Cell Number
Pairwise Corr.
I
TEST Pairwise Correlation
SAMPLE Pairwise Correlation
More Concentrated
More Diffuse
w.r.t. red
J
Strong Corr. Change
Weak Corr. Change
p = 1.4 × 10^-4
p=0.03
p=0.84
p=0.002
p=0.820
p=0.07
K
Memory
Non-Memory
Sessions
Weak Pairs
Strong Pairs
p=1.4 × 10^-7
p=0.0152
Retention

memory task (Figure 2J). Individual strongly correlated pairs at SAMPLE were more likely to be retained at TEST compared to weakly correlated pairs in both tasks (Figure 1.2K). Thus, while at the population level the tails of the spike correlation distributions were differently modulated by the two tasks, the strength of individual correlations in SAMPLE determined to what extent they were carried over to the TEST epoch. The relationship between the values of place map and spike train correlations did not appear to have a straightforward interpretation, suggesting that these analyses captured different aspects of neural dynamics (Figure 1S.2). Taken together, these results delineate the distinct dynamics of firing rate and spike timing correlations between the memory and non-memory tasks.

Goal location is overrepresented in the memory task

To further characterize the neural dynamics that might support behavioral performance, we examined the distribution of place representations in the two tasks (Figure 1.3A). Cells typically had multiple discrete place fields scattered throughout the maze (Figure 1.3B). Cells with a place field on the goal arm (labeled “goal cells”) constituted roughly 10.4% and 4.9% of the population of simultaneously recorded cells in the memory and non-memory tasks, respectively (Figure 1.3C, $z = 4.84$, rank sum = 15344.5, $p = 1.3 \times 10^{-6}$, rank sum test). Intriguingly, compared to non-goal cells (place selective cells without a place field on the goal arm), the goal cells were overrepresented in both tasks (10.4% vs. 3.1% in memory, $z = 10.88$, rank sum = 27037.5, $p = 1.5 \times 10^{-27}$; and 4.9% vs. 2.6% in non-memory tasks, $z = 3.00$, rank sum = 3429, $p = 0.0027$; rank sum tests). To account for possible disparities in the number of place fields per cell, we recounted the goal arm place fields as a fraction of all place fields (Figure 1.3D). The proportion of all place fields expressed within an experimental session was greater on the goal arm compared to the non-goal arms only in the memory task (memory: 20% vs. 11.0%,

$z = 5.02$, rank sum = 9954, $p = 5.3 \times 10^{-7}$; non-memory 12.5% vs. 13.4%, $z = -0.224$, rank sum = 1799, $p = 0.82$; rank sum tests). Furthermore, the proportion of goal cell place fields was greater in the memory task than in the non-memory task ($z = 3.68$, rank sum = 10372.5, $p = 2.3 \times 10^{-4}$, rank sum test). Thus, the goal arm was overrepresented in the memory task both when calculated as a fraction of all hippocampal cells and as a fraction of all place fields expressed within an experimental session.

To assess whether the goal-representing cells have distinct coding properties, we calculated the proportion of such cells that retained their spatial selectivity across the SAMPLE and TEST behavioral epochs. In the memory task, but not the non-memory task, goal cells were more likely to continue to be spatially selective (Figure 1.3E; Mem: 88.4% vs. 76.6%, $p = 0.0016$; NMem: 88.7% vs. 76.0%, $p = 0.05014$, chi-square tests), although their place fields were no more likely to remain on the same arm of the maze compared to non-goal cells (Figure 1.3F; Mem: goal vs. non-goal 66.7% vs. 68.4%, $p = 0.46$; NMem: 69.2% vs. 71.1%, $p = 0.62$, chi-square tests). Cells that represented the goal arm at SAMPLE had a higher average firing rate at baseline (Figure 1.3G; mean firing rates in PRE: Mem, 0.30 Hz vs. 0.57 Hz goal vs. non-goal, $p = 0.043$; NMem, 0.25 Hz vs. 0.23 Hz goal vs. non-goal, $p = 0.95$) and higher peak firing rate in the SAMPLE epoch (Figure 1.3H; Median peak SAMPLE firing rates: Mem, 11.41 Hz vs. 8.12 Hz, goal vs. non-goal, $p = 0.0018$; NMem, 13.44 Hz vs. 8.98 Hz, goal vs. non-goal, $p = 0.0329$; rank sum tests) compared to non-goal representing cells. Interestingly, in the memory task goal cells fired at a significantly higher rate upon the rat's first pass through the goal arm field (which took place in trial S0; see Methods) compared to the subsequent visits (trials S1-S5), as well as compared to the first pass through the place fields of non-goal cells (Figure 3I; firing rates during first field traversal: Mem, 19.86 Hz vs. 15.08 Hz, goal vs. non-goal, $p = 0.0087$; NMem, 17.27

Figure 1.3: Goal arm is overrepresented in the hippocampal population by the more excitable cells. (A) Schematics of the counting methods for estimation of overrepresentation. Top: in the by-cell method, overrepresentation of the goal arm was calculated as the number of goal cells (cells with at least one place field on the goal arm) as a fraction of the number of simultaneously recorded hippocampal cells. Bottom: in the by-field method, overrepresentation was calculated as a fraction of place fields expressed on the goal arm out of all discrete place fields. **(B)** Examples of non-goal (top two rows) and non-goal cells (bottom row). **(C)** The goal arm was overrepresented in both tasks when counted by-cell. In the memory task, the overrepresentation was more pronounced. **(D)** The goal arm was overrepresented in the memory task when counted by-field. **(E)** Goal cells were more likely to retain their place selectivity in the memory task. **(F)** Retention of place selectively was not arm-specific as both goal and non-goal cell populations had a similar probability of representing the same arm in both SAMPLE and TEST epochs. **(G)** Baseline firing rate of goal cells calculated in the PRE epoch (before any new learning took place) was higher than non-goal cells in the memory task. **(H)** Peak firing rate of the goal cell population was higher during SAMPLE, evident in the upward shift of the QQ-plots. **(I)** In-field firing rate of goal cells was higher during the first pass through the place field (which occurred in trial S0) compared to subsequent visits (S1 to S5). This was not the case for non-goal cells (first visit occurring in trial S1, compared to subsequent visits in S2 to S5). Though a similar pattern was observed in the non-memory task, the effect was less pronounced. **(J)** Goal cells expressed more place fields than non-goal cells in both tasks, on average. The vertical lines indicate the means.

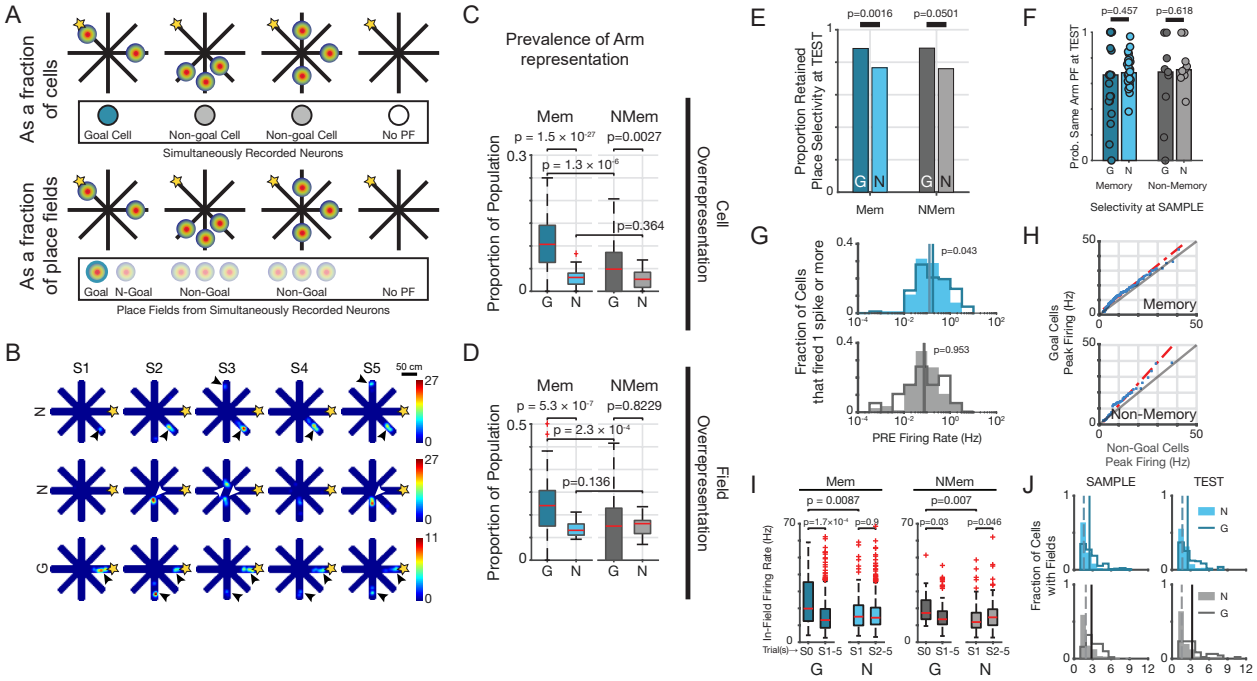
A
As a fraction of cells
Goal Cell
Non-goal Cell
Non-goal Cell
No PF
Simultaneously Recorded Neurons
As a fraction of place fields
Goal
N-Goal
Non-Goal
Non-Goal
No PF
Place Fields from Simultaneously Recorded Neurons
B
S1
S2
S3
S4
S5
50 cm
N
N
G
27
0
27
0
11
0
C
Prevalence of Arm representation
Mem
NMem
p = 1.5 × 10-27
p=0.0027
p = 1.3 × 10-6
p=0.364
Proportion of Population
0.3
0
G
N
G
N
Cell Overrepresentation
D
Mem
NMem
p = 5.3 × 10-7
p=0.8229
p = 2.3 × 10-4
p=0.136
Proportion of Population
0.5
0
G
N
G
N
Field Overrepresentation
E
p=0.0016
p=0.0501
Proportion Retained Place Selectivity at TEST
1
0
G
N
G
N
Mem
NMem
F
p=0.457
p=0.618
Prob. Same Arm PF at TEST
1
0
G
N
G
N
Memory
Non-Memory
Selectivity at SAMPLE
G
p=0.043
p=0.953
Fraction of Cells that fired 1 spike or more
0.4
0
0.4
0
10-4
10-2
100
102
PRE Firing Rate (Hz)
H
50
0
Memory
50
0
50
0
Non-Memory
50
0
Goal Cells Peak Firing (Hz)
Non-Goal Cells Peak Firing (Hz)
I
Mem
NMem
p = 0.0087
p=0.007
p=1.7×10-4
p=0.9
p=0.03
p=0.046
In-Field Firing Rate (Hz)
70
0
70
0
Trial(s)→
S0
S1-5
S1
S2-5
S0
S1-5
S1
S2-5
G
N
G
N
J
SAMPLE
TEST
Fraction of Cells with Fields
1
0
1
0
N
G
1
0
1
0
N
G
0
3
6
9
12
0
3
6
9
12

Hz vs. 11.91 Hz, goal vs. non-goal, $p = 0.007$; rank sum tests). Goal cells were also more likely to have more place fields compared to non-goal cells in both task epochs (Figure 3J; number of place fields at SAMPLE: Mem, mean: 2.49 vs. 1.57, median: 2 vs. 1; NMem, mean: 2.82 vs. 1.89, median: 3 vs. 1; medians $p < 10^{-6}$, rank sum tests). Together, these results identify cell excitability and intrinsic spiking propensity as the physiological properties that play a role in determining functional cell fate to represent each session's goal location.

Distinct pairwise place representations and spiking dynamics in relation to goal cells

Next, we sought to characterize the interactions between the goal cells and the rest of the population to determine how they shape neural dynamics in each task. Place map correlations between goal cells were significantly stronger than between a goal cell and a non-goal cell, or between non-goal cells (Figure 1S.3; $p < 10^{-80}$, Kruskal-Wallis test; post-hoc comparisons $p < 0.01$). In addition, place map correlations between one non-goal and one goal cell were stronger than between non-goal cells (Figure 1S.3, post-hoc comparisons $p < 0.01$). At SAMPLE, the median place map correlation between goal and non-goal cells was -9.7×10^{-4} in the memory task and 0.012 in the non-memory task, with 49.5% and 55.1% of the values, respectively, in the positive (Figure 1.4A, $p = 2.4 \times 10^{-8}$, $\chi^2 = 31.16$, chi-square test for proportions). In contrast, at TEST time about 38.7% and 36.1% of place map correlations between goal and non-goal cells were positive ($p = 0.0073$, $\chi^2 = 7.20$, chi-square test for proportions). Of the positive correlations between goal and non-goal cells at SAMPLE, 54.6% and 48.4% remained positive also at TEST (Figure 4B, $p = 8.2 \times 10^{-6}$, $\chi^2 = 19.90$, chi-square test for proportions). When pairs of goal cells alone were considered, 63.4% and 54.9% of the positive SAMPLE correlations were retained at TEST (Figure 4B, $p = 0.0041$, $\chi^2 = 8.25$, chi-square test for proportions). We also found

significant interactions between the number of goal cells in a given pair (0, 1, or 2) and the task performed (memory or non-memory) (Figure 1S.4): weakly correlated pairs in the SAMPLE epoch enhanced their place representation correlation at TEST to a greater extent when at least one member of the pair was a goal cell only in the memory task (interaction term F-value = 8.53, p = 0.0002; two-factor ANOVA). In contrast, the correlation between strongly correlated pairs at SAMPLE was reduced to a greater extent at TEST when at least one pair member was a non-goal cell in the memory task (interaction term F-value = 3.91, p = 0.0203; two-factor ANOVA). When exactly one pair member was a goal cell, weakly-, moderately-, and strongly correlated cell pairs exhibited a median change in correlation between SAMPLE and TEST of 0.046, -0.08, and -0.33 in the memory task, and of 0.032, -0.079, and -0.194 in the non-memory task (Figure 1.4C). All values were statistically significantly different across the two tasks (Figure 1.4C, $p < 0.05$, rank sum tests), though the greatest effect was observed for the pairs with high SAMPLE correlations. Taken together, these analyses suggest that the goal-selective cell population might have an enhancing effect on positive correlations between place maps from SAMPLE to TEST.

We next grouped cell pairs by their goal-selectivity and inspected the spike train correlation matrices of each session based on this grouping (Figure 1.4D). Overall, the correlation matrices of the TEST epoch appeared sparser compared to their SAMPLE counterparts in the memory task (Figure 1.4D), with the sparsification mainly evident in the non-goal population (Figure 1.4D-E). The comparison between how the samples were distributed relative to each via QQ-plots showed that the strong correlations between non-goal cells were skewed rightward compared to those in the goal cell population evident in the upward divergence of quantiles from the equidistribution line (Figure 1.4E-F). In contrast, when at least one member of a weakly correlated spike train pair was drawn from the non-goal cell population, the

Figure 1.4: Dynamics of pairwise spatiotemporal co-firing profiles in relation to the goal selective population. (A) Distribution of spatial co-firing similarity between goal selective and non-goal selective cell pairs in the memory (blue) and non-memory (gray) tasks with SAMPLE and TEST data displayed as solid line or shaded histogram, respectively. **(B)** Proportions of SAMPLE spatial co-firing retained at TEST for cell pairs with exactly one or two goal selective members. **(C)** Quantitative changes in co-firing of cells pairs with exactly one goal-selective member. Pairs with a high co-firing score ($r > 0.4$) show the greatest change between SAMPLE and TEST epochs. **(D)** Example spike train correlation matrices from the memory task. Goal selective and non-goal selective cells are sorted into blocks (note the labels). **(E)** QQ-plots of memory task correlation matrices separated by goal-selectivity. **(F)** Changes in strongly correlated cell pairs in the memory task sorted by goal-selectivity. **(G)** Changes in weakly correlated cell pairs in the memory task sorted by goal-selectivity. **(H-K)** Organized as in (D-G) but for the non-memory task. **(L)** Distribution of the correlation values of spike train pairs in the memory (left) and non-memory (right) tasks. Insets show the proportion of strongly correlated pairs ($r > 0.1$). **(M-N)** Histograms of the proportion of pairwise weak or strong SAMPLE spike train correlation values that were retained at TEST for the memory (M) and non-memory (N) tasks, separated by goal-selectivity. In each pair one member was fixed to be a non-goal selective cell, while the second member was chosen to be either a goal selective cell (darker histograms) or non-goal selective cell (lighter histograms). Strong and weak values are shown separately as shaded or solid line histograms, respectively.

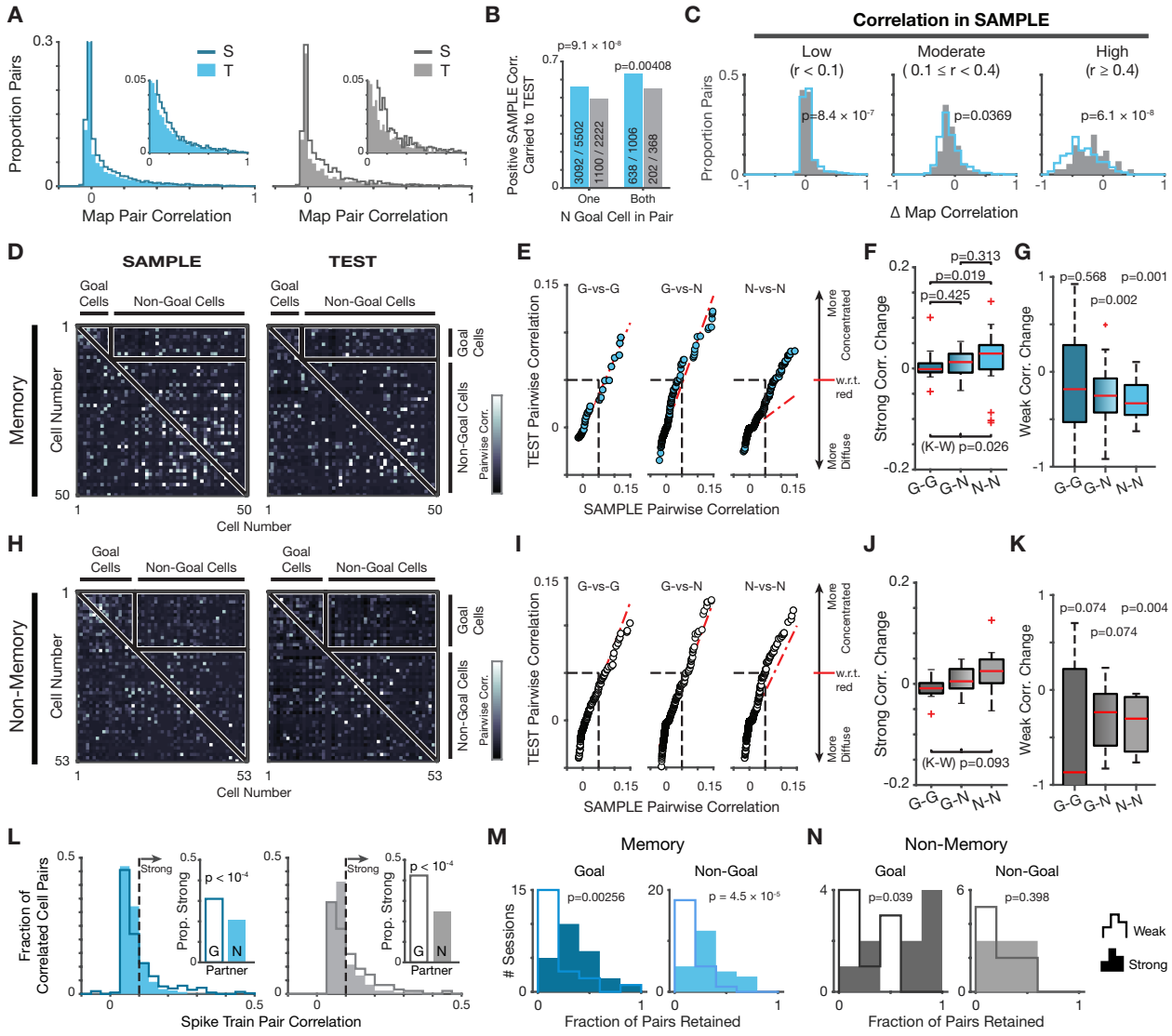
A
Proportion Pairs
S
T
Map Pair Correlation
B
Positive SAMPLE Corr. Carried to TEST
p=9.1 × 10⁻⁸
p=0.00408
3092 / 5502
1100 / 2222
638 / 1006
202 / 368
One
Both
N Goal Cell in Pair
C
Correlation in SAMPLE
Low (r < 0.1)
Moderate (0.1 ≤ r < 0.4)
High (r ≥ 0.4)
p=8.4 × 10⁻⁷
p=0.0369
p=6.1 × 10⁻⁸
Proportion Pairs
Δ Map Correlation
D
SAMPLE
TEST
Goal Cells
Non-Goal Cells
Memory
Cell Number
Pairwise Corr.
E
G-vs-G
G-vs-N
N-vs-N
More Concentrated
w.r.t. red
More Diffuse
TEST Pairwise Correlation
SAMPLE Pairwise Correlation
F
p=0.313
p=0.019
p=0.425
(K-W) p=0.026
Strong Corr. Change
G
p=0.568
p=0.001
p=0.002
Weak Corr. Change
H
Non-Memory
I
J
(K-W) p=0.093
K
p=0.074
p=0.004
p=0.074
L
Fraction of Correlated Cell Pairs
Strong
p < 10⁻⁴
Prop. Strong
Partner
Spike Train Pair Correlation
M
Memory
Goal
Non-Goal
p=0.00256
p = 4.5 × 10⁻⁵
# Sessions
Fraction of Pairs Retained
N
Non-Memory
p=0.039
p=0.398
Weak
Strong

correlation was further weakened compared to goal cell-goal cell interactions which on average remained intact (Figure 1.4G). These correlation strength-specific effects were not found in the non-memory task (Figure 1.4H-K), except for the further weakening of weakly correlated spike train pairs drawn exclusively from the non-goal population (Figure 1.4K). The strength of a non-goal cell's spike train correlation depended on the identity of its partner: in both tasks spike train correlations with a goal cell were stronger ($r > 0.10$) than with non-goal cells (Figure 1.4L, insets: $p < 10^{-4}$, chi-squared tests). Finally, between SAMPLE and TEST in the memory task weak spike train correlations were eliminated at a higher rate than strong ones (Figure 1.4M, fig 1S.5). In contrast, spike trains correlated with goal cells were differentially retained between SAMPLE and TEST depending on the initial correlation strength at SAMPLE (Figure 1.4N, fig 1S.5). In summary, cells that develop a representation of the goal arm in the memory task mediate distinct place map and spike train correlations across the population. Furthermore, in the memory task the hippocampus shapes the neural dynamics in such a way to promote goal representations and eliminate the non-goal representations.

Population spatial firing rates predict behavioral choices

How can the hippocampus take advantage of goal overrepresentation? Theories of hippocampal function based on reinforcement learning (Stachenfeld *et al.*, 2017) predict that hippocampal representations quantify the animal's expected visit probability to various spatial locations in the environment. We tested this prediction by comparing the total neural activity expressed on each of the eight arms of the maze with the probability of the behavioral visits to that arm. In the memory task, we found that the per-arm total neural firing activity was strongly predictive of the total number of visits to that arm at TEST (Figure 1.5A-B; Spearman's rank correlation $r = 0.282$, $p = 5.1 \times 10^{-5}$). However, importantly, this was not the case in the neural

data recorded from rats performing the non-memory task (Figure 1.5B; Spearman's rank correlation $r = 0.131$, $p = 0.27$). This is crucial for two reasons. First, because the relationship is not present in the non-memory task, it indicates that the fact that rats visit a certain arm more often does not automatically lead to a greater level of hippocampal firing rate on that arm. Rather, this is indicative of some form of learning related to the task objectives. Second, supports the hypothesis that the learning objective of the hippocampus, in a mathematical sense, is to provide a mechanism to enable future discovery of remembered locations. The pairwise dynamics delineated in the previous section are consistent with this interpretation. Thus, goal overrepresentation might indicate a readily detectable signal quantifying the rat's estimate of the probability of future visits to discrete locations in an environment once learning has taken place.

Memory task engagement primes the population to spike in longer ripples

So far, our results demonstrate that although memory task performance drives the hippocampal network to alter the single-cell spatial maps, these changes are far from random and maintain a level of higher-order coherence in the memory task above and beyond what was observed in the non-memory task which suggests a role for supporting memory-guided behaviors. Because these dynamics were characterized by comparing the SAMPLE and TEST behavior epochs, we reasoned that the changes we uncovered must arise from the neuronal events occurring in the intervening period. Thus, we sought to elucidate the dynamics of hippocampal spiking in the six hour long memory retention period between the two behavioral epochs (i.e., MID sleep). Sharp-wave ripple activity has been proposed to reorganize hippocampal synapses (Norimoto *et al.*, 2018; Sadowski *et al.*, 2016), specifically when rats are engaged in a memory task (Dupret *et al.*, 2010; Kovács *et al.*, 2016; Roux *et al.*, 2017). In

Figure 1.5: Population firing rate distributions over the maze at TEST predict visits to individual maze arms. (A) Example of correlation between visit counts to each maze arm (left) and population firing rates across the maze (right). The average arm firing rate (AAFR) across the population is displayed as arcs near each arm. The color coding indicates the number of visits to each arm in the left panel and rank of the values in the right panel. **(B)** Spearman's rank correlation between AAFR and arm visit counts is significant only in the memory task, indicating learning is necessary for firing rate reorganization to guide future behavior.

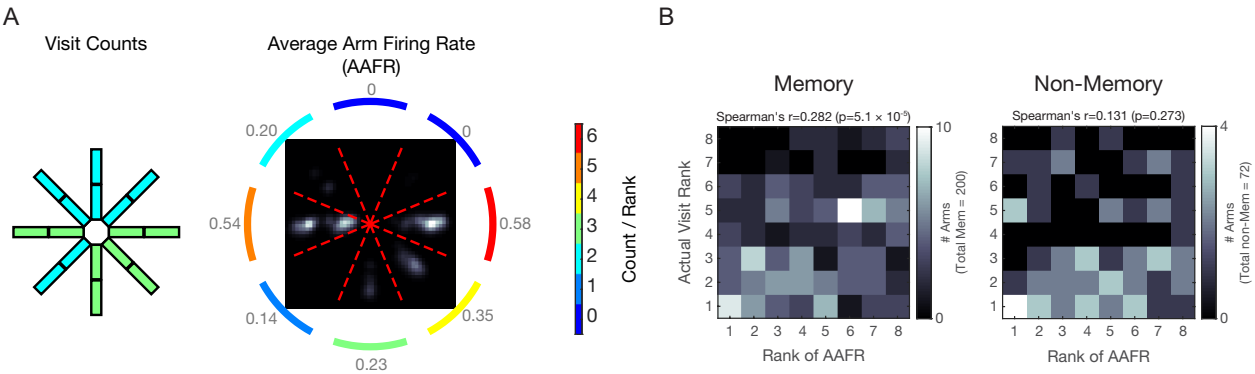
A
Visit Counts
Average Arm Firing Rate
(AAFR)
0
0.20
0
0.54
0.58
0.14
0.35
0.23
Count / Rank
6
5
4
3
2
1
0
B
Memory
Non-Memory
Spearman's r=0.282 (p=5.1 × 10^-9)
Spearman's r=0.131 (p=0.273)
Actual Visit Rank
Rank of AAFR
Arms
(Total Mem = 200)
(Total non-Mem = 72)
10
4
0

addition, spiking in long-duration SWRs in the awake state has been shown to be important for memory task performance (Fernández-Ruiz *et al.*, 2019). We, therefore, quantified the ripple length preference (RLP) of hippocampal cells by calculating the ratio between the proportion of long ripples a cell fired in and the expected proportion of the cell's spikes in ripples of various lengths assuming the cell fired with equal probability in ripples of any length (Figure 1.6A; see Methods). Hippocampal cells became more likely to fire in longer ripples in the memory task in the MID sleep epoch and less likely to fire in shorter ripples (Figure 1.6B). However, the preferred ripple length was less specific when the rats performed the memory task (Figure 1.6C). Goal cells had a higher ripple sensitivity (i.e., probability of firing a spike when a ripple event occurs) compared to non-goal cells in the memory task (Figure 1.6D). Likewise, memory task goal cells had a higher ripple sensitivity compared to cells recorded in the non-memory task (Figure 1.6D). To characterize how ripple-specific cell pair co-firing is modulated by memory demand, we quantified the ripple length preference of cell pairs in a similar manner as before (Figure 1.6E). As in the single-cell case, hippocampal cell pairs became more selective for firing in longer ripple events in MID sleep (Figure 1.6F). Thus, single and pairwise hippocampal cell spiking during rest ripple events is modulated by memory demand.

Strong and weak spike correlations in behavior are differentially re-expressed in sharp-wave ripple events

We have so far shown that a) single-cell place representations change to a greater extent in the memory task than in the non-memory task, b) pairwise spike timing correlations follow distinct dynamics for weak and strong correlations during behavior, and c) single- and pairwise cell spiking becomes biased to take place in longer ripple events in the intervening period between SAMPLE and TEST epochs. Because of the interaction of spiking and MID sleep ripple

Figure 1.6: Long-term SWR-associated spiking dynamics during memory retention. (A) Ripple length preference (RLP) of spiking in the memory (top) and non-memory (bottom) tasks. Short and long ripple thresholds are defined as one standard deviation below or above the mean, respectively. These values amounted to 304 ms and 575 ms. **(B)** Quantification of RLP as the area under curve (AUC) below (top) and above (bottom) the respective thresholds from panel **A**. Data from the memory task are summarized by the teal histograms, while the non-memory task data are summarized by the gray shaded histograms. The vertical lines are the medians. **(C)** Variability of RLP expressed as the coefficient of variation. Color coding same as in (B). **(D)** The empirical probability distributions of spiking in SWRs of various durations (left), and post-hoc comparisons (95% confidence intervals) after a Kruskall-Wallis test (right). G: Goal cells, N: non-goal cells, O: Cells with no place field in behavior. **(E)** RLP of pairwise firing in the memory (top) and non-memory (bottom) tasks. **(F)** Quantification of pairwise RLP, similar to (B). **(G)** Coactivity re-expression index (i.e., correlation between pairs of correlation matrices obtained from SAMPLE and 30-minute long bins of MID epoch).

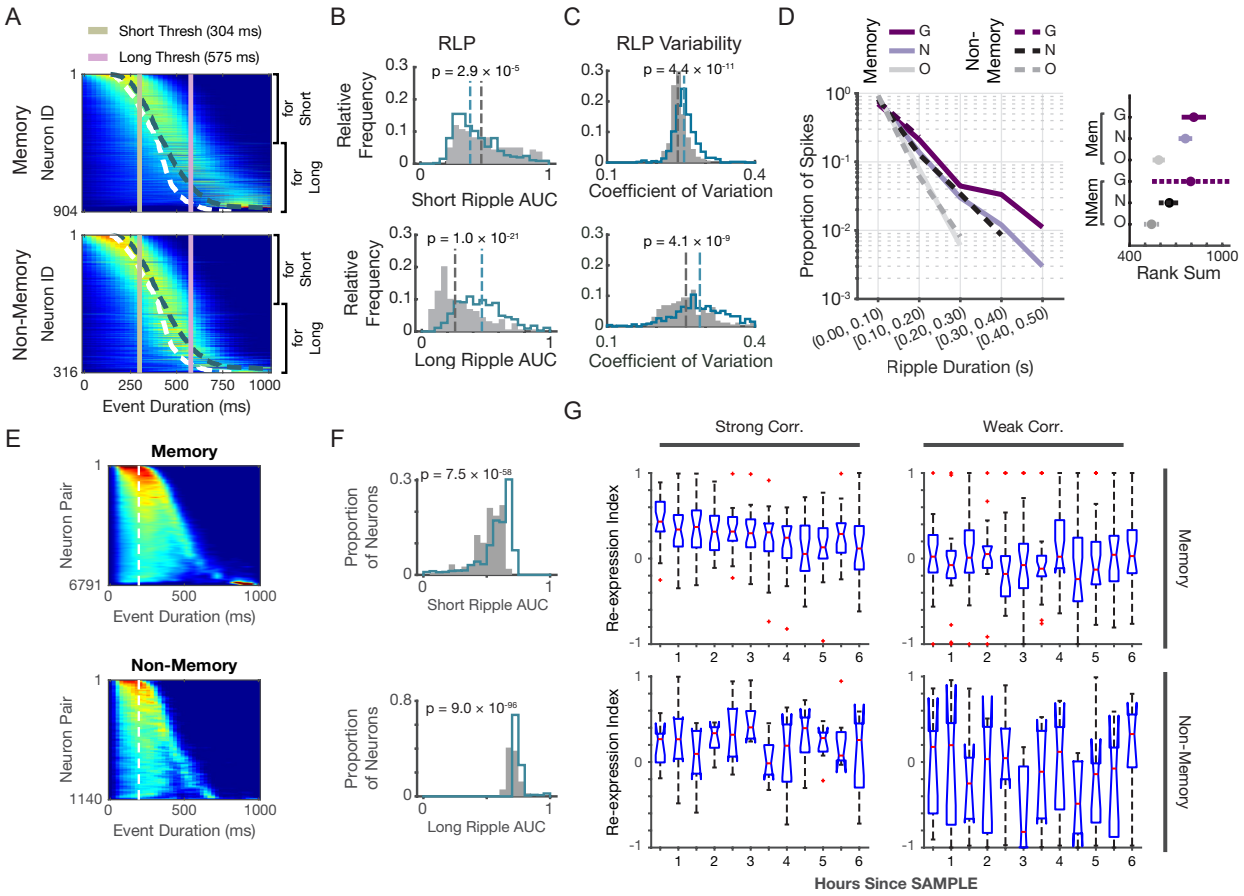
A
Short Thresh (304 ms)
Long Thresh (575 ms)
Memory
Neuron ID
Non-Memory
Neuron ID
for Short
for Long
Event Duration (ms)
B
RLP
Relative Frequency
p = 2.9 × 10-5
Short Ripple AUC
p = 1.0 × 10-21
Long Ripple AUC
C
RLP Variability
p = 4.4 × 10-11
Coefficient of Variation
p = 4.1 × 10-9
Coefficient of Variation
D
Memory
Non-Memory
G
N
O
Proportion of Spikes
Ripple Duration (s)
Mem
NMem
Rank Sum
E
Memory
Non-Memory
Neuron Pair
Event Duration (ms)
F
Proportion of Neurons
p = 7.5 × 10-58
Short Ripple AUC
p = 9.0 × 10-96
Long Ripple AUC
G
Strong Corr.
Weak Corr.
Re-expression Index
Memory
Non-Memory
Hours Since SAMPLE

length, we wondered whether ripple-specific spiking might play a role in weakening or strengthening relative spiking dynamics between cell pairs. We thus asked to what extent the correlated firing found in the SAMPLE epoch was re-expressed within the ripple events after the SAMPLE epoch was over. We computed the similarity between the correlation matrices obtained in SAMPLE and from the ripple-specific spiking in MID sleep. Strong SAMPLE correlation between pairs of cells' spike trains were re-expressed during SWRs for the entire six hour duration of MID sleep (Figure 1.6G), but was heightened preferentially in the memory task (three factor ANOVA with task, correlation strength, and time as factors; correlation strength, memory: 0.245 vs. non-memory: -0.051, $p = 7.3 \times 10^{-6}$; task, memory: 0.125 vs. non-memory: 0.016, $p = 0.0021$). Interestingly, these correlations continued to be re-expressed even after the animals had been tested (in the POST rest session) in the memory, but not non-memory, task (Figure 1S.6). Taken together, these observations hint at the idea that neural dynamics are altered in important ways specifically in long ripple events during hours-long memory retention periods.

Discussion

Hippocampal function is marked by highly spatially selective firing of individual neurons. We studied the reorganization of hippocampal representations for up to 8 hours while rats performed one of two tasks, one involving the encoding, retention, and retrieval of a spatial goal location and the other matching the behavioral variables of the first task without the task memory-dependent elements. Motivated by verifying whether memory engagement alter the profile of code reorganization for future behaviorally relevant navigation, we found, surprisingly, that in fact the hippocampal population reorganized *more* than expected from passive exploration of the environment. We demonstrated that this code "instability" is detrimental for the decoding of spatial information conveyed by hippocampal activity because after many hours the

correspondence between spatially selective firing and external variables was less precise. We next sought to elucidate what dynamics would permit the hippocampus to continue to support memory-based task performance despite this apparent reorganization. Pairwise correlation analyses of spatial and temporal co-firing of cell pairs illustrated the heterogeneous dynamics of hippocampal reorganization: strong spatial correlations were reduced, while strong temporal correlations were retained. These strong temporal correlations were re-expressed in the sharp-wave ripples of the rest period between learning and testing and continued past testing in the memory task alone. Spiking was also biased to manifest in long duration SWRs in the memory task.

Ziv *et al.* (2013) have shown that the remaining overlap among active hippocampal populations across many days is informative as to the spatial position of an animal on a linear track. Thus, based on this one could argue that the degraded decoder performance at TEST in our experiments would be inconsequential in the brain. However, there are two major differences between this study and ours. First, in the Ziv et al. study a linear track was used to investigate long-term hippocampal dynamics. In our tasks the environment consisted of an 8-arm radial maze that spanned a two-dimensional space. On the eight arms of the maze neuronal firing was direction selective as would be expected when the rats' trajectories are stereotyped (McNaughton *et al.*, 1983). In the stem area of our maze (the center platform), the travel direction of the rats was not restricted. These topological and geometrical differences may result in different spatial coding properties in the hippocampus. Perhaps more importantly, the second difference between our design and that in the Ziv et al. study was that one group of rats in our experiments performed a spatial memory task in which they were required to learn a new goal location each day and remember it until testing six hours later. In fact, one of our major findings was that

memory task performance *further reduced* the accuracy of hippocampal representations. We monitored neural activity for during behavioral epochs separated by only six hours. It is conceivable that over much longer time periods of days or weeks, the hippocampal representations might undergo much more drastic reorganization, which would further undermine the decoding accuracy of a downstream readout. Because this would happen over a slow enough time-course, it could be accompanied by concomitant recalibration of cortical circuits that receive spatial information from the hippocampus. This could act as a remedy to ensure stable memories. However, these ideas remain to be tested in the future.

The higher order correlation structure of neural networks likely represents the smallest computational units in the brain (Harris, Csicsvari, Hirase, Dragoi, & Buzsáki, 2003). We observed that pairwise spatial firing correlations were reduced specifically in cell pairs that started out with significant co-firing. In particular, this occurred at an exaggerated rate in the memory task compared to the non-memory task. On the other hand, temporal correlations between cell pairs were differentially modulated for strong and weak pairwise correlations, but in a similar quantitative manner in both tasks. Whereas weak correlations were selectively eliminated between learning and testing, strongly correlated temporal firing of cell pairs was selectively retained. This was particularly interesting in relation to SWR-associated spiking wherein cell pairs that were strongly correlated in learning, were selectively re-expressed for the duration of the rest session. Although this co-firing re-expression in SWRs was statistically significant in both tasks, it was markedly more pronounced in the memory task (Figure 1.6G). Previous studies have suggested that sharp-wave ripples work to stabilize hippocampal codes (Roux *et al.*, 2017), and as such our results are consistent with these reports. The selective exclusion of weakly correlated cell pairs from sharp-wave ripples could be either due to a lack of

statistical power in our study or because these correlations are in fact rapidly eliminated early on in SWRs of MID sleep. Corroborating this is work that shows that in slice preparations sharp-wave ripples can actively diminish and eliminated synapses (Norimoto *et al.*, 2018). Mediated by phase precession (Skaggs *et al.*, 1996), Strongly correlated cell pairs, on the other hand, may be "tagged" through precisely organized spike timing during theta states (Sanders *et al.*, 2015). We further saw that goal-selective cells exhibited indirect markers of high excitability as well as a higher propensity to participate in SWRs, which is consistent with previous reports (Mizunuma *et al.*, 2014). These results also shed light onto an important, previously unanswered (Buzsáki, 2015) question of the determinants of cell participation in sharp wave ripple-associated firing in support of memory task performance.

Goal overrepresentation has previously been shown to occur when a behaviorally relevant location is defined in the environment (Dupret *et al.*, 2010; Fyhn *et al.*, 2002; Hok *et al.*, 2007). Goal overrepresentation can be promoted by dopaminergic inputs as rats receive a reward on the goal arm (McNamara *et al.*, 2014). However, in our task this is unlikely as the goal arm was already overrepresented in the very first trial each day (trial S0). Goal selective cells likely did not became selective for the goal arm due to repeated visits to the same arm as overrepresentation was evident in the non-memory task (fig 1.3C-D) where the baited arm changed in each SAMPLE trial. A more likely origin of such overrepresentation is probably by excitability. There is a rich literature on the mechanisms of memory allocation that proposes that cAMP response element binding protein (CREB)-mediated excitability determines competitive cell responses to new incoming stimuli (Josselyn & Tonegawa, 2020; Rogerson *et al.*, 2014; Silva *et al.*, 2009). This is a potential explanation for why in the non-memory version of our task the rats seemed to show traces of memory of the goal arm (arm presented in trial S0) when tested

30 minutes after learning (Figure 1S.1A). The same set of rats were not biased to visit the goal arm after six hours (Figure 1.1B), suggesting that excitable cells rapidly acquire the memory of a location upon the first visit, compatible with the one-short learning requirements of episodic memory.

Once neurons are recruited to represent a location, they could help the rat solve the memory-guided navigation problem in two ways. First, these cells directly draw the animal to highly valued locations. Recent in vivo experiments bolster this view by showing that targeted stimulation of place cells can bias behavior toward their specific place fields (Robinson *et al.*, 2020). The overrepresentation ensures that the bias force generated by the goal-representing cells overrides the bias that could originate from cells representing other locations. In addition, goal-selective cells can bias the content of awake replay events which have been shown to be instrumental in guiding ongoing decision making during behavior (Jadhav *et al.*, 2012; Pfeiffer & Foster, 2013). The second way in which goal-selective cells can support memory performance is by coordinating the response of the rest of the network. We showed that non-goal selective cells that co-fire with goal selective cells had a higher probability of displaying stronger correlations (Figure 1.4L, insets). In the spatial domain, the same pattern was observed: correlations between goal-selective and non-goal selective cells were better retained than between two non-goal-selective pairs (Figure 1.4C). Thus, arguments presented above regarding the mechanisms by which excitable, goal-selective cells can guide behavior would be applicable to the non-goal selective cells.

The picture that emerges suggests the following model. A goal location is encoded in the excitable cell population, aided by dopamine when the goal is associated with a reward, as was the case in our memory task. Because of our task design (goal location visited on first trial, S0)

the confluence of reward, first visit, and prior knowledge about the goal location being the first arm that's visited each day, learning can take place very rapidly (in as few as 5 trials). Memory traces acquired are then further potentiated on subsequent visits and retained for many hours only if they can inform future behavior. If so, offline processing during SWR-associated firing promotes the stability of recently acquired traces. Cells that represent locations other than the goal arm are selectively weakened both in terms of their spatial and temporal correlations. Because of the natural fluctuations in excitability each day (Cai *et al.*, 2016), memory traces do not necessarily interference as the identity of goal selective cells changes from day to day. These results shed light on the question of how memory can be retained in a stable way despite time-dependent changes in the spatial coding of the hippocampal population. Future studies should investigate how precisely the memory traces encoded in the CA1 population are read out in downstream areas. Ideally, the exact targets of goal-selective and non-goal selective cells can be identified and simultaneously studied in a memory task.

Methods

Experimental Procedures

Approvals

All experimental procedures were approved by the Institutional Animal Care and Use Committee at the University of California, San Diego, and conducted at the University of California, San Diego according to National Institutes of Health guidelines.

Subjects and surgeries

Thirteen experimentally naive, male Long-Evans rats weighing between 250 g and 350 g were food restricted and maintained at ~85%-90% of their *ad libitum* weight. The rats were randomly assigned to the memory (N = 9) or non-memory (control; N = 4) tasks and pre-trained for 3 to 27 days on an 8-arm radial maze. Food was made available *ad libitum* two to three days prior to the rats. The animals were then implanted with hyperdrives containing 14 individually movable tetrodes over the right hippocampus targeted at AP: -4.0 mm, ML: +2.8 to +3.0 mm (from bregma). Otherwise, surgeries followed the procedures previously published (Sabariego *et al.*, 2019). Rats were housed individually on a reversed 12 h light/dark cycle, with behavioral testing and recording sessions performed in the dark phase of the light-dark cycle.

Behavioral task and apparatus

Over the course of three to five weeks following implantation, the tetrodes were advanced to the principal cell layers of CA1. After seven days of postop recovery, subjects were once again food deprived to 85%-90% of their baseline weight, and trained to run on the maze for sugar pellet rewards. An 8-arm radial maze (189 cm in diameter; 11.4 cm wide arms; octagonal stem with a circumradius of 13.75 cm) was used to habituate, train, and test the rats.

At the end of each arm (at ~90 cm radius from the center), a small (5 cm diameter, 2.5 cm tall) black cup was affixed to the maze with Velcro to hold the sugar pellet rewards. Each arm of the maze was independently controllable by the experimenter to be in one of two positions: lowered or raised. In the lowered position, an arm would be completely detached from the stem and inaccessible to the rat.

Each experimental session consisted of 5 recording epochs in the following order: PRE, SAMPLE, MID, TEST, POST. The PRE, MID, and POST epochs were rest periods during which the animals were placed in a Plexiglas box in a different room than the behavioral testing was performed, and allowed to rest for 30 minutes, 6 hours, and 30 minutes, respectively. Unlimited water was available to the rats during the rest epochs. The behavior took place in the SAMPLE and TEST epochs. To start the SAMPLE epoch, a rat was brought to the experiment room and placed in a pedestal that was separated from the 8-arm maze by a black curtain. Before the start of each trial within SAMPLE the maze surface was wiped with 70% EtOH and the appropriate goal reward cup was baited with 15-20 (45 mg) or 45-60 (20 mg) sugar pellets. In each trial, a new set of three additional (randomly chosen) cups were baited with only 2 (45 mg) or 5 (20 mg) sugar pellets to incentivize the rats to explore the maze. Before the start of each trial and after wiping and baiting, all maze arms were lowered and the rat was placed on the stem of the maze. For trial S0, only the day's goal arm was raised (i.e., made accessible to the rat). Rats typically ran down the arm to consume the reward as soon as the arm was raised. Once they finished consuming the reward, they turned around and return to the stem at which point they were removed from the maze and placed in the pedestal again. For subsequent trials (S1 to S5), the same procedure was repeated for the rats in the memory task group, except instead of one arm, all eight arms were simultaneously raised at the start of each trial and the rat was given 2-3

minutes to freely explore the maze to maximize spatial sampling. In three sessions (from two rats) only four trials after S0 (i.e., S1-S4) were recorded. For the TEST epoch, the same protocol was used except the rats were allowed to explore the maze for up to 10 minutes. For the non-memory task rats, the only difference was that the arm with the large reward was randomly chosen per trial (both for trials S1-S5 and at TEST). For two rats doing the memory task, and in three sessions from two non-memory task rats, the TEST epoch was executed exactly like trials S1-S5.

Neural recordings

Neural data were collected using the Neuralynx Cheetah data acquisition system. During recording, the position of the animal's head was tracked with an overhead camera recording the position of a diode array on the headstage preamplifiers. Spike data were recorded relative to a reference tetrode left the cortex, sampled at 32 kHz, digitally filtered between 600 Hz and 6 kHz, and threshold crossing events as well as the spike waveforms were saved to disk. Local field potentials (LFPs) were sampled at 2 kHz and digitally filtered between 0.5 Hz and 900 Hz.

Putative single neurons were identified by clustering spikes in MClust (A. David Redish, University of Minnesota) using peak amplitude, peak-to-valley distance, and energy (i.e., sum of squared amplitudes of waveform samples) features. Each cluster was manually assigned a "quality score" between 1 and 5, with a score of 5 representing an excellent cluster with no "noise", well separated from the rest of the threshold-crossing events. In practice, no clusters were assigned a score of 1 (any "cluster" that would have received this score was ignored) while only a handful of clusters had a score of 2. Clusters with a score of 2 were not included in the study. Quantitatively an analysis of variance showed that scores of 3, 4, and 5 had strictly increasing Isolation Distances and strictly decreasing L-Ratios on the log scale, as desired. We

opted to use subjective scores because, compared to quantitative cluster quality metrics (Isolation Distance and L-Ratio), they better accounted for several aspects of neural recordings unique to our study. These included the confirmation of clusters stability over time, high-quality waveforms, distance from multi-unit activity cloud, distance from the high-dimensional identity hyperplane, and accounted for any discrepancies between sleep and behavior firing rates.

Histology and recording site assignment

After the last day of recording, each subject was euthanized with pentobarbital and perfused intracardially with PBS followed by 4% paraformaldehyde in PBS. The brain was post-fixed *in situ* for several hours, after which the tetrodes were retracted and the brain extracted and stored in 30% sucrose in PBS for one or two days until it sank to the bottom of the solution. Coronal sections (30 μm) were taken with a cryostat. All sections were Nissl-stained with cresyl violet. In 2 rats, immunohistochemistry was used to stain for CA2 marker α-actinin as previously described (Mankin *et al.*, 2015). CA2 recording sites were designated as those in which the end of tetrode track overlapped with the CA2 stain or dispersed cytoarchitectural zone characteristic of CA2 (Mankin *et al.*, 2015).

Data analysis

All analyses were carried out using custom software written in Matlab 2018b (Mathworks).

Behavioral performance

Two measures were used to quantify behavioral performance. First, behavioral performance was quantified as the time from the start of the TEST trial to the moment the head of the animal was within the reward zone. Second, the eight arms of the maze were sorted by the

rank of the rats' entry. The rank of entry to the reward arm was used as another measure of behavioral performance. Entry into the arm was defined as traveling at least 35 cm down an arm (measured from the center of the maze).

To estimate chance level performance, a null distribution of visit ranks to each arm was simulated based on the visitation behavior of the animals. During actual behavior, the rats did not choose the arms of the maze randomly; for instance, following a visit they were much less likely to choose the arm from which they had just exited compared to any other arm. To mimic this behavior, the visit behavior was modeled as a distribution describing the probability of each egocentric "turn" (the angle between the arm just exited and the arm taken next). 100,000 trials were simulated as follows. For each simulated trial, first a random arm was chosen from 1 to 8. Next, for a maximum of MAX_VISITS iterations (i.e., trial lengths), an arm was randomly drawn based on the egocentric probability of turns. Various trial lengths were used because the behavioral paradigm did not cap the number of visits a rat could in fact make. While a higher caps would lead to a more accurate estimate of actual chance level performance, because the rats were not allowed to make an unbounded number of visits a cap of 11 was chosen to closely match actual behavior (Figure 1.1B).

Neural data

A subset of recordings with high cell recording yield and good behavioral performance was selected for further analysis.

Spatial firing rate maps (place maps) and estimates of map stability

For each neuron, the number of spikes falling into each 4 cm by 4 cm spatial bin covering the entirety of the maze was counted which was then normalized by the amount of time each bin

was occupied by the animal during behavioral epochs. The normalized spike density was smoothed with a 2 dimensional Gaussian kernel with a standard deviation of 6 cm. Only periods of running (> 2 cm/s) were used to construct place maps. Bins that were not visited are not displayed where place maps are shown in this paper. Importantly, each behavioral session was parsed and separated into four distinct periods: stem running, reward zones, outbound running (from the stem to reward zones), and inbound running (from reward zones to the stem). Thus, each behavioral epoch had four distinct place maps. Throughout the paper only the outbound maps were analyzed, except for position reconstruction in Figure 1.1F where all four maps were used (see below). Several key analyses were replicated with inbound maps with similar results (data not shown).

Place map stability was quantified by taking the correlation coefficient (corrcoef function in Matlab) between the place maps of two neurons, or those of the same neuron across two behavioral epochs. Only neurons with place selectivity in both epochs were included.

Place field definition

Conceptually, a place field was defined as the set of all adjacent pixels in a place map with a peak rate above a given threshold. Specifically, all map pixels with a value above 2 Hz were extracted. A graph representation of suprathreshold pixels was then built with the nodes representing the suprathreshold pixels. Pixels with touching edges and corners were considered adjacent in the graph. Next, for each connected component of the graph, a depth-first search (DFS) was started from the peak node to find all connected nodes that exceeded 20% of the starting node's value. Nodes visited by the DFS were considered a candidate place field. When overlapping fields were discovered, the overlap region was taken to be the final place field. A minimum of 3 and a maximum of 40 bins were required for a place field to be retained. Smaller

and larger fields were discarded. A cell was considered to be place selective in an experimental epoch if it had at least one place field as defined above.

Goal overrepresentation was quantified in two ways. The number of cells with a place field on the goal arm was divided by the total number of simultaneously recorded cells in each session (Figure 1.3A, C) for a by-cell overrepresentation estimate. To account for possible disparities in the number of fields per cell, goal overrepresentation was also estimated by dividing the number of place fields (from any cell) on the goal arm by the total number of place fields in a given trial (from any cell). This gave a by-field estimate of overrepresentation (Figure 1.3A, D). The values in Figure 1.3C, D, I were obtained from individual trials in SAMPLE or TEST.

Position reconstruction

A previously described Bayesian decoder (Pfeiffer & Foster, 2013; Zhang *et al.*, 1998) was used to reconstruct position in Figure 1.1F-G. Non-overlapping windows of 250 ms long were used. The place maps for the four running direction/zones (i.e., reward zones, stem, inbound runs, and outbound runs) were concatenated. In other words, the training data for each session was a 50 x 200 x N matrix of smoothed firing map, where each map was 50 x 50 bins (four maps per cell, concatenated along the second dimension) and N is the number of simultaneously recorded cells in that session. Decoding was done only for bins with at least 5 spikes and 5 active neurons.

To estimate the generalization capacity of the decoder in the SAMPLE epoch, it was trained on trials S1 to S5 with the data from one out of the five trials excluded, and evaluated on the data from the excluded trial (e.g., training on data from S1, S2, S4, and S5; testing on S3).

This resulted in a five-fold leave-one-out cross-validation (LOOCV) scheme. The generalization capacity of the decoder across the SAMPLE and TEST behavioral epochs was quantified by training the decoder on all data from the SAMPLE and evaluating it on TEST data.

Figure 1.1F shows the cumulative distribution of the absolute errors of the decoder. The absolute error was calculated as the Euclidean distance between the position estimate and the actual rat position. The actual position was the position of the rat at the video tracking sample closest in time to the center of the time bin in which position was decoded. To obtain a null distribution for position estimate errors, we shuffled the identity of the cells for each session and performed the decoding as described. The error bars in Figure 1.1F are standard errors of the mean across sessions.

Pairwise correlations

Map pair correlations were calculated as the correlation coefficient between the place maps of pairs of cells with at least one spike in a given behavioral epoch. Autocorrelations were excluded. For spike train correlations, the entirety of the behavioral epochs of interest was divided into 30 ms long bins and the number of spikes within each bin was counted. The spike train correlation was calculated as the correlation coefficient between such spike count vectors for pairs of cells. Statistically significant ($p < 10^{-4}$) spike correlation values between 0 and 0.05 were considered weak; those greater than 0.05 were considered strong.

Quantifying QQ-plots

To quantify how the distribution of strong and weak spike train correlations compared across SAMPLE and TEST epochs, the shape of the QQ-plots was quantified via two techniques. First, a linear regression model was fit the QQ-plot points between 0 and 0.01 on the horizontal

axis. The difference between the slope of the regression model and the expected distribution line in the QQ-plot (red dashed line) was taken to indicate the “squishing” of the weak correlations. Second, the average sum of the square deviation between the QQ-plot points and the expected distribution line (red dashed line) was taken to indicate the skewing of extreme SAMPLE values at TEST. For this measure, only points with a SAMPLE value of at least 0.05 were used.

Goal and non-goal cells

Cells with at least one place field on the goal arm at SAMPLE were considered goal cells. Cells with at least one place field on an arm other than the goal arm, but no fields on the goal arm, were considered non-goal cells. In the non-memory task, the goal arm was defined as the arm visited in trial S0. This would ensure that the novelty factor of a large reward at the beginning of an experimental session was similar across the two tasks.

Baseline firing rate estimation

The baseline firing rate in PRE (Figure 1.3G) was calculated simply as the total number of spikes divided by the total length of the PRE epoch in which the cell was recorded.

SWR detection

LFPs from all tetrodes were filtered between 150–250 Hz and the average of the envelope of the filtered signal (computed via a Hilbert transform) was taken. The resulting signal was then smoothed with a Gaussian kernel ($\sigma = 12.5$ ms). Periods when the signal exceeded 1 s.d. of the recording epoch mean for at least 40 ms, during which the signal amplitude reached at least 3 s.d. were identified. In addition, multi-unit activity (MUA) periods exceeding 3 s.d. above mean MUA rate were marked. Ripple periods were defined as such MUA periods that had an overlap with the strong 150-250 Hz LFP periods as described above (Csicsvari & Dupret, 2014).

Ripple length preference

First, the spikes of each cell falling within a ripple event were identified. Next, the deviation from the expected number of spikes in each of 40 time bins from 0 to 1 second (bin width of 25 ms) was quantified as the ratio of the (discrete) probability mass functions of spike ripple length and ripple incidence for each temporal bin. Prior to computing the quotient, the probability mass functions were linearly smoothed with a kernel of 75 ms. The resulting ratios quantified whether the length distribution of the ripples in which the spikes of a given cell occurred followed the overall distribution of ripple lengths, and if not how it deviated from the "expected" distribution. This approach also accounted for any disparities between firing rates and ripple incidence across cells and sessions. The panels in Figure 1.6A-B show the smoothed (kernel: 100 ms) probability-normalized such discrete ratios (normalization done row-wise). To increase the signal-to-noise ratio of the estimates, cell that spiked in 10 or fewer ripple events were excluded.

To quantify the differences between ripple length preference (RLP) for short and long ripples across the two tasks, the area under curve of the normalized ratios was calculated for time bins less than 1 s.d. below and 1 s.d. above the mean, respectively. Figure 1.6B shows the distribution of total mass falling to the left ("Short Ripple Mass") and right ("Long Ripple Mass") of the cutoffs. To quantify the specificity of RLPs, the coefficient of variation for the top and bottom halves of the RLPs were calculated from Figure 1.6A and plotted in Figure 1.6C.

Statistics

All statistical tests were two-sided at $\alpha = 0.05$ unless otherwise noted. When the assumptions of parametric tests were not violated, parametric tests were used; otherwise, an appropriate non-parametric test was applied. The Anderson-Darling and F tests were used to

evaluate whether assumptions of normality and homoscedasticity were met, respectively. Effect size was calculated as Cohen's d defined as follows:

$$d = \frac{\overline{x_1} - \overline{x_2}}{s}$$

where $\overline{x_i}$ is the sample mean for group i and s is the pooled variance calculated as

$$s = \sqrt{\frac{(n_1 - 1)s_1^2 + (n_2 - 1)s_2^2}{n_1 + n_2 - 2}}$$

with s_i^2 being the sample variance for group i.

Code availability

All custom-written code is available upon reasonable request to jleutgeb@ucsd.edu.

Acknowledgements

Chapter 1, in full, is material that is unpublished and coauthored by Ahmadi, S, Leutgeb, S, and Leutgeb, JK. The dissertation author was the primary investigator and author of this material.

Appendix 1.1: Supplementary figures

Figure 1S.1: Rats remember the S0 arm and return to it better than expected by chance in both tasks. **A, (Left)** Because an F-test rejected the null hypothesis of equal variances between the two groups ($F_{44,18}$ = 0.4658, p = 0.040), we compared the time-to-reward measure of performance with Wilcoxon's rank sum test, which did not reveal a difference between the tasks (rank sum = 1351, z = -1.631, p = 0.1029). **(Center)** Performance, as measured by the median rank of entry to the S0 arm at TEST, was different between the two tasks (rank sum = 1315, z = -2.2582 p = 0.0239). **(Right)** However, the performance in the non-memory task was better than chance as compared with simulation data (see Methods). **B,** The probability of egocentric turns at the end of an inbound run was not uniform. These probabilities were used to simulated random-choice performance for a fair evaluation of the rats' memory of the target arm. All data are from the same rats used for the results reported in the main text.

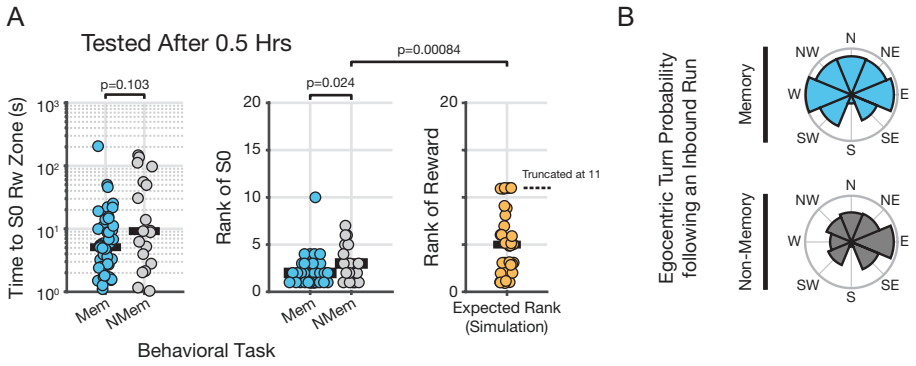
A
Tested After 0.5 Hrs
p=0.00084
p=0.103
p=0.024
Time to S0 Rw Zone (s)
Rank of S0
Rank of Reward
Truncated at 11
Mem
NMem
Expected Rank
(Simulation)
Behavioral Task
B
Egocentric Turn Probability
following an Inbound Run
Memory
Non-Memory
N
NE
E
SE
S
SW
W
NW

Figure 1S.2: Spatial map and spike train pairwise correlations provide distinct information about hippocampal dynamics. Correlation between measures of spatial and temporal co-firing in the memory (left) and non-memory (right) tasks are shown. The absence of a linear relationship suggests that the two analysis methods reveal different information about neural computations in our tasks.

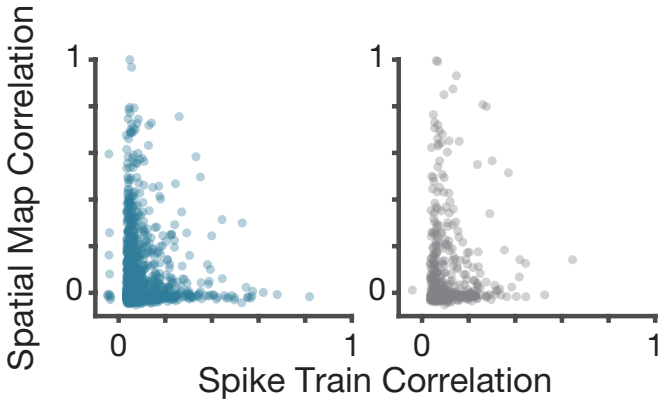
Spatial Map Correlation
1
0
0
1
1
0
0
1
Spike Train Correlation

Figure 1S.3: Place map correlation strength depends on the goal-selectivity of the cell pairs. Top: In the memory task, place map correlation strengths decrease from the strongest to the weakest between two goal cells, one non-goal and one goal-cell, and two non-goal cells. Bottom: A similar pattern is observed in the non-memory task. Multiple comparison results following Kruskal-Wallis tests are displayed ($p < 10^{-80}$ in each panel). The horizontal lines are 99% confidence intervals. Thus, the lack of overlap indicates a statistical difference between the values after post-hoc tests.

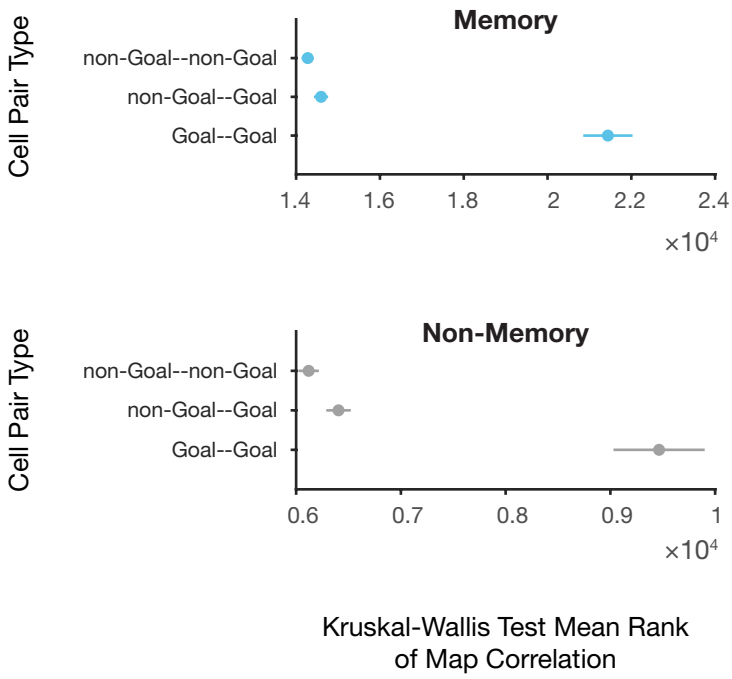
Memory
Cell Pair Type
non-Goal--non-Goal
non-Goal--Goal
Goal--Goal
1.4
1.6
1.8
2
2.2
2.4
×10^4
Non-Memory
Cell Pair Type
non-Goal--non-Goal
non-Goal--Goal
Goal--Goal
0.6
0.7
0.8
0.9
1
×10^4
Kruskal-Wallis Test Mean Rank
of Map Correlation

Figure 1S.4: Quantitative changes in spatial co-firing of cells grouped by place selectivity. The difference between pairwise spatial map correlations at SAMPLE and TEST are shown for pairs with both members being non-goal selective (A), one member being goal selective and the other non-goal selective (B), and both goal selective (C). Data from the memory and non-memory tasks are plotted in blue and gray, respectively. In addition, in the three columns to the right, the changes are shown separately for pairs with low ($r < 0.1$), moderate ($0.1 < r < 0.4$), or high ($r > 0.4$) initial (i.e., SAMPLE) place co-firing.

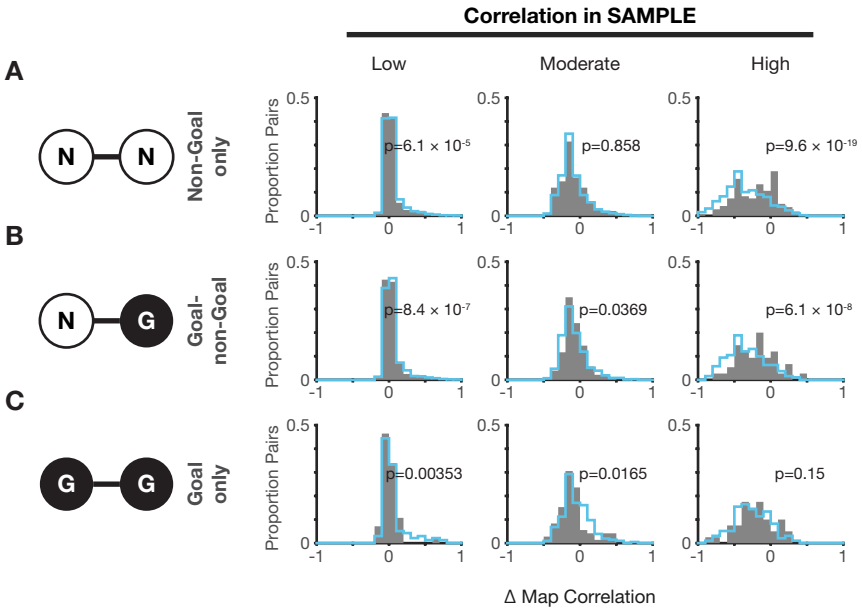
Correlation in SAMPLE
Low
Moderate
High
A
N
N
Non-Goal only
B
N
G
Goal-non-Goal
C
G
G
Goal only
Proportion Pairs
p=6.1 × 10-5
p=0.858
p=9.6 × 10-19
p=8.4 × 10-7
p=0.0369
p=6.1 × 10-8
p=0.00353
p=0.0165
p=0.15
0.5
0
-1
0
1
Δ Map Correlation

Figure 1S.5: Three-factor ANOVA results for the spike train interactions between the goal selective and non-goal selective populations. (A) Post-hoc comparisons of groups with 99% confidence intervals displayed. **(B)** ANOVA table. Variables are follows: Task: {MEM, NMEM}, CorrStrength: {STRONG, WEAK}, S0_PF: {GOAL, NONGOAL}.

A

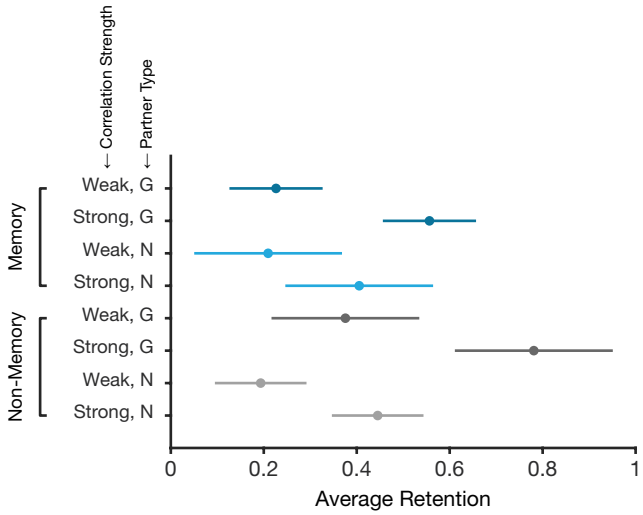

B

3-Way Analysis of Variance

Source	Sum Sq.	d.f.	Mean Sq.	F	Prob>F
Task	0.1949	1	0.1949	4.03	0.047
CorrStrength	2.22698	1	2.22698	46.01	0
S0_PF	0.74929	1	0.74929	15.48	0.0001
Task*CorrStrength	0.00061	1	0.00061	0.01	0.9106
Task*S0_PF	0.25147	1	0.25147	5.2	0.0244
CorrStrength*S0_PF	0.13174	1	0.13174	2.72	0.1016
Task*CorrStrength*S0_PF	0.0273	1	0.0273	0.56	0.4541
Error	5.85659	121	0.0484		
Total	9.60542	128			

Figure 1S.6: Re-expression of behavioral coactivations continues throughout the experimental session preferentially in the memory task. (Left) Re-expression index is high for strongly co-firing pairs early in the MID sleep epoch (EM) and continues to the rest epoch after testing (POST) only in the memory task. **(Right)** Weak co-firing of pairs is not re-expressed in sleep in the memory task but marginal re-expression is detected in the initial portion of MID sleep (EM) in the non-memory task. Red crosses are outliers (1.5 times mid-quartile interval). * $p < 0.05$, *** $p < 0.001$, **** $p < 0.0001$.

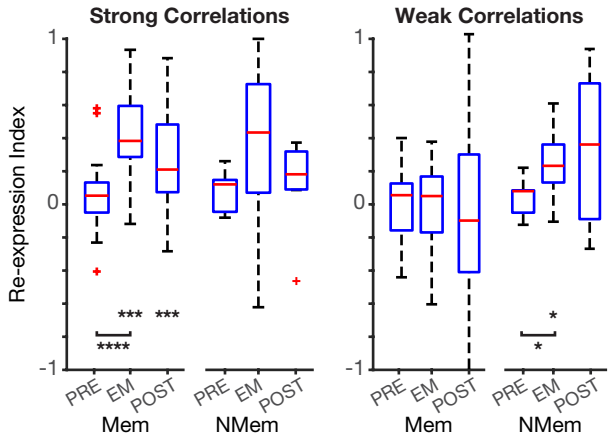
Strong Correlations
Weak Correlations
Re-expression Index
1
0
-1
***
***
****
*
*
PRE
EM
POST
Mem
NMem

CHAPTER 2: Distinct roles of dentate gyrus and medial entorhinal cortex inputs for phase precession and temporal correlations in hippocampal CA3 place cells

Abstract

The CA3 recurrent circuit is a hippocampal subregion known to support memory consolidation and route planning by the activation of stored sequences of neurons organized during experience. The precise temporal firing patterns of CA3 ensembles during behavior is evident in the relationship of spike timing to the local theta oscillation, which is characterized by phase precession of spikes. Although this computation is thought to be critical for building behavioral sequences during learning, the origins of its computation are unknown. By assessing CA3 network activity in the absence of each of its theta modulated excitatory inputs, the dentate gyrus (DG) and the medial entorhinal cortex (MEC), we show necessary and unique contributions of each region. The DG-CA3 circuit is essential for organizing the temporal order of compressed behavioral sequences, by promoting the expression of prospective “look-ahead” spiking during theta states, whereas the MEC modulates the gain of excitation. We propose a simple computational model that accounts for this double dissociation where the two feedforward pathways exert differential effects on inhibitory subnetworks. DG inputs affect the phase and MEC inputs affect the amplitude of the inhibitory theta signal. Our results thus describe the circuit mechanisms that contribute to the generation of sequence coding in the CA3 recurrent circuit.

Introduction

Although the hippocampus and the timing of its neuronal activity have long been recognized as critical for episodic memory and spatial navigation (Buzsáki & Moser, 2013; Squire, 1992), many of the underlying computations within hippocampal circuits are not described at a level of detail to understand how these functions are supported. In particular, the hippocampal CA3 area is thought to be a key hub for autoassociative and sequence computations because of its recurrent connectivity and the integration of inputs from two major excitatory pathways (Hopfield, 1982; Marr, 1971; McNaughton & Morris, 1987). The inputs originate from the medial entorhinal cortex (MEC), which synapse onto the distal apical dendrites of CA3 pyramidal cells, and from the dentate gyrus (DG), which make highly potent synapses on proximal dendrites (Amaral & Witter, 1989) that enable single granule cells to drive CA3 spiking (Henze *et al.*, 2002). In theory, such specialized connectivity can provide the DG-CA3 circuitry with a means to determine which patterns received through the perforant pathway are selected for encoding (Romani & Tsodyks, 2015; Treves & Rolls, 1992).

A prerequisite for encoding sequences is that they are organized in the correct temporal order, but compressed in time compared to a behavioral sequence. Sequence compression is thought to be supported by phase precession, which entails that the spiking of principal cells systematically advances from late to early over successive cycles of the 6-10 Hz theta rhythm as an animal traverses the spatial receptive field of place cells in rats (O'Keefe & Recce, 1993; Skaggs *et al.*, 1996). The remarkable temporal organization of single-cell phase precession implies that multiple place cells fire in a temporal order within each theta cycle that matching the behavioral-scale order in which their place fields are visited (Dragoi & Buzsáki, 2006; Foster & Wilson, 2007). Sequences so established are called theta sequences. The time differences that are

generated between pairs of cells by precise theta-scale spike timing are such that long-term potentiation between synapses may be facilitated to store sequence information (McNaughton & Morris, 1987; Mizuseki *et al.*, 2009). Thus, phase precession can play an instrumental role in producing appropriate sequences and selection of memory items for storage, although the network mechanisms of its generation remain poorly understood. Because phase precession is also observed in the medial entorhinal cortex (MEC), it is possible that hippocampus inherits phase precession from MEC through its direct perforant path axons (Hafting *et al.*, 2008; Jaramillo *et al.*, 2014; Schlesiger *et al.*, 2015). If MEC input were to sustain phase precession in the hippocampus, then lesioning the second theta modulated input to CA3, namely DG, should not interfere with normal CA3 phase precession. Alternatively, it has been proposed that the DG can support the *de novo* generation of phase precession in CA3 (Thurley *et al.*, 2008; Tsodyks *et al.*, 1996), and as a result ensure the encoding of correct sequences of experienced items in the subsequent processing stages in CA3 and CA1.

A third, possibility is that both DG and MEC inputs are simultaneously required for normal CA3 phase precession. In this case, it would still be possible that the two inputs have distinct, yet complementary, roles in supporting CA3 phase precession. For instance, based on its role in supporting physiological signatures of sequence formation and CA3 prospective firing to distinguish similar items in dentate-dependent task (Drieu *et al.*, 2018; Sasaki *et al.*, 2018; van Dijk & Fenton, 2018), the dentate gyrus could be critical for supporting prospective firing in CA3 during theta states, a mode of firing expressed late in the theta cycle but early in a place field traversal. To complement this, MEC may provide the content of the memory items to be encoded in an all or none manner by the proper timing of its convergent inputs onto the same CA3 pyramidal cell (Lisman & Redish, 2009; Lisman *et al.*, 2005; Treves & Rolls, 1992). In

other words, MEC input may modulate the gain of excitation on CA3 pyramidal cells, while DG input organizes the phase information to support correct sequential ordering of memory items. To test these possibilities, we performed recordings of CA3 cells with either diminished MEC or with diminished DG inputs.

Here, we show that the integrity of the DG-to-CA3 connections, in particular, promote the precise temporal firing of CA3 for phase precession. Surprisingly, we find that the DG-CA3 circuit is both necessary and sufficient for two critical functions. First, it promotes the temporally reliable expression of prospective "look-ahead" spiking during theta states (Hasselmo, Bodelón, & Wyble, 2002; Lisman *et al.*, 2005; Sanders *et al.*, 2015). Second, it supports the theta time-scale spike timing compression of behavioral time-scale sequences. Integrating these experimental findings via computational modeling, we suggest that the *in vivo* results are explained by two distinct feedforward pathways exerting differential effects particularly on their associated inhibitory subnetworks: DG inputs affect the phase, whereas MEC inputs affect the amplitude of the inhibitory theta signal.

Results

To test the role of DG and MEC inputs for CA3 phase precession, single-unit activity in the CA3 region of the rat hippocampus from two previously published datasets (Sabariego *et al.*, 2019; Sasaki *et al.*, 2018) were analyzed. In each of these datasets, CA3 cells were recorded in hippocampus-dependent working memory tasks after lesioning either the dentate granule neurons or the medial entorhinal cortex (Figure 2S.1a,b), and each lesion group was paired with a respective control group (DG lesioned and control: 16 sessions from 9 rats and 7 sessions from 4 rats; MEC lesioned and control: 20 sessions from 8 rats and 18 sessions from 7 rats). Because our analysis was focused on the precise timing of neuronal activity over a series of theta cycles,

we began by selecting periods of 5 or more spikes that occurred within spike intervals of less than 500 ms and while animals were moving and theta oscillations are thus likely to occur (Figure 2S.1c). Because rat trajectory shape and spatial coverage in the working memory tasks were irregular, we used spike train analysis to avoid systematic errors in estimating the extent of place fields or extracting spikes from individual place field traversals. Along with identifying spike trains, we identified the corresponding behavioral characteristics, such as running speed and distance travelled (see Methods; Figure 2S.1d). We confirmed that a sufficient proportion of all recorded spikes (29.2% in control and 15.9% in lesion data sets) were assigned to some train (Figure 2S.2a). While this method of defining periods of increased spiking focuses on temporal, not on spatial characteristics, the analyzed trains of both datasets gave rise to similar standard spatial coding characteristics (Figure 2S.2b-h). Using spike trains, we then investigated the dynamics of phase precession in each data set to gain insight into the contributions to CA3 temporal firing patterns.

DG granule cell input is necessary for the expression of phase precession in downstream CA3 neurons

Although it has long been known that there is substantial phase precession in DG cells (Skaggs *et al.*, 1996), it has not been clear whether DG inputs are necessary for phase precession in its direct target cells in CA3. We therefore compared phase precession between CA3 cells that were recorded in DG-lesioned and control animals in rats that were trained to perform a dentate-dependent radial 8-arm maze task (Table 2S.1) (Sasaki *et al.*, 2018). We began by determining the level of phase precession in control CA3 cells. We plotted theta phase of all spikes of qualifying trains of a cell against the distance that the animal travelled from the beginning to the end of each train ("slope-by-cell" analysis). In control CA3 cells, phase precession was evident

in the negative circular-linear regression slope (Figure 2.1a). In rats with DG lesions, substantial loss of mossy fiber innervation has previously been confirmed for all recording sites that are included in the analysis, and the extent of DG granule cell loss was previously quantified by a measure between 0 and 4, 0 indicating the complete absence of TIMM staining, and 4 indicating control TIMM stain intensity (Sasaki *et al.*, 2018). Here, we included cells from all recordings at sites with partial or complete mossy fiber loss (scores 0, 1, and 2) as a separate analysis of tetrodes in each score category was not possible to due small N. In CA3 cells recorded from tetrodes with reduced mossy fiber input, phase precession was less apparent and more variable than in controls (Figure 2.1b). In the slope-by-cell analysis, the median circular-linear regression slope value was -149.4° for the control cells which was less than 0° (Figure 2.1c; Sign Rank test; z-value = -6.19, signed rank = 396, $p = 2.96 \times 10^{-10}$). The median slope of cells from the DG-lesioned animals was -79.2°, which was also less than zero (Figure 2.1c; Sign Rank test; z-value = -2.63, signed rank = 742, $p = 0.0043$), but less negative than in controls (Figure 2.1c; Wilcoxon's rank sum test; z-value = -3.63, rank sum = 5446, $p = 2.84 \times 10^{-4}$). In addition, a lower proportion of CA3 cells in lesioned rats displayed phase precession (88.1% versus 69.1% in $CTRL^{(DG)}$ and $LESION^{(DG)}$, respectively; χ^2 test for proportions, χ^2 test statistic = 8.34, $p = 0.0039$). This trend was preserved when only negative slopes that were statistically significant were considered (Figure 2.1c, shaded bars; 61.9% versus 38.2% in $CTRL^{(DG)}$ and $LESION^{(DG)}$, respectively; χ^2 test for proportions, χ^2 test statistic = 8.47, $p = 0.0037$).

To reveal any remaining phase precession that might have been masked by trains without phase precession, we re-ran the circular-linear regression on the pool of trains with significant single-train phase precession (Figure 2.1d). This analysis too indicated impaired phase precession in lesioned rats (Figure 2.1d, left; $CTRL^{(DG)}$ less than zero: z-value = -6.17, signed

Figure 2.1: Dentate granule cell input is required for intact phase precession in CA3. a, Examples of intact phase precession in CA3 cells. Left, schematic of the circuitry of interest with the major theta-modulated excitatory inputs to CA3. Right, spike trains and session phase-position plots for two example CA3 cell. Solid magenta lines indicate significant phase precession ($p < 0.05$). The example train is highlighted in red. 1 cycle = 360°. **b**, Data presented as in panel **a**, for cells in the DG lesion experiment. Dashed magenta lines indicate no phase precession. **c**, Slope-by-cell analysis (i.e., spikes from all trains of each cell were pooled and a circular-linear regression line was fit to this pool for each cell). Median magnitude of slopes (violin plots) and the proportion of negative slopes (bar plots) are reduced by the DG lesions. Stippled horizontal line over the bar plots indicates chance level (0.05). **d**, When only trains with a significant slope were pooled for each cell, the slopes were significantly less negative for control compared to DG lesioned rats. Organized similar to panel **c**. **e**, Regression slopes for each train in $CTRL^{(DG)}$ (left) and $LESION^{(DG)}$ (right). Each row contains the slope values of one cell's trains, plotted with blue vertical ticks. Rows are sorted from top to bottom by the median value of each cell's slopes, indicated with black ticks when negative, and magenta ticks when positive. The shaded regions mark negative values. **f**, Slope-by-train analysis. Violin plots of the per-cell average train slopes (left). The proportion of the distributions below zero are plotted as bar graphs (right). Organized similar to panel **c**. Scale bars: vertical bars 500 μV, LFP scale bars 250 ms, path scale bars 50 cm.

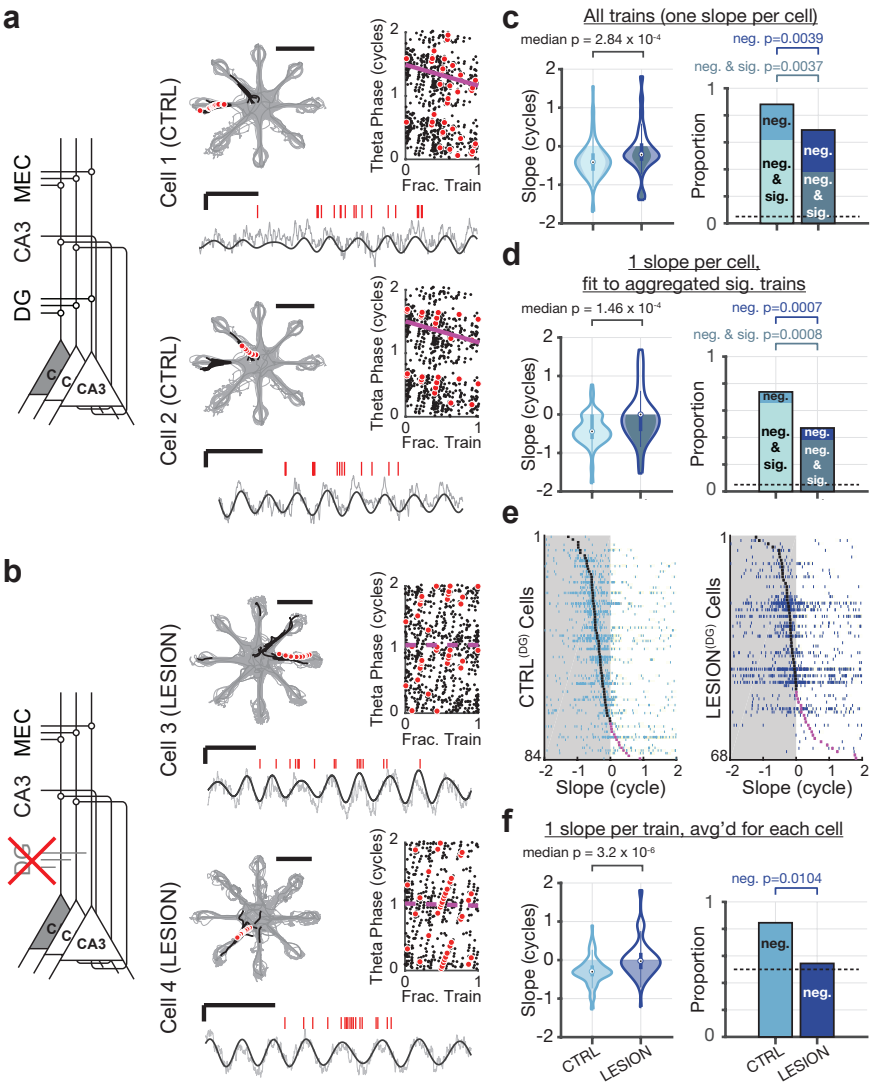
a
MEC
CA3
DG
CA3
Cell 1 (CTRL)
Cell 2 (CTRL)
Theta Phase (cycles)
Frac. Train
b
MEC
CA3
CA3
Cell 3 (LESION)
Cell 4 (LESION)
c
All trains (one slope per cell)
median p = 2.84 x 10-4
neg. p=0.0039
neg. & sig. p=0.0037
Slope (cycles)
Proportion
neg.
neg. & sig.
d
1 slope per cell,
fit to aggregated sig. trains
median p = 1.46 x 10-4
neg. p=0.0007
neg. & sig. p=0.0008
e
CTRL (DG) Cells
LESION (DG) Cells
Slope (cycle)
f
1 slope per train, avg'd for each cell
median p = 3.2 x 10-6
neg. p=0.0104
CTRL
LESION

rank = 151, $p = 3.45 \times 10^{-10}$; $LESION^{(DG)}$: z-value = -1.30, signed rank = 441, $p = 0.0974$; $CTRL^{(DG)}$ vs. $LESION^{(DG)}$: z-value = -3.79, rank sum = 5409, $p = 1.46 \times 10^{-4}$), with a lower proportion of CA3 cells having negative (73.8% versus 47.1% in $CTRL^{(DG)}$ and $LESION^{(DG)}$, respectively; χ^2 test for proportions, χ^2 test statistic = 11.3958, $p = 7.36 \times 10^{-4}$) or significant negative (shaded bars; 65.5% versus 38.2% in $CTRL^{(DG)}$ and $LESION^{(DG)}$, respectively; χ^2 test for proportions, χ^2 test statistic = 11.203, $p = 8.17 \times 10^{-4}$) correlations (Figure 2.1d, right).

Differences between the two groups were also apparent from the distribution of slopes obtained from the circular-linear regression analysis of single train data ("slope-by-train" analysis; Figure 2.1e). For statistical comparison, we averaged the circular-linear slopes of all train's for each cell (Figure 2.1f) and then compared the cell's averages across groups. The median value of cell-averaged slopes was significantly less than zero in control but not DG lesioned rats ($CTRL^{(DG)}$: z-value = -5.942, signed rank = 452, $p = 1.40 \times 10^{-9}$, $LESION^{(DG)}$: z-value = -0.529, signed rank = 1086, $p = 0.299$), with the median of $LESION^{(DG)}$ significantly different from $CTRL^{(DG)}$ (z-value = -4.6597, rank sum = 5168, $p = 3.17 \times 10^{-6}$). Further, the proportion of CA3 cells on the negative end of the distribution was lower in $LESION^{(DG)}$ than $CTRL^{(DG)}$ (χ^2 test statistic = 6.5657, $p = 0.0104$). Taken together, these analyses demonstrate that CA3 phase precession is disrupted when the dentate granule input to CA3 neurons is reduced. In particular, the averaging of single train slopes revealed that the remaining inputs to CA3 after DG lesions, although maintaining minimal phase precession on average, are not sufficient to sustain the reliable, single-train phase precession thought to be required for real-time encoding and retrieval of episodic memories.

MEC inputs to CA3 are also necessary for the expression of phase precession in CA3 neurons

The medial entorhinal cortex is known to be necessary for CA1 phase precession. However, it is not known whether CA3 also requires MEC input to produce phase precession or can generate phase precession together with DG through their reciprocal connections. Thus, we next tested whether DG alone can support CA3 phase precession by analyzing recordings of CA3 cells in MEC-lesioned rats. The MEC lesions were consistent between rats and included 93.0% of the total volume, with damage approximately matched across cell layers (95.3% of layer II, 92.4% of layer III, and 91.4% of deep layers) (Sabariego *et al.*, 2019). We extracted qualifying spike trains recorded in the CA3 of MEC-lesioned animals according to the abovementioned criteria (Table 2S.1). Our slope-by-cell analysis revealed that the CA3 cells of control rats displayed tight, negative correlations between the theta phase and position of the spikes (Figure 2.2a) while correlations were significantly diminished in MEC-lesioned animals (Figure 2.2b). As a population, the median slope shifted from -120.4° per train-length to -66.9° per train-length when the MEC was lesioned (Figure 2.2c; Wilcoxon's rank sum test; z-value = -2.34, rank sum = 11754, $p = 0.0193$). However, both medians were significantly less than zero ($CTRL^{(MEC)}$, z-value = -6.18, signed rank = 750, $p = 3.16 \times 10^{-10}$; $LESION^{(MEC)}$, z-value = -3.6, signed rank = 4204, $p = 1.57 \times 10^{-4}$; Sign tests). The proportion of slope values was significantly lower in the MEC lesioned rats both when all negative slopes (83.2% and 70.3%, $CTRL^{(MEC)}$ vs. $LESION^{(MEC)}$; χ^2 test statistic = 5.52, $p = 0.0188$) and only negative slopes that reached statistical significance (54.4% and 38.6%, $CTRL^{(MEC)}$ vs. $LESION^{(MEC)}$, χ^2 test statistic = 6.26, $p = 0.0124$; χ^2 tests for proportions) were considered. These trends were confirmed in the slope-by-cell analysis of slope values that reached statistics significance (Figure 2.2d; Medians less than zero: $CTRL^{(MEC)}$, z-value = -5.824, signed rank = 423, $p = 2.87 \times 10^{-9}$; $LESION^{(MEC)}$, z-value = -1.863, signed rank = 2766, $p = 0.0312$; Median of $CTRL^{(MEC)}$ vs. $LESION^{(MEC)}$: z-value

Figure 2.2: Medial entorhinal cortical input is required for intact phase precession in CA3. This Figure follows the presentation of Figure 2.1, with data from the MEC lesion experiment. **a-b**, Examples of CA3 phase precession in control (**a**) and MEC-lesioned rats (**b**). Schematics of the circuitry of interest are shown to the left of each panel, with the phase-position plots to the right. Significant phase precession ($p < 0.05$) is indicated with a solid magenta line. Example trains are highlighted in red. **c**, Slope-by-cell analysis. Median magnitude of slopes (violin plots) and the proportion of negative slopes (bar plots) are reduced by the MEC lesions. Stippled horizontal line over the bar plots indicates chance level (0.05). **d**, When instead only trains with a significant slope were pooled for each cell, the slopes were significantly smaller in magnitude for MEC lesioned rats. **e**, Regression slopes for each train in $CTRL^{(MEC)}$ (left) and $LESION^{(MEC)}$ (right) **f**, Slope-by-train analysis. Violin plots of the per-cell average train slopes (left). The proportion of the distributions below zero are plotted as bar graphs (right). Scale bars: vertical bars 500 μV, LFP scale bars 250 ms, path scale bars 50 cm. 1 cycle = 360°.

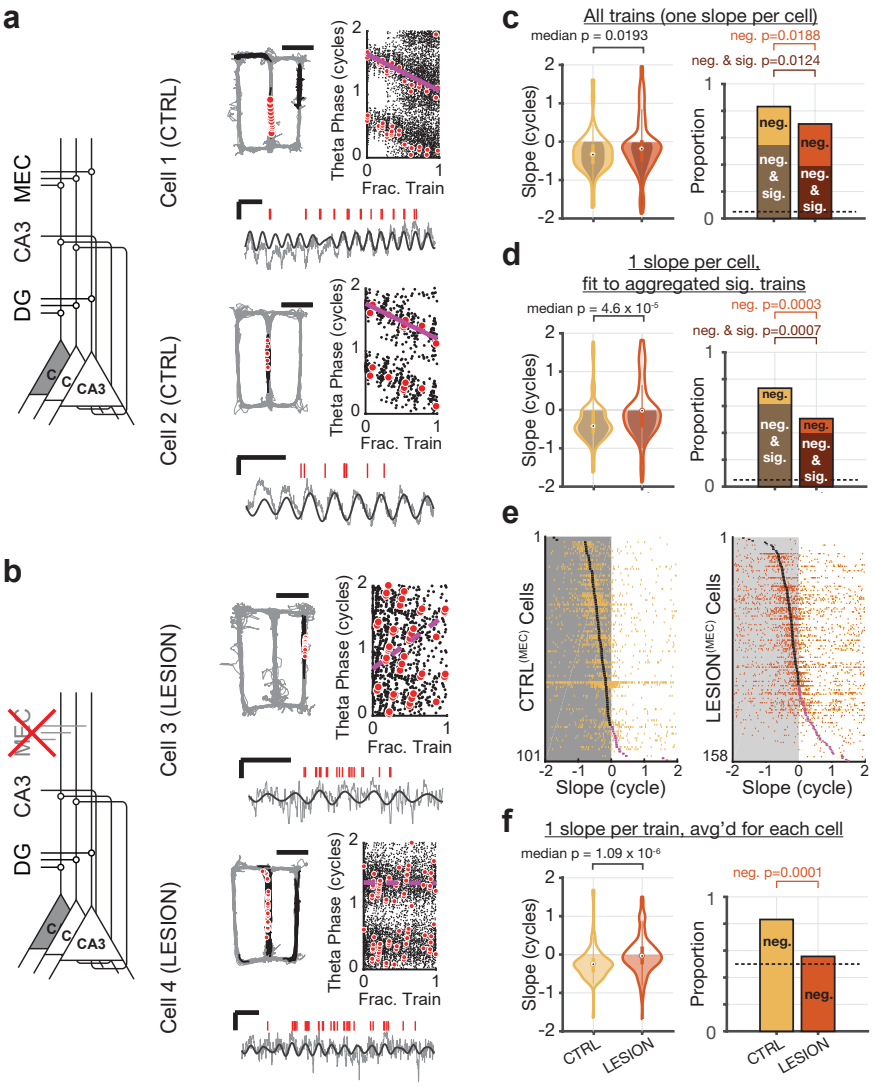
a
MEC
CA3
DG
CA3
Cell 1 (CTRL)
Cell 2 (CTRL)
Theta Phase (cycles)
Frac. Train
b
MEC
CA3
DG
CA3
Cell 3 (LESION)
Cell 4 (LESION)
Theta Phase (cycles)
Frac. Train
c
All trains (one slope per cell)
median p = 0.0193
neg. p=0.0188
neg. & sig. p=0.0124
Slope (cycles)
Proportion
neg.
neg. & sig.
d
1 slope per cell,
fit to aggregated sig. trains
median p = 4.6 x 10-5
neg. p=0.0003
neg. & sig. p=0.0007
Slope (cycles)
Proportion
neg.
neg. & sig.
e
CTRL(MEC) Cells
LESION(MEC) Cells
101
158
Slope (cycle)
Slope (cycle)
f
1 slope per train, avg'd for each cell
median p = 1.09 x 10-6
neg. p=0.0001
Slope (cycles)
Proportion
neg.
CTRL
LESION
CTRL
LESION

= -4.075, signed rank = 10749, $p = 4.60 \times 10^{-5}$; Proportions: 73.3% and 50.6%, negative slopes of $CTRL^{(MEC)}$ vs. $LESION^{(MEC)}$, χ^2 test statistic = 10.50, $p = 0.0012$; 61.4% and 39.9%, significant negative slopes of $CTRL^{(MEC)}$ vs. $LESION^{(MEC)}$, χ^2 test statistic = 15.48, $p = 8.32 \times 10^{-5}$; χ^2 tests for proportions). In a similar manner to the effects of DG lesions, the positive shift of the slopes with MEC lesions was visually appreciable from the slope-by-train analysis (Figure 2.2e). Statistical comparisons in the slope-by-train analysis confirmed the slope-by-cell analysis results (Figure 2.2f; Medians less than zero: $CTRL^{(MEC)}$, z-value = -6.30, signed rank = 716, $p = 1.51 \times 10^{-10}$; $LESION^{(MEC)}$, z-value = -1.15, signed rank = 5615, $p = 0.124$; Median of $CTRL^{(MEC)}$ vs. $LESION^{(MEC)}$: z-value = -4.87, signed rank = 10263, $p = 1.09 \times 10^{-6}$; Proportions: 83.2% and 55.7%, negative slopes of $CTRL^{(MEC)}$ vs. $LESION^{(MEC)}$, χ^2 test statistic = 14.459, $p = 1.43 \times 10^{-4}$). These observations support a role for MEC in the generation of robust phase precession in the CA3 of rats. Therefore, the DG-CA3 network alone is incapable of generating phase precession at control levels—for this, both the DG and MEC inputs are necessary.

DG and MEC support CA3 phase precession via qualitatively distinct mechanisms

After confirming that both the DG and MEC are necessary for CA3 phase precession, we asked whether there are qualitative differences in the mechanism by which each of these inputs supports phase precession in CA3. Loss of phase precession can be either due to reduced theta phase range over which spiking occurs, or heightened variability around a monotonically decreasing precession slope, or both. To determine how the theta phase range was altered by the lesions, we calculated the onset and offset theta phase of CA3 spike trains. The onset phase of trains – defined as the circular mean of the theta phase of train spikes in the first theta cycle of each train – showed a marked shift toward earlier phases in CA3 cells of DG lesioned rats

compared to control rats (Figure 2.3a). The distribution of the onset phase (Φ_{on}) of all trains was left-skewed, with a peak in the rising half of theta and a circular mean of 242.4°, in the DG-lesioned rats, this distribution appeared more symmetrical, with a circular mean of 202.5°. The difference between the two circular means was significant (Figure 2.3a; Watson-Williams test; $F_{1,2900} = 160.86$, $p < 10^{-35}$). In contrast, the distributions of offset phases (Φ_{off}) – defined as the circular mean theta phase of train spikes in the last theta cycle of each train – were more similar between control and lesioned rats, though there was a statistically significant shift in the mean phase from 123.9° in the control group to 102.7° in lesions (Figure 2.3b; Watson-Williams test; $F_{1,2900} = 27.27$, $p = 1.89 \times 10^{-7}$). The effect size was greater for the onset phase (Cohen's d = -0.6670) compared with offset phase (Cohen's d = -0.2998). The offset phase showed a considerably smaller shift (Figure 2.3b), indicating that the DG granule cell drive primarily determines the phase of early spikes in the theta cycle, in line with the idea of "look-ahead" spikes (Hasselmo *et al.*, 2002; Lisman *et al.*, 2005; Sanders *et al.*, 2015).

These effects on CA3 spike timing were unique to DG lesions as MEC lesions had no effect on either the onset or the offset phases of the train spikes (Figure 2.3c,d). The onset of phase of the MEC-lesioned CA3 trains had a mean of 236.7° compared with 237.1° in controls (Figure 2.3c; difference not significant, $F_{1,5456} = 0.0334$, $p = 0.8549$; Watson-Williams test). Similarly, the mean offset phase of MEC-lesioned CA3 cells (246.6°) was very close to that of controls (242.9°), with their difference not statistically significant (Figure 2.3d; Watson-Williams test; $F_{1,5456} = 1.6962$, $p = 0.1928$). These changes suggest it is predominantly the DG rather than the MEC input to CA3 that is involved in setting the theta phase of CA3, in particular the onset phase within the theta cycle.

The onset phase specific shift of spike timing within the theta cycle can be produced in at

Figure 2.3: DG, but not MEC, lesions selectively alter the onset phase of CA3 phase precession. a, **Left**, Onset phase (Φ_{on}) of each train in control rats ($CTRL^{(DG)}$). Rows represent single units sorted as in Figure 2.1c. Note the clustering of the median onset phases in the rising portion of theta. Data are repeated from 2π to 4π for clarity, and two theta cycles are displayed above for reference. **Right**, Onset phase of the trains in $LESION^{(DG)}$, showing more dispersed values compared to control rats. Organization as on the left. **b**, Single-pass offset phase (Φ_{off}) distribution is similar for $CTRL^{(DG)}$ and $LESION^{(DG)}$. Organization as in **a**. Note that the offset phases cluster in the descending portion of theta. **c,** Population onset phase for the $CTRL^{(DG)}$ (light blue bars) and $LESION^{(DG)}$ (dark blue line) data sets are different with an effect size of d = -0.667. Data are repeated from 2π to 4π for clarity. **d**, Population offset phase of the $CTRL^{(DG)}$ (light blue bars) and $LESION^{(DG)}$ (dark blue line) data sets are different with an effect size of d = -0.299. **e-h**, As in panels (**a-d**) but for the MEC lesion experiment. Onset and offset phase values in CA3 are similarly dispersed with and without MEC inputs. **e**, Onset phases of $CTRL^{(MEC)}$ and $LESION^{(MEC)}$. **f**, Offset phases of $CTRL^{(MEC)}$ and $LESION^{(MEC)}$. **g**, Population onset phase distribution is not different in control and MEC-lesioned animals. **h**, Population offset phase distribution is also not different in control and MEC-lesioned animals.

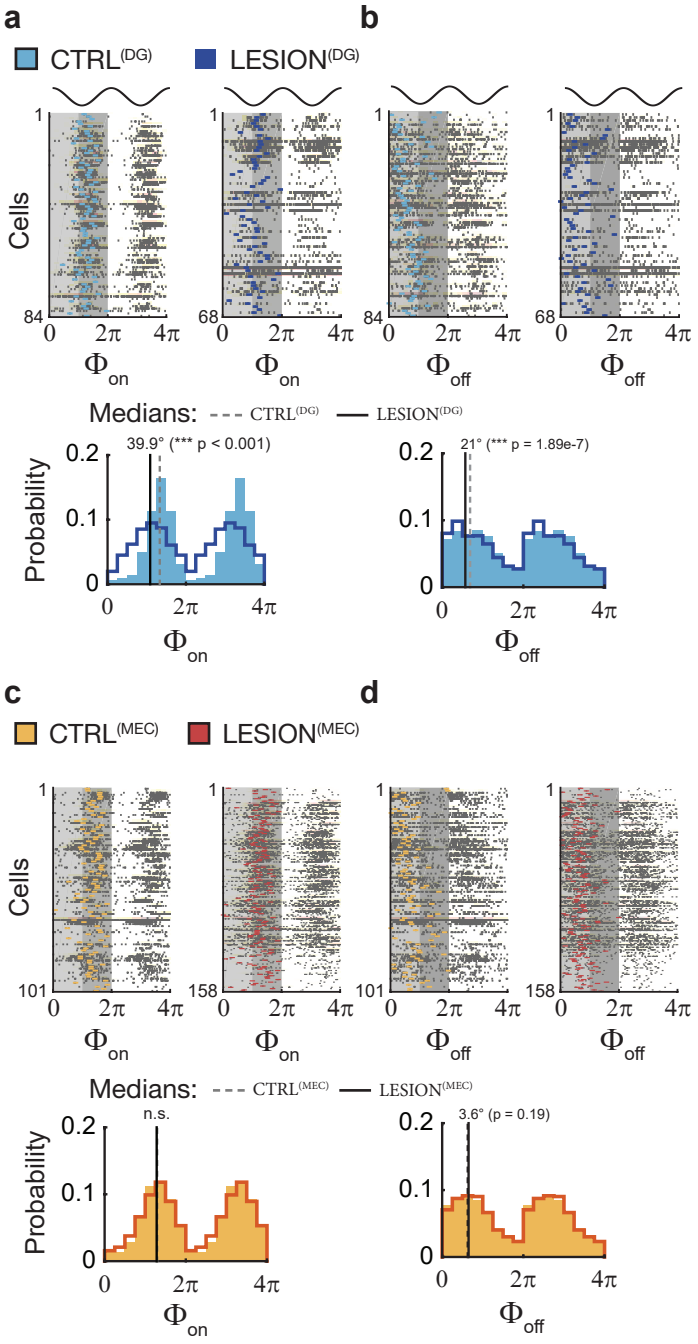
a
b
CTRL(DG)
LESION(DG)
Cells
1
84
68
0
2π
4π
Φon
Φoff
Medians:
CTRL(DG)
LESION(DG)
Probability
0.2
0.1
0
39.9° (*** p < 0.001)
21° (*** p = 1.89e-7)
c
d
CTRL(MEC)
LESION(MEC)
101
158
n.s.
3.6° (p = 0.19)

Figure 2.4: In the absence of DG input, peak probability of CA3 spiking shifts to earlier phases of the theta cycle, corresponding to exiting the place field. a, Distribution of CA3 spike incidence in the early, mid, and late theta cycle bins. As expected, the middle of the theta cycle contains more spikes than the early or late phases. **b,** The proportion of CA3 spikes occurring early in the theta cycle was markedly increased without the DG granule cell input ($LESION^{(DG)}$; top) (χ^2 statistic = 973.199, $p = 4.7 \times 10^{-212}$, χ^2 test for independence of dimensions of tabulated data), suggesting that the remaining inputs, notably the MEC, tend to drive CA3 firing later in place fields. Total number of spikes in $LESION^{(DG)}$ was 28,704. The bottom plot shows that although in the absence the MEC inputs ($LESION^{(MEC)}$), CA3 spikes tended to occur later in the theta cycle (corresponding to a shift to place field entry; χ^2 statistic = 191.408, $p = 2.7 \times 10^{-42}$, χ^2 test), this shift was small. The remaining inputs (such as DG) seem to have a slight tendency to drive CA3 firing at the entry to CA3 place fields, especially as compared to MEC inputs. The total number of spikes in $LESION^{(MEC)}$ was 68,385. The control rats' plots from (**a**) are superimposed with dotted lines to aid direct visual comparison. **c,** Fraction of CA3 spikes in each bin of the theta cycle as a function of normalized (%) distance through the train, displayed as stacked bars. Notice the increase in the relative incidence of early-phase spikes in the DG lesioned rats (top right plot). **d,** (Top) DG lesions selectively increase the variability of spike phase in the first half of a field traversal (compare bar pairs from 5% to 45% of normalized distance). (Bottom) MEC lesions, on the other hand, do not alter the reliability of theta phase preference in a major way. The theta cycle was split into 3 equally sized bins. E: early theta cycle, M: mid theta cycle, L: late theta cycle. * $p < 0.05$, ** $p < 0.01$, *** $p < 0.001$, Wilcoxon's rank sum tests (uncorrected for multiple comparisons).

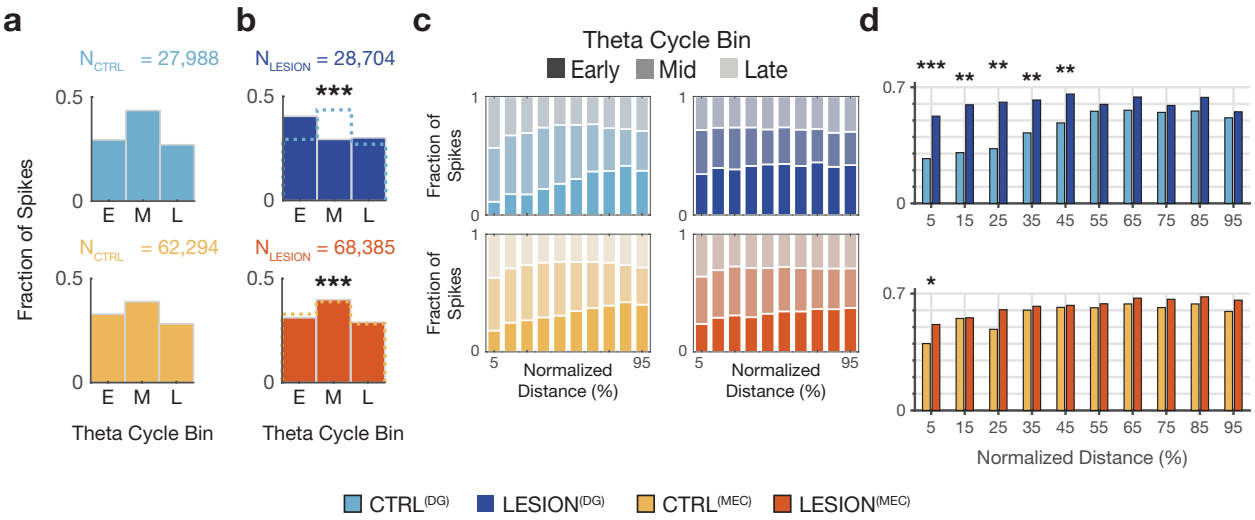
a
b
c
d
N_CTRL = 27,988
N_LESION = 28,704
N_CTRL = 62,294
N_LESION = 68,385
Fraction of Spikes
Theta Cycle Bin
E M L
Theta Cycle Bin
Early Mid Late
Normalized Distance (%)
Normalized Distance (%)
Normalized Distance (%)
CTRL(DG) LESION(DG) CTRL(MEC) LESION(MEC)

least two distinct ways. First, it is possible that the mean theta phase shifts without a change in the phase variance. Second, it is possible that the mean and variance of the phase shift simultaneously. This possibility can be interpreted as the addition of "noise" spikes to early theta phases at the entry to the place field which would increase the phase variance and shift the mean to earlier phases. To distinguish these two possibilities, we analyzed two independent measures of the spike phase distribution. First, we examined how spike phase is distributed across the theta cycle regardless of distance (Figure 2.4a-b). In control animals, CA3 spike phase was concentrated in the middle of the theta cycle, as expected (Figure 2.4a). However, in DG-lesioned, but not in MEC-lesioned animals, CA3 spike phase shifted from the expected distribution to earlier phases (Figure 2.4b; DG experiment (top): χ^2 statistic = 973.199, $p = 4.7 \times 10^{-212}$; MEC experiment (bottom): χ^2 statistic = 191.408, $p = 2.7 \times 10^{-42}$; χ^2 test for independence of dimensions of tabulated data). Second, after binning the normalized distance within spike trains into 10 bins we considered the joint distribution of spike phase and normalized distance (Figure 2.4c). Here, we found that phase shifts caused by DG lesions were smoothly distributed between the beginning and middle of trains, but were particularly pronounced in the early bins. The circular variance of CA3 spike theta phase was selectively increased in the first half of a field traversal (Figure 2.4d, top; pairwise comparisons between $\text{CTRL}^{(\text{DG})}$ and $\text{LESION}^{(\text{DG})}$ $p < 0.01$ for the first five bins, rank sum tests). In contrast, circular variance took on similar values in MEC control and lesioned rats (Figure 2.4d, bottom; pairwise comparisons between $\text{CTRL}^{(\text{MEC})}$ and $\text{LESION}^{(\text{MEC})}$ $p < 0.05$ only for the first bin, rank sum tests). Taken together, these findings thus favor the second possibility. In other words, the DG to CA3 input is critically involved in supporting late-theta phase ("prospective") CA3 spiking by inhibiting spurious spikes in the early phases of the theta cycle.

Is the temporal profile of granule cell spiking precise enough to organize the onset phase of CA3 neurons? In rats where we were able to record single units from the dentate gyrus (N = 5, see Methods), both putative granule cells and putative mossy cells displayed phase precession (Figure 2S.3a,b). At the onset of trains, a striking theta phase preference was evident in putative granule cells, which gradually diminished with distance traversed through a cell's place field (Figure 2S.3c). In contrast, putative mossy cells and CA3 pyramidal cells did not show a distinct pattern of theta phase variability as a function of distance through the place field (Figure 2S.3c). These findings are consistent with the results of the lesion experiments, suggesting that the DG granule cells play an active role in supporting the precise temporal coding of CA3 pyramidal cell population on the theta time-scale.

If a lesion impairs phase precession via increasing the variance of the conditional phase probability (i.e., spread of the distribution of spikes at a given position), one should be able to rescue phase precession if one artificially reduces this variance by replacing, for each theta cycle, all spikes with their mean timestamp. However, if the lesion causes a reduction in the rhythmic spiking frequency (quantified by slope), replacing the spikes with their cycle mean should not rescue the effect. Indeed, when we did this, the effect could be largely rescued in MEC lesioned rats, evident both when all trains were considered together as well as in individual trains (Figure 2S.4). On the population level, the median of the cells' slopes in MEC lesioned rats was no longer distinguishable from control rats ($CTRL^{(MEC)}$ vs. $LESION^{(MEC)}$: z-value = -1.436, rank sum = 12285, p = 0.1509, Wilcoxon's rank sum test), while it remained different from controls in DG lesioned rats ($CTRL^{(DG)}$ vs. $LESION^{(DG)}$: z-value = -4.226, rank sum = 5285, $p = 2.37 \times 10^{-5}$, Wilcoxon's rank sum test) (Figure 2.5a-c). Testing this directly by quantifying phase variability, we observed that the variance of the conditional phase probability over all trains of

Figure 2.5: Distinct mechanisms for temporal organization of CA3 spiking by DG and MEC networks. a-b, Phase-position plots of an example CA3 cell from an MEC lesioned rat using all train spikes (**a**) or only the theta cycle mean of the spikes (**b**). The opacity of points is reduced so that the presence of an underlying negative slope is more readily appreciated. Replacing spike times in each theta cycle with their mean leads to a negative precession slope by removing "noisy" spikes. **c,** Slope distribution of all-trains aggregate phase-position circular-linear regression slopes for each group. Only in the case of MEC lesions did replacing each cycle's spikes with their mean reduce the regression slopes to the point that they were no longer statistically distinguishable from controls, indicating that in MEC lesioned rats, broad spike spread over the theta cycle prevents the aggregate spike trains from being identified as phase precessing. In all cases, however, the median slope was statistically less than 0 ($CTRL^{(DG)}$: N = 84, $p = 2.15 \times 10\text{-}14$, $LESION^{(DG)}$: N = 68, $p = 9.7 \times 10\text{-}5$, exact left-tailed sign tests; $CTRL^{(MEC)}$: N = 101, z-value = -7.7613, $p = 4.2 \times 10\text{-}15$, $LESION^{(MEC)}$: N = 158, z-value = -8.5125, $p = 8.5 \times 10\text{-}18$, approximate left-tailed sign tests). Also note the reduction in the density of outlier slope values, especially on the positive end (compare with Figures 2.1d and 2.2d). **d,** Circular variance of theta phase either with all spikes (bar histograms) or only with the each cycle's spike mean (line histograms). Top left: $CTRL^{(DG)}$, top right: $LESION^{(DG)}$, bottom left: $CTRL^{(MEC)}$, bottom right: $LESION^{(MEC)}$. In all groups, the circular variance decreases after replacing each cycle's spikes with their mean, though the effect is less pronounced in the CA3 of DG lesioned rats. **e,** Schematic summary of mechanism by which DG lesions might disrupt CA3 temporal coding. DG lesions appear to cause CA3 spiking to commence earlier in the theta cycle than it would under physiological conditions. This early commencement is manifested as the "addition" of new spikes early in the theta cycle, exclusively in the beginning of trains, thereby reducing the slope of the resulting circular-linear regression slope (top middle plot). Therefore, early phase CA3 spiking is effectively inhibited via the mossy fibers. Theta averaging is unable to rescue the phase precession effect because after theta averaging the slope remains diminished. **f,** Schematic summary of mechanism by which MEC lesions might disrupt CA3 temporal coding. Although the window of firing in a single theta cycle is slightly narrower in single trains, spike phase is more variable across multiple trains (i.e., greater variability around the mean spike phase at each position) at each position along the train. This lowers the probability of detecting a significant slope indicative of phase precession. MEC, thus, appears to support reliable theta phase coding of CA3 pyramidal cells upon successive visits to each cell's place field. Theta averaging rescues phase precession because, effectively, it reverses the increase in the variability around mean spike phase at each position. *p*-values displayed are obtained via rank sum tests. Scale bars: horizontal: 200 ms, vertical: 200 μV.

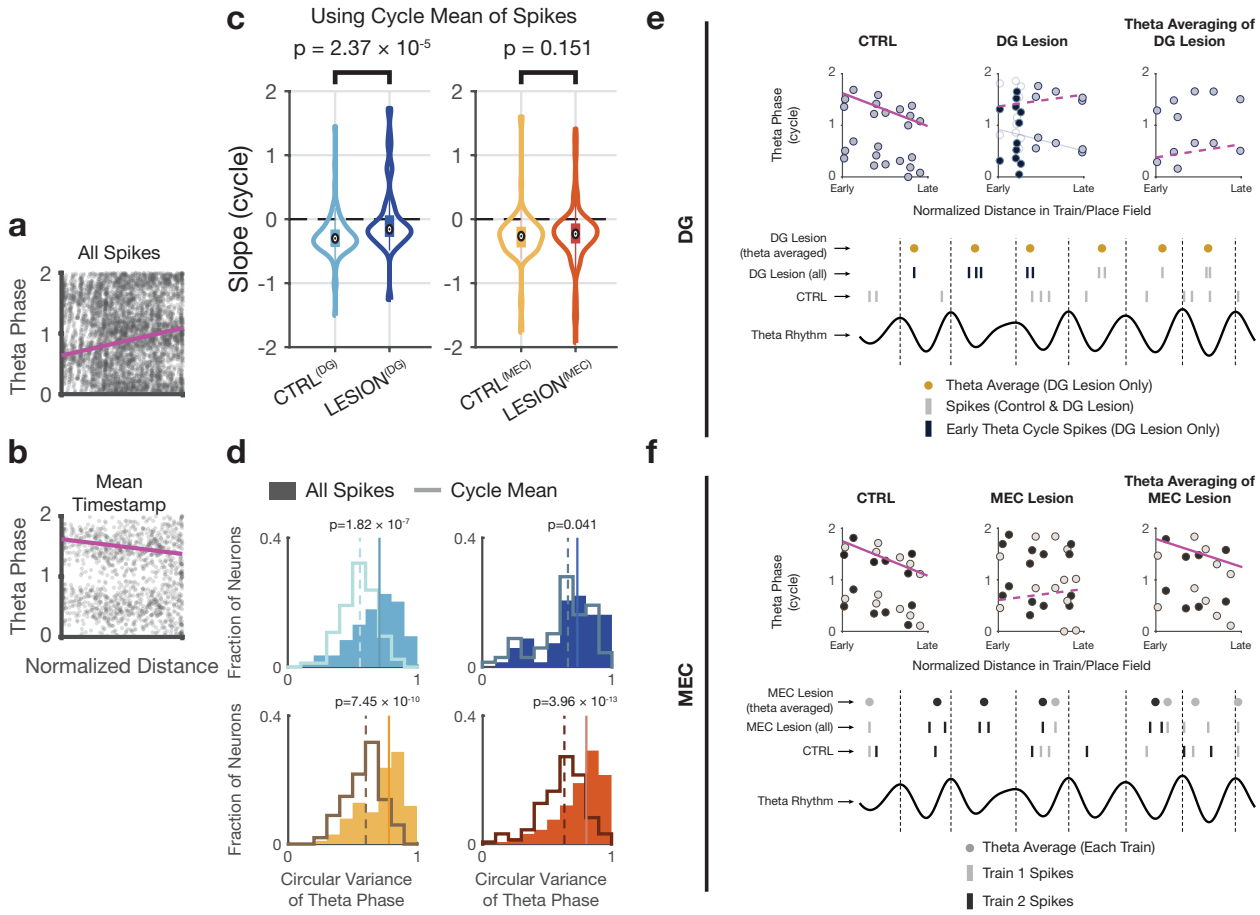
a
All Spikes
Theta Phase
Normalized Distance
b
Mean Timestamp
c
Using Cycle Mean of Spikes
p = 2.37 × 10-5
p = 0.151
Slope (cycle)
CTRL(DG)
LESION(DG)
CTRL(MEC)
LESION(MEC)
d
All Spikes
Cycle Mean
p=1.82 × 10-7
p=0.041
p=7.45 × 10-10
p=3.96 × 10-13
Fraction of Neurons
Circular Variance of Theta Phase
e
DG
CTRL
DG Lesion
Theta Averaging of DG Lesion
Theta Phase (cycle)
Early
Late
Normalized Distance in Train/Place Field
DG Lesion (theta averaged)
DG Lesion (all)
CTRL
Theta Rhythm
Theta Average (DG Lesion Only)
Spikes (Control & DG Lesion)
Early Theta Cycle Spikes (DG Lesion Only)
f
MEC
CTRL
MEC Lesion
Theta Averaging of MEC Lesion
MEC Lesion (theta averaged)
MEC Lesion (all)
Theta Average (Each Train)
Train 1 Spikes
Train 2 Spikes

each neuron was similar between the original and cycle-mean analyses specifically in DG lesioned rats (Figure 2.5d; compare, for each panel, the difference of medians indicated by the solid and dashed vertical lines). Taken together, these results suggest two distinct mechanisms by which DG and MEC circuits contribute to the organization of precise temporal profile of CA3 spiking (Figure 2.5e-f). Accordingly, upon entry to the place field of a CA3 neuron, DG inputs effectively inhibit spiking that would have otherwise occurred early in the theta cycles (Figure 2.5e). In contrast, in the middle and near the exit from the place field, MEC inputs ensure the start and end of CA3 spiking at an appropriate, consistent theta phase by driving CA3 neurons in tight windows around a monotonically decreasing mean theta phase (Figure 2.5f).

DG, but not MEC, supports the preservation of CA3 cells' behavioral order of firing on the theta scale

It has been suggested that phase precession and hippocampal cell assemblies manifested in theta sequences are dissociable (Dragoi & Buzsáki, 2006; Feng *et al.*, 2015). However, even though theta sequences have not been observed in the absence of phase precession, the question still remains whether phase precession is indeed a prerequisite for the formation of such sequences (Foster & Wilson, 2007). In previous experiments (Schlesiger *et al.*, 2015) it was shown that cell pairs in CA1 lose their sequence information, accompanied by a concomitant decrease in the level of phase precession. We asked if in the CA3 network the temporal relationship on the theta time-scale reflect that on the behavioral time-scale in the absence of either of its two theta-modulated inputs. We measured this by calculating the correlation between the temporal shift in the spike cross-correlation of such pairs and the physical distance between their peak firing locations in physical space (Dragoi & Buzsáki, 2006).

We found that in the DG-lesioned rats the simultaneously recorded cells did not preserve

Figure 2.6: DG, but not MEC, inputs are required for a matched order of CA3 coactive pairs in behavior and theta cycles. (a-d) Effect of DG inputs on CA3 pairwise spiking. **a,** The place field activity of two pairs of simultaneously recorded cells with shared theta cycle firing is displayed (1-2 pair from a control rat, and 3-4 pair from a DG lesioned rat, as labeled at the top). Each place field is delineated by its 20% max firing contour, with the peaks marked by filled circles inside each contour. The place field visited first in each pair (and the corresponding neuron) is always displayed in black, while the second place field (and the corresponding neuron) is in red. This pairwise ordering is also marked by a black arrow beside the place field. **b,** Session-aggregated phase-position plots of the spiking of cells in (**a**). Only those trains in the direction indicated by the horizontal arrows are selected and analyzed for each group. **c,** Cross-correlation of the spikes from the two cells. The peak of the cross-correlation function nearest 0 is indicated with a small arrow pointing down. The inset shows the cross-correlogram for a window of width of 4 seconds. **d,** Left: Phase shift of the theta firing of the two cells plotted against the physical distance of the peaks of the respective place fields. The dashed line is the linear regression. Right: proportion of pairs shown in the scatter plots to the where 0 (“neither”), 1 (“one”), or 2 (“both”) neurons in the pair displayed phase precession. Although a substantial number of pairs in the DG lesion scatter were indeed phase precessing, this phase precession did not automatically guarantee the pairwise correlations between spiking order in behavior and theta cycles. **(e-h)** Same as **(a-d)** except the data are from the MEC lesion experiment. Despite marked deficits in phase precession, CA3 pairwise correlations are strong, indicating that, unlike DG, MEC does not seem to be necessary for CA3 pairwise correlations. ** $p < 0.01$, *** $p < 0.001$, n.s. not significant.

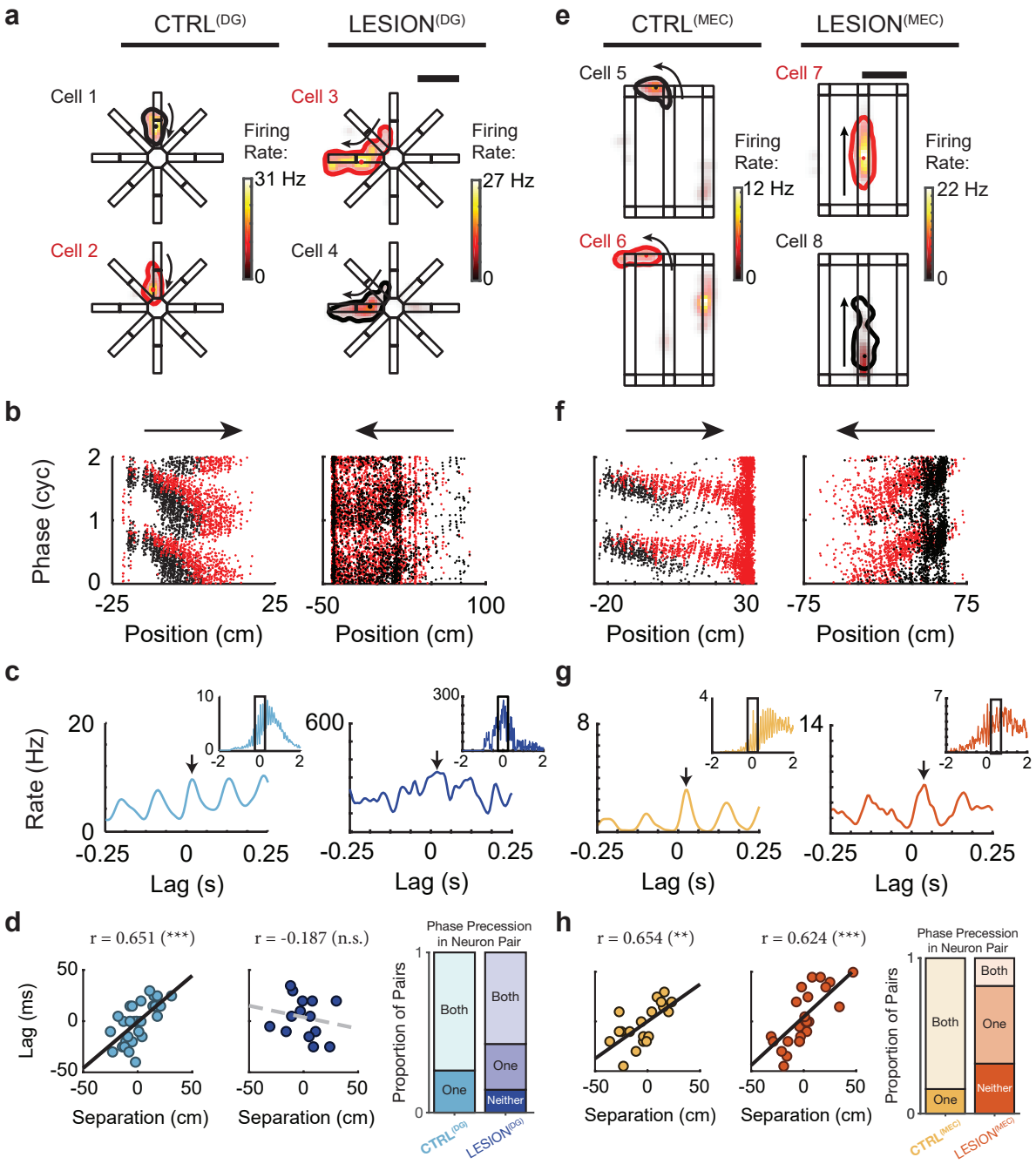
a
CTRL(DG)
LESION(DG)
Cell 1
Cell 2
Cell 3
Cell 4
Firing Rate:
31 Hz
0
Firing Rate:
27 Hz
0
e
CTRL(MEC)
LESION(MEC)
Cell 5
Cell 6
Cell 7
Cell 8
Firing Rate:
12 Hz
0
Firing Rate:
22 Hz
0
b
Phase (cyc)
2
1
0
-25
25
Position (cm)
-50
100
Position (cm)
f
-20
30
Position (cm)
-75
75
Position (cm)
c
Rate (Hz)
20
0
10
0
-2
0
2
-0.25
0
0.25
Lag (s)
600
300
-2
0
2
-0.25
0
0.25
Lag (s)
g
8
4
-2
0
2
-0.25
0
0.25
Lag (s)
14
7
-2
0
2
-0.25
0
0.25
Lag (s)
d
r = 0.651 (***)
Lag (ms)
50
0
-50
-50
0
50
Separation (cm)
r = -0.187 (n.s.)
-50
0
50
Separation (cm)
Phase Precession in Neuron Pair
Proportion of Pairs
1
0
Both
One
Both
One
Neither
CTRL(DG)
LESION(DG)
h
r = 0.654 (**)
-50
0
50
Separation (cm)
r = 0.624 (***)
-50
0
50
Separation (cm)
Phase Precession in Neuron Pair
Proportion of Pairs
1
0
Both
One
Both
One
Neither
CTRL(MEC)
LESION(MEC)

their behavioral order of firing within individual theta cycles (Figure 2.6a-d). While the correlation between the spatial separation and theta phase shift of place field peaks was significant in $CTRL^{(DG)}$ (N = 30 pairs, r = 0.651, $p = 9.87 \times 10^{-5}$, Pearson's correlation), it was not so in $LESION^{(DG)}$ (N = 14 pairs, r = -0.187, $p = 0.523$, Pearson's correlation) even though the proportion of neuron pairs with phase precession in DG lesioned rats was comparable to that in control rats (Figure 2.6d). Surprisingly, despite reduced phase precession in comparison to neuron pairs from control rats, the CA3 pairs in the MEC-lesioned rats maintained their spiking order in theta cycles according to their firing order on the maze (Figure 2.6e-h; $CTRL^{(MEC)}$ N = 19 pairs, r = 0.654, $p = 0.0024$; $LESION^{(MEC)}$ N = 27 pairs, r = 0.624, $p = 5.02 \times 10^{-4}$; Pearson's correlations), unlike what has been previously reported in CA1 (Schlesiger *et al.*, 2015). These effects were not due to errors in spike sorting or low quality clusters (Figure 2S.5). Thus, it seems that though the MEC is critical in maintaining hippocampal phase precession, the recurrent CA3 network together with its reciprocal connections with the DG organizes fine ensemble-level temporal relationships within theta cycles to compress behavioral-scale sequences to time-scales suitable for encoding and retrieval of memories.

Computational modeling supports distinct modulatory roles for DG and MEC to reproduce empirical CA3 phase precession measures

To evaluate whether the interpretations of our findings are feasible, we devised a minimalistic phenomenological model based on oscillatory interference to simulate the spiking dynamics of a model CA3 pyramidal cell as the animal moved through the cell's place field at constant velocity. Although our manipulations involved only two inputs to CA3, it should be noted that if a computational model based on oscillatory interference is to emulate the lesions, it must account for inputs beyond the inputs to be lesioned. Inhibition has been shown to mediate

input gain control, precise spike timing and enhanced coding in networks (Denève & Machens, 2016; Klyachko & Stevens, 2006; Lytton & Sejnowski, 1991; Milstein *et al.*, 2015) and could control the theta phase of pyramidal cell spikes (Losonczy *et al.*, 2010). Therefore, we included an inhibitory oscillation. The model CA3 cell thus received three inputs. Two of these were excitatory waves oscillating at slightly above LFP theta frequency, analogous to the major theta modulated excitatory inputs (i.e., the MEC and DG granule cell afferents), while the third input was an inhibitory oscillation at the LFP theta frequency. We allowed the model to have three free parameters: a phase shift between excitation and inhibition denoted by ϕ_{inh}, the oscillatory amplitude of inhibition denoted by A, and a DC component for the inhibitory oscillation (baseline inhibition) denoted by I_{DC}. We estimated and fixed the excitatory phase offset at place field entry (phase differential between the two excitatory oscillations that modeled DG and MEC inputs) from Mizuseki *et al.* (2009) (their Figure 3) to be $\psi = -39°$. The output of the model CA3 cell was determined by the place modulated (Schmidt-Hieber & Nolan, 2017; Silver, 2010) difference between a combination of the three inputs and a membrane threshold value, constant across the place field. Spikes were generated stochastically via an inhomogeneous Poisson point process with an intensity measure defined by the total excitatory drive minus the membrane threshold. The simulated spike phases were extracted with respect to an 8 Hz oscillation representing the LFP theta oscillation (see Methods).

We simulated CA3 model neuron spikes for a broad range of parameter values. We observed that when all three input components are present (Figure 2.7a), phase precession can be obtained for a wide range of parameter values (Figure 2.7b). Different values of the phase precession slope and onset phase could be obtained by an appropriate choice of inhibition phase offset for each excitatory phase offset value (Figure 2S.6). The peak of the simulated place field

was most sensitive to the phase shifts between the inputs (Figure 2S.7). However, when either of the two excitatory components was removed, we observed that phase precession was diminished (Figure 2.7c). This recapitulated the behavior of real CA3 neurons in the absence of either MEC or DG inputs.

To determine which parameter values under this model would correspond to the underlying biological values, we selected for each of the four phase precession measures (i.e., slope, onset phase, offset phase, or explained variance r^2) the middle two quartiles where slope, onset phase, and explained variance reasonably closely matched the empirical observations from the DG and MEC lesion experiments. This analysis revealed that the empirical values for the abovementioned four measures when the DG was lesioned took on a broader and shifted set of values compared to the controls along the ϕ_{inh} axis (Figure 2.7d). In contrast, the same measures from the MEC lesion data set took on a set of larger values of A, compared to controls (Figure 2.7e). Interestingly, the third free parameter in the model did not influence the state space substantially as values as high as 25 times larger produced similar ranges of matching with empirical data (Figure 2S.8). Since the difference between the control and lesion data spread simulated by the model arises along two independent dimensions (ϕ_{inh} and A for DG and MEC, respectively), we conclude that, under our proposed model, the inhibition phase offset is mostly set by the DG population, whereas the inhibition amplitude is mostly set by the MEC population, corroborating our empirical findings on the distinct role of the DG and MEC inputs for CA3 temporal precision (Figure 2.5e-f). By comparing model values matching either empirical control data or empirical lesion data (Figure 2S.9), we further note that the full-width at half maximum (FWHM) of the ϕ_{inh} distributions is most consistent with value ranges for feedforward inhibition due to DG input at 190°–225° theta phase offset with respect to DG excitatory input for controls.

Figure 2.7: A model of two oscillating excitatory inputs and an inhibitory input recapitulates the main empirical results. a, Model construction. The three inputs are modeled after DG, MEC, and local inhibition converging onto the CA3 model neuron. The excitatory DG and MEC inputs oscillate at faster-than-LFP frequencies (ω_{DG} = 8.6 Hz, ω_{MEC} = 8.5 Hz). The inhibitory input oscillates at 8 Hz across the place field, corresponding to LFP theta. A small Gaussian noise is added to the inhibitory input to ensure robustness against small perturbations. The excitatory inputs contribute positively at phase differential y and spatial gain function, while the inhibitory input contributes negatively to the total drive at phase differential ϕ_{inh} relative to excitation at place field entry, before the sum-square step (see Methods for details). The total excitatory input is gain modulated (γ) and displayed at the bottom along with an 8-Hz oscillation, the LFP theta. Not all steps are displayed for brevity (see Methods for full details). **b,** Phase-position relationship of spikes generated by the model show phase precession. The A (inhibitory oscillation amplitude), *I* (inhibition DC component) and ψ (excitatory phase differential) values are the same across the four plots as displayed at the top. However, the inhibition phase offset, ϕ_{inh}, varies in each panel. A broad range of phase precession profiles can be obtained, confirming the expressive power of the simple model. **c,** Lesion experiments were simulated by setting the DG input (left) or MEC input (right) to 0. In both cases phase precession is diminished and the slopes are reduced. **d-e,** The parameter space is shown for various values of A and ϕ, with fixed *I* = 0.5. The ranges for which the values of onset phase, offset phase, slope, and explained variance are similar to those of physiological values are delineated in black. The intersection of all four such zones is displayed in the Overlap plots and color coded from dark blue (1) to light blue (4) to indicate the number of overlapping measures at each parameter pair. An overlap of 4 is delineated in black (control) or pink (lesion), and repeated in the respective plots on the top left for comparison (high-frequency polygons removed to aid clear visualization). The light blue zone is the prediction of the physiological values for inhibition oscillatory amplitude and phase differential. To match empirical phase precession measures in the DG lesioned rats, the model is forced to take on a larger set of ϕ_{inh} values (**d**, compare black and pink outlines in Overlap plots). In contrast, to match empirical phase precession measures in the MEC lesioned rats, the model is forced to take on a larger set of A values (**e**, compare black and pink outlines in Overlap plots). See Figure 2S.9 for the quantification of these comparisons.

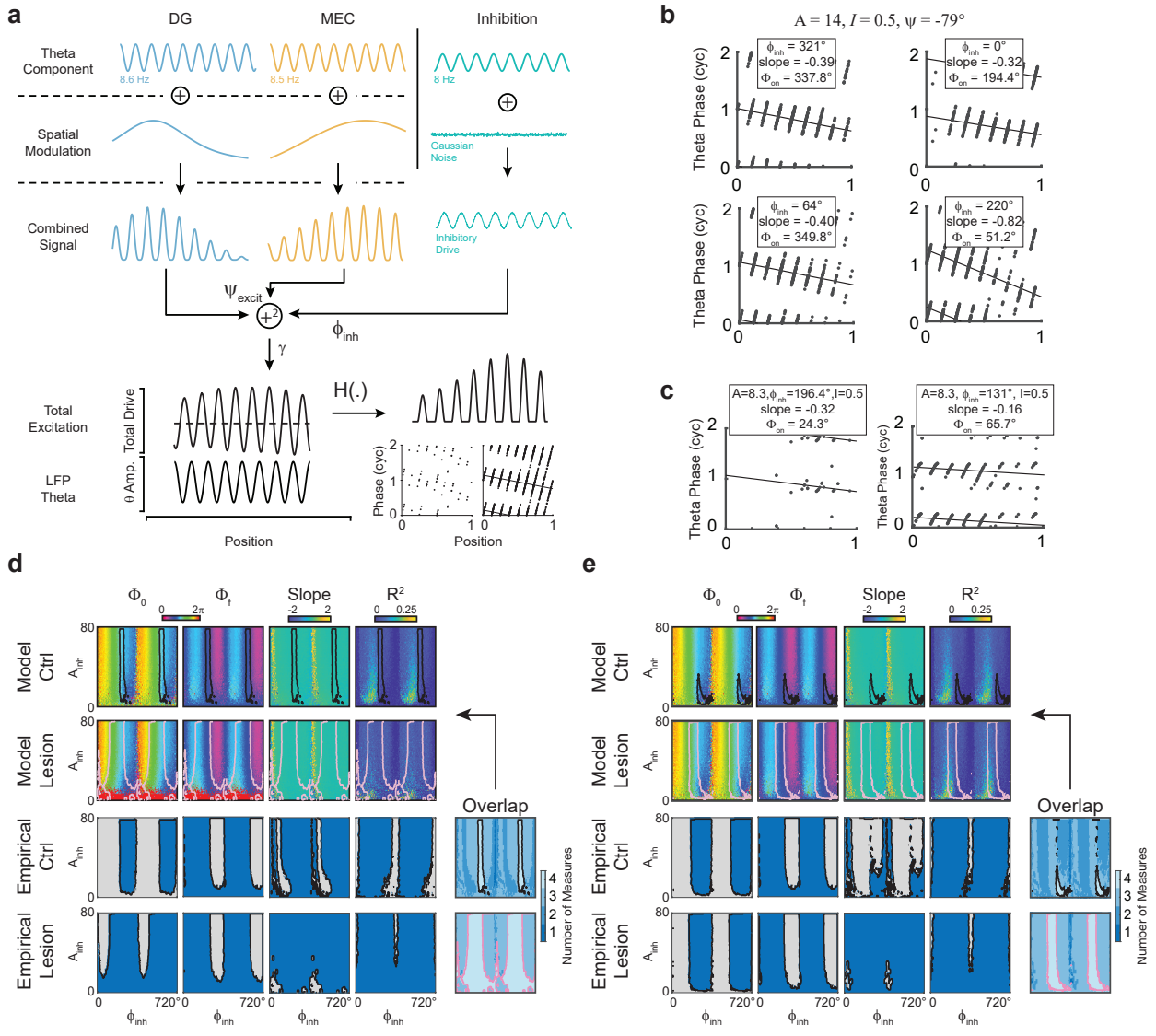
a
DG
MEC
Inhibition
Theta Component
8.6 Hz
8.5 Hz
8 Hz
Spatial Modulation
Gaussian Noise
Combined Signal
Inhibitory Drive
ψexcit
+2
ϕinh
γ
Total Excitation
Total Drive
LFP Theta
θ Amp.
H(.)
Phase (cyc)
Position
b
A = 14, I = 0.5, ψ = -79°
ϕinh = 321°
slope = -0.39
Φon = 337.8°
ϕinh = 0°
slope = -0.32
Φon = 194.4°
ϕinh = 64°
slope = -0.40
Φon = 349.8°
ϕinh = 220°
slope = -0.82
Φon = 51.2°
Theta Phase (cyc)
c
A=8.3,ϕinh=196.4°,I=0.5
slope = -0.32
Φon = 24.3°
A=8.3, ϕinh=131°, I=0.5
slope = -0.16
Φon = 65.7°
d
e
Φ0
Φf
Slope
R2
Model Ctrl
Model Lesion
Empirical Ctrl
Empirical Lesion
Overlap
Ainh
ϕinh
720°
Number of Measures

For DG lesions, the range expanded to 95°–245°. A similar comparison for A is most consistent with a ratio of inhibitory amplitude between MEC lesions and controls between 1x to > 5x, possibly with great variability. Finally, to investigate whether higher frequency gamma oscillations found in the hippocampus play a role in modulating phase precession, we added a gamma component to each of the excitatory inputs (Figure 2S.10a). This modification, however, did not qualitatively change the state space of generated values or the value ranges of the model regarding the values of A and ϕ_{inh} (Figure 2S.10b,c). Taken together, these simulations demonstrate that phase precession in the CA3 circuit can, in principle, be generated by the interaction of the two major theta-modulated excitatory inputs and the local inhibitory neuronal population innervating the CA3 pyramidal cells.

Discussion

Causal experiments on the mechanism of the generation of phase precession outside CA1 are rare. Previous studies on the modulation of GABA release by local cannabinoid release (Robbe & Buzsáki, 2009) and theta sequences (Wang *et al.*, 2015) suggested a role for intrahippocampal synaptic computations in sustaining phase precession. The convergence onto CA3 of two major excitatory theta-modulated inputs (Hafting *et al.*, 2008; Skaggs *et al.*, 1996), from the dentate gyrus of the hippocampus and the medial entorhinal cortex, provides an opportunity to investigate the role of the two inputs in the generation of phase precession. Lesioning each input separately allowed us to uncover their distinct roles in generating phase precession in area CA3 of the hippocampus of rats. Specifically, we showed that both the dentate gyrus (DG) and medial entorhinal cortex (MEC) inputs to CA3 are necessary for phase precession in the CA3 area of the hippocampus. Furthermore, we found that DG lesions specifically altered the temporal organization of the prospective firing during the theta cycle by

selectively broadening the phase window of spikes early in the place field, thereby shifting the average onset of spikes to earlier phases in the cycle. We note that these phase shifts were unlikely to be a result of traveling wave theta phase differences due to tetrode placement (Muller, Chavane, Reynolds, & Sejnowski, 2018) as this would have shifted both onset and offset phases to the same extent without altering the shape of the distribution, both contrary to our observations. Interestingly, the MEC lesions did not alter the average onset or offset timing of CA3 spikes with respect to the theta rhythm but reduced phase variability. Finally, we showed that pairwise correlations between the behavioral- and theta-scale firing of CA3 cells were disrupted only when the DG, but not the MEC, input was abolished. Our findings, therefore, provide critical insights into the circuit mechanisms of phase precession and establish the dentate gyrus as a major contributor for organizing CA3 sequential computations during the theta-state.

Even though the ablation of DG and MEC inputs reduced phase precession, many CA3 pyramidal neurons in the lesioned rats retained normal phase precession. In addition to the fact that individual neurons in lesioned rats may have favorable parameter combinations that allow them to express temporal spiking profiles that appear normal, the remaining phase precession may also be due to mechanisms other than a simple combination of rhythmic excitatory and inhibitory drive, including interactions between neuromodulation and the ion channel-mediated biophysics of neurons (Losonczy *et al.*, 2010; Magee, 2001; Robbe *et al.*, 2006). Supporting this hypothesis, previous finding showed that the instantaneous firing rate of hippocampal cells is not predictive of their theta phase in the absence of MEC (Schlesiger *et al.*, 2015). In addition to these mechanisms, it is important to note that the lateral entorhinal cortex (LEC) exhibits considerable, albeit significantly diminished (compared to MEC), spatial (Hargreaves *et al.*, 2005) and theta (Deshmukh *et al.*, 2010) modulation. Furthermore, in our experiments the

recurrent projections of CA3 pyramidal population together with non-DG or MEC inputs could in principle support phase precession given that theta-modulated inhibition from the medial septum was intact. The specific mechanisms in this case, however, remain to be determined.

Surprisingly, pairwise correlations of the sequential activation of CA3 cells in behavior found in controls were not detectable on the theta scale without the DG input, despite remaining phase precession in the analyzed neuron pairs. The versatility of the DG network in supporting prospective coding in different brain states as shown here and previously (Sasaki *et al.*, 2018) suggests the intriguing possibility that the DG-CA3 feedback network is involved in sequence computations ascribed to CA3. In line with this, we also showed that pairwise correlations were sustained without the MEC despite a marked reduction in phase precession of the analyzed pairs, suggesting that the recurrent CA3 network together with its backprojections to DG support such associations. Although the interaction of CA3 with DG has been the subject of some interest (Hasselmo *et al.*, 2002; Lisman *et al.*, 2005; Treves & Rolls, 1992), elsewhere CA3 has often been considered in isolation from DG. This double dissociation highlights the unique role of DG in supporting CA3 sequential coding and suggest that the dynamics of DG-CA3 circuit should be considered a whole in analyzing processes thought to be important for memory storage (Sasaki *et al.*, 2018). Furthermore, given the nuances of the roles of dentate granule and mossy cells firing patterns (Danielson *et al.*, 2017; GoodSmith *et al.*, 2017; Senzai & Buzsáki, 2017), identification of the role of specific cells in sequence coding remains an interesting future direction to be explored.

To explain our empirical observations, we introduced a phenomenological model of CA3 phase precession. We sought to model theta modulated inputs to a model CA3 cell which included the two excitatory inputs that we were able to experimentally manipulate, as well as the

oscillatory inhibition which we considered to be a latent factor not directly observed in our experiments, but which could be inferred by studying the results of changing input parameters on the output in a model. Studies of the role of inhibition in cortical computations have emphasized its importance and prevalence (Isaacson & Scanziani, 2011). Indeed, previous models of phase precession have concluded that phase precession can arise as the result of the oscillatory interference of a somatic inhibitory drive with dendritic excitation (Kamondi *et al.*, 1998; Losonczy *et al.*, 2010; O'Keefe & Recce, 1993). We arrived at a similar conclusion via a different logic. Given our simple oscillatory interference framework, the direct, monosynaptic effect of excitation from DG and MEC inputs should produce symmetric effects on observed measurements. Because DG affected prospective theta firing in CA3 whereas MEC did not, we reasoned that this effect must be mediated indirectly via local interneurons. Model parameters that gave rise to phase precession measures similar to the empirical observations included the theta phase shift between the excitatory and inhibitory inputs and the oscillatory amplitude of inhibition. Biologically, this effect could be mediated via two separate classes of interneurons with distinct connectivity patterns with the upstream inputs. Entorhinal cortex inputs impinge on apical dendrites of hippocampal cells, whereas the intrahippocampally sourced inputs tend to converge on their basal dendrites (Megías, Emri, Freund, & Gulyás, 2001; Steward & Scoville, 1976). One possibility is that the dentate gyrus modulates the theta phase of cholecystokinin (CCK), soma-targeting basket cells (Klausberger *et al.*, 2005), which in turn leads to the resulting interference pattern with the monosynaptic excitation to promote the prospective firing of CA3 pyramidal neurons during late parts of the theta cycle. Alternatively, parvalbumin positive (PV) interneurons could be the intermediary since the spikes of pyramidal cells occurring late in the theta cycle shifts to earlier phases when the PV interneuron drive is

diminished in the network (Royer *et al.*, 2012). On the other hand, the MEC input could modulate the inhibition strength on CA3 cells via somatostatin (SOM) interneuron (Amilhon *et al.*, 2015; Royer *et al.*, 2012), contributing to the range of phase precession as suggested by our model.

While many important scientific insights can be gained by studying how experimental manipulations alter the first moment (i.e., mean) of a parameter's distribution, understanding how the second (central) moment (i.e., variance) of the parameter distribution is affected by the manipulations can provide additional novel insights. Indeed, we showed that DG and MEC lesions alter CA3 spike phase variability in different ways (Figure 2.3-2.4). Together with previous experiments, these findings suggest that phase precession is a result of phase delayed onset of spiking at low levels of excitation (corresponding to entry to place field) rather than a phase advance with increased excitation (corresponding to exit from place field) as both distal dendritic excitation alone (Losonczy *et al.*, 2010) (that is, not paired with somatic inhibition) as well as proximal dendritic excitation paired with somatic inhibition (Magee, 2001) reproduce a time-advanced temporal profile of action potential initiation reminiscent of the phase-advanced spikes when distal dendritic excitation is paired with somatic inhibition. This suggests that spike initiation is a function of current integration biophysics of the cell which in turn could be altered by modulating the phase of the coincident excitation and inhibition. While in previous experimental setups the dendritic and somatic stimuli were always 180° out-of-phase (Harris *et al.*, 2002; Kamondi *et al.*, 1998; Losonczy *et al.*, 2010; Magee, 2001), our computational model suggests that the dentate gyrus could regulate spike timing due to the phase differential between the respective inputs via its projections to the local inhibitory circuit. Computationally, delaying the early spikes in CA3 may serve to segregate entorhinal and DG signals over the theta cycle to

filter out the mismatched inputs thereby preventing their potentiation in the synaptic matrix. Thus, a lack of phase precession should lead to the saturation of the synapses and destructive interference among memories.

The degree to which neural firing obeys the accurate ordering experienced in behavior correlates with the quality of subsequent replay sequences in sleep (Drieu *et al.*, 2018). Our phenomenological model was not aimed at explaining how the DG-CA3 circuitry ensures that, over the course of an ordered visit to two overlapping place fields, the spikes of the first cell occur earlier in the theta cycle despite lack of phase precession. Mechanistically, it remains an open question how the dentate gyrus contributes to this phenomenon. In particular, the fine temporal structure of coordinated firing of the DG-CA3 network with regards to replay both in awake behavior (Sasaki *et al.*, 2018) and sleep is yet to be elucidated. Moreover, future efforts are required to integrate our model with a model in which the temporal pattern separation by DG is mapped out.

Approvals

All experimental procedures were approved by the Institutional Animal Care and Use Committee at the University of California, San Diego, and conducted at the University of California, San Diego according to National Institutes of Health guidelines.

Methods

Subjects and Surgical Procedures

Subjects

All data used in the present study has been previously collected and published (Sabariego *et al.*, 2019; Sasaki *et al.*, 2018). We reanalyzed and compared these data from a total of 31 rats in the present report (Table 2S.1). These included 4 control and 9 lesioned rats in the DG lesion experiment with CA3 or dual CA3-DG (2 of 4 control rats) single-unit recordings; 7 control and 8 lesioned rats in the MEC lesion experiment with CA3 single-unit recordings; and 3 control rats with only DG recordings. Neural data from DG recordings were analyzed exclusively for Figure 2S.3. All subjects were male Long-Evans rats and between the ages of 3 and 6 months old at 300-350g of weight. The animals were kept on a 12 hour light-dark cycle (7 AM to 7 PM dark) and housed individually. Once the animals were habituated to the laboratory environment and ready for the experiments, they were food deprived to obtain a body weight of 85% or more *ad lib* baseline. Water access was not restricted.

Experimental Procedures and Brain Lesions

The details of the DG lesion and MEC lesion experiments were published previously and should be consulted as needed (Sabariego *et al.*, 2019; Sasaki *et al.*, 2018). In brief, rats in the DG lesion experiment were trained on the 8-arm radial maze to perform a working memory task

(see below). Those rats that were initially designated to receive DG lesions (N = 9; $LESION^{(DG)}$) underwent a surgical procedure during which colchicine was bilaterally infused into the dorsal and ventral dentate gyrus. The remaining rats (N = 4; $CTRL^{(DG)}$) were subjected to a sham lesion procedure (infusion of vehicle). During the same surgical procedure, a hyperdrive of 14 independently moving tetrodes was implanted above the right hippocampus for electrophysiology as described below. Rats in the MEC lesion experiment were trained on the figure-8 continuous spatial alternation task (described below). These rats underwent a single surgical procedure whereby the control rats (N = 7; $CTRL^{(MEC)}$) received a sham lesion (injection of vehicle) and the experimental rats (N = 8; $LESION^{(MEC)}$) received an excitotoxic lesion of MEC via the injection of NMDA.

In post-mortem histological material, the final position of the recording tetrodes was confirmed by performing cresyl violet staining of the sectioned brain tissue. In the DG Lesion experiment, the loss of dentate granule input to CA3 cells was confirmed by TIMM stains as previously described in detail (Sasaki *et al.*, 2018). The extent of DG granule cell damage was quantified in a localized fashion. Specifically, each tetrode ending location was scored based on the intensity of the TIMM-positive staining in histological sections. Scores of 0 (~0% TIMM-positive signal), 1 (< 30% signal), or 2 (< 70% signal), 3 (> 70% signal) were assigned to tetrodes obtained from DG lesioned animals, and tetrodes with scores of 0, 1, and 2 were included in the $LESION^{(DG)}$ data set. A score of 4 was used for control data, which are included as $CTRL^{(DG)}$ data. The extent of MEC lesions was confirmed quantitatively (Sabariego *et al.*, 2019) to be 93.0% of total MEC volume (95.3% of layer II, 92.4% of layer III, and 91.4% of deep layers), with the majority of sparing in the most ventral portions of MEC.

Hyperdrive Implants

An array of 14 independently moving tetrodes was implanted over the right hippocampus in all 28 rats (control group: 4.0 mm posterior and +2.7 to +2.9 mm lateral to bregma; DG lesion group: 3.5 to 4.4 mm posterior and +2.8 to +3.2 lateral to bregma; MEC lesion group: -4.0 mm posterior and +2.8 lateral to bregma). The hyperdrive was secured with skull screws and dental cement to prevent mechanical instability. The tetrodes (with tips platinum plated to 150-300 kΩ at 1 kHz) were slowly lowered each day over a period of 2-4 weeks to ensure recording stability and minimizing damage to the brain. Depth records, LFP signals, and neural spiking markers were used to estimate tetrode distance from the target region. After an initial period of larger advances, the tetrodes were moved only in small increments over several days until a satisfactory signal (i.e., low-amplitude multiunit activity) was observed. Once near CA3, the tetrodes were allowed to settle inside the stratum pyramidale of the CA3 of the hippocampus with no further active movement of the tetrodes to maximize recording quality (i.e., high-amplitude multiunit activity).

Electrophysiological Recordings

A Neuralynx Cheetah recording system with a multichannel head-mounted preamplifier was used for LFP and single-unit recordings. A signal from a skull screw was used as animal ground, and a reference signal from the neocortex was subtracted from the hippocampal signals to increase the hippocampal signal to noise ratio. Unit recordings were filtered at 600 Hz to 6 kHz, and spike waveforms above an amplitude of 40 μV were time-stamped and recorded at 32 kHz for 1 ms. LFP recordings were filtered between 1 and 425 Hz in the DG lesion experiment and between 1 and 450 Hz in the MEC lesion experiment.

Behavioral Tasks

DG Lesion Experiment (Spatial working memory on the 8-arm radial maze)

We trained the animals in the DG lesion experiment to perform a DG-dependent spatial working memory task (Sasaki *et al.*, 2018). The task used a maze with a central platform and 8 radial arms that each had a proximal segment that could be lowered and raised. The rats were first placed on the central platform (i.e., "stem") of the 8-arm maze with all 8 arms lowered such that the reward cups at the end of each arm were inaccessible to the animal (Figure 2S.1a). Next, the experimenter raised one arm at a time, for four arms, following a previously generated pseudorandom sequence. The rat was allowed to run down each raised arm and upon its return to the stem that arm was lowered and the next arm in the sequence was raised. Once the rat had visited all four experimenter-forced arms ("forced choice" phase), all 8 arms were raised and available for the rat to visit ("free choice" phase). The optimal strategy would consist of the rat visiting every one of the four arms unvisited during the forced-choice phase without reentering any arm. A total of 13 rats (N = 4 $CTRL^{(DG)}$; N = 9 $LESION^{(DG)}$, dentate granule cell lesions) were trained and tested in this task while CA3 single-unit recordings were made.

MEC Lesion Experiment (Figure-8 continuous alternation working memory task)

In the MEC lesion experiment, the rats were trained to perform a hippocampus dependent alternation task on the figure-8 maze (Sabariego *et al.*, 2019). In this task, a rat is placed in a delay zone at the base of the figure-8 maze (Figure 2S.1b) and is required to run up the "stem" of the maze toward a T-junction from where it can choose between reward locations on either the left or right before returning on a side arm to the delay zone. Blocks of trials with and without delays were performed. In non-delayed trial blocks the delay site is not actually used to restrict the animal's movements. In delayed trial blocks a barrier restricted the rat's progress for 2, 10, or 60 seconds for each trial. These blocks were not distinguished for the analyses presented here. This first trial ("trial 0") is discarded. However, it is used on the following lap to determine the

success of the animal in choosing the right or left reward. From the second trial onwards (trial 1 and later), a trial is "correct" if and only if the animal chooses to visit the reward location not visited on the preceding trial. If the animal chooses the same side more than once, it will not receive a reward at the visited reward site. It will, however, continue to receive reward items at the appropriate reward sites as soon as it chooses the side not chosen on the previous trial. A total of 19 rats (N = 7 $CTRL^{(MEC)}$; N = 8 $LESION^{(MEC)}$, with complete lesions to the medial entorhinal cortex) were trained and tested on this task.

Data Analysis

All statistical tests were chosen to appropriately match the underlying data distributions. In the case of testing proportions, χ^2 tests were used. In the case of testing for means, first the normality and homoscedasticity were tested with Anderson-Darling and F-test, respectively. If the data were concluded to be normal, t-tests or ANOVAs were performed as appropriate. Otherwise, rank-sum or Kruskal-Wallis tests were applied as appropriate. For comparing the distributions, the Kolmogorov-Smirnov test was used. The α level was set to 0.05 for all experiments and tests.

Spike Sorting.

Spike sorting was performed offline using a custom version of MClust (A. David Redish, University of Minnesota). Clusters were selected in the sleep sessions before and after a behavior and matched to the data recorded during the behavior to ensure consistency and reliability. The cross-correlogram was used as an additional criterion to ensure cluster independence. Only well separated clusters were retained for analysis.

Spatial Firing Properties.

The measures included in Figure 2S.2 are defined as follows. Let N be the total number of spikes of a given cell, and the number of such spikes that were part of a detected train (as defined below) denoted N_t. The proportion of spikes assigned to a train is defined N_t/N. The firing rate is defined as $\lambda = N / T$ where T is the summed total duration in seconds of all behavioral trials in a given session. The number of spikes per train is calculated for each cell as the N / N_{tr} where N_{tr} is the number of detected trains for that cell. To calculate the train length we first found the physical position of the first and last spikes of a train on the maze (points $P_1 = (x_1, y_1)$ and $P_N = (x_N, y_N)$). The train length L is calculated as $L = \sum_{i=2}^{N} ||P_i - P_{i-1}||$, where $||\cdot||$ is the L_2 norm. The number of bins covered was calculated as the total number of square bins of size 2 centimeters that contained at least one point from the path of a detected train. The information content measure was adapted from (Skaggs, McNaughton, Gothard, & Markus, 1992) and was calculated as $H = \sum_x \lambda(x) \log_2 \frac{\lambda(x)}{\lambda} p(x) dx$, where λ is the mean firing rate and p is the probability mass function of the rat's position over the spatial bins of the maze. The selectivity and sparsity measures were drawn from (Skaggs *et al.*, 1996) and are defined, respectively, as $S = \frac{E[\lambda]}{E[\lambda^2]}$ and $s = \frac{\lambda_{max}}{\lambda}$, where E is the expected value over the spatial bins and λ is the mean rate as defined above.

Rate map construction.

First, those intervals during the periods delimited by trial timestamps in which the velocity of the animal exceeded 2 cm/s were selected. For each cell, all spikes that occurred outside these intervals were excluded for the purpose of rate maps construction. Next, the environment was divided into square bins of side length 5 cm and the spikes that occurred in each such bin were counted. The occupancy matrix was constructed similarly by counting the number of position tracking points falling in each spatial bin multiplied by the tracking

acquisition rate (29.97 FPS). The rate map was the result of the element-wise division of the spike count matrix by the occupancy matrix, spatially smoothed with a 2-d Gaussian of kernel size 15 cm.

Spike Train Detection.

A spike train was defined as the set of 5 or more consecutive spikes with a maximal inter-spike interval of 500 ms. Additional criteria were imposed on the selection of spike trains for analysis as follows (Figure 2S.2c). A spike train (a.k.a. "pass") was deemed valid for analysis if it was at least 300 ms and no more than 2500 ms in duration, its corresponding path was at least 20 cm long (see above for the calculation of pass length), its corresponding path endpoints were at least 10 cm apart in physical space, and if the average velocity of the animal during the pass exceeded 2 cm/s. All of a cell's detected trains were discarded if its mean firing rate over the duration of the behavior was smaller than 0.1 Hz or greater than 5 Hz.

LFP Analysis and Theta Phase Extraction.

Local field potentials were recorded from one of the electrodes for each tetrode. The raw LFP signal was filtered in the theta range (6-10 Hz) and the channel with the largest theta rectified RMS power was selected as the reference for phase precession analysis. The phase estimate was obtained by $\phi = \tan^{-1}\frac{\Im\mathfrak{m}(H(s))}{\Re\mathfrak{e}(H(s))}$ under linear interpolation, where $H(\cdot)$ is the Hilbert transform and s is the 6 Hz to 10 Hz filtered LFP signal.

Quantification of Phase Precession.

The distance and theta phase variables were extracted from the detected trains. For each train, the last tracked point before the first spike, and the first tracked point after the last spike were marked as the Start and the End of that train's corresponding trajectory. Next, every spike timestamp was normalized with respect to the Start and End points' timestamps, yielding vector

d of normalized distances. Taken together with the theta phase vector ϑ described above, the circular-linear regression was then computed on the (d, ϑ) pairs for each train or cell, as described below. The circular-linear regression produced a slope value s and the estimate of explained variance r^2. The onset phase Φ_{on} was calculated for each train as the circular mean theta phase of the spikes occurring in the first (possibly truncated) theta cycle of the train. The offset phase Φ_{off} was defined similarly, except over the last theta cycle of the train. These four values are referred to as phase precession "measures" in the modeling section.

Population level quantification of remaining phase precession.

Two methods were employed for the quantification of the phase precession in each data set.

Slope-by-cell analysis. In this method, first the $\left(d^{(i)}, \vartheta^{(i)}\right)$ pairs were calculated for the N detected trains for a CA3 cell. Next, all such pairs were concatenated to obtain a single pair (d, ϑ) of length equal to the total number of spikes from the CA3 cell. The circular-linear regression was then performed on this pair to obtain the slope and explained variance measures (described above) for the CA3 cell in question. This was then done for every qualifying CA3 cell. The quantifications of proportions and cells were performed on the values thus obtained. A cell was deemed to exhibit "phase precession", if the circular-linear regression p-value was less than $\alpha = 0.05$.

Slope-by-train analysis. Here, the circular-linear regression was directly performed on the $\left(d^{(i)}, \vartheta^{(i)}\right)$ pairs to produce values of slope $s^{(i)}$ and explained variance ${r^2}_{(i)}$. The statistics of proportions were then performed on the cell-averaged values (such that each cell contributed a single slope and r^2 value regardless of the number of its trains). The Φ_{on} and Φ_{off} values were

only defined for trains, though instead of averaging them per train, they were directly used to find the distributions used in Figure 2.3.

Spike phase variance analysis.

For Figure 2.5d, circular variance was calculated either across all spikes of each neuron or across the timestamps resulting from replacing each cycle's spikes with their mean. Notice that even though this operation reduces the total number of spikes, it will not necessarily reduce the variance; this would depend on the distribution of spikes within the theta cycle and the phase reliability firing windows of a cell over multiple trains. This in turn is depends on the brain circuitry which is manipulated by experimental conditions (CTRL, DG lesions, or MEC lesions). For Figure 2S.3c, we used a similar binning scheme as for Figure 2.5d but the binning was performed on the actual place field of the neuron, defined as the area within the 20% contour of the place maps. We then calculated the circular standard deviation across all spikes of each cell in each bin and plotted the mean values together with the error bars representing the standard error of the mean.

Onset, offset and binned theta phase estimation.

The onset firing phase was defined as the circular mean phase of the spikes occurring in the first (partial) theta cycle of each train. The offset firing phase was analogously defined as the circular mean phase of the spikes occurring in the last (partial) theta cycle of each train. The histograms in Figure 2.3 are obtained from the single train onset and offset phase values for each group. To estimate firing probability in the binned theta cycle (Figure 2.4), we assigned a bin label (early, mid, or late, corresponding to $[0, 2\pi/3)$, $[2\pi/3, 4\pi/3)$, $(4\pi/3, 2\pi)$, respectively) to each spike and plotted the resulting discrete probability distribution (panels a and b). This

approach was repeated for each of 10 equal bins of the normalized position of spikes within a train to get a "position-resolved" theta bin firing probability estimate (panel c).

Cell pair sequence analysis.

Let $S = \{tr_i\}$ be the set of all spike trains detected in a given recording session, where tr_i is the $\underline{i}^{th}$ spike train (ordering not important) with spike timestamps $ts^{(i)}_j$ where $j = 1 \ldots n_i$, and n_i is the number of spikes in tr_i. Let $I_k(ts^{(i)}_j)$ be an indicator function that assumes 1 if an l exists for which $|ts^{(i)}_j - ts^{(k)}_l| < 125$ ms when $i \neq k$, and 0 otherwise. Spike train pairs (tr_i, tr_j) were selected for inclusion in this analysis whenever $\frac{\sum_j I_k(ts_j^{(i)}) + \sum_k I_i\left(ts_l^{(k)}\right)}{n_i + n_k} \geq 0.15$. The cross-correlogram was computed for such pairs and the relative time, τ, of the peak closest to the 0 time lag was found. The physical separation of the peaks of the two cells' place fields, d, was computed and used to make the pair (d, τ). In the case of the 8-arm maze where runs in opposite outbound and inbound directions were possible, each pair was treated twice—once for the inbound run and once for the outbound. In all cases only one of the two run directions had enough spikes to reliably assess pair co-modulation (i.e., the unreliable direction did not contribute a (d, τ) pair). Once all (d, τ) pairs were obtained for each experimental group, a linear regression line was fit to the data to assess the significance of the relationship between place field separation and theta co-modulation, as reported in Figure 2.6. For the phase precession plots in Figure 2.6b and Figure 2.6f, trains from each cell are first mapped to the animal's path and projected via dot product onto the line segment connecting the place field peaks of the of the two cells. The midpoint of this line segment was considered the origin (x = 0) and used on the x-axis of the phase-position plots. The sign of the direction of travel was defined to be positive if Cell 1's place field was visited before Cell 2's place field; otherwise, it was set to negative.

Computational model

Model description.

The model CA3 neuron received three distinct inputs. Two of these were excitatory (i.e., positively contributed to the model neuron's total drive) and one was inhibitory (i.e., negatively contributed to the total drive). The excitatory inputs modeled the DG and MEC monosynaptic excitatory drive that CA3 principal cells receive, while the inhibitory input modeled the total inhibitory input that these neurons receive. The equations governing the value of each of the three functions took the following forms:

$$G_{DG}(t) = \gamma_{DG}\left(\frac{g_{DG}}{2}\left[1 + cos\left(2\pi {\nu_1}^{(DG)} t\right)\right] + \frac{1}{2}\left[1 + cos\left(2\pi {\nu_2}^{(DG)} t\right)\right]\right)$$

$$G_{MEC}(t) = \gamma_{MEC}\left(\frac{g_{MEC}}{2}\left[1 + cos\left(2\pi {\nu_1}^{(MEC)} t\right)\right] + \frac{1}{2}\left[1 + cos\left(\psi + 2\pi {\nu_2}^{(MEC)} t\right)\right]\right)$$

$$G_{INH}(t) = I_{DC} + Acos(\phi + 2\pi\nu_{INH} t)$$

where ${\nu_1}^{(DG)} = 35Hz, {\nu_1}^{(MEC)} = 75Hz, {\nu_2}^{(DG)} = 8.6Hz, {\nu_2}^{(MEC)} = 8.5Hz, g_{DG} = 0.25, g_{MEC} = 0.075$, and $\nu_{INH} = 8Hz$, and I_{DC} represented the DC (baseline) component of inhibition. The gamma oscillation frequencies were chosen to represent the mid points of generally accepted slow (20-50 Hz) and fast (50-100 Hz) gamma oscillations *in vivo*. Gain coefficients γ_{DG} and γ_{MEC} were chosen appropriately for each section of the experiments (see Results). In the above equations, ψ controls the phase difference of the two excitatory inputs by essentially timing only the MEC input while the DG input remains the same. Effectively, this could cause the place field to shift around slightly which we shall ignore. Here, ϕ denotes the excitatory-inhibitory phase differential, which in the text is referred to by ϕ_{inh} for clarity. I_{DC} was drawn from a Gaussian with a constant mean between 0.5 and 25 (with specific values given in Results) and variance 0.025.

To produce the total drive, the inputs combined as follows:

$$G(t) = \gamma\left(H\left(\left(M_{DG}(t)\cdot G_{DG}(t) + M_{MEC}(t)\cdot G_{MEC}(t) - G_{INH}(t)\right)^2\right)\right)$$

where $\gamma(x) = \sqrt[4]{x^3}$, H is the Heaviside function and M represents a spatial modulation function. A spatial modulation function to each of these inputs to mimic the influence of DG and MEC inputs to the early and late portions of place fields, respectively (see Figure 2.4) (Sanders *et al.*, 2015). These functions are defined as follows:

$$M_{DG}(x) = \frac{exp\left(\left[\frac{1}{2} + N_x(0.3,0.65)\right]^{\eta_{DG}}\right)}{max_{[0,1]}\left(exp\left(\left[\frac{1}{2} + N_x(0.3,0.65)\right]^{\eta_{DG}}\right)\right)}$$

$$M_{MEC}(x) = \frac{N_x(0.7,0.45)^{\eta_{MEC}}}{max_{[0,1]}(N(0.7,0.45)^{\eta_{MEC}})}$$

where $\eta_{DG} = 2$ and $\eta_{MEC} = 4$ are concentration parameters and $N_x(\mu, \sigma)$ is the Gaussian distribution with mean μ and standard deviation σ. The argument to the Heaviside function is referred to as the "sum-square" step in Figure 2.7. We set the G_{DG} or G_{MEC} terms to 0 to simulate DG or MEC "lesions", respectively.

Spike generation.

The total drive obtained in the previous step was normalized to define a probability distribution and used as an intensity function for an inhomogeneous Poisson process to generate the spikes. The phase precession measures were calculated for these simulated trains as described for the empirical data.

Mapping of model output to empirical data.

The phase precession measures (slope, variance explained, onset phase, offset phase) obtained by simulating the model with various combinations of free parameters (A, I_{DC}, and ϕ_{inh})

were individually compared to those obtained by analyzing the experimental data from control, DG lesioned, or MEC lesioned rats. Each set of empirical phase precession measures was compared to the phase precession measures obtained from analyzing the corresponding model instantiation (CTRL to full model (no terms set to 0), $\text{LESION}^{(\text{DG})}$ to "DG-lesioned" model, and $\text{LESION}^{(\text{MEC})}$ to "MEC-lesioned" model). Each measure from the model that was within a quartile (in each direction) of the empirical median of the measures was considered admissible (blue regions in the binary plots of Figure 2.7d,e). Free parameter combinations that produced four admissible measures were accepted (Overlap plots in Figure 2.7d,e). Finally, the accepted free parameters were compared between lesion and control instantiations of the model by plotting the histogram of their distribution (Figure 2S.9). The model predictions were obtained by comparing full-width at half maximum (FWHM) intervals in these histograms.

Acknowledgements

Chapter 2, in full, is currently being prepared for submission for publication of the material by Ahmadi, S, Sasaki, T, Sabariego, M, Leibold, C, Leutgeb, S, and Leutgeb, JK. The dissertation author was the primary investigator and author of this material.

Appendix 2.1: Supplementary Figures

Figure 2S.1: Behavioral tasks and spike train detection. (a-b) Behavioral tasks. In rats, successful completion of these spatial working memory tasks depends on the hippocampus, making it possible to study effects of selectively DG and MEC lesions on CA3 information processing. The gray areas indicate the maze regions covered by a rat during an example trial. **a**, The radial 8-arm maze spatial working memory task. **b**, The figure-8 alternation spatial working memory task. **c**, Criteria applied to detect spike trains. The Train Detection step starts by extracting sets of at least 5 spikes whose inter-spike interval is 500 ms or less. Of these trains, those with duration ≥ 300 ms, path length ≥ 20 cm, path end points at least 10 cm apart, and an average velocity ≥ 2 cm/s were selected for further analysis. This results in 0 or more trains per cell. Cells with 0 qualifying trains or firing rate ≥ 5 Hz are excluded from further analysis. These criteria ensured that trains across recordings had statistically comparable behavioral characteristics with sufficient sampling to minimize artefactual findings. **d**, The train detection method visualized. Left, single trial with spikes from a cell in the $CTRL^{(DG)}$ group. The subset of spikes that meets the criteria is shown in red. The other spikes which do not qualify as a train are in light blue and dark blue. The spikes are mapped onto space and displayed on the path of the rat in the trial. The numbers in the rasters are in milliseconds. Two more example trains are shown to the right. The top example is excluded because the train length is less than 20 cm to reduce errors due to insufficient spatial and theta cycle sampling.

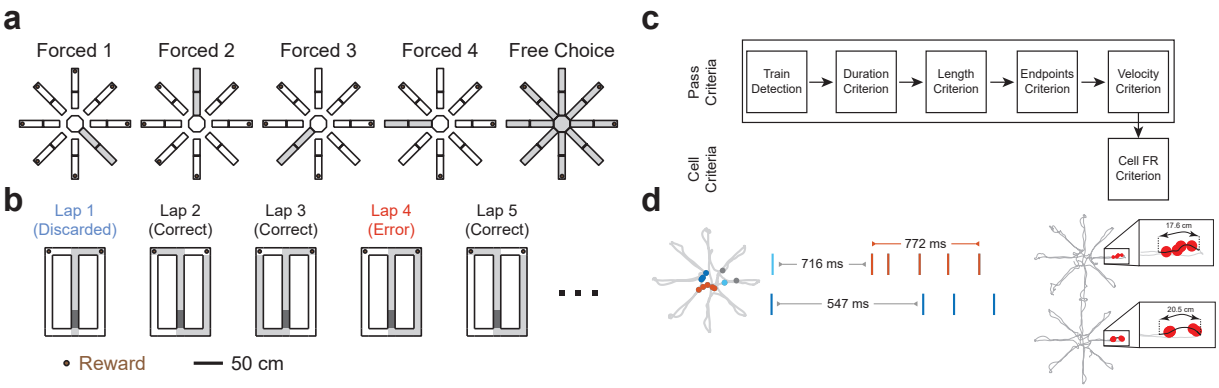
a
Forced 1
Forced 2
Forced 3
Forced 4
Free Choice
b
Lap 1
(Discarded)
Lap 2
(Correct)
Lap 3
(Correct)
Lap 4
(Error)
Lap 5
(Correct)
Reward
50 cm
c
Pass Criteria
Train Detection
Duration Criterion
Length Criterion
Endpoints Criterion
Velocity Criterion
Cell Criteria
Cell FR Criterion
d
772 ms
716 ms
547 ms
17.6 cm
20.5 cm

Figure 2S.2: Differences in the requirements of the two spatial working memory tasks had minimal effects on physiological neural coding. Control data in the two spatial working memory tasks were largely comparable, indicating that comparison of the respective roles of DG and MEC inputs to CA3 in the tasks was justified. **blue**: Control data from rats performing the radial 8-arm maze spatial working memory task, **red**: Control data from rats performing the figure-8 maze spatial working memory task. **a**, Proportion of the recorded spikes that were assigned to trains ($p = 0.185$). **b**, Average firing rate in the selected trains log-transformed to obtain normally distributed data ($p = 0.142$). **c**, The number of spikes per train was different between the two groups ($t_{183} = -3.6226$, $p = 3.78 \times 10^{-4}$; log-transformed two-sample *t*-test). **d**, The train length in cm was also different across the control groups (*z*-value = -2.3012, rank sum = 6977, $p = 0.0214$; Wilcoxon's rank sum test). **e**, The spatial extent of the mazes was divided into a grid of 2 cm by 2 cm bins. The number of bins that contained any portion of a train's corresponding path was counted and displayed ($p = 0.941$). **f**, Information content of the trains measured in bits per spike was not different ($p = 0.183$). **g**, Selectivity, as defined by Skaggs and colleagues [2], was not different ($p = 0.209$). **h**, Sparsity, as defined by Skaggs and colleagues [2], was not different ($p = 0.375$). All data tested for normality with the Anderson-Darling test. If both the original and log-transformed data were deemed not normal by the test, Wilcoxon's rank sum test was used to test differences; otherwise, a two-sample *t*-test was used on the original data (not log-transformed). Error bars mean ± s.e.m.

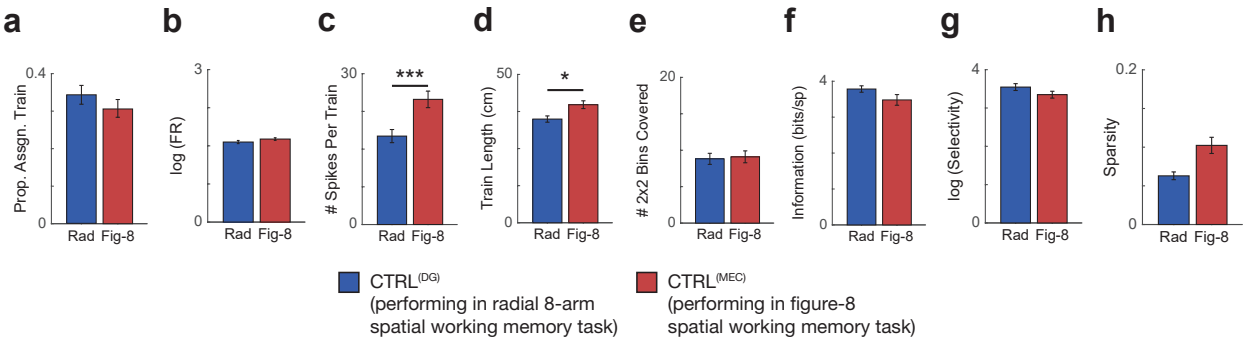
a
b
c
d
e
f
g
h
Prop. Assgn. Train
0.4
0
Rad Fig-8
log (FR)
3
0
Rad Fig-8
Spikes Per Train
30
0
***
Rad Fig-8
Train Length (cm)
50
0
*
Rad Fig-8
2x2 Bins Covered
20
0
Rad Fig-8
Information (bits/sp)
4
0
Rad Fig-8
log (Selectivity)
4
0
Rad Fig-8
Sparsity
0.2
0
Rad Fig-8
CTRL(DG)
(performing in radial 8-arm
spatial working memory task)
CTRL(MEC)
(performing in figure-8
spatial working memory task)

Figure 2S.3: Neurons recorded in the granule cell layer of the dentate gyrus increase their spike phase variability from the beginning to the end of place fields. a, Phase position plots of all neurons that were recorded on tetrodes confined by histology to end in the granule cell layer (N = 5 cells, 10 place fields, from 3 rats). The plots are sorted into a group with a clear pattern of increased phase variability later in the field (top) or little change in phase variability (bottom). **b,** Six examples of neurons recorded on tetrodes ending in the dentate gyrus but not in the granule cell layer (total recorded N = 13 neurons, 34 place fields, from 4 rats). From histology, tetrode endings in the hilar region or the subgranular zone are labeled "Hilus" here. **c,** Quantification of the variability (circular standard deviation) at various distances through the place field. These plots show that, compared to hilar and CA3 recordings, putative granule cell phase coding tends to be more reliable across multiple passes through the same place field. This is consistent with a role for granule cells' controlling the onset phase of CA3 pyramidal cells. Data are grouped into 10 bins along the normalized position. GCL, granule cell layer. Hilus: hilar or subgranular zone.

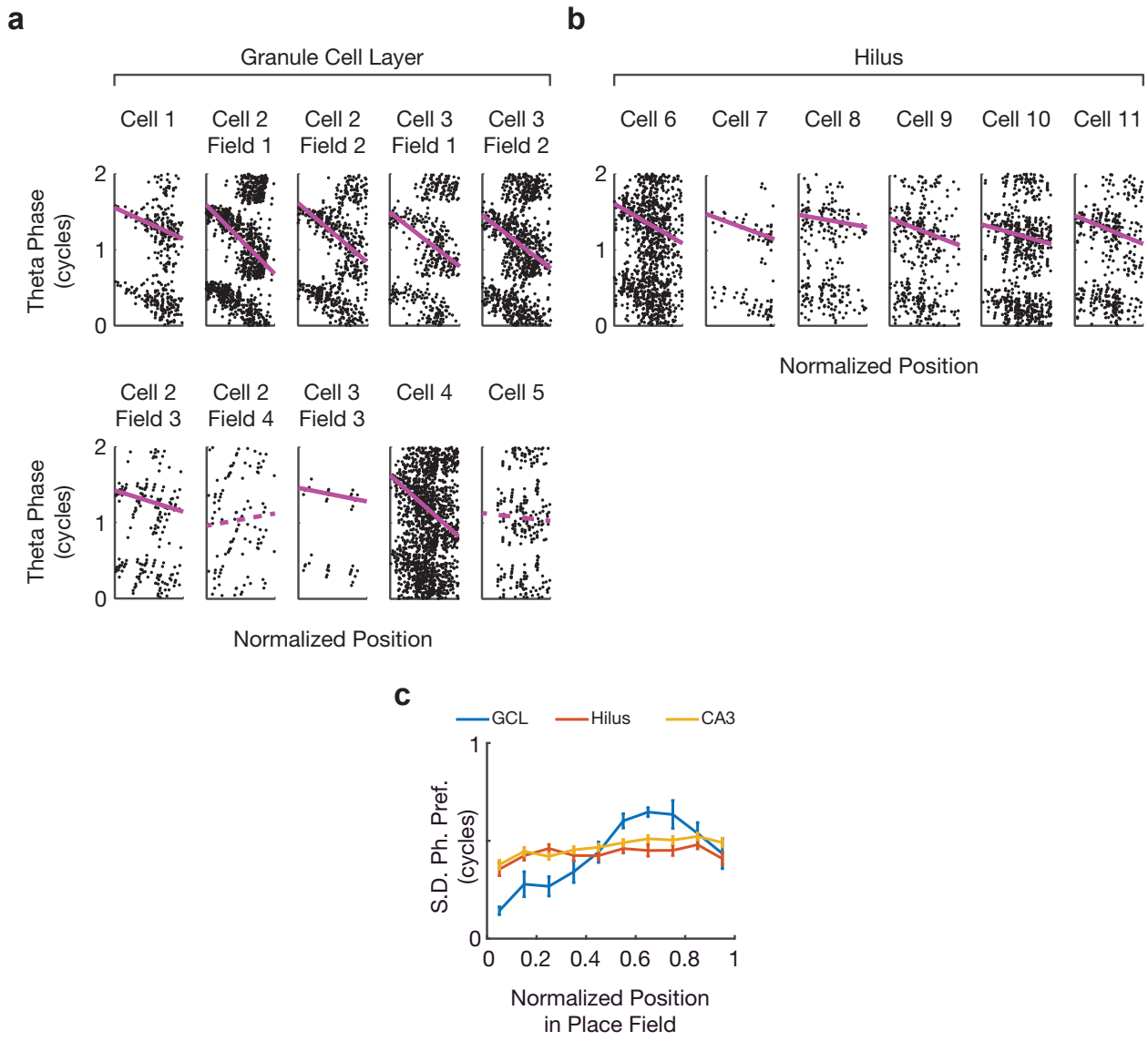
a
Granule Cell Layer
Cell 1
Cell 2 Field 1
Cell 2 Field 2
Cell 3 Field 1
Cell 3 Field 2
Theta Phase (cycles)
2
1
0
Cell 2 Field 3
Cell 2 Field 4
Cell 3 Field 3
Cell 4
Cell 5
Normalized Position
b
Hilus
Cell 6
Cell 7
Cell 8
Cell 9
Cell 10
Cell 11
Normalized Position
c
GCL
Hilus
CA3
S.D. Ph. Pref. (cycles)
1
0
0
0.2
0.4
0.6
0.8
1
Normalized Position in Place Field

Figure 2S.4: Replacing each cycle's spikes with their mean rescues CA3 phase precession in the absence of MEC, but not DG, inputs. a, Examples of a single train where replacing each cycle's spikes with their mean converts a positive circular-linear phase-position regression slope to a negative value. Below each example phase-position plot pair, the spike train and the mean timestamp for each cycle are displayed alongside the simultaneously recorded LFPs and theta rhythm. The example train on the far right had a statistically significant slope when the theta cycle mean of the spikes was considered. **b,** Additional examples of single trains from MEC lesioned rats where replacing each cycle's spikes with their mean led to a negative circular-linear regression slope. As in **(a)**, below each phase-position plot pair the spike train and the mean timestamp for each cycle are shown along with the LFPs and theta rhythm. Scale bars: horizontal: 200 ms, vertical: 200 μV.

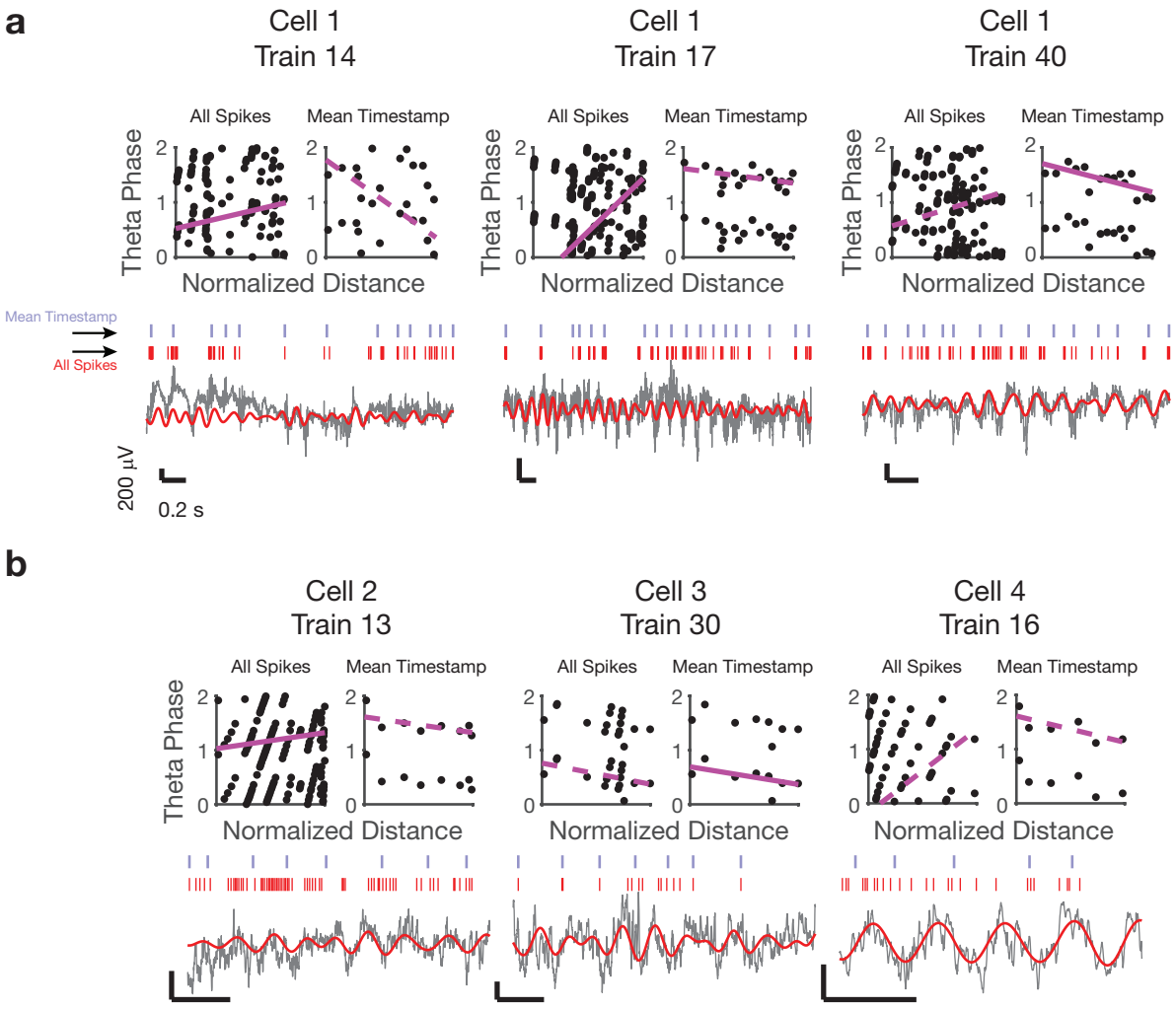
a
Cell 1
Train 14
Cell 1
Train 17
Cell 1
Train 40
All Spikes
Mean Timestamp
Theta Phase
Normalized Distance
Mean Timestamp
All Spikes
200 µV
0.2 s
b
Cell 2
Train 13
Cell 3
Train 30
Cell 4
Train 16

Figure 2S.5: Spike sorted clusters were of high quality and were well-separated. The clusters corresponding to the two members of each neuron pair shown in Figure 2.6 are marked in each panel. **a,** Clusters of the example pair for CTRL$^{(DG)}$ were simultaneously recorded on two different tetrodes and formed nice clusters. **b,** Clusters of the example pair for LESION$^{(DG)}$ were simultaneously recorded on two different tetrodes and formed nice clusters. **c,** Clusters of the example pair for CTRL$^{(MEC)}$ were simultaneously recorded on the same tetrodes but were well-separated and formed nice clusters. **d,** Clusters of the example pair for LESION$^{(DG)}$ were simultaneously recorded on two different tetrodes and formed nice clusters.

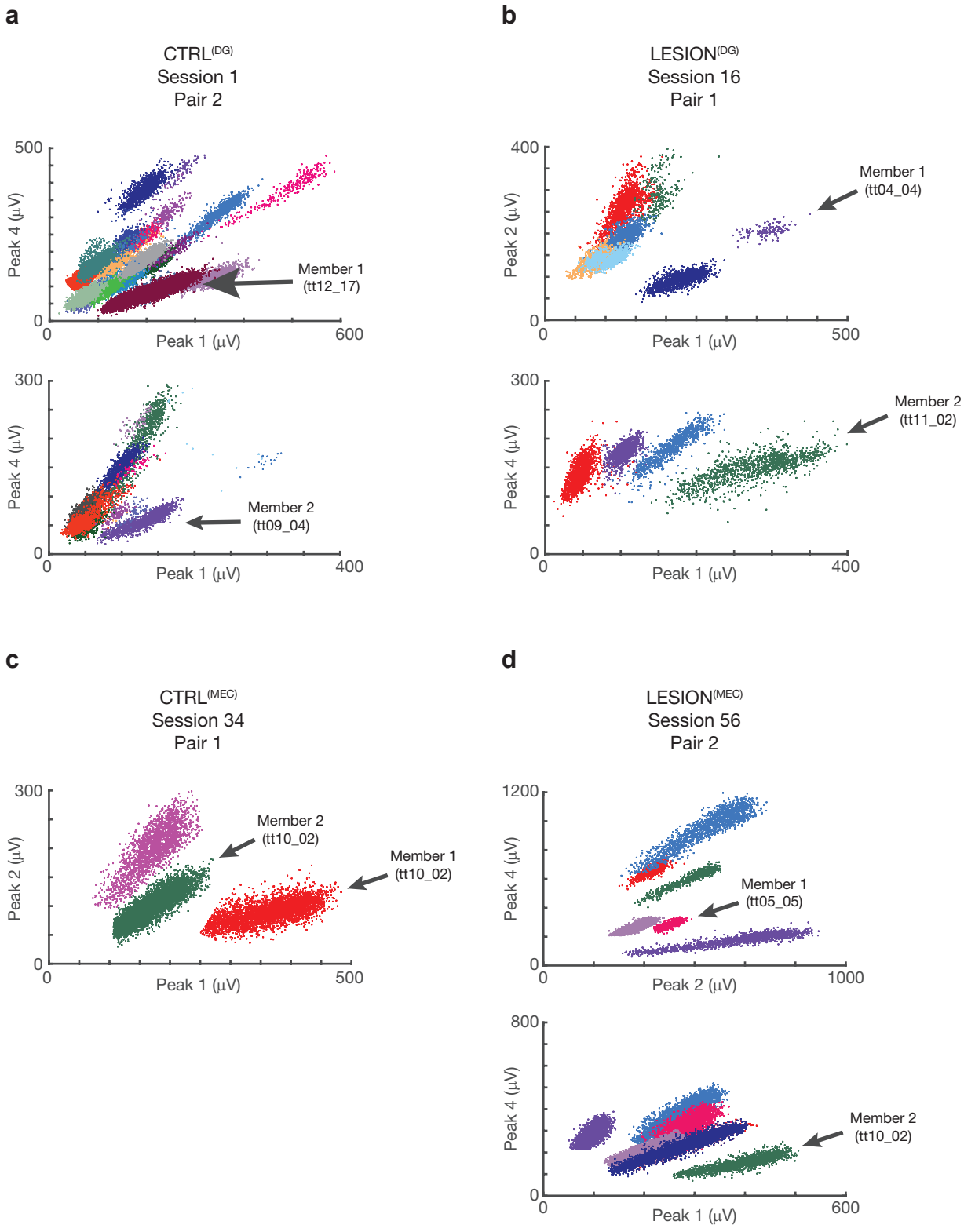
a
CTRL(DG)
Session 1
Pair 2
Peak 4 (μV)
Peak 1 (μV)
Member 1
(tt12_17)
Member 2
(tt09_04)
b
LESION(DG)
Session 16
Pair 1
Peak 2 (μV)
Peak 4 (μV)
Peak 1 (μV)
Member 1
(tt04_04)
Member 2
(tt11_02)
c
CTRL(MEC)
Session 34
Pair 1
Peak 2 (μV)
Peak 1 (μV)
Member 2
(tt10_02)
Member 1
(tt10_02)
d
LESION(MEC)
Session 56
Pair 2
Peak 4 (μV)
Peak 2 (μV)
Peak 1 (μV)
Member 1
(tt05_05)
Member 2
(tt10_02)

Figure 2S.6: Shifts in the phase relationship among DG, MEC, and inhibitory inputs result in a variety of phase precession profiles. These examples demonstrate the model's expressive power to capture a variety of possible scenarios arising in the analysis of phase precession, including both negative, zero, and positive slopes. **(a-i)** In each panel, the excitatory (ψ) and inhibitory (ϕ) phase shifts are indicated at the top. The slope and onset phase value pairs are, respectively, (-0.93, 50.9°), (+0.24, 123.9°), (-0.03, 189.3°), (+0.04, 114.3°), (-0.04, 150.9°), (-0.07, 169.2°), (+0.17, 144.1°), (+0.14, 152.6°), and (+0.14, 158.7°). For all panels, A = 14, I = 0.65.

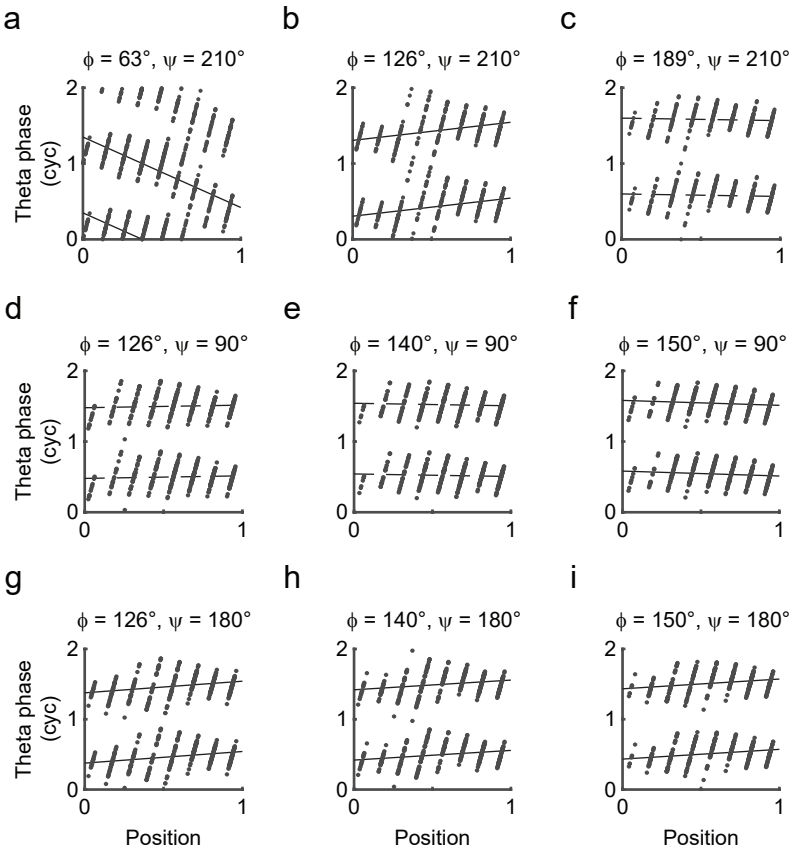
a
b
c
d
e
f
g
h
i
ϕ = 63°, ψ = 210°
ϕ = 126°, ψ = 210°
ϕ = 189°, ψ = 210°
ϕ = 126°, ψ = 90°
ϕ = 140°, ψ = 90°
ϕ = 150°, ψ = 90°
ϕ = 126°, ψ = 180°
ϕ = 140°, ψ = 180°
ϕ = 150°, ψ = 180°
Theta phase (cyc)
Position
0
1
2

Figure 2S.7: Relative phase shifts are the key parameters that determine the profile of virtual place fields. a, The color coded position of the largest peak resulting from the combined excitation and inhibition in the model, as a function of the excitatory (ψ) and inhibitory (ϕ) phase shifts with different spatial modulation concentration parameters (left, $\eta_{DG} = 2$, $\eta_{MEC} = 4$; right, $\eta_{DG} = 8$, $\eta_{MEC} = 8$). The peak is calculated separately for the relative phase shifts marked by black dots as a function of either the spatial modulation parameters or the gain coefficients and displayed below in **b** and **c**. **b,** Peak position is a fairly constant function of the concentration parameters (η). Peak position is calculated for various relative phase shifts and in all cases the variability is much less than in panel **(a)** where this is shown as a function of the relative phase shifts. **c,** Similar to **b**, peak position is a fairly constant function of the gain coefficients (manifested as large areas of constant color coding). The color bar above panel **(a)** applies to all panels. Thus, overall phase shifts drive a greater deal of variability in a virtual place field's peak than do other parameters.

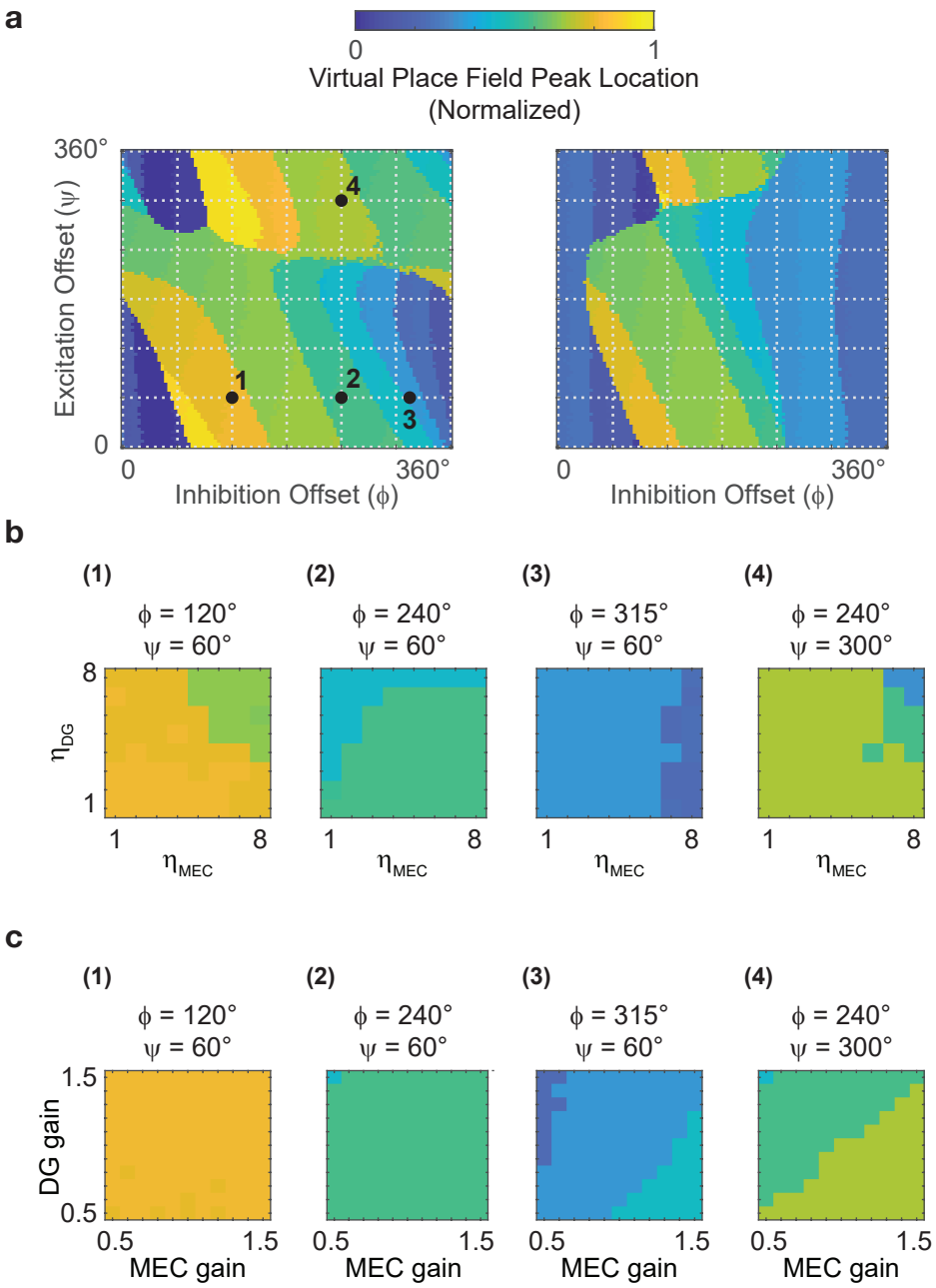
a
0
1
Virtual Place Field Peak Location
(Normalized)
360°
Excitation Offset (ψ)
0
4
1
2
3
0
360°
Inhibition Offset (ϕ)
0
360°
Inhibition Offset (ϕ)
b
(1)
ϕ = 120°
ψ = 60°
(2)
ϕ = 240°
ψ = 60°
(3)
ϕ = 315°
ψ = 60°
(4)
ϕ = 240°
ψ = 300°
8
1
η_DG
1
8
η_MEC
c
(1)
ϕ = 120°
ψ = 60°
(2)
ϕ = 240°
ψ = 60°
(3)
ϕ = 315°
ψ = 60°
(4)
ϕ = 240°
ψ = 300°
1.5
0.5
DG gain
0.5
1.5
MEC gain

Figure 2S.8: Baseline inhibition level (*I*) does not qualitatively alter the model state space. Model state space was explored by linear search along the *I* parameter. Three instances for each experiment are shown as described: **(a-b)** The state space obtained at $I = 4.5$ (9x that shown in Figure 2.7) via comparisons to empirical CA3 data in DG lesioned rats and the associated control rats **(a)**, or to empirical CA3 data in MEC lesioned rats and the associated control rats **(b)**. **(c-d)** $I = 8.5$ (13x) with empirical data from the DG **(c)** or MEC **(d)** lesion experiments, and **(e-f)** $I = 12.5$ (25x) with empirical data from the DG **(e)** or MEC **(f)** lesion experiments. The Overlap plots across all panels reveal state space matches that resemble those reported in Figure 2.7, indicating minimal effect of the baseline inhibition parameter (*I*).

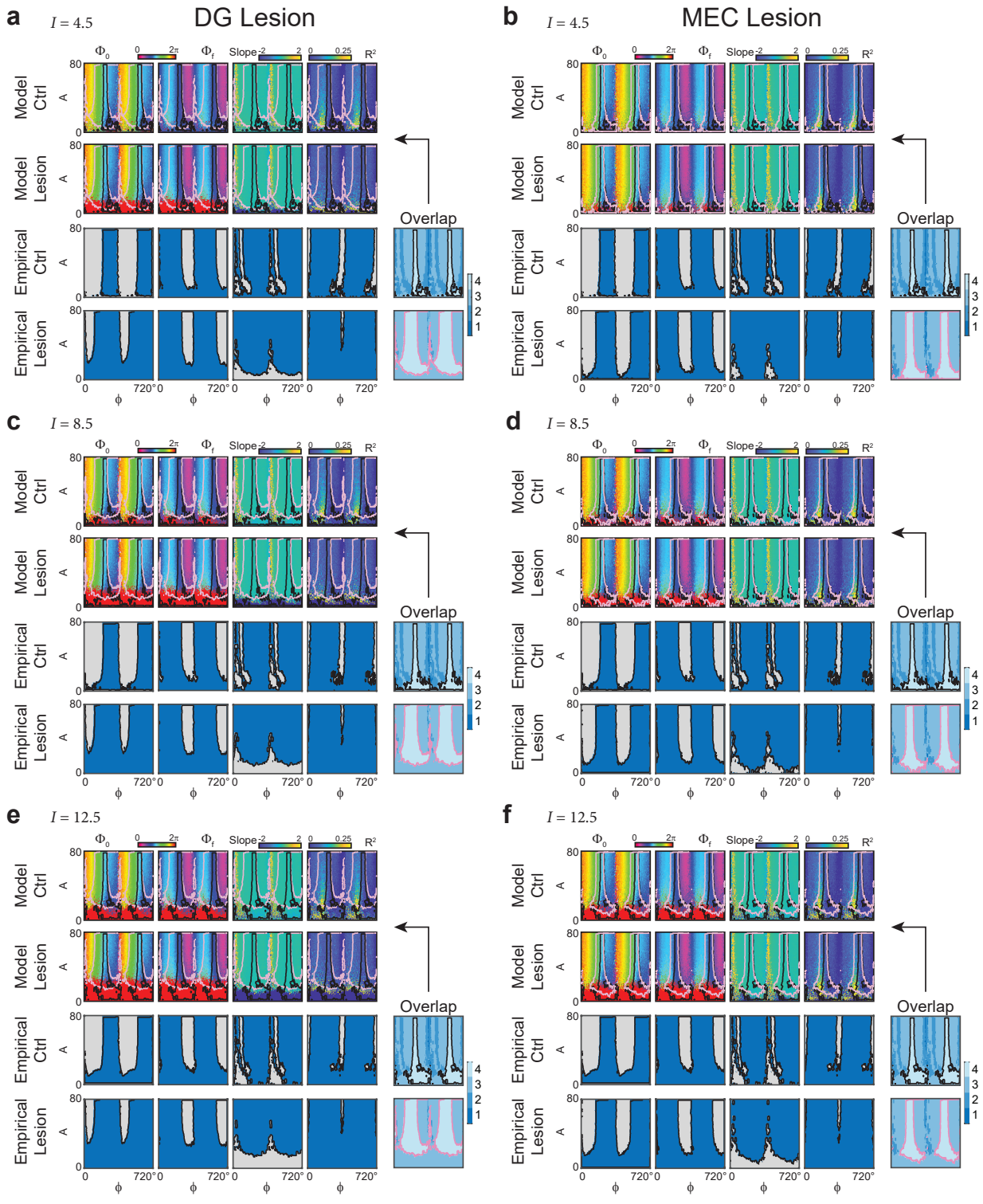
a
I = 4.5
DG Lesion
b
I = 4.5
MEC Lesion
c
I = 8.5
d
I = 8.5
e
I = 12.5
f
I = 12.5
Model Ctrl
Model Lesion
Empirical Ctrl
Empirical Lesion
Overlap
Slope
R²
A
ϕ
720°

Figure 2S.9: DG and MEC lesions alter CA3 phase precession along largely orthogonal dimensions. **a,** Distribution of parameter values A and ϕ_{inh} that reproduce the control (light blue) and lesion (dark blue) data in the DG lesion experiment. The histograms show the spread of regions of overlap in Figure 2.7d and Figure 2.7e for the ϕ_{inh} (top) and A (bottom) parameters, namely inhibitory phase shift and inhibitory amplitude. The DG lesions strikingly alter the profile of the ϕ_{inh} parameter (compare light and dark blue double arrows) while leaving the A parameter largely intact, up to a small shift (black arrow). Full-width at half maximum (FWHM) of the ϕ_{inh} histograms is indicated with stippled lines. **b,** As in **(a)** but for the MEC lesion experiment. In contrast to **(a)**, the MEC lesions mainly affect the profile of A parameter spread (compare the yellow and orange double arrows), while leaving the ϕ parameter largely intact, up to a small shift (black arrow). FWHM of the *A* histograms is indicated with stippled lines.

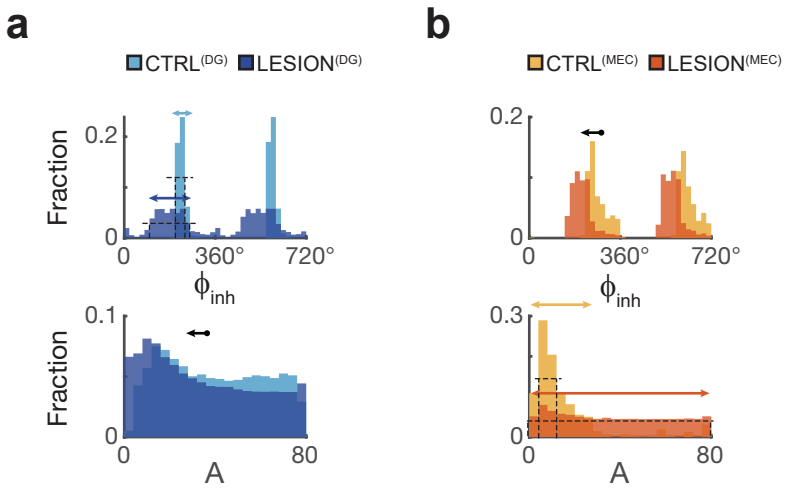
a
CTRL(DG)
LESION(DG)
Fraction
0.2
0
0
360°
720°
ϕinh
Fraction
0.1
0
0
80
A
b
CTRL(MEC)
LESION(MEC)
0.2
0
0
360°
720°
ϕinh
0.3
0
0
80
A

Figure 2S.10: Addition of gamma oscillations to the model does not qualitatively change the results. a, Model construction with the inclusion of gamma components. These components account for the presence of slow and mid gamma oscillations in the DG and MEC input terminals in the hippocampus, respectively (35 Hz and 75 Hz; see Methods). The rest of this panel follows the conventions of Figure 2.7. **b,** Similar to Figure 2.7d, but with the simulated values generated by the model that includes gamma components. **c,** Similar to Figure 2.7e, but with simulated values generated by the model that includes gamma components. In (**b**) and (**c**) the regions in overlap plots delineated by pink resemble those in Figure 2.7 obtained without gamma oscillations.

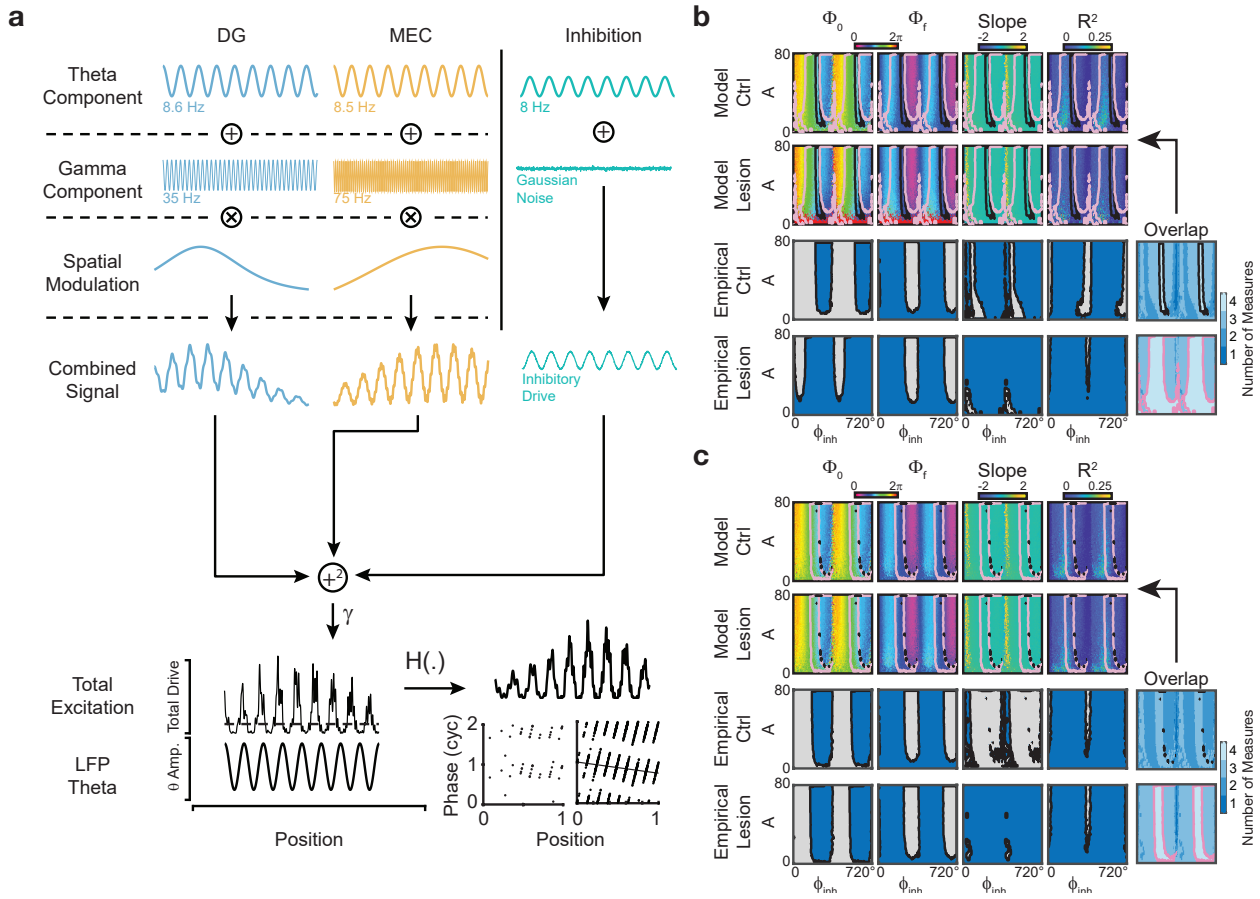
a
DG
MEC
Inhibition
Theta Component
8.6 Hz
8.5 Hz
8 Hz
Gamma Component
35 Hz
75 Hz
Gaussian Noise
Spatial Modulation
Combined Signal
Inhibitory Drive
γ
H(.)
Total Excitation
LFP Theta
Total Drive
θ Amp.
Position
Phase (cyc)
Position
b
c
Slope
Model Ctrl
Model Lesion
Empirical Ctrl
Empirical Lesion
Overlap
Number of Measures

Appendix 2.2: Supplementary Tables

Table 2S.1: Summary of rats used in this study.

Rat ID	Experiment	Experimental Condition	# Qualifying CA3 Units	# Qualifying DG Units	# Sessions
122	DG	CTRL	N/A	5	1
147	DG	CTRL	N/A	6	1
194	DG	CTRL	N/A	4	1
600	DG	CTRL	50	N/A	2
601	DG	CTRL	19	2	2
632	DG	CTRL	7	1	2
650	DG	CTRL	8	N/A	1
Total			84	18	10
599	DG	LESION	4	N/A	1
633	DG	LESION	5	N/A	2
648	DG	LESION	11	N/A	2
649	DG	LESION	4	N/A	2
656	DG	LESION	2	N/A	1
669	DG	LESION	20	N/A	2
672	DG	LESION	7	N/A	3
675	DG	LESION	7	N/A	1
684	DG	LESION	8	N/A	2
		Total	68	N/A	16
3661	MEC	CTRL	23	N/A	5
3839	MEC	CTRL	11	N/A	3
3840	MEC	CTRL	2	N/A	1
3906	MEC	CTRL	13	N/A	2
3931	MEC	CTRL	4	N/A	1
3958	MEC	CTRL	39	N/A	3
3959	MEC	CTRL	9	N/A	3
		Total	101	N/A	18
3656	MEC	LESION	5	N/A	1
3754	MEC	LESION	17	N/A	5
3756	MEC	LESION	10	N/A	2
3837	MEC	LESION	6	N/A	2
3903	MEC	LESION	9	N/A	2
3928	MEC	LESION	29	N/A	3
3978	MEC	LESION	48	N/A	3
3979	MEC	LESION	34	N/A	2
Total			158	N/A	20

CHAPTER 3: CONCLUSIONS AND FUTURE DIRECTIONS

By combining experiments, data analysis, and computational modeling, I was able to elucidate several aspects of the neural code that supports episodic memories. Specifically, I showed that the representations that develop in CA1 upon learning new spatial information follow a broad stability distribution, which suggests a mechanism for storing stable and unstable aspects of experience within the same population. Moreover, I showed how this could enable the hippocampus to implement an effective search algorithm to guide the animal's behavior towards remembered goal locations. I next showed that the two major theta-modulated inputs to the sequence generating core of the hippocampal CA3 area played distinct roles in supporting its theta phase precession. Through computational modeling, I illustrated how the underlying circuitry might in fact be implemented to give rise to the observed experimental data. This involved demonstrating that differences in how each input stream influences the inhibition onto the CA3 circuit determine the phase precession profile, suggesting the distinct involvement of different inhibitory interneuron types.

As neuroscientists we segregate behavioral epochs and the neural codes that support them for better experimental control and for breaking down a complex problem into manageable parts. The brain, however, is always active and continually performing its computations to support ongoing behavior, whether or not the rats are aware that they are being used in experiments. While my studies might appear to be focused on disparate phenomena, they were attempts at uncovering mutually interacting neural dynamics. From the point of view of the brain, the internal and external worlds are constantly influencing one another: the external world affects brain organization through sensation and additional internal processing, while the brain

influences the external world by driving the animal to perform different behaviors (e.g., via motor actions to actively sample the environment). By this perspective, the study of Chapter 2 was concerned with the first half of this interaction, while the study of Chapter 1 investigated the second half of it. In neuroscientific terms, I first showed how a heterogeneous population with diverse levels of representational stability could enable an effective search algorithm to guide the behavior of the animals toward remembered goal locations. Conversely, I next shed light on how the hippocampus develops a new representation upon being presented with new information, and how it might determine which synapses to prime for strengthening and weakening in "offline" states to retain this information (i.e., once behavior is over). While these studies advance our understanding of learning and memory, they also pave the way for asking novel questions via targeted experiments.

It is typical that once a scientific question is answered, multiple new ones emerge. One of the questions that my results raise is how sequences of ensemble activity get selected for further potentiation. As shown in the thesis, phase precession is observed across a large proportion of hippocampal neurons, and thus it is expected that a large number of ensembles coherently phase precess to form theta sequences. Of these, a subset will be more strongly potentiated as suggested by the results of the first chapter. How do such subsets get selected? It is possible that the reward centers of the brain contribute to this. Multiple such areas have been implicated in supporting long-term hippocampal memory stabilization, including ventral tegmental area (Mamad *et al.*, 2017; Martig & Mizumori, 2011; McNamara *et al.*, 2014; Rosen, Cheung, & Siegelbaum, 2015), locus coeruleus(Kempadoo *et al.*, 2016; Takeuchi *et al.*, 2016), nucleus accumbens (LeGates *et al.*, 2018; Sosa, Joo, & Frank, 2020), ventral striatum(van der Meer & Redish, 2011), and the thalamic nucleus reuniens (Ito, Zhang, Witter, Moser, & Moser, 2015;

Vertes, 2015). It would be interesting to investigate how in the same hippocampus-dependent memory task (such as that used in Chapter 1), these diverse areas interact and coordinate to promote the selection of sequences for storage and maintenance of goal-related memories. Simultaneous recordings from multiple such areas could provide important insights.

Another avenue for future research would be to develop a computational account of the observations reported in Chapter 1. A simple neural network model based on Hebbian learning can be developed in which neurons have diverse excitability profiles. In the setting of goal learning tasks, excitable neurons in the network become associated with the goal items. Using this model, questions about optimality of excitability profiles and how they should change across a battery of goal-directed tasks may be answered and compared to data. Importantly, in Chapter 1 we saw that while the accumulation of neural responses at goal locations correlated with future behavior in the setting of goal learning, this was not the case when the task did not involve goal learning (Figure 1.5). What should the patterns of goal selectivity be to allow downstream networks to read out behaviorally relevant information from this network in order to guide behavior? The initial stages of such computations might take place in the entorhinal cortex (Ólafsdóttir, Carpenter, & Barry, 2016), which should provide some constraints on how the model is developed. Once the properties of this computational mechanism are worked out, one can search for their anatomical locus based on the roadmap obtained from the theoretical studies.

Another future direction could involve causal experiments with optogenetics. For example, in Chapter 2 we used lesions to eliminate one or the other of CA3's major theta-modulated inputs to study how phase precession is generated. However, lesion studies suffer from poor temporal specificity as well as risking altering intrinsic network function by inducing compensatory plasticity. Using viral techniques, however, one could exert simultaneous

optogenetic control over these two inputs with different light wavelengths. This way, phase precession can be studied even at the level of single passes through place fields of identified cells. This would allow the experimenter to directly test the relationship between phase precession, theta sequences, and subsequent replay for memory performance. In the study of Chapter 1, optogenetics could be deployed to silence or activate either highly active cells or the less active population to identify the rules by which goal-selectivity is induced. This approach has been successfully applied to contextual fear memory paradigms in the dentate gyrus (Tonegawa *et al.*, 2015), but it remains to be successfully applied to the CA1 in conjunction with the performance of a memory task over extended time periods. Optogenetic control of such populations might also allow one to imprint specific memory trajectories encoded in a sequence of CA3/CA1 ensembles and ask whether behavior would follow it. This would be a direct, causal test of the computational model developed in this thesis. A similar idea has successfully been implemented previously (de Lavilléon *et al.*, 2015; Robinson *et al.*, 2020), but the new results in the thesis can guide the design of a much more specific test of the model.

REFERENCES

Amaral, D. G., Ishizuka, N., & Claiborne, B. (1990). Neurons, numbers and the hippocampal network. In J. Storm-Mathisen, J. Zimmer, & O. P. Ottersen (Eds.), *Progress in brain research* (Vol. 83, pp. 1-11): Elsevier.

Amaral, D. G., & Witter, M. P. (1989). The three-dimensional organization of the hippocampal formation: A review of anatomical data. *Neuroscience, 31*(3), 571-591. doi:https://doi.org/10.1016/0306-4522(89)90424-7

Amilhon, B., Huh, Carey Y. L., Manseau, F., Ducharme, G., Nichol, H., Adamantidis, A., & Williams, S. (2015). Parvalbumin interneurons of hippocampus tune population activity at theta frequency. *Neuron, 86*(5), 1277-1289. doi:https://doi.org/10.1016/j.neuron.2015.05.027

Annese, J., Schenker-Ahmed, N. M., Bartsch, H., Maechler, P., Sheh, C., Thomas, N., Kayano, J., Ghatan, A., Bresler, N., Frosch, M. P., Klaming, R., & Corkin, S. (2014). Postmortem examination of patient h.M.'s brain based on histological sectioning and digital 3d reconstruction. *Nature Communications, 5*(1), 3122. doi:10.1038/ncomms4122

Arnal, L. H., & Giraud, A.-L. (2012). Cortical oscillations and sensory predictions. *Trends in Cognitive Sciences, 16*(7), 390-398. doi:https://doi.org/10.1016/j.tics.2012.05.003

Babb, S. J., & Crystal, J. D. (2005). Discrimination of what, when, and where: Implications for episodic-like memory in rats. *Learning and Motivation, 36*(2), 177-189. doi:https://doi.org/10.1016/j.lmot.2005.02.009

Babb, S. J., & Crystal, J. D. (2006). Episodic-like memory in the rat. *Current Biology, 16*(13), 1317-1321. doi:https://doi.org/10.1016/j.cub.2006.05.025

Battaglia, F. P., Sutherland, G. R., & McNaughton, B. L. (2004). Hippocampal sharp wave bursts coincide with neocortical "up-state" transitions. *Learn Mem, 11*(6), 697-704. doi:10.1101/lm.73504

Bengio, Y., Courville, A., & Vincent, P. (2013). Representation learning: A review and new perspectives. *IEEE Transactions on Pattern Analysis and Machine Intelligence, 35*(8), 1798-1828. doi:10.1109/TPAMI.2013.50

Bennett, M. R., Gibson, W. G., & Robinson, J. (1994). Dynamics of the ca3 pyramidial neuron autoassociative memory network in the hippocampus. *Philosophical Transactions of the Royal Society of London. Series B: Biological Sciences, 343*(1304), 167-187. doi:doi:10.1098/rstb.1994.0019

Bi, G. Q., & Poo, M. M. (1998). Synaptic modifications in cultured hippocampal neurons: Dependence on spike timing, synaptic strength, and postsynaptic cell type. *J Neurosci, 18*(24), 10464-10472. doi:10.1523/jneurosci.18-24-10464.1998

Bieri, Kevin W., Bobbitt, Katelyn N., & Colgin, Laura L. (2014). Slow and fast gamma rhythms coordinate different spatial coding modes in hippocampal place cells. *Neuron, 82*(3), 670-681. doi:https://doi.org/10.1016/j.neuron.2014.03.013

Bittner, K. C., Grienberger, C., Vaidya, S. P., Milstein, A. D., Macklin, J. J., Suh, J., Tonegawa, S., & Magee, J. C. (2015). Conjunctive input processing drives feature selectivity in hippocampal ca1 neurons. *Nature Neuroscience, 18*(8), 1133-1142. doi:10.1038/nn.4062

Bliss, T. V. P., & Collingridge, G. L. (1993). A synaptic model of memory: Long-term potentiation in the hippocampus. *Nature, 361*(6407), 31-39. doi:10.1038/361031a0

Bliss, T. V. P., & Lømo, T. (1973). Long-lasting potentiation of synaptic transmission in the dentate area of the anaesthetized rabbit following stimulation of the perforant path. *The Journal of Physiology, 232*(2), 331-356. doi:10.1113/jphysiol.1973.sp010273

Boehringer, R., Polygalov, D., Huang, A. J. Y., Middleton, S. J., Robert, V., Wintzer, M. E., Piskorowski, R. A., Chevaleyre, V., & McHugh, T. J. (2017). Chronic loss of ca2 transmission leads to hippocampal hyperexcitability. *Neuron, 94*(3), 642-655.e649. doi:https://doi.org/10.1016/j.neuron.2017.04.014

Bosch, S. E., Jehee, J. F. M., Fernández, G., & Doeller, C. F. (2014). Reinstatement of associative memories in early visual cortex is signaled by the hippocampus. *The Journal of Neuroscience, 34*(22), 7493-7500. doi:10.1523/jneurosci.0805-14.2014

Bostock, E., Muller, R. U., & Kubie, J. L. (1991). Experience-dependent modifications of hippocampal place cell firing. *Hippocampus, 1*(2), 193-205. doi:10.1002/hipo.450010207

Bragin, A., Jando, G., Nadasdy, Z., Hetke, J., Wise, K., & Buzsaki, G. (1995). Gamma (40-100 hz) oscillation in the hippocampus of the behaving rat. *The Journal of Neuroscience, 15*(1), 47-60. doi:10.1523/jneurosci.15-01-00047.1995

Breton-Provencher, V., & Sur, M. (2019). Active control of arousal by a locus coeruleus gabaergic circuit. *Nat Neurosci, 22*(2), 218-228. doi:10.1038/s41593-018-0305-z

Brown, E. N., Frank, L. M., Tang, D., Quirk, M. C., & Wilson, M. A. (1998). A statistical paradigm for neural spike train decoding applied to position prediction from ensemble firing patterns of rat hippocampal place cells. *J Neurosci, 18*(18), 7411-7425. doi:10.1523/jneurosci.18-18-07411.1998

Buzsáki, G. (1986). Hippocampal sharp waves: Their origin and significance. *Brain Research, 398*(2), 242-252. doi:https://doi.org/10.1016/0006-8993(86)91483-6

Buzsáki, G. (1989). Two-stage model of memory trace formation: A role for "noisy" brain states. *Neuroscience, 31*(3), 551-570. doi:https://doi.org/10.1016/0306-4522(89)90423-5

Buzsáki, G. (2006). *Rhythms of the brain*. New York, NY, US: Oxford University Press.

Buzsáki, G. (2015). Hippocampal sharp wave-ripple: A cognitive biomarker for episodic memory and planning. *Hippocampus, 25*(10), 1073-1188. doi:https://doi.org/10.1002/hipo.22488

Buzsáki, G., Anastassiou, C. A., & Koch, C. (2012). The origin of extracellular fields and currents — eeg, ecog, lfp and spikes. *Nature Reviews Neuroscience, 13*(6), 407-420. doi:10.1038/nrn3241

Buzsáki, G., Lai-Wo S, L., & Vanderwolf, C. H. (1983). Cellular bases of hippocampal eeg in the behaving rat. *Brain Research Reviews, 6*(2), 139-171. doi:https://doi.org/10.1016/0165-0173(83)90037-1

Buzsáki, G., & Moser, E. I. (2013). Memory, navigation and theta rhythm in the hippocampal-entorhinal system. *Nature Neuroscience, 16*, 130. doi:10.1038/nn.3304

Buzsáki, G., & Tingley, D. (2018). Space and time: The hippocampus as a sequence generator. *Trends in Cognitive Sciences, 22*(10), 853-869. doi:10.1016/j.tics.2018.07.006

Cai, D. J., Aharoni, D., Shuman, T., Shobe, J., Biane, J., Song, W., Wei, B., Veshkini, M., La-Vu, M., Lou, J., Flores, S. E., Kim, I., Sano, Y., Zhou, M., Baumgaertel, K., Lavi, A., Kamata, M., Tuszynski, M., Mayford, M., Golshani, P., & Silva, A. J. (2016). A shared neural ensemble links distinct contextual memories encoded close in time. *Nature, 534*(7605), 115-118. doi:10.1038/nature17955

Carstens, K. E., & Dudek, S. M. (2019). Regulation of synaptic plasticity in hippocampal area ca2. *Current opinion in neurobiology, 54*, 194-199. doi:https://doi.org/10.1016/j.conb.2018.07.008

Castro, C. A., Silbert, L. H., McNaughton, B. L., & Barnes, C. A. (1989). Recovery of spatial learning deficits after decay of electrically induced synaptic enhancement in the hippocampus. *Nature, 342*(6249), 545-548. doi:10.1038/342545a0

Cei, A., Girardeau, G., Drieu, C., Kanbi, K. E., & Zugaro, M. (2014). Reversed theta sequences of hippocampal cell assemblies during backward travel. *Nat Neurosci, 17*(5), 719-724. doi:10.1038/nn.3698

Chance, F. S. (2012). Hippocampal phase precession from dual input components. *The Journal of Neuroscience, 32*(47), 16693-16703. doi:10.1523/jneurosci.2786-12.2012

Chawla, M. K., Guzowski, J. F., Ramirez-Amaya, V., Lipa, P., Hoffman, K. L., Marriott, L. K., Worley, P. F., McNaughton, B. L., & Barnes, C. A. (2005). Sparse, environmentally selective expression of arc rna in the upper blade of the rodent fascia dentata by brief spatial experience. *Hippocampus, 15*(5), 579-586. doi:10.1002/hipo.20091

Chenani, A., Sabariego, M., Schlesiger, M. I., Leutgeb, J. K., Leutgeb, S., & Leibold, C. (2019). Hippocampal ca1 replay becomes less prominent but more rigid without inputs from medial entorhinal cortex. *Nature Communications, 10*(1), 1341. doi:10.1038/s41467-019-09280-0

Cheng, S., & Frank, L. M. (2008). New experiences enhance coordinated neural activity in the hippocampus. *Neuron, 57*(2), 303-313. doi:10.1016/j.neuron.2007.11.035

Chevaleyre, V., & Siegelbaum, S. A. (2010). Strong ca2 pyramidal neuron synapses define a powerful disynaptic cortico-hippocampal loop. *Neuron, 66*(4), 560-572. doi:https://doi.org/10.1016/j.neuron.2010.04.013

Chrobak, J. J., & Buzsáki, G. (1994). Selective activation of deep layer (v-vi) retrohippocampal cortical neurons during hippocampal sharp waves in the behaving rat. *J Neurosci, 14*(10), 6160-6170. doi:10.1523/jneurosci.14-10-06160.1994

Ciliberti, D., Michon, F., & Kloosterman, F. (2018). Real-time classification of experience-related ensemble spiking patterns for closed-loop applications. *eLife, 7*, e36275. doi:10.7554/eLife.36275

Clayton, N. S., & Dickinson, A. (1998). Episodic-like memory during cache recovery by scrub jays. *Nature, 395*(6699), 272-274. doi:10.1038/26216

Clopath, C., Bonhoeffer, T., Hübener, M., & Rose, T. (2017). Variance and invariance of neuronal long-term representations. *Philosophical Transactions of the Royal Society B: Biological Sciences, 372*(1715), 20160161. doi:doi:10.1098/rstb.2016.0161

Colgin, L. L. (2013). Mechanisms and functions of theta rhythms. *Annual Review of Neuroscience, 36*(1), 295-312. doi:10.1146/annurev-neuro-062012-170330

Colgin, L. L. (2016). Rhythms of the hippocampal network. *Nat Rev Neurosci, 17*(4), 239-249. doi:10.1038/nrn.2016.21

Colgin, L. L., Denninger, T., Fyhn, M., Hafting, T., Bonnevie, T., Jensen, O., Moser, M.-B., & Moser, E. I. (2009). Frequency of gamma oscillations routes flow of information in the hippocampus. *Nature, 462*(7271), 353-357. doi:10.1038/nature08573

Colgin, L. L., Leutgeb, S., Jezek, K., Leutgeb, J. K., Moser, E. I., McNaughton, B. L., & Moser, M. B. (2010). Attractor-map versus autoassociation based attractor dynamics in the hippocampal network. *J Neurophysiol, 104*(1), 35-50. doi:10.1152/jn.00202.2010

Collingridge, G. L., Kehl, S. J., & McLennan, H. (1983). Excitatory amino acids in synaptic transmission in the schaffer collateral-commissural pathway of the rat hippocampus. *The Journal of Physiology, 334*(1), 33-46. doi:https://doi.org/10.1113/jphysiol.1983.sp014478

Corkin, S. (1984). Lasting consequences of bilateral medial temporal lobectomy: Clinical course and experimental findings in h.M. *Seminars in Neurology, 4*(02), 249-259. doi:10.1055/s-2008-1041556

Corkin, S. (2002). What's new with the amnesic patient h.M.? *Nature Reviews Neuroscience, 3*(2), 153-160. doi:10.1038/nrn726

Corkin, S., Amaral, D. G., González, R. G., Johnson, K. A., & Hyman, B. T. (1997). H. M.'s medial temporal lobe lesion: Findings from magnetic resonance imaging. *The Journal of Neuroscience, 17*(10), 3964-3979. doi:10.1523/jneurosci.17-10-03964.1997

Csicsvari, J., & Dupret, D. (2014). Sharp wave/ripple network oscillations and learning-associated hippocampal maps. *Philos Trans R Soc Lond B Biol Sci, 369*(1635), 20120528. doi:10.1098/rstb.2012.0528

Csicsvari, J., Jamieson, B., Wise, K. D., & Buzsáki, G. (2003). Mechanisms of gamma oscillations in the hippocampus of the behaving rat. *Neuron, 37*(2), 311-322. doi:10.1016/s0896-6273(02)01169-8

Cui, Z., Gerfen, C. R., & Young, W. S., 3rd. (2013). Hypothalamic and other connections with dorsal ca2 area of the mouse hippocampus. *J Comp Neurol, 521*(8), 1844-1866. doi:10.1002/cne.23263

Czurkó, A., Hirase, H., Csicsvari, J., & Buzsáki, G. (1999). Sustained activation of hippocampal pyramidal cells by 'space clamping' in a running wheel. *Eur J Neurosci, 11*(1), 344-352. doi:10.1046/j.1460-9568.1999.00446.x

D'Albis, T., Jaramillo, J., Sprekeler, H., & Kempter, R. (2015). Inheritance of hippocampal place fields through hebbian learning: Effects of theta modulation and phase precession on structure formation. *Neural Computation, 27*(8), 1624-1672. doi:10.1162/NECO_a_00752 %M 26079752

Danielson, Nathan B., Kaifosh, P., Zaremba, Jeffrey D., Lovett-Barron, M., Tsai, J., Denny, Christine A., Balough, Elizabeth M., Goldberg, Alexander R., Drew, Liam J., Hen, R., Losonczy, A., & Kheirbek, Mazen A. (2016). Distinct contribution of adult-born hippocampal granule cells to context encoding. *Neuron, 90*(1), 101-112. doi:https://doi.org/10.1016/j.neuron.2016.02.019

Danielson, N. B., Turi, G. F., Ladow, M., Chavlis, S., Petrantonakis, P. C., Poirazi, P., & Losonczy, A. (2017). In vivo imaging of dentate gyrus mossy cells in behaving mice. *Neuron, 93*(3), 552-559.e554. doi:https://doi.org/10.1016/j.neuron.2016.12.019

Dasgupta, S., Stevens, C. F., & Navlakha, S. (2017). A neural algorithm for a fundamental computing problem. *Science, 358*(6364), 793-796. doi:10.1126/science.aam9868

Davidson, T. J., Kloosterman, F., & Wilson, M. A. (2009). Hippocampal replay of extended experience. *Neuron, 63*(4), 497-507. doi:https://doi.org/10.1016/j.neuron.2009.07.027

de Lavilléon, G., Lacroix, M. M., Rondi-Reig, L., & Benchenane, K. (2015). Explicit memory creation during sleep demonstrates a causal role of place cells in navigation. *Nature Neuroscience, 18*(4), 493-495. doi:10.1038/nn.3970

Denève, S., & Machens, C. K. (2016). Efficient codes and balanced networks. *Nature Neuroscience, 19*, 375. doi:10.1038/nn.4243

Deshmukh, S. S., & Knierim, J. J. (2011). Representation of non-spatial and spatial information in the lateral entorhinal cortex. *Front Behav Neurosci, 5*, 69. doi:10.3389/fnbeh.2011.00069

Deshmukh, S. S., Yoganarasimha, D., Voicu, H., & Knierim, J. J. (2010). Theta modulation in the medial and the lateral entorhinal cortices. *Journal of Neurophysiology, 104*(2), 994-1006. doi:10.1152/jn.01141.2009

Diba, K., & Buzsáki, G. (2007). Forward and reverse hippocampal place-cell sequences during ripples. *Nature Neuroscience, 10*(10), 1241-1242. doi:10.1038/nn1961

Diehl, G. W., Hon, O. J., Leutgeb, S., & Leutgeb, J. K. (2017). Grid and nongrid cells in medial entorhinal cortex represent spatial location and environmental features with complementary coding schemes. *Neuron, 94*(1), 83-92.e86. doi:https://doi.org/10.1016/j.neuron.2017.03.004

Diehl, G. W., Hon, O. J., Leutgeb, S., & Leutgeb, J. K. (2019). Stability of medial entorhinal cortex representations over time. *Hippocampus, 29*(3), 284-302. doi:10.1002/hipo.23017

Dragoi, G., & Buzsáki, G. (2006). Temporal encoding of place sequences by hippocampal cell assemblies. *Neuron, 50*(1), 145-157.

Dragoi, G., Harris, K. D., & Buzsáki, G. (2003). Place representation within hippocampal networks is modified by long-term potentiation. *Neuron, 39*(5), 843-853. doi:https://doi.org/10.1016/S0896-6273(03)00465-3

Drieu, C., Todorova, R., & Zugaro, M. (2018). Nested sequences of hippocampal assemblies during behavior support subsequent sleep replay. *Science, 362*(6415), 675-679. doi:10.1126/science.aat2952

Driscoll, L. N., Pettit, N. L., Minderer, M., Chettih, S. N., & Harvey, C. D. (2017). Dynamic reorganization of neuronal activity patterns in parietal cortex. *Cell, 170*(5), 986-999.e916. doi:10.1016/j.cell.2017.07.021

Dudek, S. M., Alexander, G. M., & Farris, S. (2016). Rediscovering area ca2: Unique properties and functions. *Nature Reviews Neuroscience, 17*(2), 89-102. doi:10.1038/nrn.2015.22

Dupret, D., O'Neill, J., Pleydell-Bouverie, B., & Csicsvari, J. (2010). The reorganization and reactivation of hippocampal maps predict spatial memory performance. *Nature Neuroscience, 13*(8), 995-1002. doi:10.1038/nn.2599

Eichenbaum, H. (2017). The role of the hippocampus in navigation is memory. *J Neurophysiol, 117*(4), 1785-1796. doi:10.1152/jn.00005.2017

Eichenbaum, H., & Cohen, N. J. (2014). Can we reconcile the declarative memory and spatial navigation views on hippocampal function? *Neuron, 83*(4), 764-770. doi:10.1016/j.neuron.2014.07.032

Eichenbaum, H., Fortin, N. J., Ergorul, C., Wright, S. P., & Agster, K. L. (2005). Episodic recollection in animals: "If it walks like a duck and quacks like a duck…". *Learning and Motivation, 36*(2), 190-207. doi:https://doi.org/10.1016/j.lmot.2005.02.006

Epsztein, J., Brecht, M., & Lee, A. K. (2011). Intracellular determinants of hippocampal ca1 place and silent cell activity in a novel environment. *Neuron, 70*(1), 109-120. doi:10.1016/j.neuron.2011.03.006

Estes, W. K. (1955). Statistical theory of spontaneous recovery and regression. *Psychological review, 62*(3), 145-154. doi:http://dx.doi.org/10.1037/h0048509

Farooq, U., Sibille, J., Liu, K., & Dragoi, G. (2019). Strengthened temporal coordination within pre-existing sequential cell assemblies supports trajectory replay. *Neuron, 103*(4), 719-733.e717. doi:https://doi.org/10.1016/j.neuron.2019.05.040

Feldman, Daniel E. (2012). The spike-timing dependence of plasticity. *Neuron, 75*(4), 556-571. doi:https://doi.org/10.1016/j.neuron.2012.08.001

Feng, T., Silva, D., & Foster, D. J. (2015). Dissociation between the experience-dependent development of hippocampal theta sequences and single-trial phase precession. *The Journal of Neuroscience, 35*(12), 4890-4902. doi:10.1523/jneurosci.2614-14.2015

Fernández-Ruiz, A., Oliva, A., Fermino de Oliveira, E., Rocha-Almeida, F., Tingley, D., & Buzsáki, G. (2019). Long-duration hippocampal sharp wave ripples improve memory. *Science, 364*(6445), 1082-1086. doi:10.1126/science.aax0758

Fernández-Ruiz, A., Oliva, A., Nagy, G. A., Maurer, A. P., Berényi, A., & Buzsáki, G. (2017). Entorhinal-ca3 dual-input control of spike timing in the hippocampus by theta-gamma coupling. *Neuron, 93*(5), 1213-1226.e1215. doi:https://doi.org/10.1016/j.neuron.2017.02.017

Foster, D. J., Morris, R. G., & Dayan, P. (2000). A model of hippocampally dependent navigation, using the temporal difference learning rule. *Hippocampus, 10*(1), 1-16. doi:10.1002/(sici)1098-1063(2000)10:1<1::Aid-hipo1>3.0.Co;2-1

Foster, D. J., & Wilson, M. A. (2006). Reverse replay of behavioural sequences in hippocampal place cells during the awake state. *Nature, 440*(7084), 680-683. doi:10.1038/nature04587

Foster, D. J., & Wilson, M. A. (2007). Hippocampal theta sequences. *Hippocampus, 17*(11), 1093-1099. doi:10.1002/hipo.20345

Foster, T. C., Castro, C. A., & McNaughton, B. L. (1989). Spatial selectivity of rat hippocampal neurons: Dependence on preparedness for movement. *Science, 244*(4912), 1580-1582. doi:10.1126/science.2740902

Frank, L. M., Brown, E. N., & Wilson, M. (2000). Trajectory encoding in the hippocampus and entorhinal cortex. *Neuron, 27*(1), 169-178. doi:10.1016/s0896-6273(00)00018-0

Fu, Y., Tucciarone, Jason M., Espinosa, J. S., Sheng, N., Darcy, Daniel P., Nicoll, Roger A., Huang, Z. J., & Stryker, Michael P. (2014). A cortical circuit for gain control by behavioral state. *Cell, 156*(6), 1139-1152. doi:https://doi.org/10.1016/j.cell.2014.01.050

Fuhs, M. C., & Touretzky, D. S. (2007). Context learning in the rodent hippocampus. *Neural Comput, 19*(12), 3173-3215. doi:10.1162/neco.2007.19.12.3173

Fyhn, M., Molden, S., Hollup, S., Moser, M. B., & Moser, E. (2002). Hippocampal neurons responding to first-time dislocation of a target object. *Neuron, 35*(3), 555-566. doi:10.1016/s0896-6273(02)00784-5

Gallego, J. A., Perich, M. G., Naufel, S. N., Ethier, C., Solla, S. A., & Miller, L. E. (2018). Cortical population activity within a preserved neural manifold underlies multiple motor behaviors. *Nature Communications, 9*(1), 4233. doi:10.1038/s41467-018-06560-z

Gatome, C. W., Slomianka, L., Lipp, H. P., & Amrein, I. (2010). Number estimates of neuronal phenotypes in layer ii of the medial entorhinal cortex of rat and mouse. *Neuroscience, 170*(1), 156-165. doi:10.1016/j.neuroscience.2010.06.048

Gauthier, J. L., & Tank, D. W. (2018). A dedicated population for reward coding in the hippocampus. *Neuron, 99*(1), 179-193.e177. doi:10.1016/j.neuron.2018.06.008

Gershman, S. J. (2018). The successor representation: Its computational logic and neural substrates. *J Neurosci, 38*(33), 7193-7200. doi:10.1523/jneurosci.0151-18.2018

Girardeau, G., Benchenane, K., Wiener, S. I., Buzsáki, G., & Zugaro, M. B. (2009). Selective suppression of hippocampal ripples impairs spatial memory. *Nature Neuroscience, 12*, 1222. doi:10.1038/nn.2384

https://www.nature.com/articles/nn.2384#supplementary-information

Girardeau, G., Cei, A., & Zugaro, M. (2014). Learning-induced plasticity regulates hippocampal sharp wave-ripple drive. *J Neurosci, 34*(15), 5176-5183. doi:10.1523/jneurosci.4288-13.2014

Gonzalez, W. G., Zhang, H., Harutyunyan, A., & Lois, C. (2019). Persistence of neuronal representations through time and damage in the hippocampus. *Science, 365*(6455), 821-825. doi:10.1126/science.aav9199

Goode, T. D., Tanaka, K. Z., Sahay, A., & McHugh, T. J. (2020). An integrated index: Engrams, place cells, and hippocampal memory. *Neuron, 107*(5), 805-820. doi:https://doi.org/10.1016/j.neuron.2020.07.011

GoodSmith, D., Chen, X., Wang, C., Kim, S. H., Song, H., Burgalossi, A., Christian, K. M., & Knierim, J. J. (2017). Spatial representations of granule cells and mossy cells of the dentate gyrus. *Neuron, 93*(3), 677-690.e675. doi:https://doi.org/10.1016/j.neuron.2016.12.026

GoodSmith, D., Lee, H., Neunuebel, J. P., Song, H., & Knierim, J. J. (2019). Dentate gyrus mossy cells share a role in pattern separation with dentate granule cells and proximal ca3 pyramidal cells. *The Journal of Neuroscience, 39*(48), 9570-9584. doi:10.1523/jneurosci.0940-19.2019

Gordon Hayman, C. A., Macdonald, C. A., & Tulving, E. (1993). The role of repetition and associative interference in new semantic learning in amnesia: A case experiment. *J Cogn Neurosci, 5*(4), 375-389. doi:10.1162/jocn.1993.5.4.375

Granger, A. J., & Nicoll, R. A. (2014). Expression mechanisms underlying long-term potentiation: A postsynaptic view, 10 years on. *Philos Trans R Soc Lond B Biol Sci, 369*(1633), 20130136. doi:10.1098/rstb.2013.0136

Gray, C. M., & Singer, W. (1989). Stimulus-specific neuronal oscillations in orientation columns of cat visual cortex. *Proceedings of the National Academy of Sciences, 86*(5), 1698-1702. doi:10.1073/pnas.86.5.1698

Greenberg, M. E., Ziff, E. B., & Greene, L. A. (1986). Stimulation of neuronal acetylcholine receptors induces rapid gene transcription. *Science, 234*(4772), 80-83. doi:10.1126/science.3749894

Gridchyn, I., Schoenenberger, P., O'Neill, J., & Csicsvari, J. (2020). Assembly-specific disruption of hippocampal replay leads to selective memory deficit. *Neuron, 106*(2), 291-300.e296. doi:10.1016/j.neuron.2020.01.021

Grieves, R. M., & Jeffery, K. J. (2017). The representation of space in the brain. *Behav Processes, 135*, 113-131. doi:10.1016/j.beproc.2016.12.012

Gupta, A. S., van der Meer, M. A., Touretzky, D. S., & Redish, A. D. (2012). Segmentation of spatial experience by hippocampal θ sequences. *Nat Neurosci, 15*(7), 1032-1039. doi:10.1038/nn.3138

Gupta, A. S., van der Meer, M. A. A., Touretzky, D. S., & Redish, A. D. (2010). Hippocampal replay is not a simple function of experience. *Neuron, 65*(5), 695-705. doi:https://doi.org/10.1016/j.neuron.2010.01.034

Guzman, S. J., Schlögl, A., Frotscher, M., & Jonas, P. (2016). Synaptic mechanisms of pattern completion in the hippocampal ca3 network. *Science, 353*(6304), 1117-1123. doi:10.1126/science.aaf1836

Guzowski, J. F., McNaughton, B. L., Barnes, C. A., & Worley, P. F. (1999). Environment-specific expression of the immediate-early gene arc in hippocampal neuronal ensembles. *Nat Neurosci, 2*(12), 1120-1124. doi:10.1038/16046

Hafting, T., Fyhn, M., Bonnevie, T., Moser, M.-B., & Moser, E. I. (2008). Hippocampus-independent phase precession in entorhinal grid cells. *Nature, 453*, 1248. doi:10.1038/nature06957

https://www.nature.com/articles/nature06957#supplementary-information

Hafting, T., Fyhn, M., Molden, S., Moser, M. B., & Moser, E. I. (2005). Microstructure of a spatial map in the entorhinal cortex. *Nature, 436*(7052), 801-806. doi:10.1038/nature03721

Hainmueller, T., & Bartos, M. (2020). Dentate gyrus circuits for encoding, retrieval and discrimination of episodic memories. *Nature Reviews Neuroscience, 21*(3), 153-168. doi:10.1038/s41583-019-0260-z

Han, J. H., Kushner, S. A., Yiu, A. P., Cole, C. J., Matynia, A., Brown, R. A., Neve, R. L., Guzowski, J. F., Silva, A. J., & Josselyn, S. A. (2007). Neuronal competition and selection during memory formation. *Science, 316*(5823), 457-460. doi:10.1126/science.1139438

Hargreaves, E. L., Rao, G., Lee, I., & Knierim, J. J. (2005). Major dissociation between medial and lateral entorhinal input to dorsal hippocampus. *Science, 308*(5729), 1792-1794. doi:10.1126/science.1110449

Harris, K. D., Csicsvari, J., Hirase, H., Dragoi, G., & Buzsáki, G. (2003). Organization of cell assemblies in the hippocampus. *Nature, 424*(6948), 552-556. doi:10.1038/nature01834

Harris, K. D., Henze, D. A., Hirase, H., Leinekugel, X., Dragoi, G., Czurkó, A., & Buzsáki, G. (2002). Spike train dynamics predicts theta-related phase precession in hippocampal pyramidal cells. *Nature, 417*(6890), 738.

Harvey, C. D., Collman, F., Dombeck, D. A., & Tank, D. W. (2009). Intracellular dynamics of hippocampal place cells during virtual navigation. *Nature, 461*(7266), 941.

Hasselmo, M. E., Bodelón, C., & Wyble, B. P. (2002). A proposed function for hippocampal theta rhythm: Separate phases of encoding and retrieval enhance reversal of prior learning. *Neural Computation, 14*(4), 793-817. doi:10.1162/089976602317318965

Hebb, D. O. (1949). *The organization of behavior; a neuropsychological theory*. Oxford, England: Wiley.

Helfrich, R. F., & Knight, R. T. (2016). Oscillatory dynamics of prefrontal cognitive control. *Trends Cogn Sci, 20*(12), 916-930. doi:10.1016/j.tics.2016.09.007

Henze, D. A., Wittner, L., & Buzsáki, G. (2002). Single granule cells reliably discharge targets in the hippocampal ca3 network in vivo. *Nature Neuroscience, 5*(8), 790-795. doi:10.1038/nn887

Hindy, N. C., Avery, E. W., & Turk-Browne, N. B. (2019). Hippocampal-neocortical interactions sharpen over time for predictive actions. *Nature Communications, 10*(1), 3989. doi:10.1038/s41467-019-12016-9

Hirase, H., Czurkó, A., Csicsvari, J., & Buzsáki, G. (1999). Firing rate and theta-phase coding by hippocampal pyramidal neurons during 'space clamping'. *Eur J Neurosci, 11*(12), 4373-4380. doi:10.1046/j.1460-9568.1999.00853.x

Hitti, F. L., & Siegelbaum, S. A. (2014). The hippocampal ca2 region is essential for social memory. *Nature, 508*(7494), 88-92. doi:10.1038/nature13028

Hok, V., Lenck-Santini, P.-P., Roux, S., Save, E., Muller, R. U., & Poucet, B. (2007). Goal-related activity in hippocampal place cells. *The Journal of Neuroscience, 27*(3), 472-482. doi:10.1523/jneurosci.2864-06.2007

Hollup, S. A., Molden, S., Donnett, J. G., Moser, M.-B., & Moser, E. I. (2001). Accumulation of hippocampal place fields at the goal location in an annular watermaze task. *The Journal of Neuroscience, 21*(5), 1635-1644. doi:10.1523/jneurosci.21-05-01635.2001

Hopfield, J. J. (1982). Neural networks and physical systems with emergent collective computational abilities. *Proceedings of the National Academy of Sciences, 79*(8), 2554-2558. doi:10.1073/pnas.79.8.2554

Howard, M. W., & Kahana, M. J. (2002). A distributed representation of temporal context. *Journal of Mathematical Psychology, 46*(3), 269-299. doi:https://doi.org/10.1006/jmps.2001.1388

Hsiao, Y.-T., Zheng, C., & Colgin, L. L. (2016). Slow gamma rhythms in ca3 are entrained by slow gamma activity in the dentate gyrus. *Journal of Neurophysiology, 116*(6), 2594-2603. doi:10.1152/jn.00499.2016

Huerta, P. T., & Lisman, J. E. (1993). Heightened synaptic plasticity of hippocampal ca1 neurons during a cholinergically induced rhythmic state. *Nature, 364*(6439), 723-725. doi:10.1038/364723a0

Huerta, P. T., & Lisman, J. E. (1995). Bidirectional synaptic plasticity induced by a single burst during cholinergic theta oscillation in ca1 in vitro. *Neuron, 15*(5), 1053-1063. doi:https://doi.org/10.1016/0896-6273(95)90094-2

Huxter, J., Burgess, N., & O'Keefe, J. (2003). Independent rate and temporal coding in hippocampal pyramidal cells. *Nature, 425*(6960), 828-832. doi:10.1038/nature02058

Isaacson, Jeffry S., & Scanziani, M. (2011). How inhibition shapes cortical activity. *Neuron, 72*(2), 231-243. doi:https://doi.org/10.1016/j.neuron.2011.09.027

Ito, H. T., Zhang, S.-J., Witter, M. P., Moser, E. I., & Moser, M.-B. (2015). A prefrontal–thalamo–hippocampal circuit for goal-directed spatial navigation. *Nature, 522*(7554), 50-55. doi:10.1038/nature14396

Jackson, J. C., Johnson, A., & Redish, A. D. (2006). Hippocampal sharp waves and reactivation during awake states depend on repeated sequential experience. *The Journal of Neuroscience, 26*(48), 12415-12426. doi:10.1523/jneurosci.4118-06.2006

Jadhav, S. P., Kemere, C., German, P. W., & Frank, L. M. (2012). Awake hippocampal sharp-wave ripples support spatial memory. *Science, 336*(6087), 1454-1458. doi:10.1126/science.1217230

Jaramillo, J., & Kempter, R. (2017). Phase precession: A neural code underlying episodic memory? *Current opinion in neurobiology, 43*, 130-138. doi:https://doi.org/10.1016/j.conb.2017.02.006

Jaramillo, J., Schmidt, R., & Kempter, R. (2014). Modeling inheritance of phase precession in the hippocampal formation. *The Journal of Neuroscience, 34*(22), 7715-7731. doi:10.1523/jneurosci.5136-13.2014

Jensen, O., & Lisman, J. E. (1996). Hippocampal ca3 region predicts memory sequences: Accounting for the phase precession of place cells. *Learning & Memory, 3*(2-3), 279-287.

Jerman, T., Kesner, R. P., & Hunsaker, M. R. (2006). Disconnection analysis of ca3 and dg in mediating encoding but not retrieval in a spatial maze learning task. *Learn Mem, 13*(4), 458-464. doi:10.1101/lm.246906

Johnson, A., & Redish, A. D. (2007). Neural ensembles in ca3 transiently encode paths forward of the animal at a decision point. *The Journal of Neuroscience, 27*(45), 12176-12189. doi:10.1523/jneurosci.3761-07.2007

Jones, M. W., & Wilson, M. A. (2005). Phase precession of medial prefrontal cortical activity relative to the hippocampal theta rhythm. *Hippocampus, 15*(7), 867-873. doi:10.1002/hipo.20119

Josselyn, S. A., Köhler, S., & Frankland, P. W. (2017). Heroes of the engram. *J Neurosci, 37*(18), 4647-4657. doi:10.1523/jneurosci.0056-17.2017

Josselyn, S. A., & Tonegawa, S. (2020). Memory engrams: Recalling the past and imagining the future. *Science, 367*(6473), eaaw4325. doi:10.1126/science.aaw4325

Káli, S., & Dayan, P. (2004). Off-line replay maintains declarative memories in a model of hippocampal-neocortical interactions. *Nature Neuroscience, 7*(3), 286-294. doi:10.1038/nn1202

Kamondi, A., Acsády, L., Wang, X.-J., & Buzsáki, G. (1998). Theta oscillations in somata and dendrites of hippocampal pyramidal cells in vivo: Activity-dependent phase-precession of action potentials. *Hippocampus, 8*(3), 244-261. doi:10.1002/(sici)1098-1063(1998)8:3<244::Aid-hipo7>3.0.Co;2-j

Karlsson, M. P., & Frank, L. M. (2008). Network dynamics underlying the formation of sparse, informative representations in the hippocampus. *J Neurosci, 28*(52), 14271-14281. doi:10.1523/jneurosci.4261-08.2008

Karlsson, M. P., & Frank, L. M. (2009). Awake replay of remote experiences in the hippocampus. *Nat Neurosci, 12*(7), 913-918. doi:10.1038/nn.2344

Kart-Teke, E., De Souza Silva, M. A., Huston, J. P., & Dere, E. (2006). Wistar rats show episodic-like memory for unique experiences. *Neurobiol Learn Mem, 85*(2), 173-182. doi:10.1016/j.nlm.2005.10.002

Kelly, K., Cochran, B. H., Stiles, C. D., & Leder, P. (1983). Cell-specific regulation of the c-myc gene by lymphocyte mitogens and platelet-derived growth factor. *Cell, 35*(3, Part 2), 603-610. doi:https://doi.org/10.1016/0092-8674(83)90092-2

Kemere, C., Carr, M. F., Karlsson, M. P., & Frank, L. M. (2013). Rapid and continuous modulation of hippocampal network state during exploration of new places. *PLOS ONE, 8*(9), e73114. doi:10.1371/journal.pone.0073114

Kempadoo, K. A., Mosharov, E. V., Choi, S. J., Sulzer, D., & Kandel, E. R. (2016). Dopamine release from the locus coeruleus to the dorsal hippocampus promotes spatial learning and memory. *Proceedings of the National Academy of Sciences, 113*(51), 14835-14840. doi:10.1073/pnas.1616515114

Kennard, M. A. (1943). Electroencephalogram of decorticate monkeys. *Journal of Neurophysiology, 6*(4), 233-242. doi:10.1152/jn.1943.6.4.233

Kentros, C. G., Agnihotri, N. T., Streater, S., Hawkins, R. D., & Kandel, E. R. (2004). Increased attention to spatial context increases both place field stability and spatial memory. *Neuron, 42*(2), 283-295. doi:10.1016/s0896-6273(04)00192-8

Kesner, R. P., Hunsaker, M. R., & Warthen, M. W. (2008). The ca3 subregion of the hippocampus is critical for episodic memory processing by means of relational encoding in rats. *Behav Neurosci, 122*(6), 1217-1225. doi:10.1037/a0013592

Khodagholy, D., Gelinas, J. N., & Buzsáki, G. (2017). Learning-enhanced coupling between ripple oscillations in association cortices and hippocampus. *Science, 358*(6361), 369-372. doi:10.1126/science.aan6203

Kim, J. J., & Fanselow, M. S. (1992). Modality-specific retrograde amnesia of fear. *Science, 256*(5057), 675-677. doi:10.1126/science.1585183

Kitamura, T., Pignatelli, M., Suh, J., Kohara, K., Yoshiki, A., Abe, K., & Tonegawa, S. (2014). Island cells control temporal association memory. *Science, 343*(6173), 896-901. doi:10.1126/science.1244634

Klausberger, T., Marton, L. F., O'Neill, J., Huck, J. H. J., Dalezios, Y., Fuentealba, P., Suen, W. Y., Papp, E., Kaneko, T., Watanabe, M., Csicsvari, J., & Somogyi, P. (2005). Complementary roles of cholecystokinin- and parvalbumin-expressing gabaergic neurons in hippocampal network oscillations. *The Journal of Neuroscience, 25*(42), 9782-9793. doi:10.1523/jneurosci.3269-05.2005

Klyachko, V. A., & Stevens, C. F. (2006). Excitatory and feed-forward inhibitory hippocampal synapses work synergistically as an adaptive filter of natural spike trains. *PLOS Biology, 4*(7), e207. doi:10.1371/journal.pbio.0040207

Knierim, J. J., & Neunuebel, J. P. (2016). Tracking the flow of hippocampal computation: Pattern separation, pattern completion, and attractor dynamics. *Neurobiology of Learning and Memory, 129*, 38-49. doi:https://doi.org/10.1016/j.nlm.2015.10.008

Kohara, K., Pignatelli, M., Rivest, A. J., Jung, H.-Y., Kitamura, T., Suh, J., Frank, D., Kajikawa, K., Mise, N., Obata, Y., Wickersham, I. R., & Tonegawa, S. (2014). Cell type–specific genetic and optogenetic tools reveal hippocampal ca2 circuits. *Nature Neuroscience, 17*(2), 269-279. doi:10.1038/nn.3614

Kovács, K. A., O'Neill, J., Schoenenberger, P., Penttonen, M., Ranguel Guerrero, D. K., & Csicsvari, J. (2016). Optogenetically blocking sharp wave ripple events in sleep does not interfere with the formation of stable spatial representation in the ca1 area of the hippocampus. *PLOS ONE, 11*(10), e0164675. doi:10.1371/journal.pone.0164675

Kropff, E., Carmichael, J. E., Moser, M. B., & Moser, E. I. (2015). Speed cells in the medial entorhinal cortex. *Nature, 523*(7561), 419-424. doi:10.1038/nature14622

Kudrimoti, H. S., Barnes, C. A., & McNaughton, B. L. (1999). Reactivation of hippocampal cell assemblies: Effects of behavioral state, experience, and eeg dynamics. *J Neurosci, 19*(10), 4090-4101. doi:10.1523/jneurosci.19-10-04090.1999

Kvitsiani, D., Ranade, S., Hangya, B., Taniguchi, H., Huang, J. Z., & Kepecs, A. (2013). Distinct behavioural and network correlates of two interneuron types in prefrontal cortex. *Nature, 498*(7454), 363-366. doi:10.1038/nature12176

Langston, R. F., Ainge, J. A., Couey, J. J., Canto, C. B., Bjerknes, T. L., Witter, M. P., Moser, E. I., & Moser, M.-B. (2010). Development of the spatial representation system in the rat. *Science, 328*(5985), 1576-1580. doi:10.1126/science.1188210

Lapray, D., Lasztoczi, B., Lagler, M., Viney, T. J., Katona, L., Valenti, O., Hartwich, K., Borhegyi, Z., Somogyi, P., & Klausberger, T. (2012). Behavior-dependent specialization of identified hippocampal interneurons. *Nature Neuroscience, 15*(9), 1265-1271. doi:10.1038/nn.3176

Larson, J., & Lynch, G. (1986). Induction of synaptic potentiation in hippocampus by patterned stimulation involves two events. *Science, 232*(4753), 985-988. doi:10.1126/science.3704635

Larson, J., Wong, D., & Lynch, G. (1986). Patterned stimulation at the theta frequency is optimal for the induction of hippocampal long-term potentiation. *Brain Research, 368*(2), 347-350. doi:https://doi.org/10.1016/0006-8993(86)90579-2

Lashley, K. S. (1950). In search of the engram. In *Physiological mechanisms in animal behavior. (society's symposium iv.).* (pp. 454-482). Oxford, England: Academic Press.

LeCun, Y., Bengio, Y., & Hinton, G. (2015). Deep learning. *Nature, 521*(7553), 436-444. doi:10.1038/nature14539

Lee, A. K., & Wilson, M. A. (2002). Memory of sequential experience in the hippocampus during slow wave sleep. *Neuron, 36*(6), 1183-1194. doi:10.1016/s0896-6273(02)01096-6

Lee, D., Lin, B. J., & Lee, A. K. (2012). Hippocampal place fields emerge upon single-cell manipulation of excitability during behavior. *Science, 337*(6096), 849-853. doi:10.1126/science.1221489

Lee, I., & Kesner, R. P. (2004). Encoding versus retrieval of spatial memory: Double dissociation between the dentate gyrus and the perforant path inputs into ca3 in the dorsal hippocampus. *Hippocampus, 14*(1), 66-76. doi:10.1002/hipo.10167

Lee, J. S., Briguglio, J. J., Cohen, J. D., Romani, S., & Lee, A. K. (2020). The statistical structure of the hippocampal code for space as a function of time, context, and value. *Cell, 183*(3), 620-635.e622. doi:10.1016/j.cell.2020.09.024

LeGates, T. A., Kvarta, M. D., Tooley, J. R., Francis, T. C., Lobo, M. K., Creed, M. C., & Thompson, S. M. (2018). Reward behaviour is regulated by the strength of hippocampus–nucleus accumbens synapses. *Nature, 564*(7735), 258-262. doi:10.1038/s41586-018-0740-8

Lenck-Santini, P.-P., Fenton, A. A., & Muller, R. U. (2008). Discharge properties of hippocampal neurons during performance of a jump avoidance task. *The Journal of Neuroscience, 28*(27), 6773-6786. doi:10.1523/JNEUROSCI.5329-07.2008

Lengyel, M., Szatmáry, Z., & Érdi, P. (2003). Dynamically detuned oscillations account for the coupled rate and temporal code of place cell firing. *Hippocampus, 13*(6), 700-714. doi:https://doi.org/10.1002/hipo.10116

Leung, L.-W. S., Da Silva, F. H. L., & Wadman, W. J. (1982). Spectral characteristics of the hippocampal eeg in the freely moving rat. *Electroencephalography and Clinical Neurophysiology, 54*(2), 203-219. doi:https://doi.org/10.1016/0013-4694(82)90162-6

Leutgeb, J. K., Leutgeb, S., Moser, M.-B., & Moser, E. I. (2007). Pattern separation in the dentate gyrus and ca3 of the hippocampus. *Science, 315*(5814), 961-966. doi:10.1126/science.1135801

Leutgeb, J. K., Leutgeb, S., Treves, A., Meyer, R., Barnes, C. A., McNaughton, B. L., Moser, M. B., & Moser, E. I. (2005a). Progressive transformation of hippocampal neuronal representations in "morphed" environments. *Neuron, 48*(2), 345-358. doi:10.1016/j.neuron.2005.09.007

Leutgeb, S., & Leutgeb, J. K. (2007). Pattern separation, pattern completion, and new neuronal codes within a continuous ca3 map. *Learn Mem, 14*(11), 745-757. doi:10.1101/lm.703907

Leutgeb, S., Leutgeb, J. K., Barnes, C. A., Moser, E. I., McNaughton, B. L., & Moser, M.-B. (2005b). Independent codes for spatial and episodic memory in hippocampal neuronal ensembles. *Science, 309*(5734), 619-623. doi:10.1126/science.1114037

Leutgeb, S., Leutgeb, J. K., Moser, M. B., & Moser, E. I. (2005c). Place cells, spatial maps and the population code for memory. *Curr Opin Neurobiol, 15*(6), 738-746. doi:10.1016/j.conb.2005.10.002

Leutgeb, S., Leutgeb, J. K., Treves, A., Moser, M. B., & Moser, E. I. (2004). Distinct ensemble codes in hippocampal areas ca3 and ca1. *Science, 305*(5688), 1295-1298. doi:10.1126/science.1100265

Levy, W. B. (1989). A computational approach to hippocampal function. In R. D. Hawkins & G. H. Bower (Eds.), *Psychology of learning and motivation* (Vol. 23, pp. 243-305): Academic Press.

Lisman, J., Buzsáki, G., Eichenbaum, H., Nadel, L., Ranganath, C., & Redish, A. D. (2017). Viewpoints: How the hippocampus contributes to memory, navigation and cognition. *Nature Neuroscience, 20*(11), 1434-1447. doi:10.1038/nn.4661

Lisman, J., & Redish, A. D. (2009). Prediction, sequences and the hippocampus. *Philosophical Transactions of the Royal Society B: Biological Sciences, 364*(1521), 1193-1201. doi:doi:10.1098/rstb.2008.0316

Lisman, J. E. (1999). Relating hippocampal circuitry to function: Recall of memory sequences by reciprocal dentate–ca3 interactions. *Neuron, 22*(2), 233-242. doi:https://doi.org/10.1016/S0896-6273(00)81085-5

Lisman, J. E., Talamini, L. M., & Raffone, A. (2005). Recall of memory sequences by interaction of the dentate and ca3: A revised model of the phase precession. *Neural Networks, 18*(9), 1191-1201. doi:https://doi.org/10.1016/j.neunet.2005.08.008

Liu, X., Ramirez, S., Pang, P. T., Puryear, C. B., Govindarajan, A., Deisseroth, K., & Tonegawa, S. (2012). Optogenetic stimulation of a hippocampal engram activates fear memory recall. *Nature, 484*(7394), 381-385. doi:10.1038/nature11028

Losonczy, A., Zemelman, B. V., Vaziri, A., & Magee, J. C. (2010). Network mechanisms of theta related neuronal activity in hippocampal ca1 pyramidal neurons. *Nature Neuroscience, 13*, 967. doi:10.1038/nn.2597

https://www.nature.com/articles/nn.2597#supplementary-information

Louie, K., & Wilson, M. A. (2001). Temporally structured replay of awake hippocampal ensemble activity during rapid eye movement sleep. *Neuron, 29*(1), 145-156. doi:10.1016/s0896-6273(01)00186-6

Lytton, W. W., & Sejnowski, T. J. (1991). Simulations of cortical pyramidal neurons synchronized by inhibitory interneurons. *Journal of Neurophysiology, 66*(3), 1059-1079. doi:10.1152/jn.1991.66.3.1059

MacDonald, C. J., Lepage, K. Q., Eden, U. T., & Eichenbaum, H. (2011). Hippocampal "time cells" bridge the gap in memory for discontiguous events. *Neuron, 71*(4), 737-749. doi:10.1016/j.neuron.2011.07.012

Magee, J. C. (2001). Dendritic mechanisms of phase precession in hippocampal ca1 pyramidal neurons. *Journal of Neurophysiology, 86*(1), 528-532.

Magee, J. C., & Grienberger, C. (2020). Synaptic plasticity forms and functions. *Annual Review of Neuroscience, 43*(1), 95-117. doi:10.1146/annurev-neuro-090919-022842

Maingret, N., Girardeau, G., Todorova, R., Goutierre, M., & Zugaro, M. (2016). Hippocampo-cortical coupling mediates memory consolidation during sleep. *Nature Neuroscience, 19*, 959. doi:10.1038/nn.4304

https://www.nature.com/articles/nn.4304#supplementary-information

Mamad, O., Stumpp, L., McNamara, H. M., Ramakrishnan, C., Deisseroth, K., Reilly, R. B., & Tsanov, M. (2017). Place field assembly distribution encodes preferred locations. *PLoS Biol, 15*(9), e2002365. doi:10.1371/journal.pbio.2002365

Mankin, Emily A., Diehl, Geoffrey W., Sparks, Fraser T., Leutgeb, S., & Leutgeb, Jill K. (2015). Hippocampal ca2 activity patterns change over time to a larger extent than between spatial contexts. *Neuron, 85*(1), 190-201. doi:https://doi.org/10.1016/j.neuron.2014.12.001

Mankin, E. A., Sparks, F. T., Slayyeh, B., Sutherland, R. J., Leutgeb, S., & Leutgeb, J. K. (2012). Neuronal code for extended time in the hippocampus. *Proceedings of the National Academy of Sciences, 109*(47), 19462-19467. doi:10.1073/pnas.1214107109

Manns, J. R., Howard, M. W., & Eichenbaum, H. (2007). Gradual changes in hippocampal activity support remembering the order of events. *Neuron, 56*(3), 530-540. doi:https://doi.org/10.1016/j.neuron.2007.08.017

Markram, H., Lübke, J., Frotscher, M., & Sakmann, B. (1997). Regulation of synaptic efficacy by coincidence of postsynaptic aps and epsps. *Science, 275*(5297), 213-215. doi:10.1126/science.275.5297.213

Markram, H., Toledo-Rodriguez, M., Wang, Y., Gupta, A., Silberberg, G., & Wu, C. (2004). Interneurons of the neocortical inhibitory system. *Nature Reviews Neuroscience, 5*(10), 793-807. doi:10.1038/nrn1519

Marr, D. (1971). Simple memory: A theory for archicortex. *Philosophical Transactions of the Royal Society of London. B, Biological Sciences, 262*(841), 23-81. doi:doi:10.1098/rstb.1971.0078

Martig, A. K., & Mizumori, S. J. (2011). Ventral tegmental area disruption selectively affects ca1/ca2 but not ca3 place fields during a differential reward working memory task. *Hippocampus, 21*(2), 172-184. doi:10.1002/hipo.20734

Martin, S. J., Grimwood, P. D., & Morris, R. G. M. (2000). Synaptic plasticity and memory: An evaluation of the hypothesis. *Annual Review of Neuroscience, 23*(1), 649-711. doi:10.1146/annurev.neuro.23.1.649

Maurer, A. P., & McNaughton, B. L. (2007). Network and intrinsic cellular mechanisms underlying theta phase precession of hippocampal neurons. *Trends in Neurosciences, 30*(7), 325-333. doi:https://doi.org/10.1016/j.tins.2007.05.002

McClelland, J. L., McNaughton, B. L., & O'Reilly, R. C. (1995). Why there are complementary learning systems in the hippocampus and neocortex: Insights from the successes and failures of connectionist models of learning and memory. *Psychological review, 102*(3), 419-457. doi:10.1037/0033-295X.102.3.419

McNamara, C. G., Tejero-Cantero, Á., Trouche, S., Campo-Urriza, N., & Dupret, D. (2014). Dopaminergic neurons promote hippocampal reactivation and spatial memory persistence. *Nature Neuroscience, 17*(12), 1658-1660. doi:10.1038/nn.3843

McNaughton, B. L., Barnes, C. A., Meltzer, J., & Sutherland, R. J. (1989). Hippocampal granule cells are necessary for normal spatial learning but not for spatially-selective pyramidal cell discharge. *Exp Brain Res, 76*(3), 485-496. doi:10.1007/bf00248904

McNaughton, B. L., Barnes, C. A., & O'Keefe, J. (1983). The contributions of position, direction, and velocity to single unit activity in the hippocampus of freely-moving rats. *Exp Brain Res, 52*(1), 41-49. doi:10.1007/bf00237147

McNaughton, B. L., Barnes, C. A., Rao, G., Baldwin, J., & Rasmussen, M. (1986). Long-term enhancement of hippocampal synaptic transmission and the acquisition of spatial information. *J Neurosci, 6*(2), 563-571. doi:10.1523/jneurosci.06-02-00563.1986

McNaughton, B. L., Battaglia, F. P., Jensen, O., Moser, E. I., & Moser, M. B. (2006). Path integration and the neural basis of the 'cognitive map'. *Nat Rev Neurosci, 7*(8), 663-678. doi:10.1038/nrn1932

McNaughton, B. L., & Morris, R. G. M. (1987). Hippocampal synaptic enhancement and information storage within a distributed memory system. *Trends in Neurosciences, 10*(10), 408-415. doi:https://doi.org/10.1016/0166-2236(87)90011-7

Megías, M., Emri, Z., Freund, T. F., & Gulyás, A. I. (2001). Total number and distribution of inhibitory and excitatory synapses on hippocampal ca1 pyramidal cells. *Neuroscience, 102*(3), 527-540. doi:https://doi.org/10.1016/S0306-4522(00)00496-6

Mehta, M., Lee, A., & Wilson, M. (2002). Role of experience and oscillations in transforming a rate code into a temporal code. *Nature, 417*(6890), 741.

Mensink, G.-J. M., & Raaijmakers, J. G. W. (1989). A model for contextual fluctuation. *Journal of Mathematical Psychology, 33*(2), 172-186. doi:https://doi.org/10.1016/0022-2496(89)90029-1

Middleton, S. J., & McHugh, T. J. (2016). Silencing ca3 disrupts temporal coding in the ca1 ensemble. *Nature Neuroscience, 19*, 945. doi:10.1038/nn.4311

https://www.nature.com/articles/nn.4311#supplementary-information

Milstein, Aaron D., Bloss, Erik B., Apostolides, Pierre F., Vaidya, Sachin P., Dilly, Geoffrey A., Zemelman, Boris V., & Magee, Jeffrey C. (2015). Inhibitory gating of input comparison in the ca1 microcircuit. *Neuron, 87*(6), 1274-1289. doi:https://doi.org/10.1016/j.neuron.2015.08.025

Mishra, R. K., Kim, S., Guzman, S. J., & Jonas, P. (2016). Symmetric spike timing-dependent plasticity at ca3–ca3 synapses optimizes storage and recall in autoassociative networks. *Nature Communications, 7*(1), 11552. doi:10.1038/ncomms11552

Mizunuma, M., Norimoto, H., Tao, K., Egawa, T., Hanaoka, K., Sakaguchi, T., Hioki, H., Kaneko, T., Yamaguchi, S., Nagano, T., Matsuki, N., & Ikegaya, Y. (2014). Unbalanced excitability underlies offline reactivation of behaviorally activated neurons. *Nature Neuroscience, 17*(4), 503-505. doi:10.1038/nn.3674

Mizuseki, K., Sirota, A., Pastalkova, E., & Buzsáki, G. (2009). Theta oscillations provide temporal windows for local circuit computation in the entorhinal-hippocampal loop. *Neuron, 64*(2), 267-280. doi:https://doi.org/10.1016/j.neuron.2009.08.037

Morgan, J., Cohen, D., Hempstead, J., & Curran, T. (1987). Mapping patterns of c-fos expression in the central nervous system after seizure. *Science, 237*(4811), 192-197. doi:10.1126/science.3037702

Morgan, J. I., & Curran, T. (1986). Role of ion flux in the control of c-fos expression. *Nature, 322*(6079), 552-555. doi:10.1038/322552a0

Morgan, J. I., & Curran, T. (1989). Stimulus-transcription coupling in neurons: Role of cellular immediate-early genes. *Trends Neurosci, 12*(11), 459-462. doi:10.1016/0166-2236(89)90096-9

Morris, R. G. M., Anderson, E., Lynch, G. S., & Baudry, M. (1986). Selective impairment of learning and blockade of long-term potentiation by an n-methyl-d-aspartate receptor antagonist, ap5. *Nature, 319*(6056), 774-776. doi:10.1038/319774a0

Morris, R. G. M., Garrud, P., Rawlins, J. N. P., & O'Keefe, J. (1982). Place navigation impaired in rats with hippocampal lesions. *Nature, 297*(5868), 681-683. doi:10.1038/297681a0

Moser, E. I., Krobert, K. A., Moser, M.-B., & Morris, R. G. M. (1998). Impaired spatial learning after saturation of long-term potentiation. *Science, 281*(5385), 2038-2042. doi:10.1126/science.281.5385.2038

Muessig, L., Lasek, M., Varsavsky, I., Cacucci, F., & Wills, T. J. (2019). Coordinated emergence of hippocampal replay and theta sequences during post-natal development. *Current Biology, 29*(5), 834-840.e834. doi:https://doi.org/10.1016/j.cub.2019.01.005

Muller, L., Chavane, F., Reynolds, J., & Sejnowski, T. J. (2018). Cortical travelling waves: Mechanisms and computational principles. *Nature Reviews Neuroscience, 19*(5), 255-268. doi:10.1038/nrn.2018.20

Muller, R., & Kubie, J. (1987). The effects of changes in the environment on the spatial firing of hippocampal complex-spike cells. *The Journal of Neuroscience, 7*(7), 1951-1968. doi:10.1523/jneurosci.07-07-01951.1987

Muzzio, I. A., Levita, L., Kulkarni, J., Monaco, J., Kentros, C., Stead, M., Abbott, L. F., & Kandel, E. R. (2009). Attention enhances the retrieval and stability of visuospatial and olfactory representations in the dorsal hippocampus. *PLOS Biology, 7*(6), e1000140. doi:10.1371/journal.pbio.1000140

Nádasdy, Z., Hirase, H., Czurkó, A., Csicsvari, J., & Buzsáki, G. (1999). Replay and time compression of recurring spike sequences in the hippocampus. *The Journal of Neuroscience, 19*(21), 9497-9507. doi:10.1523/jneurosci.19-21-09497.1999

Nakashiba, T., Young, J. Z., McHugh, T. J., Buhl, D. L., & Tonegawa, S. (2008). Transgenic inhibition of synaptic transmission reveals role of ca3 output in hippocampal learning. *Science, 319*(5867), 1260-1264. doi:10.1126/science.1151120

Nakazawa, K., Quirk, M. C., Chitwood, R. A., Watanabe, M., Yeckel, M. F., Sun, L. D., Kato, A., Carr, C. A., Johnston, D., Wilson, M. A., & Tonegawa, S. (2002). Requirement for hippocampal ca3 nmda receptors in associative memory recall. *Science, 297*(5579), 211-218. doi:10.1126/science.1071795

Nakazawa, K., Sun, L. D., Quirk, M. C., Rondi-Reig, L., Wilson, M. A., & Tonegawa, S. (2003). Hippocampal ca3 nmda receptors are crucial for memory acquisition of one-time experience. *Neuron, 38*(2), 305-315. doi:https://doi.org/10.1016/S0896-6273(03)00165-X

Naqshbandi, M., Feeney, M. C., McKenzie, T. L. B., & Roberts, W. A. (2007). Testing for episodic-like memory in rats in the absence of time of day cues: Replication of babb and crystal. *Behavioural Processes, 74*(2), 217-225. doi:https://doi.org/10.1016/j.beproc.2006.10.010

Nicoll, R. A. (2017). A brief history of long-term potentiation. *Neuron, 93*(2), 281-290. doi:https://doi.org/10.1016/j.neuron.2016.12.015

Nicoll, R. A., & Schmitz, D. (2005). Synaptic plasticity at hippocampal mossy fibre synapses. *Nat Rev Neurosci, 6*(11), 863-876. doi:10.1038/nrn1786

Niedermeyer, E. (1999). The normal eeg of the waking adult. In E. Niedermeyer & F. H. Lopes da Silva (Eds.), *Electroencephalography: Basic principles, clinical applications and related fields* (pp. 149-173). Baltimore, MD: Lippincott Williams & Wilkins.

Norimoto, H., Makino, K., Gao, M., Shikano, Y., Okamoto, K., Ishikawa, T., Sasaki, T., Hioki, H., Fujisawa, S., & Ikegaya, Y. (2018). Hippocampal ripples down-regulate synapses. *Science, 359*(6383), 1524-1527. doi:10.1126/science.aao0702

Nyberg, L., McLntosh, A. R., Houle, S., Nilsson, L. G., & Tulving, E. (1996). Activation of medial temporal structures during episodic memory retrieval. *Nature, 380*(6576), 715-717. doi:10.1038/380715a0

O'Kane, G., Kensinger, E. A., & Corkin, S. (2004). Evidence for semantic learning in profound amnesia: An investigation with patient h.M. *Hippocampus, 14*(4), 417-425. doi:10.1002/hipo.20005

O'Keefe, J. (1976). Place units in the hippocampus of the freely moving rat. *Experimental Neurology, 51*(1), 78-109. doi:https://doi.org/10.1016/0014-4886(76)90055-8

O'Keefe, J., & Dostrovsky, J. (1971). The hippocampus as a spatial map. Preliminary evidence from unit activity in the freely-moving rat. *Brain Research, 34*(1), 171-175. doi:https://doi.org/10.1016/0006-8993(71)90358-1

O'Keefe, J., & Nadel, L. (1978). *The hippocampus as a cognitive map*: Clarendon Press.

O'Keefe, J., & Recce, M. L. (1993). Phase relationship between hippocampal place units and the eeg theta rhythm. *Hippocampus, 3*(3), 317-330. doi:10.1002/hipo.450030307

O'Neill, J., Senior, T. J., Allen, K., Huxter, J. R., & Csicsvari, J. (2008). Reactivation of experience-dependent cell assembly patterns in the hippocampus. *Nature Neuroscience, 11*(2), 209-215. doi:10.1038/nn2037

Okamoto, K., & Ikegaya, Y. (2019). Recurrent connections between ca2 pyramidal cells. *Hippocampus, 29*(4), 305-312. doi:10.1002/hipo.23064

Ólafsdóttir, H. F., Carpenter, F., & Barry, C. (2016). Coordinated grid and place cell replay during rest. *Nature Neuroscience, 19*(6), 792-794. doi:10.1038/nn.4291

Oliva, A., Fernández-Ruiz, A., Buzsáki, G., & Berényi, A. (2016). Role of hippocampal ca2 region in triggering sharp-wave ripples. *Neuron, 91*(6), 1342-1355. doi:10.1016/j.neuron.2016.08.008

Olton, D. S., & Samuelson, R. J. (1976). Remembrance of places passed: Spatial memory in rats. *Journal of Experimental Psychology: Animal Behavior Processes, 2*(2), 97-116. doi:10.1037/0097-7403.2.2.97

Olton, D. S., Walker, J. A., & Gage, F. H. (1978). Hippocampal connections and spatial discrimination. *Brain Res, 139*(2), 295-308. doi:10.1016/0006-8993(78)90930-7

Pacheco Estefan, D., Sánchez-Fibla, M., Duff, A., Principe, A., Rocamora, R., Zhang, H., Axmacher, N., & Verschure, P. F. M. J. (2019). Coordinated representational reinstatement in the human hippocampus and lateral temporal cortex during episodic memory retrieval. *Nature Communications, 10*(1), 2255. doi:10.1038/s41467-019-09569-0

Pastalkova, E., Itskov, V., Amarasingham, A., & Buzsáki, G. (2008). Internally generated cell assembly sequences in the rat hippocampus. *Science, 321*(5894), 1322-1327. doi:10.1126/science.1159775

Pavlides, C., & Winson, J. (1989). Influences of hippocampal place cell firing in the awake state on the activity of these cells during subsequent sleep episodes. *J Neurosci, 9*(8), 2907-2918. doi:10.1523/jneurosci.09-08-02907.1989

Perez-Orive, J., Mazor, O., Turner, G. C., Cassenaer, S., Wilson, R. I., & Laurent, G. (2002). Oscillations and sparsening of odor representations in the mushroom body. *Science, 297*(5580), 359-365. doi:10.1126/science.1070502

Pernía-Andrade, Alejandro J., & Jonas, P. (2014). Theta-gamma-modulated synaptic currents in hippocampal granule cells in vivo define a mechanism for network oscillations. *Neuron, 81*(1), 140-152. doi:https://doi.org/10.1016/j.neuron.2013.09.046

Peyrache, A., Battaglia, F. P., & Destexhe, A. (2011). Inhibition recruitment in prefrontal cortex during sleep spindles and gating of hippocampal inputs. *Proc Natl Acad Sci U S A, 108*(41), 17207-17212. doi:10.1073/pnas.1103612108

Peyrache, A., & Seibt, J. (2020). A mechanism for learning with sleep spindles. *Philos Trans R Soc Lond B Biol Sci, 375*(1799), 20190230. doi:10.1098/rstb.2019.0230

Pfeiffer, B. E., & Foster, D. J. (2013). Hippocampal place-cell sequences depict future paths to remembered goals. *Nature, 497*, 74. doi:10.1038/nature12112

https://www.nature.com/articles/nature12112#supplementary-information

Rasch, B., & Born, J. (2007). Maintaining memories by reactivation. *Current opinion in neurobiology, 17*(6), 698-703. doi:https://doi.org/10.1016/j.conb.2007.11.007

Rebola, N., Carta, M., & Mulle, C. (2017). Operation and plasticity of hippocampal ca3 circuits: Implications for memory encoding. *Nature Reviews Neuroscience, 18*(4), 208-220. doi:10.1038/nrn.2017.10

Redish, A. D., & Touretzky, D. S. (1998). The role of the hippocampus in solving the morris water maze. *Neural Comput, 10*(1), 73-111. doi:10.1162/089976698300017908

Reifenstein, E. T., Ebbesen, C. L., Tang, Q., Brecht, M., Schreiber, S., & Kempter, R. (2016). Cell-type specific phase precession in layer ii of the medial entorhinal cortex. *J Neurosci, 36*(7), 2283-2288. doi:10.1523/jneurosci.2986-15.2016

Reijmers, L. G., Perkins, B. L., Matsuo, N., & Mayford, M. (2007). Localization of a stable neural correlate of associative memory. *Science, 317*(5842), 1230-1233. doi:10.1126/science.1143839

Repa, J. C., Muller, J., Apergis, J., Desrochers, T. M., Zhou, Y., & LeDoux, J. E. (2001). Two different lateral amygdala cell populations contribute to the initiation and storage of memory. *Nat Neurosci, 4*(7), 724-731. doi:10.1038/89512

Robbe, D., & Buzsáki, G. (2009). Alteration of theta timescale dynamics of hippocampal place cells by a cannabinoid is associated with memory impairment. *The Journal of Neuroscience, 29*(40), 12597-12605. doi:10.1523/jneurosci.2407-09.2009

Robbe, D., Montgomery, S. M., Thome, A., Rueda-Orozco, P. E., McNaughton, B. L., & Buzsaki, G. (2006). Cannabinoids reveal importance of spike timing coordination in hippocampal function. *Nature Neuroscience, 9*(12), 1526-1533. doi:10.1038/nn1801

Roberts, W. A., Feeney, M. C., MacPherson, K., Petter, M., McMillan, N., & Musolino, E. (2008). Episodic-like memory in rats: Is it based on when or how long ago? *Science, 320*(5872), 113-115. doi:10.1126/science.1152709

Robinson, N. T. M., Descamps, L. A. L., Russell, L. E., Buchholz, M. O., Bicknell, B. A., Antonov, G. K., Lau, J. Y. N., Nutbrown, R., Schmidt-Hieber, C., & Häusser, M. (2020). Targeted activation of hippocampal place cells drives memory-guided spatial behavior. *Cell*. doi:10.1016/j.cell.2020.09.061

Robinson, N. T. M., Priestley, J. B., Rueckemann, J. W., Garcia, A. D., Smeglin, V. A., Marino, F. A., & Eichenbaum, H. (2017). Medial entorhinal cortex selectively supports temporal coding by hippocampal neurons. *Neuron, 94*(3), 677-688.e676. doi:10.1016/j.neuron.2017.04.003

Rogerson, T., Cai, D. J., Frank, A., Sano, Y., Shobe, J., Lopez-Aranda, M. F., & Silva, A. J. (2014). Synaptic tagging during memory allocation. *Nature Reviews Neuroscience, 15*(3), 157-169. doi:10.1038/nrn3667

Rokni, U., Richardson, A. G., Bizzi, E., & Seung, H. S. (2007). Motor learning with unstable neural representations. *Neuron, 54*(4), 653-666. doi:https://doi.org/10.1016/j.neuron.2007.04.030

Rolls, E. T. (1989). Functions of neuronal networks in the hippocampus and neocortex in memory. In J. H. Byrne & W. O. Berry (Eds.), *Neural models of plasticity* (pp. 240-265): Academic Press.

Rolls, E. T. (1996). A theory of hippocampal function in memory. *Hippocampus, 6*(6), 601-620. doi:10.1002/(sici)1098-1063(1996)6:6<601::Aid-hipo5>3.0.Co;2-j

Rolls, E. T. (2010). A computational theory of episodic memory formation in the hippocampus. *Behavioural Brain Research, 215*(2), 180-196. doi:https://doi.org/10.1016/j.bbr.2010.03.027

Rolls, E. T. (2013). The mechanisms for pattern completion and pattern separation in the hippocampus. *Frontiers in Systems Neuroscience, 7*(74). doi:10.3389/fnsys.2013.00074

Romani, S., & Tsodyks, M. (2015). Short-term plasticity based network model of place cells dynamics. *Hippocampus, 25*(1), 94-105. doi:10.1002/hipo.22355

Rosen, Z. B., Cheung, S., & Siegelbaum, S. A. (2015). Midbrain dopamine neurons bidirectionally regulate ca3-ca1 synaptic drive. *Nature Neuroscience, 18*(12), 1763-1771. doi:10.1038/nn.4152

Rosenbaum, R. S., Köhler, S., Schacter, D. L., Moscovitch, M., Westmacott, R., Black, S. E., Gao, F., & Tulving, E. (2005). The case of k.C.: Contributions of a memory-impaired person to memory theory. *Neuropsychologia, 43*(7), 989-1021. doi:https://doi.org/10.1016/j.neuropsychologia.2004.10.007

Roux, L., & Buzsáki, G. (2015). Tasks for inhibitory interneurons in intact brain circuits. *Neuropharmacology, 88*, 10-23. doi:https://doi.org/10.1016/j.neuropharm.2014.09.011

Roux, L., Hu, B., Eichler, R., Stark, E., & Buzsáki, G. (2017). Sharp wave ripples during learning stabilize the hippocampal spatial map. *Nat Neurosci, 20*(6), 845-853. doi:10.1038/nn.4543

Rowland, D. C., Weible, A. P., Wickersham, I. R., Wu, H., Mayford, M., Witter, M. P., & Kentros, C. G. (2013). Transgenically targeted rabies virus demonstrates a major monosynaptic projection from hippocampal area ca2 to medial entorhinal layer ii neurons. *The Journal of Neuroscience, 33*(37), 14889-14898. doi:10.1523/jneurosci.1046-13.2013

Roy, D. S., Arons, A., Mitchell, T. I., Pignatelli, M., Ryan, T. J., & Tonegawa, S. (2016). Memory retrieval by activating engram cells in mouse models of early alzheimer's disease. *Nature, 531*, 508. doi:10.1038/nature17172

Royer, S., Zemelman, B. V., Losonczy, A., Kim, J., Chance, F., Magee, J. C., & Buzsáki, G. (2012). Control of timing, rate and bursts of hippocampal place cells by dendritic and somatic inhibition. *Nature Neuroscience, 15*, 769. doi:10.1038/nn.3077

https://www.nature.com/articles/nn.3077#supplementary-information

Rubin, A., Geva, N., Sheintuch, L., & Ziv, Y. (2015). Hippocampal ensemble dynamics timestamp events in long-term memory. *eLife, 4*, e12247. doi:10.7554/eLife.12247

Rule, M. E., O'Leary, T., & Harvey, C. D. (2019). Causes and consequences of representational drift. *Current opinion in neurobiology, 58*, 141-147. doi:https://doi.org/10.1016/j.conb.2019.08.005

Sabariego, M., Schönwald, A., Boublil, B. L., Zimmerman, D. T., Ahmadi, S., Gonzalez, N., Leibold, C., Clark, R. E., Leutgeb, J. K., & Leutgeb, S. (2019). Time cells in the hippocampus are neither dependent on medial entorhinal cortex inputs nor necessary for spatial working memory. *Neuron, 102*(6), 1235-1248.e1235. doi:10.1016/j.neuron.2019.04.005

Sadowski, J. H., Jones, M. W., & Mellor, J. R. (2016). Sharp-wave ripples orchestrate the induction of synaptic plasticity during reactivation of place cell firing patterns in the hippocampus. *Cell Rep, 14*(8), 1916-1929. doi:10.1016/j.celrep.2016.01.061

Samsonovich, A., & McNaughton, B. L. (1997). Path integration and cognitive mapping in a continuous attractor neural network model. *J Neurosci, 17*(15), 5900-5920. doi:10.1523/jneurosci.17-15-05900.1997

Sanders, H., Rennó-Costa, C., Idiart, M., & Lisman, J. E. (2015). Grid cells and place cells: An integrated view of their navigational and memory function. *Trends in Neurosciences, 38*(12), 763 - 775. doi:https://doi.org/10.1016/j.tins.2015.10.004

Sanders, H., Wilson, M. A., & Gershman, S. J. (2020). Hippocampal remapping as hidden state inference. *eLife, 9*. doi:10.7554/eLife.51140

Sargolini, F., Fyhn, M., Hafting, T., McNaughton, B. L., Witter, M. P., Moser, M. B., & Moser, E. I. (2006). Conjunctive representation of position, direction, and velocity in entorhinal cortex. *Science, 312*(5774), 758-762. doi:10.1126/science.1125572

Sasaki, T., Leutgeb, S., & Leutgeb, J. K. (2015). Spatial and memory circuits in the medial entorhinal cortex. *Current opinion in neurobiology, 32*, 16-23. doi:https://doi.org/10.1016/j.conb.2014.10.008

Sasaki, T., Piatti, V. C., Hwaun, E., Ahmadi, S., Lisman, J. E., Leutgeb, S., & Leutgeb, J. K. (2018). Dentate network activity is necessary for spatial working memory by supporting ca3 sharp-wave ripple generation and prospective firing of ca3 neurons. *Nature Neuroscience, 21*(2), 258-269. doi:10.1038/s41593-017-0061-5

Schacter, D. L., Eich, J. E., & Tulving, E. (1978). Richard semon's theory of memory. *Journal of Verbal Learning and Verbal Behavior, 17*(6), 721-743. doi:https://doi.org/10.1016/S0022-5371(78)90443-7

Scharfman, H. E. (2007). The ca3 "backprojection" to the dentate gyrus. *Prog Brain Res, 163*, 627-637. doi:10.1016/s0079-6123(07)63034-9

Schlesiger, M. I., Cannova, C. C., Boublil, B. L., Hales, J. B., Mankin, E. A., Brandon, M. P., Leutgeb, J. K., Leibold, C., & Leutgeb, S. (2015). The medial entorhinal cortex is necessary for temporal organization of hippocampal neuronal activity. *Nature Neuroscience, 18*, 1123. doi:10.1038/nn.4056

https://www.nature.com/articles/nn.4056#supplementary-information

Schmidt-Hieber, C., & Nolan, M. F. (2017). Synaptic integrative mechanisms for spatial cognition. *Nature Neuroscience, 20*, 1483. doi:10.1038/nn.4652

Schmidt, B., Duin, A. A., & Redish, A. D. (2019). Disrupting the medial prefrontal cortex alters hippocampal sequences during deliberative decision making. *J Neurophysiol, 121*(6), 1981-2000. doi:10.1152/jn.00793.2018

Schomburg, Erik W., Fernández-Ruiz, A., Mizuseki, K., Berényi, A., Anastassiou, Costas A., Koch, C., & Buzsáki, G. (2014). Theta phase segregation of input-specific gamma patterns in entorhinal-hippocampal networks. *Neuron, 84*(2), 470-485. doi:https://doi.org/10.1016/j.neuron.2014.08.051

Schwartz, B. L., Hoffman, M. L., & Evans, S. (2005). Episodic-like memory in a gorilla: A review and new findings. *Learning and Motivation, 36*(2), 226-244. doi:https://doi.org/10.1016/j.lmot.2005.02.012

Scoville, W. B., & Milner, B. (1957). Loss of recent memory after bilateral hippocampal lesions. *Journal of Neurology, Neurosurgery & Psychiatry, 20*(1), 11-21. doi:10.1136/jnnp.20.1.11

Sejnowski, T. J., & Paulsen, O. (2006). Network oscillations: Emerging computational principles. *The Journal of Neuroscience, 26*(6), 1673-1676. doi:10.1523/JNEUROSCI.3737-05d.2006

Senzai, Y., & Buzsáki, G. (2017). Physiological properties and behavioral correlates of hippocampal granule cells and mossy cells. *Neuron, 93*(3), 691-704.e695. doi:https://doi.org/10.1016/j.neuron.2016.12.011

Shin, J. D., Tang, W., & Jadhav, S. P. (2019). Dynamics of awake hippocampal-prefrontal replay for spatial learning and memory-guided decision making. *Neuron*. doi:https://doi.org/10.1016/j.neuron.2019.09.012

Shirvalkar, P. R., Rapp, P. R., & Shapiro, M. L. (2010). Bidirectional changes to hippocampal theta-gamma comodulation predict memory for recent spatial episodes. *Proc Natl Acad Sci U S A, 107*(15), 7054-7059. doi:10.1073/pnas.0911184107

Siapas, A. G., & Wilson, M. A. (1998). Coordinated interactions between hippocampal ripples and cortical spindles during slow-wave sleep. *Neuron, 21*(5), 1123-1128. doi:https://doi.org/10.1016/S0896-6273(00)80629-7

Silva, A. J., Zhou, Y., Rogerson, T., Shobe, J., & Balaji, J. (2009). Molecular and cellular approaches to memory allocation in neural circuits. *Science, 326*(5951), 391-395. doi:10.1126/science.1174519

Silver, R. A. (2010). Neuronal arithmetic. *Nature Reviews Neuroscience, 11*, 474. doi:10.1038/nrn2864

https://www.nature.com/articles/nrn2864#supplementary-information

Singer, Annabelle C., Carr, Margaret F., Karlsson, Mattias P., & Frank, Loren M. (2013). Hippocampal swr activity predicts correct decisions during the initial learning of an alternation task. *Neuron, 77*(6), 1163-1173. doi:https://doi.org/10.1016/j.neuron.2013.01.027

Singer, A. C., & Frank, L. M. (2009). Rewarded outcomes enhance reactivation of experience in the hippocampus. *Neuron, 64*(6), 910-921. doi:https://doi.org/10.1016/j.neuron.2009.11.016

Singer, A. C., Karlsson, M. P., Nathe, A. R., Carr, M. F., & Frank, L. M. (2010). Experience-dependent development of coordinated hippocampal spatial activity representing the similarity of related locations. *The Journal of Neuroscience, 30*(35), 11586-11604. doi:10.1523/jneurosci.0926-10.2010

Skaggs, W. E., & McNaughton, B. L. (1996). Replay of neuronal firing sequences in rat hippocampus during sleep following spatial experience. *Science, 271*(5257), 1870-1873. doi:10.1126/science.271.5257.1870

Skaggs, W. E., McNaughton, B. L., Gothard, K. M., & Markus, E. J. (1992). *An information-theoretic approach to deciphering the hippocampal code*. Paper presented at the Proceedings of the 5th International Conference on Neural Information Processing Systems, Denver, Colorado.

Skaggs, W. E., McNaughton, B. L., Wilson, M. A., & Barnes, C. A. (1996). Theta phase precession in hippocampal neuronal populations and the compression of temporal sequences. *Hippocampus, 6*(2), 149-172.

Solstad, T., Boccara, C. N., Kropff, E., Moser, M.-B., & Moser, E. I. (2008). Representation of geometric borders in the entorhinal cortex. *Science, 322*(5909), 1865-1868. doi:10.1126/science.1166466

Sosa, M., Joo, H. R., & Frank, L. M. (2020). Dorsal and ventral hippocampal sharp-wave ripples activate distinct nucleus accumbens networks. *Neuron, 105*(4), 725-741.e728. doi:10.1016/j.neuron.2019.11.022

Squire, L. R. (1992). Memory and the hippocampus: A synthesis from findings with rats, monkeys, and humans. *Psychological review, 99*(2), 195.

Stachenfeld, K. L., Botvinick, M. M., & Gershman, S. J. (2017). The hippocampus as a predictive map. *Nature Neuroscience, 20*, 1643. doi:10.1038/nn.4650

https://www.nature.com/articles/nn.4650#supplementary-information

Steward, O., & Scoville, S. A. (1976). Cells of origin of entorhinal cortical afferents to the hippocampus and fascia dentata of the rat. *Journal of Comparative Neurology, 169*(3), 347-370. doi:10.1002/cne.901690306

Sugar, J., & Moser, M. B. (2019). Episodic memory: Neuronal codes for what, where, and when. *Hippocampus, 29*(12), 1190-1205. doi:10.1002/hipo.23132

Sun, Q., Sotayo, A., Cazzulino, A. S., Snyder, A. M., Denny, C. A., & Siegelbaum, S. A. (2017). Proximodistal heterogeneity of hippocampal ca3 pyramidal neuron intrinsic properties,

connectivity, and reactivation during memory recall. *Neuron, 95*(3), 656-672.e653. doi:https://doi.org/10.1016/j.neuron.2017.07.012

Takeuchi, T., Duszkiewicz, A. J., Sonneborn, A., Spooner, P. A., Yamasaki, M., Watanabe, M., Smith, C. C., Fernández, G., Deisseroth, K., Greene, R. W., & Morris, R. G. M. (2016). Locus coeruleus and dopaminergic consolidation of everyday memory. *Nature, 537*(7620), 357-362. doi:10.1038/nature19325

Tanaka, Kazumasa Z., Pevzner, A., Hamidi, Anahita B., Nakazawa, Y., Graham, J., & Wiltgen, Brian J. (2014). Cortical representations are reinstated by the hippocampus during memory retrieval. *Neuron, 84*(2), 347-354. doi:https://doi.org/10.1016/j.neuron.2014.09.037

Tang, W., & Jadhav, S. P. (2019). Sharp-wave ripples as a signature of hippocampal-prefrontal reactivation for memory during sleep and waking states. *Neurobiology of Learning and Memory, 160*, 11-20. doi:https://doi.org/10.1016/j.nlm.2018.01.002

Tang, Y.-P., Shimizu, E., Dube, G. R., Rampon, C., Kerchner, G. A., Zhuo, M., Liu, G., & Tsien, J. Z. (1999). Genetic enhancement of learning and memory in mice. *Nature, 401*(6748), 63-69. doi:10.1038/43432

Taylor, K., Mandon, S., Freiwald, W. A., & Kreiter, A. K. (2005). Coherent oscillatory activity in monkey area v4 predicts successful allocation of attention. *Cerebral Cortex, 15*(9), 1424-1437. doi:10.1093/cercor/bhi023

Thompson, L. T., & Best, P. J. (1990). Long-term stability of the place-field activity of single units recorded from the dorsal hippocampus of freely behaving rats. *Brain Research, 509*(2), 299-308. doi:https://doi.org/10.1016/0006-8993(90)90555-P

Thurley, K., Leibold, C., Gundlfinger, A., Schmitz, D., & Kempter, R. (2008). Phase precession through synaptic facilitation. *Neural Computation, 20*(5), 1285-1324. doi:10.1162/neco.2008.07-06-292

Tolman, E. C. (1948). Cognitive maps in rats and men. *Psychological review, 55*(4), 189-208. doi:10.1037/h0061626

Tonegawa, S., Liu, X., Ramirez, S., & Redondo, R. (2015). Memory engram cells have come of age. *Neuron, 87*(5), 918-931. doi:10.1016/j.neuron.2015.08.002

Treves, A., & Rolls, E. T. (1992). Computational constraints suggest the need for two distinct input systems to the hippocampal ca3 network. *Hippocampus, 2*(2), 189-199. doi:10.1002/hipo.450020209

Treves, A., & Rolls, E. T. (1994). Computational analysis of the role of the hippocampus in memory. *Hippocampus, 4*(3), 374-391. doi:10.1002/hipo.450040319

Tsodyks, M. (1999). Attractor neural network models of spatial maps in hippocampus. *Hippocampus, 9*(4), 481-489. doi:10.1002/(sici)1098-1063(1999)9:4<481::Aid-hipo14>3.0.Co;2-s

Tsodyks, M. V., Skaggs, W. E., Sejnowski, T. J., & McNaughton, B. L. (1996). Population dynamics and theta rhythm phase precession of hippocampal place cell firing: A spiking neuron model. *Hippocampus, 6*(3), 271-280. doi:10.1002/(sici)1098-1063(1996)6:3<271::Aid-hipo5>3.0.Co;2-q

Tulving, E. (1983). Elements of episodic memory.

Tulving, E., Hayman, C. A., & Macdonald, C. A. (1991). Long-lasting perceptual priming and semantic learning in amnesia: A case experiment. *J Exp Psychol Learn Mem Cogn, 17*(4), 595-617. doi:10.1037//0278-7393.17.4.595

van de Ven, G. M., Trouche, S., McNamara, C. G., Allen, K., & Dupret, D. (2016). Hippocampal offline reactivation consolidates recently formed cell assembly patterns during sharp wave-ripples. *Neuron, 92*(5), 968-974. doi:https://doi.org/10.1016/j.neuron.2016.10.020

van der Meer, M. A., & Redish, A. D. (2011). Theta phase precession in rat ventral striatum links place and reward information. *J Neurosci, 31*(8), 2843-2854. doi:10.1523/jneurosci.4869-10.2011

van Dijk, M. T., & Fenton, A. A. (2018). On how the dentate gyrus contributes to memory discrimination. *Neuron, 98*(4), 832-845.e835. doi:https://doi.org/10.1016/j.neuron.2018.04.018

Vanderwolf, C. H. (1969). Hippocampal electrical activity and voluntary movement in the rat. *Electroencephalography and Clinical Neurophysiology, 26*(4), 407-418. doi:https://doi.org/10.1016/0013-4694(69)90092-3

Varga, C., Lee, S. Y., & Soltesz, I. (2010). Target-selective gabaergic control of entorhinal cortex output. *Nature Neuroscience, 13*(7), 822-824. doi:10.1038/nn.2570

Vazdarjanova, A., & Guzowski, J. F. (2004). Differences in hippocampal neuronal population responses to modifications of an environmental context: Evidence for distinct, yet complementary, functions of ca3 and ca1 ensembles. *J Neurosci, 24*(29), 6489-6496. doi:10.1523/jneurosci.0350-04.2004

Vertes, R. P. (2015). Major diencephalic inputs to the hippocampus: Supramammillary nucleus and nucleus reuniens. Circuitry and function. *Prog Brain Res, 219*, 121-144. doi:10.1016/bs.pbr.2015.03.008

Vesuna, S., Kauvar, I. V., Richman, E., Gore, F., Oskotsky, T., Sava-Segal, C., Luo, L., Malenka, R. C., Henderson, J. M., Nuyujukian, P., Parvizi, J., & Deisseroth, K. (2020). Deep posteromedial cortical rhythm in dissociation. *Nature, 586*(7827), 87-94. doi:10.1038/s41586-020-2731-9

Vyazovskiy, V. V., Cirelli, C., Pfister-Genskow, M., Faraguna, U., & Tononi, G. (2008). Molecular and electrophysiological evidence for net synaptic potentiation in wake and depression in sleep. *Nat Neurosci, 11*(2), 200-208. doi:10.1038/nn2035

Wallenstein, G. V., & Hasselmo, M. E. (1997). Gabaergic modulation of hippocampal population activity: Sequence learning, place field development, and the phase precession effect. *Journal of Neurophysiology, 78*(1), 393-408. doi:10.1152/jn.1997.78.1.393

Walter, W. G., & Dovey, V. J. (1944). Electro-encephalography in cases of sub-cortical tumour. *J Neurol Neurosurg Psychiatry, 7*(3-4), 57-65. doi:10.1136/jnnp.7.3-4.57

Wang, M., Foster, D. J., & Pfeiffer, B. E. (2020). Alternating sequences of future and past behavior encoded within hippocampal theta oscillations. *Science, 370*(6513), 247-250. doi:10.1126/science.abb4151

Wang, Y., Romani, S., Lustig, B., Leonardo, A., & Pastalkova, E. (2015). Theta sequences are essential for internally generated hippocampal firing fields. *Nature Neuroscience, 18*, 282-288. doi:10.1038/nn.3904

https://www.nature.com/articles/nn.3904#supplementary-information

Whishaw, I. Q., & Vanderwolf, C. H. (1973). Hippocampal eeg and behavior: Changes in amplitude and frequency of rsa (theta rhythm) associated with spontaneous and learned movement patterns in rats and cats. *Behav Biol, 8*(4), 461-484. doi:10.1016/s0091-6773(73)80041-0

Whittington, J. C. R., Muller, T. H., Mark, S., Chen, G., Barry, C., Burgess, N., & Behrens, T. E. J. (2020). The tolman-eichenbaum machine: Unifying space and relational memory through generalization in the hippocampal formation. *Cell*. doi:10.1016/j.cell.2020.10.024

Wikenheiser, A. M., & Redish, A. D. (2015). Hippocampal theta sequences reflect current goals. *Nature Neuroscience, 18*, 289. doi:10.1038/nn.3909

https://www.nature.com/articles/nn.3909#supplementary-information

Wills, T. J., Lever, C., Cacucci, F., Burgess, N., & O'Keefe, J. (2005). Attractor dynamics in the hippocampal representation of the local environment. *Science, 308*(5723), 873-876. doi:10.1126/science.1108905

Wilson, M. A., & McNaughton, B. L. (1993). Dynamics of the hippocampal ensemble code for space. *Science, 261*(5124), 1055-1058. doi:10.1126/science.8351520

Wilson, M. A., & McNaughton, B. L. (1994). Reactivation of hippocampal ensemble memories during sleep. *Science, 265*(5172), 676-679. doi:10.1126/science.8036517

Wilson, N. R., Runyan, C. A., Wang, F. L., & Sur, M. (2012). Division and subtraction by distinct cortical inhibitory networks in vivo. *Nature, 488*(7411), 343-348. doi:10.1038/nature11347

Wilson, R. I., & Laurent, G. (2005). Role of gabaergic inhibition in shaping odor-evoked spatiotemporal patterns in the drosophila antennal lobe. *J Neurosci, 25*(40), 9069-9079. doi:10.1523/jneurosci.2070-05.2005

Witter, M. P. (2007). Intrinsic and extrinsic wiring of ca3: Indications for connectional heterogeneity. *Learning & Memory, 14*(11), 705-713. doi:10.1101/lm.725207

Witter, M. P., Groenewegen, H. J., Lopes da Silva, F. H., & Lohman, A. H. M. (1989). Functional organization of the extrinsic and intrinsic circuitry of the parahippocampal region. *Progress in Neurobiology, 33*(3), 161-253. doi:https://doi.org/10.1016/0301-0082(89)90009-9

Womelsdorf, T., Schoffelen, J. M., Oostenveld, R., Singer, W., Desimone, R., Engel, A. K., & Fries, P. (2007). Modulation of neuronal interactions through neuronal synchronization. *Science, 316*(5831), 1609-1612. doi:10.1126/science.1139597

Wood, E. R., Dudchenko, P. A., & Eichenbaum, H. (1999). The global record of memory in hippocampal neuronal activity. *Nature, 397*(6720), 613-616. doi:10.1038/17605

Wood, E. R., Dudchenko, P. A., Robitsek, R. J., & Eichenbaum, H. (2000). Hippocampal neurons encode information about different types of memory episodes occurring in the same location. *Neuron, 27*(3), 623-633. doi:10.1016/s0896-6273(00)00071-4

Yamaguchi, Y., Aota, Y., McNaughton, B. L., & Lipa, P. (2002). Bimodality of theta phase precession in hippocampal place cells in freely running rats. *J Neurophysiol, 87*(6), 2629-2642. doi:10.1152/jn.2002.87.6.2629

Yamamoto, J., Suh, J., Takeuchi, D., & Tonegawa, S. (2014). Successful execution of working memory linked to synchronized high-frequency gamma oscillations. *Cell, 157*(4), 845-857. doi:https://doi.org/10.1016/j.cell.2014.04.009

Yiu, Adelaide P., Mercaldo, V., Yan, C., Richards, B., Rashid, Asim J., Hsiang, H.-Lin L., Pressey, J., Mahadevan, V., Tran, Matthew M., Kushner, Steven A., Woodin, Melanie A., Frankland, Paul W., & Josselyn, Sheena A. (2014). Neurons are recruited to a memory trace based on relative neuronal excitability immediately before training. *Neuron, 83*(3), 722-735. doi:https://doi.org/10.1016/j.neuron.2014.07.017

Ylinen, A., Bragin, A., Nádasdy, Z., Jandó, G., Szabó, I., Sik, A., & Buzsáki, G. (1995). Sharp wave-associated high-frequency oscillation (200 hz) in the intact hippocampus: Network and intracellular mechanisms. *J Neurosci, 15*(1 Pt 1), 30-46. doi:10.1523/jneurosci.15-01-00030.1995

Zhang, K., Ginzburg, I., McNaughton, B. L., & Sejnowski, T. J. (1998). Interpreting neuronal population activity by reconstruction: Unified framework with application to

hippocampal place cells. *Journal of Neurophysiology, 79*(2), 1017-1044. doi:10.1152/jn.1998.79.2.1017

Zhou, Y., Won, J., Karlsson, M. G., Zhou, M., Rogerson, T., Balaji, J., Neve, R., Poirazi, P., & Silva, A. J. (2009). Creb regulates excitability and the allocation of memory to subsets of neurons in the amygdala. *Nature Neuroscience, 12*(11), 1438-1443. doi:10.1038/nn.2405

Ziv, Y., Burns, L. D., Cocker, E. D., Hamel, E. O., Ghosh, K. K., Kitch, L. J., Gamal, A. E., & Schnitzer, M. J. (2013). Long-term dynamics of ca1 hippocampal place codes. *Nature Neuroscience, 16*(3), 264-266. doi:10.1038/nn.3329

Zola-Morgan, S., & Squire, L. (1990). The primate hippocampal formation: Evidence for a time-limited role in memory storage. *Science, 250*(4978), 288-290. doi:10.1126/science.2218534

Zugaro, M. B., Monconduit, L., & Buzsáki, G. (2005). Spike phase precession persists after transient intrahippocampal perturbation. *Nat Neurosci, 8*(1), 67-71. doi:10.1038/nn1369